Académie universitaire Wallonie-Europe
Université de Liège
Faculté des Sciences Appliquées
Département d'Electricité, Electronique
et Informatique (Institut Montefiore)

Real-time Corrective Control in Active Distribution Networks

Hamid Soleimani Bidgoli

Liège, Belgium, October 2017

Submitted in partial fulfilment of the requirements for the degree of
Doctor of Philosophy (Ph.D.) in Engineering Sciences

Examining Committee

Professor Bertrand Cornélusse (President of Jury), Université de Liège, Belgium

Professor Rachid Cherkaoui, École Polytechnique Fédérale de Lausanne, Switzerland

Professor Christophe Geuzaine, Université de Liège, Belgium

Professor Stefano Massucco, Università degli studi di Genova, Italy

Professor Jean-Claude Maun, Université libre de Bruxelles, Belgium

Professor Patricia Rousseaux, Université de Liège, Belgium

Professor Thierry Van Cutsem (Ph.D. advisor), FNRS and Université de Liège, Belgium

Abstract

The continuous growth of renewable energy injected into Medium-Voltage (MV) distribution systems is expected to create new operational problem such as over- and under-voltages and/or thermal overloads of equipment. Therefore, the need for real-time corrective control will go increasing, since reinforcing the network to deal with these temporary situations is seldom an economically viable option for the Distribution System Operator (DSO). This requires monitoring the system through an appropriate measurement and communication infrastructure and taking control actions if the system is going to exceed its prescribed operational limits.

In this thesis, number of methods and algorithms have been devised, developed and tested which can allow DSOs to enhance the real-time monitoring and control of their grids, taking into account various practical challenges. The main components taking part in these corrective actions are Dispersed Generation Units and the transformer Load Tap Changer in the main sub-station. A centralized control architecture is chosen mainly for its capability of coordinating multiple control actions. Furthermore, the scheme is extended to a two-level structure in order to combine a fast but partial correction by the local controllers, followed by the smooth, coordinated control of the centralized one. Another extension deals with enabling the controller to contribute to LV network voltage corrections by adjusting voltages on the MV side of the MV/LV transformers where a voltage problem has been detected.

Finally, the time frame of the centralized controller is extended with preventive security restoration. The latter uses near-future production/consumption predictions to determine if the active distribution network is going to operate within prescribed limits and, if not, to determine appropriate preventive decisions that can be used, for instance, as reference for the real-time corrective controller.

Acknowledgements

After a period of (almost) four years, today is the day: writing this note of thanks is the finishing touch on my dissertation. Throughout this period, there were many people who have supported and helped me so much, and I would like to express my sincere appreciation to all of them in the following few paragraphs.

Foremost, I would like to express my sincere gratitude to my advisor Professor Thierry Van Cutsem. Since the first day of my Ph.D. program, it has been a period of intense learning for me, not only in the scientific area, but also on a personal level. Undoubtedly, he is the main person to whom I would be thankful. He has devoted considerable time in transferring his knowledge on active distribution networks to me, advancing my research skills, leading me working on diverse topics, discussing and developing novel ideas, and also helping me to write this thesis. Besides, I thank him for the family-like atmosphere he has built in his group. I have enjoyed and learnt a lot from interesting discussions on various non-academic topics such as culture, history, news, etc. during the lunch-time and on the walking distance between the department and the restaurant. Overall, I could not have imagined having a better advisor and mentor for my Ph.D study.

Besides my advisor, I would like to thank the rest of my thesis committee: Prof. Rachid Cherkaoui, Prof. Stefano Massucco, Prof. Jean-Claude Maun, Prof. Bertrand Cornélusse, Prof. Christophe Geuzaine and Prof. Patricia Rousseaux , for devoting their time and energy to read this report.

I would like to express my sincerest thanks to Professor Damien Ernst for involving me in the GREDOR project, and for his support throughout the whole process. I would like to extend my thanks to Public Service of Wallonia, Department of Energy and Sustainable Building for its support through the GREDOR project. Indeed, it was a unique opportunity in my professional life to broaden my knowledge and interact with academic and industrial partners, expert in the field.

A special thanks to Dr. Mevludin Glavic for his valuable supports at the beginning and during my study. His guidance and insightful discussions helped me to learn the necessary materials and to become an active member of GREDOR project quite fast. I also appreciate our talks and share of his experience during our tea/coffee breaks, helping me to make important decisions in my professional life.

During my study, I have greatly benefited from the work and friendship with my colleagues. I would like to thank Dr. Petros Aristidou for his support during my first two years in Liège. He has proved to be a valuable source of information (on technical and non-technical topics alike) and a dear friend. The collaboration with my close friend Lampros Papangelis made my life more enjoyable. We started our PhD program almost at the same time and I have spent much of my time with him at work. Although working on different topics, we have had very interesting talks and brainstorming sessions. More importantly, I appreciate the friendly talks during afternoon breaks and on the way back home. I wish him, and his girlfriend Eleftheria, the best in their private and professional lives. Special thanks to Dr. Frédéric Plumier, for being a dear friend and ready to help at any time. He patiently let me practice my French with him, which was very useful to adapt in Liège and play with his lovely son Antoine. Special thanks to Dr. Tilman Weckesser for sharing time and nice discussions during the last two years. I would like to wish the best for my junior colleague Gilles Chaspierre in his PhD program and sporting life.

My thanks to all other colleagues, visiting researchers and administrative staffs, amongst which, Dr. Angel Perez, Dr. Theodoros Kyriakidis, Dr. Boris Alcaide , Gustav Lammert, Dr. Quentin Gemine and Diane Zander. Your support and friendship are cherished.

My thoughts are also with everyone else, my friends from Iran and the ones I met here, which unfortunately I cannot list separately, due to the unsaid rule that the acknowledgements should not exceed the size of the rest of the manuscript.

The last thanks goes to my family, my lovely parents Fatemeh and Mohammad who have always encouraged me in all steps of my life; my little brother Amin, a source of joy and happiness in our family; my dear brother Omid who has admired me at all times, and also Majid and Sahar thanks to whom I will soon become an uncle. I would like to extend my thanks to Monica Moriconi who has been like my mother here in Belgium.

Hamid

‘توانا بود هر که دانا بود ز دانش دل پیر برنا بود’ [1]

‘Mighty is the one who has knowledge

By knowledge, the old hearts grow young again’[1]

[1] ***A.Q. Ferdowsi Tusi*** (c. 940 – 1020) was a Persian poet and the author of *Shahnameh* (“Book of Kings”), which is the world’s longest epic poem created by a single poet, and the national epic of Greater Persia. Ferdowsi is celebrated as the most influential figure in Persian literature and one of the greatest in the history of literature [Fer].

Contents

Chapter 1

Introduction

1.1 Context and motivation

Conventionally, the electrical energy has been mainly produced by large power plants, and shipped through the transmission and distribution grids to the end customers. However, the recent quest for reduction of greenhouse gas, use of sustainable energy sources and higher energy efficiency in the transmission grid, has led to the continuous growth of comparatively much smaller Dispersed Generation Units (DGUs) exploiting renewable sources of energy and connected to Distribution Networks (DNs) [CCC09]. On the other hand, the existing distribution grid was not designed nor equipped to host DGUs and to become an "active distribution network". This proliferation of DGUs raises challenges in many aspects of Distribution System Operator (DSO) activities, ranging from long-term planning to real-time control. From system operation viewpoint, this change is expected to create new technical problems, for instance over- or under-voltages (typically in rural networks due to the long distance from the main substation), or congestion problems (typically in urban networks serving many loads) [LHM+07].

Therefore, a major need for some adaptations arises to accommodate these DGUs while assuring network security as well as satisfying market objectives. These activities can be categorized into different time horizons, as outlined hereafter.

Planning horizon: refers to the time horizon in which decisions on investment are taken. Given the information on the distant future consumption and generation, the considered network is assessed and decisions on medium- to long-term investments are taken in this time horizon. The issues to be dealt with are mainly the necessary network reinforcements, the amount of generation that can be connected to the network and their optimal allocation as well as developing the contracts between appropriate stakeholders [CIG14, FLDV14, GH15].

Operational planning horizon: aiming at assuring a balance between consumption and production at the lowest cost, this time horizon is typically from one day ahead until a few hours before real time. Furthermore, if a risk of not satisfying operational security limits is anticipated, preventive actions may be taken such as scheduled generation modulations, load flexibility activation, or network re-configuration. To take this type of decision, scenarios of consumption and generation are first estimated. Then, if a problem is anticipated, the set of available preventive actions to circumvent this issue is assessed. This information is communicated to actors of concern in distribution and transmission networks [BBG+10, Gem16].

Real-time horizon: focusing on the secure operation of the network, in this time frame the actual situation of the network is monitored and its evolution is evaluated. If, due to incidents or unforeseen events, the operational security limits are exceeded or there is high risk that the network faces such violations, corrective actions are taken. For instance, DGU power outputs and the tap position

of the transformer(s) in the main sub-station are adjusted. Thus, in this time frame, the dedicated control offers a "last line of defence" to clear or avoid the operational limit violations [SVA+].

Ex-post horizon: after a while, it is time to make financial and technical reports including the remuneration of the flexibility services (correction of expected and unexpected imbalances) and the identified limit violations. These are reported to regulatory agencies and stakeholders for financial compensation, and also to make future operation of the system smoother and more secure.

The work presented in this thesis falls in the context of Real-time. Even if the best possible decisions have been taken ahead of time, unforeseen events may take place in the meantime, which may require further decisions. There is a need for a "back-up solution" against those unforeseen events. In addition, when security is checked preventively and decisions are taken ahead of time, generation and consumption have to be predicted. This may result in either optimistic or pessimistic decisions, owing to the inevitable prediction errors. It is well known that the longer the prediction horizon, the larger the statistical dispersion of prediction errors. This increases the need for corrective control in real-time, where the actual instead of an expected situation is to be considered. Thus, in the real-time horizon, the actual situation of the network is monitored and corrective decisions are taken without delay, if necessary.

Real-time corrective control has received a growing attention in the recent years. The various approaches can be classified according to the overall control architecture: centralized, local (or decentralized), agent-based, and multi-layer. Our choice has been a centralized scheme for its capability of coordinating multiple control actions. This requires monitoring the system through an appropriate measurement and communication infrastructure and taking corrective actions if the system is driven to operate with voltage and/or thermal limits exceeded. The main components taking part in these corrective actions are DGUs and the transformer Load Tap Changer (LTC) in the main sub-station.

The control scheme has been further extended to deal, if possible, with overvoltage problems in the low-voltage grids, as well as to a two-level structure in order to combine features offered by both local and centralized controls.

Finally, a preventive analysis is proposed which re-uses the mathematical formulation of the real-time controller, together with the near-future expected evolution of the system to identify limit violations, and suggest preventive actions. The joint operation of the real-time corrective controller with this preventive analysis can provide a more secure and cost-effective operation of DNs.

1.2 Real-time corrective control

By real-time corrective control it is meant the actions taken in real-time to modify the operating point of the system when voltages at some buses are outside the allowed/desired limits, or currents in some equipment approach the limit monitored by protections. The main motivation behind corrective control is to resort to operating point adjustments to alleviate the stressed operating conditions that take place a small fraction of the time, instead of performing expensive network reinforcements in order to prevent the occurrence of those unacceptable operating conditions (the well-known "fit-and-forget" policy [LHM+07]). In other words, expensive network reinforcements can be postponed as long as unacceptable operating conditions can be avoided by corrective actions (and the latter are not "too frequent" nor "too intrusive").

As already mentioned, the available control means are typically the active and reactive powers of DGUs, and the ratio the load tap changer of the transformer(s) connecting the Medium Voltage (MV) distribution system to the High Voltage (HV) transmission grid. Flexible loads (or demand side management) can also be used in real-time to alleviate the abnormal situations (however, for the reasons explained in Section 2.10, they are not explicitly included). In such corrective actions, the various available control means should be treated in a non-discriminatory manner. Furthermore, the curtailment of active power generations should be used in the last resort, when all other control actions (such as reactive power adjustments) have been exhausted. LTCs, on the other hand, should not be manoeuvred too often to avoid reducing their lifetime. Thus, their use should have a lower priority compared to the reactive power adjustments of DGUs.

As earlier mentioned, our choice has fallen on a centralized controller. Among the centralized control schemes, Model Predictive Control (MPC) offers some interesting features. Using some model of the system, MPC relies on a multi-step optimization over a receding horizon and offers the following advantages:

- it can compensate (at least to some extent) the inevitable modelling errors. As a result, it is possible to use a model that approximates the system behaviour, in case there are not enough measurements to set up a detailed model (a typical situation in power systems, not only at distribution level);
- it can steer the system smoothly from its current operating point to the desired one;
- it allows dynamically adding and/or removing constraints to the optimisation problem at the heart of the method;
- it can anticipate the effect of the actions taken, including those by components not under its direct control.

The principle of this approach is further presented in the next section.

1.3 Model Predictive Control

The name MPC stems from the idea of employing an explicit model of the controlled system to predict its future behavior over a prediction horizon. This prediction capability allows solving optimal control problems on line, in which for instance the difference between the predicted and the desired outputs is minimized over the next N_p steps, subject to constraints on the control inputs and outputs. If the prediction model is linear, then a quadratic programming problem has to be solved if the objective is expressed through the L_2-norm, or a linear programming problem if it is expressed through the L_1-norm [BM99].

The result of the optimization is applied using a receding horizon philosophy. Namely, at instant k, using the latest available measurements, the controller determines the optimal change of control inputs (or the optimal control inputs directly) over a control horizon N_c, i.e. from k until $k+N_c-1$, in order to meet a target at the end of the prediction horizon, i.e. at $k+N_p$. However, only the first component of the optimal command sequence ($\Delta \boldsymbol{u}(k)$ or $\boldsymbol{u}(k)$) is actually applied to the system; the remaining components are discarded. After the sampling period T (i.e. at instant $k+1$), a new optimal control problem is solved using the newly received set of measurements that reflect the system response to the applied control actions at and before time k. The horizons are illustrated in Fig. 1.1. As new measurements are collected from the network at each instant k, the receding horizon mechanism provides the controller with desirable feedback characteristics.

As presented in Fig. 1.1, the prediction horizon must be chosen such that it takes into account the expected effect of the control actions on the system. Based on this, the length of the prediction horizon should be at least equal to the length of the control horizon, i.e. $N_p \geq N_c$. To decrease the computational burden, the lengths can be chosen equal, unless the controller is requested to consider changes happening beyond the control horizon.

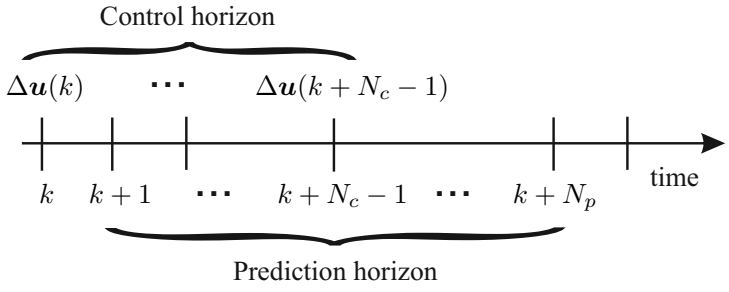

Figure 1.1: Prediction and control horizons

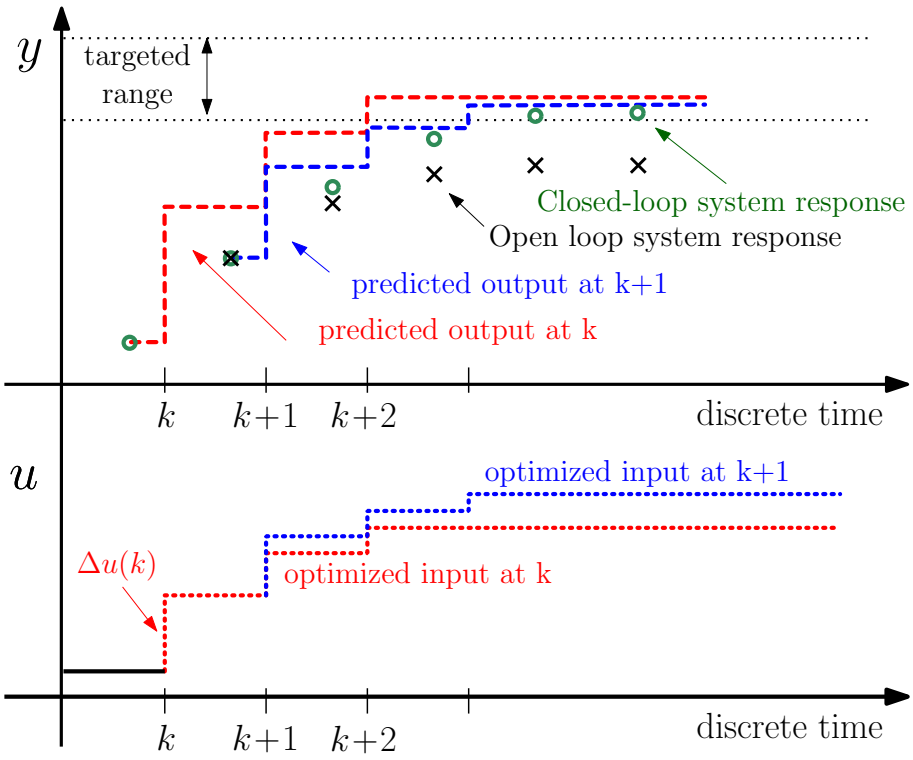

Figure 1.2: Basic principle of MPC through an illustrative example

Figure 1.2 illustrates the above-described concept of MPC for a system with a single input (control variable) and a single output (controlled variable), and with $N_c = N_p = 3$. In this example, the objective of the control scheme consists of bringing the output variable y (shown in the upper part of the figure) within the targeted range by optimum changes of the control variable u (shown in the lower part of the figure). At time k the controller calculates $\Delta u(k)$, $\Delta u(k+1)$ and $\Delta u(k+2)$ but only applies $\Delta u(k)$. Using measurements and the internal system model, it is predicted that the output will reach the desired range of operation at the end of the prediction horizon, as suggested by the red dashed line in the upper figure. However, due to model inaccuracies and measurement noises, the system response at $k+1$ is different from what was predicted for this instant. This is depicted by the green circle which is the measurement collected shortly before time $k+1$; this measured value departs from the expected trajectory shown in red. Therefore, the controller computes a new sequence of actions at $k+1$ and at subsequent times, in order to reach the objective, as shown by the circles eventually entering the targeted range.

It should be noted that the open-loop and resulting closed-loop behaviours of the system are in general different. The former would consist of applying all components of the optimal control sequence calculated at time k (i.e. $\Delta u(k)$, $\Delta u(k+1)$ and $\Delta u(k+2)$) to the system at the corresponding discrete-times ($k, k+1$ and $k+2$). In such a case, the new measurements that reflect

the system response are not exploited. Consequently, after several discrete steps, the model inaccuracies and measurement noises could result in an open-loop system response quite different from what was predicted. The crosses in Fig. 1.2 shows the open-loop system response to the optimal control sequence calculated at time k. As it can be seen, and given the above reasoning, the imprecise prediction of the system behaviour results in accumulated errors and eventually the output does not enter the targeted range.

The above receding horizon principle can be simply formulated as follows.

Typically it relies on an optimization problem, aiming at minimizing or maximizing a function (e.g. minimizing a cost) under various constraints. Assuming $\boldsymbol{x}(k+1), \ldots, \boldsymbol{x}(k+N_p)$ are state variables, grouped into the vector $\boldsymbol{X}(k)$, and $\boldsymbol{u}(k), \ldots, \boldsymbol{u}(k+N_c-1)$ into $\boldsymbol{U}(k)$, the optimization problem can be written as:

$$\min_{\boldsymbol{X},\boldsymbol{U}} \quad J(\boldsymbol{X}(k), \boldsymbol{U}(k)) \tag{1.1}$$

subject to the system evolution equality constraint, expressed symbolically through the function $\boldsymbol{f}$:

$$\boldsymbol{X}(k+1) \;=\; \boldsymbol{f}\big(\boldsymbol{X}(k), \boldsymbol{U}(k)\big) \tag{1.2}$$

and the state-output relation:

$$\boldsymbol{Y}(k) \;=\; \boldsymbol{g}\big(\boldsymbol{X}(k)\big) \tag{1.3}$$

where $\boldsymbol{Y}(k)$ is a vector grouping the outputs $\boldsymbol{y}(k+1), \ldots, \boldsymbol{y}(k+N_p)$ which have to be controlled, and are obtained from the state variables through the function $\boldsymbol{g}$. For simplicity the output variables are assumed to be all directly measured.

In addition, constraints are imposed on outputs and controls according to:

$$\boldsymbol{y}(k+N_p \mid k) \;\in\; \boldsymbol{\mathcal{Y}} \tag{1.4}$$

$$\boldsymbol{u}(k+i) \;\in\; \boldsymbol{\mathcal{U}} \qquad\qquad i = 0, \ldots, N_c - 1 \tag{1.5}$$

where $\boldsymbol{y}(k+N_p \mid k)$ denotes the predicted output at the end of prediction horizon, given the current output $\boldsymbol{y}(k)$. The control $\boldsymbol{U}(k)$ is such that $\boldsymbol{y}(k+N_p \mid k)$ falls in the acceptable set $\boldsymbol{\mathcal{Y}}$, which defines the desirable output. The latter can be either a particular set-point or some targeted range of values. This is also known as terminal constraint, and is likely to guarantee the stability of the system, if properly chosen. Alternatively, and depending on the application, variable constraints may be imposed at all steps of the prediction horizon (i.e. $\boldsymbol{y}(k+i+1 \mid k) \;\in\; \boldsymbol{\mathcal{Y}},\;\; i = 0, \ldots, N_p - 1$). Similarly, the constraints (1.5) require that $\boldsymbol{u}$ stays within the acceptable set $\boldsymbol{\mathcal{U}}$ over the control horizon. These limits must always be satisfied, since they reflect hard constraints on available control means.

Given the above-mentioned principle illustrated in Figs. 1.1 and 1.2, the procedure at time step k is the following:

1. Obtain measurements $\boldsymbol{y}(k)$.
2. Compute the optimal control sequence $\boldsymbol{u}(k+i),\ \ i=0,\ldots,N_c-1$.
3. Apply $\boldsymbol{u}(k)$ to the system.

Most of the systems behave in a non-linear manner that can be described by (ordinary) differential equations. But unfortunately, in most cases, solving non-linear differential equations is complicated. Therefore, functions $\boldsymbol{f}$ and $\boldsymbol{g}$ are obtained after time discretization by algebraization of the differential equations. Then, it is left to the closed-loop nature of MPC to compensate for the errors.

It should be noted that in most of the MPC applications (e.g. Chemical Engineering, food processing, automotive, aerospace applications, etc.), the dynamics of the system are such that, after a single control change $\Delta\boldsymbol{u}(k)$, the state variables reach steady values after a time larger than sampling period T of the MPC controller. In such a case, the dynamics of the system have to be properly taken into account in system evolution function $\boldsymbol{f}$.

In this thesis, the system has a relatively fast dynamics (in the order of a few seconds) and, thus, with the proper choice of the sampling period T (e.g. in the order of 10 seconds), the state variables have reached (almost) steady values before the next control change is applied [1]. This justifies the use of a sensitivity-type model, as detailed in the next chapter.

1.4 Description of test systems used in this work

In this section the test systems used in the following chapters are briefly presented. Some more information can be found in Appendix A.

All distribution networks are three-phase and are assumed to operate in balanced conditions. The topology of the distribution networks is also assumed unchanged.

1.4.1 32-bus system

The 32-bus test system is a 20-kV distribution network connected to the external grid through a 132/20 kV transformer with fixed tap position. The network one-line diagram is shown in Fig. 1.3

[1] which does not exclude random variations around that steady state

while the branch parameters are given in Table A.1. These data were taken from [KK09].

The network hosts three 4.5-MVA synchronous generators driven by hydro turbines and one 3.33-MVA Doubly Fed Induction Generator (DFIG) driven by wind turbine. It feeds 12 loads modelled as constant current for active power and constant impedance for reactive power, plus three equivalent induction motors. The DGU models and parameters were taken from [TNV09], [HBM99], and simplified in accordance with the type of dynamics considered in this work. All DGUs operate in reactive power control mode. This is achieved by a PI controller that regulates the reactive power output according to the set-point value requested by the centralized controller.

The following measurements are collected throughout the network: active and reactive power and voltage magnitude at the terminals of the four DGUs, active and reactive power flows in the HV/MV transformer as well as its terminal voltage on the MV side, and voltages at five load buses.

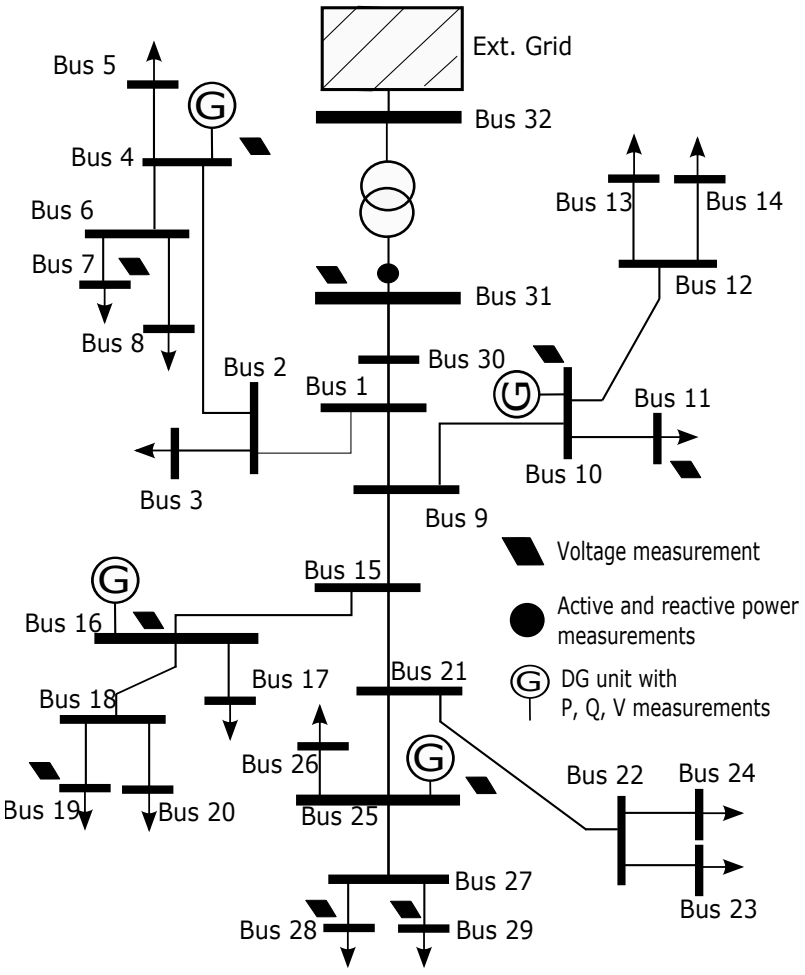

Figure 1.3: 32-bus test system: Network topology and measurement allocation

1.4.2 75-bus system

The 75-bus system is an 11-kV urban network. Its one-line diagram is presented in Fig. 1.4, while the branch parameters are given in Table A.2. The network is connected to the external grid through a 33/11 kV transformer equipped with an LTC. The data were taken from the United Kingdom Generic Distribution System repository which is a collection of models representative of UK distribution networks [tes05].

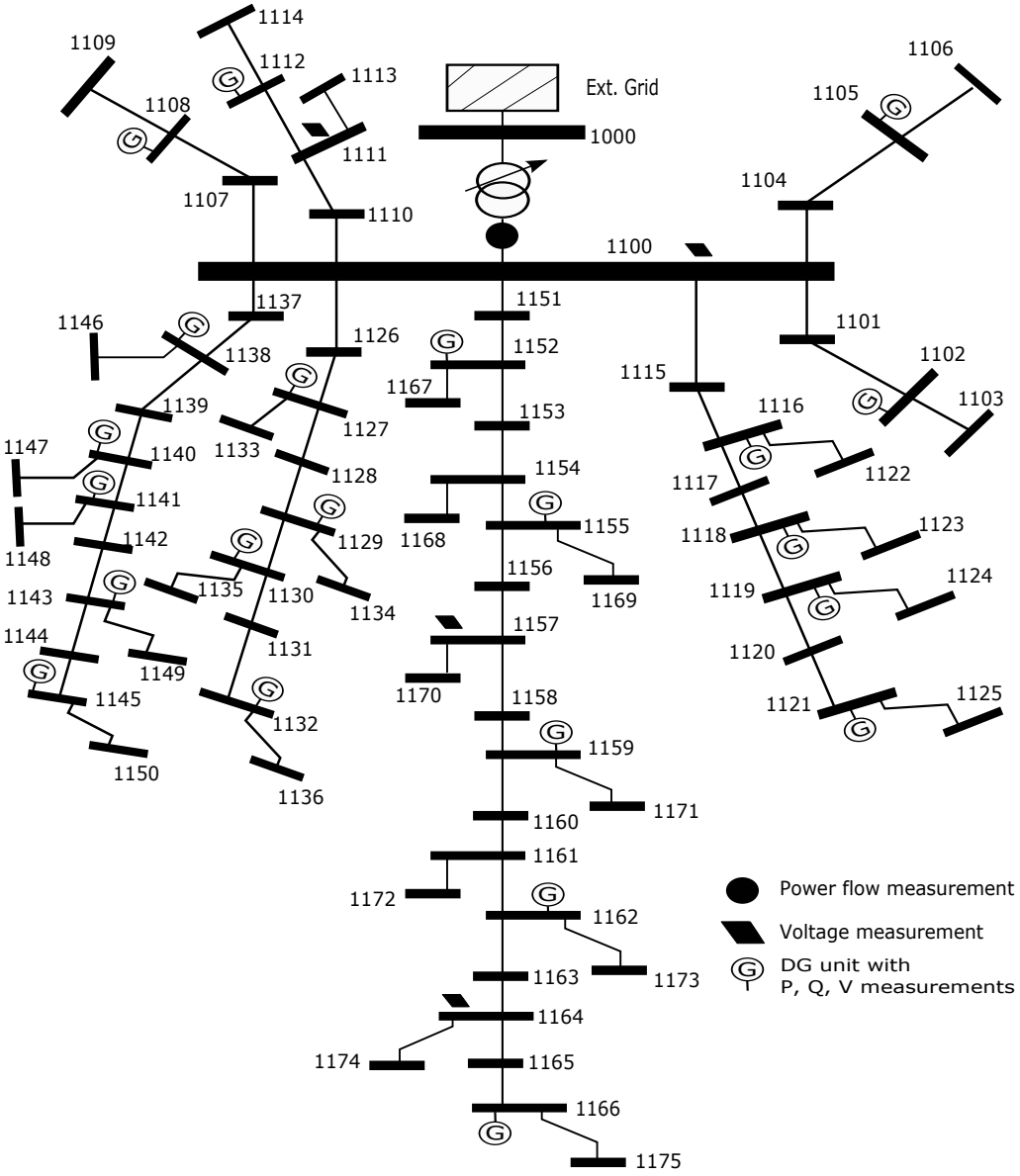

Figure 1.4: 75-bus test system: Network topology and measurement allocation

The system consists of eight short-distance underground feeders, all directly connected to the

main transformer and serving 38 loads modelled as constant current for active power and constant impedance for reactive power, and 15 more loads represented by equivalent induction motors.

Moreover, it includes 22 DGUs which are either 3-MVA synchronous generators driven by hydro turbines with 2.55-MW nominal power, or DFIG driven by wind turbines. Each DFIG is a one-machine equivalent of two 1.5-MW wind turbines operating in parallel. The nominal capacity of each DFIG is 3.33 MVA. The DGU models are identical to those of the 32-bus test system. The number of each type of DGUs has been varied in different case studies, and thus, it will be mentioned where results are presented.

It is assumed that the 22 DGUs have their active power, reactive power and voltage magnitude measurements telemetered and gathered by the centralized controller. The voltage at the 11-kV end of the transformer and the corresponding active/reactive power flows are also measured. As regards load buses, the measurement configuration is such that no load is at a distance larger than two buses from a voltage monitored bus, see Fig. 1.4.

1.4.3 YLPIC system

The YLPIC test system is largely inspired of a Belgian MV distribution network located in Wallonia and operated by ORES. It has been used in several work packages of the GREDOR project (https://gredor.be). The objective was to examine the system behaviour over future years, when more renewable DGUs (wind and PV) would be installed. To do so, a likely situation in 2030 has been considered with high penetration of renewable DGUs and new loads (mainly electrical vehicles and heat pumps).

The network is a 328-bus, 10-kV distribution grid connected through two transformers to the 70-kV transmission system. The latter is represented by a Thévenin equivalent and the transformers are equipped with Load Tap Changers (LTCs). The one-line diagram is shown in Fig. 1.5

Main substation

The main substation hosts two 70/10 kV transformers which are connected to two separate 10-kV bus-bars. The latter can be connected through a bus-coupler, if needed. Each transformer has a permanent rating of 20-MVA. In normal operation, considered here, the bus-coupler is closed and only one transformer (referred to as main transformer hereafter) is in operation. When the power exchange between the MV grid and the transmission network is high (i.e. high consumption and low generation, or low consumption and high generation), both transformers are in operation and

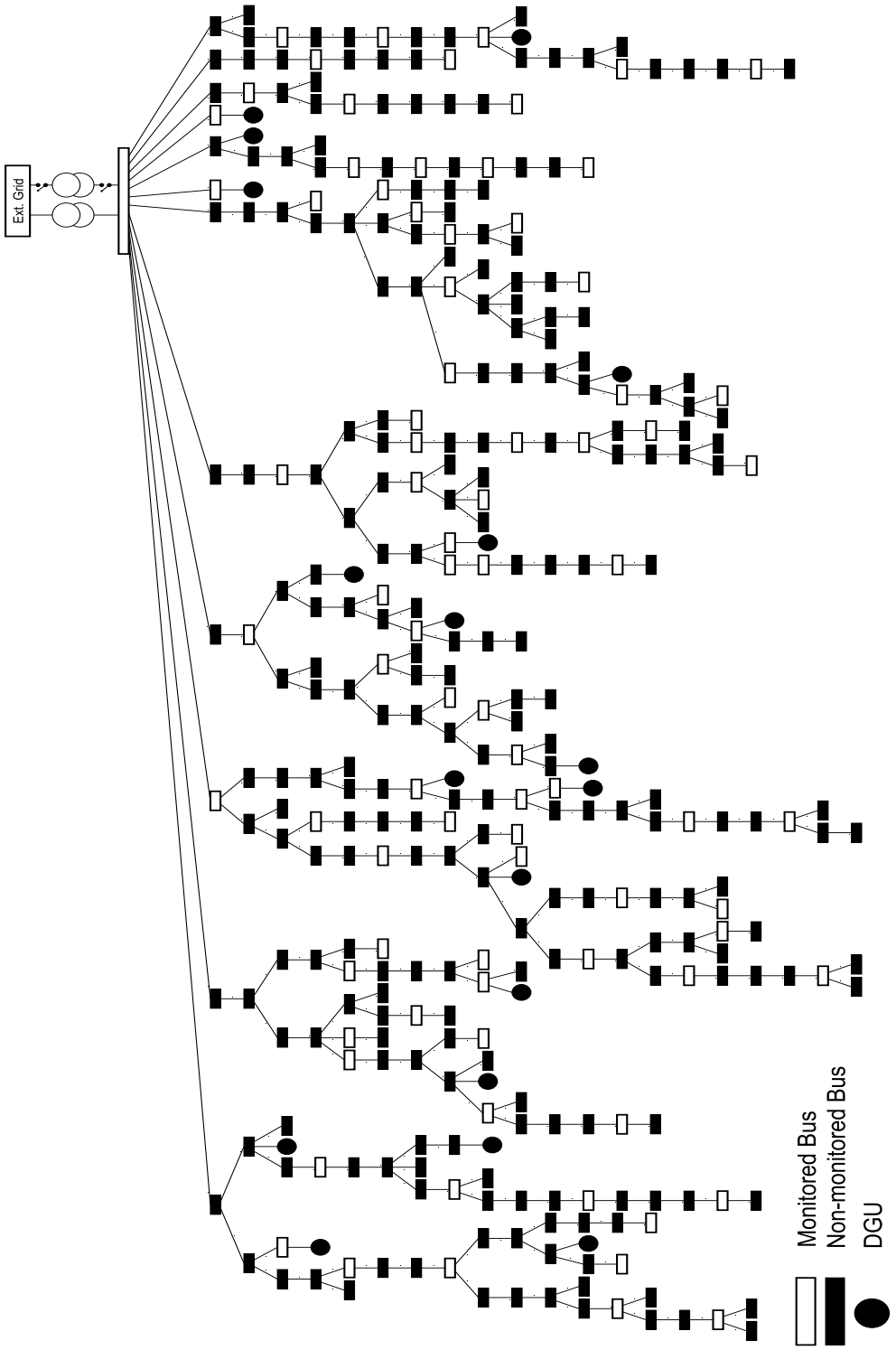

Figure 1.5: 328-bus YLPIC test system: Network topology and measurement allocation

the bus-coupler is open (this is required since both transformers do not have exactly the same nominal secondary voltages). Both transformers are equipped with LTCs.

From past recordings it is known that the voltage on the transmission side can vary from 65-kV (0.93 pu) to 77-kV (1.10 pu), depending on the system operating conditions. On the distribution side, however, voltages must be kept within a tighter interval.

Dispersed generation

Currently four wind-turbine units, with a total installed power of 20.5 MW, are connected to the MV buses. On the other hand, the existing PV installations as well as the Combined Heat and Power (CHP) units are all connected to the Low Voltage (LV) network. Since setting up a communication infrastructure down to LV level does not seem realistic, DGUs connected to LV networks are not considered controllable. Instead, the focus is on DGUs connected to the MV grid.

It is expected that, by the year 2030, the network of concern will accommodate new DGUs at MV level, for an additional installed power of 13.6 MW. The GCAN tool described in [CVGE15] has been used to locate the new DGUs in the grid. Table 1.1 details the capacities and numbers of DGUs. Including the existing wind units, it is assumed that the system will host a total of 18 DGUs, identified in Fig. 1.5. They are distributed along various feeders, enabling the real-time centralized controller to have a relatively good controllability of the system.

Table 1.1: number and installed power of the existing and new planned DGUs (for the year 2030)

DGU type	Existing number / power (MW)	New Planned number / power (MW)
Wind	4 / 20.50	9 / 8.75
PV	0 / 0.00	2 / 1.70
CHP	0 / 0.00	3 / 3.10

Consumption

The network feeds 420 residential and industrial loads connected to 297 MV buses. The various residential loads connected at LV level and fed by the same MV/LV transformer are aggregated into one load attached to the MV bus. That load also includes the losses in the LV network and in the MV/LV transformer.

The industrial loads are subdivided into three types, depending on their consumption profile within a day:

- type 1: working during the day only (e.g. manufacturers; total number of 40);
- type 2: with high thermal needs (total number of 10);
- type 3: working day and night (e.g. warehouses; total number of 10).

There are also 178 heat pumps (total capacity of 1.37 MW) and 182 electrical vehicle charging stations (total capacity of 2.66 MW). Both are categorized as residential loads.

Measurements

With the expected penetration of DGUs, a better observability of the system will be needed, to detect and correct problems in various parts of the grid. Hence, ORES plans to install in a near future additional measurement points throughout the system. The future telemetered values were assumed to be:

- the active and reactive powers injected by, and the terminal voltage of each DGU;
- the active and reactive power flows in all branches that leave the main substation;
- the active and reactive power flows in one incident branch and the voltage at each of the monitored buses shown with empty rectangles in Fig. 1.5;
- the active and reactive powers received from the transformer and the voltages on its MV side.

1.5 Simulation tool

Devising and testing the algorithms requires simulating in an off-line environment real or realistic distribution networks with their DGUs and their loads.

In this work all the control schemes have been implemented in the RAMSES simulator (acronym for "RApid Multithreaded Simulator of Electric power Systems"), a software for dynamic simulation under the phasor (or quasi-sinusoidal) approximation, developed at the University of Liège in the context of research on advanced time-domain solvers [FCHV13, AFV14, Ari15, ALV16]. The time step size is typically of 0.01 second.

The choice of RAMSES instead of a commercial product was justified by the complete knowledge and control of this software. For instance, it allowed a rather easy implementation of the

MPC-based controller: the latter is implemented as a discrete controller retrieving its inputs from RAMSES variables and acting on other variables representing the set-points of the DG units. This tight coupling between time domain simulation and control, as well as the programming of a rather complex constrained optimization in the controller, is not likely to be easy or even possible with commercial (or non-open access) software. Furthermore, the availability of a software handling detailed dynamic models has allowed simulating a variety of scenarios such as: variations of renewable energy inflow (mainly sun irradiance and wind speed), slowly varying load demand, the time-delayed response of load tap changers, etc.

The MPC-based corrective controller module has been developed and progressively extended to offer more advanced and practical features. It relies on a Quadratic Programming library, namely the VE17AD package from Harwell [hsl11].

1.6 Thesis outline

Chapter 2. The overall scope of this chapter is to first introduce the corrective control of abnormal voltages and branch overloads in DNs in the framework of MPC. Then, using the latter, a centralized control scheme is defined. Relying on the appropriate measurement and communication infrastructures, this controller acts on active and reactive powers of DGUs in order to smoothly drive the system from an unsatisfactory operating point to a targeted secure operation region. The problem is formulated as a receding-horizon multi-step optimization using a sensitivity model. Furthermore, as additional control means: (i) flexible loads are envisaged and some discussions are provided on the associated practical issues, and (ii) automatic LTCs are included into the formulation.

Chapter 3. In the context of the GREDOR project (https://gredor.be), the performance of the centralized real-time controller detailed in the previous chapter, has been evaluated on the test system introduced in Section 1.4.3, with the objective of examining the system behaviour over future years, when more DGUs would be installed. More precisely, the aim was to evaluate the capability of the real-time controller to address the over- or under-voltage and/or thermal overload issues, and, consequently, postpone network reinforcements. The main attractiveness of those tests was to assess the controller response over full days, including some periods where corrective actions were needed.

Chapter 4. The real-time controller detailed in Chapter 2 is further extended to contribute to LV network control. It is achieved by the adjustment of voltage at the MV side of the MV/LV transformers where the stressed LV grid is connected. This is relevant in so far as most LV networks are not equipped with control means (i.e. the MV/LV transformers operate with fixed or off-load

adjustable tap changer, while the rooftop PhotoVoltaic (PV) panels usually operate at unity power factor).

Chapter 5. The real-time corrective control of DNs is extended to accommodate a two-level control architecture combining the previously presented centralized controller with multiple local, simple and faster acting controllers. The developed control scheme has the following features:

- The local control provides fast response after a disturbance, reducing its impact and enhancing voltage quality.
- A hybrid control structure is also considered where, at the upper level, only a subset of the DGUs are centrally controlled.

Chapter 6. In this chapter the time frame of the centralized controller is extended with a preventive security restoration. The latter uses near-future production/ consumption predictions to determine if the active distribution network is going to operate within prescribed limits and, if not, to determine appropriate preventive decisions that can be used, for instance, as references for the real-time corrective controller. One distinctive feature of that preventive analysis is that it re-uses the multi-step constrained optimization formulation of the real-time controller.

Chapter 7. Last but not least, the contributions of this thesis are summarized and directions for future work are suggested.

1.7 Publications

This thesis expands material which has been published, or submitted, in a book chapter, various journals and conferences:

[1] **H. Soleimani Bidgoli**, M. Glavic and T. Van Cutsem. Real-time corrective control of distribution networks : validation in future scenarios of a real system. Submitted to *Applied Energy*, 2017.

[2] **H. Soleimani Bidgoli**, and T. Van Cutsem. Combined local and centralized voltage control in active distribution networks. *to appear in IEEE Transactions on Power Systems, 2017*. Also available at: http://orbi.ulg.ac.be/handle/2268/212120

[3] **H. Soleimani Bidgoli**, G. Valverde, P. Aristidou, M. Glavic, and T. Van Cutsem. Operation of distribution systems within secure limits using real-time Model Predictive Control. in Rueda Torres, Jose (Ed.) *Dynamic Vulnerability Assessment and Intelligent Control for Sustainable Power Systems (in press)*.

[4] **H. Soleimani Bidgoli**, and T. Van Cutsem. Voltage profile correction in distribution grids combining single- and two-level controllers. In Proc. *IEEE PES PowerTech conference*, Manchester (UK), June 2017.
Also available at: http://orbi.ulg.ac.be/handle/2268/212118

[5] **H. Soleimani Bidgoli**, M. Glavic and T. Van Cutsem. Receding-Horizon Control of Distributed Generation to Correct Voltage or Thermal Violations and Track Desired Schedules. In Proc. *19th Power Systems Computation Conference (PSCC)*, Genova (Italy), June 2016.
Also available at: http://hdl.handle.net/2268/194288

[6] **H. Soleimani Bidgoli**, Combined Centralized and Local Voltage correction in Active Distribution Network. In Proc. *8th IEEE Benelux Young Researchers Symposium (YRS)*, Eindhoven (The Netherlands), May 2016.
Also available at: http://orbi.ulg.ac.be/handle/2268/197020

[7] **H. Soleimani Bidgoli**, M. Glavic and T. Van Cutsem. Model Predictive Control of Congestion and Voltage Problems in Active Distribution Networks. In Proc. *CIRED Workshop*, Rome (Italy), June 2014.
Also available at http://hdl.handle.net/2268/165430

Chapter 2

Centralized control scheme for voltage control and congestion management

In this chapter the application of the MPC principle, introduced in Section 1.3, to corrective control of active DNs is presented. It is shown how the MPC principle is used to predict and correct the network operating conditions. The control problem formulation is followed by a short discussion of techniques used to reach a feasible solution and guarantee the stability of this control. Furthermore, a centralized scheme using the so introduced formulation is detailed. It aims at correcting abnormal voltages and/or managing thermal congestions using two different objectives: (i) voltage correction with minimum control effort, or (ii) minimum deviation of control variables from their references for both voltage correction and congestion management. It is shown that Objective (ii) can accommodate various contexts of applications and information transfers between entities acting on the DGUs, in accordance with the regulatory policy. The proposed method effectiveness is demonstrated on a 32-bus and a 75-bus test system followed by further tests to evaluate the robustness of the scheme in case of communication failures and slow dynamics of the system components. In addition, some discussions are provided on practical issues of controlling flexible loads. The chapter ends with an extension of the controller to make use of the automatic LTC of the transformer connecting the MV DN to the transmission grid.

2.1 Introduction

2.1.1 Motivation

One of the largest mutations that electric power systems will experience in the next decade or so is the gradual replacement of large, conventional power plants connected to transmission networks by a large number of comparatively much smaller DGUs exploiting renewable sources of energy and connected to DNs, most often through power-electronics interfaces [CCC09]. This expected proliferation of DGUs raises challenges in many aspects of DSO activities, ranging from long-term planning to real-time control [LHM+07]. From the system operation viewpoint the increasing number of DGUs, together with the intermittent nature of most renewable energy sources is going to create new problems such as over- and under-voltages and/or thermal overloads of equipment.

The traditional approach has been to reinforce the network to avoid such limit violations. However, the latter are expected to take place for limited durations (for instance, over-voltages usually take place under conditions of low load and high dispersed generation); hence, reinforcing the network to deal with these temporary situations is seldom an economically viable option for the DSO. To some extent, the problems can be anticipatively detected and corrected in operational planning, e.g. in the day-ahead time frame [BBG+10]. However, this requires taking decisions under uncertainty [GKEC13], stemming from the prediction of renewable energy input, with some risk of taking conservative or insufficient actions. In fact, operational planning appears to be the proper time frame for decisions dealing with demand response, taking into account energy consumption constraints over the whole day [Gem16].

For the above reasons, and because it is the last "line of defence" against unexpected events, the need for real-time corrective control will go increasing. This requires monitoring the system through an appropriate measurement and communication infrastructure and taking control actions if the system is driven to operate with voltage and/or thermal limits exceeded. The DGUs are the main components taking part in corrective control. This is reflected in the term "active distribution network" [CCC09]. The transformer LTC can be also used.

2.1.2 Literature review

This topic has received a growing attention over the last decade, as testified for instance by the recent surveys in [EGH16, MZ16].

The approaches can be categorized according to the overall control architecture: centralized [SGV14, SGV16, VV13b, VKWH07, DDK+12, SFC+17, GRMC16, ACA17, DNA+17], local (or de-

centralized) [KHBL13, SOH12, AZLV17], agent-based [VKWH07, BEM07, RHDG13, VZ13, SKR14, BNCP15, BCP16, BTCP16], and multi-layer [HB11, CKN+12, JWS14, FGM+15, SV].

The most widely used, and also simplest approach is local control. It is already present in a number of grid codes [KHBL13]. For example, Ref. [SOH12] proposes to perform a sensitivity analysis at each DGU location to compute the necessary, local active/reactive power adjustments; no communication is required. A decentralized control strategy for wind farms with full-scale converters is presented in [AZLV17], and the results are compared with a centralized approach. It is shown that the use of an accurate model of the wind farm internal structure as well as an accurate parametrization of transformers and cables play an important role to obtain a satisfactory response of the decentralized control.

An alternative with some more information exchange is the agent-based scheme, proposed for instance in [BEM07]. A reactive power support in distribution is provided in the latter through an optimal multi-agent scheme, assuming DGUs communicate with a single controller, either directly or through other DGUs. By using locally collected measurements, the distributed controllers mitigate the voltage violations in [RHDG13] and, when needed, initiate an additional reactive power support request from the neighbouring controllers. A distributed architecture, comprising several cooperative smart agents, was proposed in [VZ13] to solve the voltage regulation problem. After obtaining the operating values, each agent optimizes its own design. In Ref. [SKR14] an agent-based system was proposed to control the DGUs in a low-voltage grid in a distributed manner. That work also considered different local reactive power characteristics and compared the corresponding system behaviours. In Refs. [BNCP15, BCP16], using the concept of voltage sensitivity coefficients, radial active distribution networks are decomposed to several clusters. By means of energy storage devices, the bus voltages within each cluster are controlled independently relying on the Thvenin representation of adjacent areas.

Centralized control relies on a proper communication infrastructure to collect measurements and send coordinated control corrections at regular time intervals. The most widely used approach for the determination of the coordinated controls is the OPF [VKWH07, DDK+12]. Using such an algorithm, Ref. [VKWH07] discusses the impact of centralized and distributed voltage control schemes on the potential penetration of dispersed generation. In [DDK+12], using a similar algorithm, the “last-in first-out” principle is used. Thermal constraints are primarily managed in a centralized manner, but voltage constraints are also included in the formulation.

The OPF is typically an open-loop approach. In contrast, relatively few references deal with an automatic, closed-loop control capable of smoothly steering the dispersed generation units in order to bring the system back within the specified security limits. Another key feature missing in many works is the capability of the controller to compensate for model inaccuracies and failure or delays of the control actions. Model Predictive Control, one type of receding-horizon control, offers such

capabilities [Mac02, QB03] in particular owing to its closed-loop nature, as outlined in the Introduction. This control method has received some attention from the power system community, and recent references show a growing interest for this approach [LHO02, VHRW06, MH17]. It was proposed in [VV13b] for voltage control purposes using a sensitivity model. This formulation was further extended and developed as a joint voltage/thermal control scheme in [SGV14, SGV16].

Reference [VV13b] proposed an MPC-based multi-step control to correct voltages out of limits by applying optimal changes of the control variables, and smoothly drive the system from its current to the targeted operation region. The proposed controller is able to discriminate between cheap and expensive actions and select the appropriate set of control variables depending on the region of operation.

References [VV13b, VV13a] were the starting point of our research work, reported in this chapter, and published in [SGV14, SGV16].

2.2 General control problem formulation

The control variables are the active power ($\boldsymbol{P}_g$) and reactive power ($\boldsymbol{Q}_g$) of dispersed generators and possibly the voltage set-point of the transformer LTC (V_{tr}), all grouped in the $m \times 1$ vector $\boldsymbol{u}(k)$, at time k:

$$\boldsymbol{u}(k) = [\boldsymbol{P}_g^T(k), \boldsymbol{Q}_g^T(k), V_{tr}(k)]^T \tag{2.1}$$

where ^{T} denotes vector transposition. Energy storage devices are not considered in this work and the option of flexible loads as additional control means is discussed in Section 2.10. MPC calculates a sequence of control variable changes $\Delta\boldsymbol{u}(k+i) = \boldsymbol{u}(k+i) - \boldsymbol{u}(k+i-1), \;\; i = 0, \ldots, N_c - 1$ to eventually bring the monitored branch currents and bus voltages within permissible limits.

The MPC objective function may be set to minimize the sum of squared control variable changes or the sum of squared deviations between the controls and their references $\boldsymbol{u}_{ref}$, as follows:

$$\min_{\Delta\boldsymbol{u},\boldsymbol{u},\boldsymbol{\varepsilon},\boldsymbol{y}} \; \underbrace{w \sum_{i=0}^{N_c-1} ||\Delta\boldsymbol{u}(k+i)||^2_{\boldsymbol{R}_1}}_{\textbf{Objective 1}} + \underbrace{(1-w) \sum_{i=0}^{N_c-1} ||\boldsymbol{u}(k+i) - \boldsymbol{u}_{ref}(k+i)||^2_{\boldsymbol{R}_2}}_{\textbf{Objective 2}} + ||\boldsymbol{\varepsilon}||^2_{\boldsymbol{S}} \tag{2.2}$$

where $\|.\|^2$ denotes the L_2-norm and w is a binary variable: $w \in \{0, 1\}$. Note that both objectives have been included in (2.2), but for the application of concern here, only one will be used depending on what is needed. Clearly, the variable w is set to one to treat Objective 1, or zero to treat Objective 2.

In matrix form, (2.2) can be written as:

$$\min_{\Delta \boldsymbol{u}, \boldsymbol{u}, \boldsymbol{\varepsilon}, \boldsymbol{y}} \; w\, \Delta \boldsymbol{u}^T \boldsymbol{R}_1 \Delta \boldsymbol{u} + (1-w)\, (\boldsymbol{u} - \boldsymbol{u}_{ref})^T \boldsymbol{R}_2 (\boldsymbol{u} - \boldsymbol{u}_{ref}) + \boldsymbol{\varepsilon}^T \boldsymbol{S} \boldsymbol{\varepsilon} \tag{2.3}$$

Here, $\Delta \boldsymbol{u}$ and $\boldsymbol{u}$ are $mN_c \times 1$ column vectors defined by:

$$\Delta \boldsymbol{u} = \begin{bmatrix} \Delta \boldsymbol{u}(k) \\ \Delta \boldsymbol{u}(k+1) \\ \vdots \\ \Delta \boldsymbol{u}(k+N_c-1) \end{bmatrix}, \qquad \boldsymbol{u} = \begin{bmatrix} \boldsymbol{u}(k) \\ \boldsymbol{u}(k+1) \\ \vdots \\ \boldsymbol{u}(k+N_c-1) \end{bmatrix} \tag{2.4}$$

Note that $\boldsymbol{u}$ can be expressed in terms of $\Delta \boldsymbol{u}$:

$$\boldsymbol{u} = \boldsymbol{C_1} \boldsymbol{u}(k-1) + \boldsymbol{C_2} \Delta \boldsymbol{u} \tag{2.5}$$

with,

$$\boldsymbol{C_1} = \begin{bmatrix} \boldsymbol{U} \\ \boldsymbol{U} \\ \vdots \\ \boldsymbol{U} \end{bmatrix}, \qquad \boldsymbol{C_2} \begin{bmatrix} \boldsymbol{U} & \boldsymbol{0} & \dots & \boldsymbol{0} \\ \boldsymbol{U} & \boldsymbol{U} & \dots & \boldsymbol{0} \\ \vdots & \vdots & \ddots & \vdots \\ \boldsymbol{U} & \boldsymbol{U} & \boldsymbol{U} & \boldsymbol{U} \end{bmatrix} \tag{2.6}$$

where $\boldsymbol{U}$ and $\boldsymbol{0}$ are the $m \times m$ identity and zero matrices, respectively. $\boldsymbol{C_1}$ and $\boldsymbol{C_2}$ are also $mN_c \times m$ and $mN_c \times mN_c$ matrices, respectively.

Similarly, $\boldsymbol{u}_{ref}$ is the $mN_c \times 1$ vector of control variable references which may vary in the control horizon, hence:

$$\boldsymbol{u}_{ref} = \begin{bmatrix} \boldsymbol{u}_{ref}(k) \\ \boldsymbol{u}_{ref}(k+1) \\ \vdots \\ \boldsymbol{u}_{ref}(k+N_c-1) \end{bmatrix} \tag{2.7}$$

In addition, $\boldsymbol{\varepsilon}$ is the vector of slack variables used to relax some inequality constraints in case of infeasibility. These variables are heavily penalized by the diagonal matrix $\boldsymbol{S}$. Finally, $\boldsymbol{R}_1$ and $\boldsymbol{R}_2$ are $mN_c \times mN_c$ diagonal weighting matrices used to prioritize control actions.

The above objective function is minimized subject to:

$$\boldsymbol{u}^{MIN} \leq \boldsymbol{u} \leq \boldsymbol{u}^{MAX} \tag{2.8}$$

$$\Delta \boldsymbol{u}^{MIN} \leq \Delta \boldsymbol{u} \leq \Delta \boldsymbol{u}^{MAX} \tag{2.9}$$

where $\boldsymbol{u}^{MIN}$, $\boldsymbol{u}^{MAX}$, $\Delta\boldsymbol{u}^{MIN}$ and $\Delta\boldsymbol{u}^{MAX}$ are the lower and upper limits on control variables and on their rate of change, along the control horizon. More precisely:

$$\boldsymbol{u}^{MIN} = \begin{bmatrix} \boldsymbol{u}^{min} \\ \vdots \\ \boldsymbol{u}^{min} \end{bmatrix}, \qquad \boldsymbol{u}^{MAX} = \begin{bmatrix} \boldsymbol{u}^{max} \\ \vdots \\ \boldsymbol{u}^{max} \end{bmatrix} \tag{2.10}$$

where $\boldsymbol{u}^{min}$ and $\boldsymbol{u}^{max}$ are the minimum and maximum allowed control input. Similarly, $\Delta\boldsymbol{u}^{MIN}$ and $\Delta\boldsymbol{u}^{MAX}$ can be expressed in the expanded form:

$$\Delta\boldsymbol{u}^{MIN} = \begin{bmatrix} \Delta\boldsymbol{u}^{min} \\ \vdots \\ \Delta\boldsymbol{u}^{min} \end{bmatrix}, \qquad \Delta\boldsymbol{u}^{MAX} = \begin{bmatrix} \Delta\boldsymbol{u}^{max} \\ \vdots \\ \Delta\boldsymbol{u}^{max} \end{bmatrix} \tag{2.11}$$

where it has been assumed, for simplicity, that the bounds do not vary with time.

In this application, the output or controlled variables $\boldsymbol{y}$ are bus voltages and branch currents. The system components have relatively fast dynamics (in the order of a few seconds) and, thus, with the proper choice of the sampling period of discrete-time optimization (e.g. in the order of 10 seconds), it can be assumed that they have reached (almost) steady values before the next control change is applied. Therefore, a sensitivity-type model of the system can be used to express the predicted system evolution:

for $i = 1, 2, ..., N_p$:

$$\boldsymbol{y}(k+i|k) = \boldsymbol{y}(k+i-1|k) + \boldsymbol{S}_y\, \Delta\boldsymbol{u}(k+i-1) + \boldsymbol{S}_\delta\, \delta\, \gamma(k+i) \tag{2.12}$$

where $\boldsymbol{y}(k+i|k)$ is the predicted system output at time $k+i$ given the measurements at time k, and $\boldsymbol{S}_y$ is the sensitivity matrix of those variables to control changes.

It must be noted that we assume all output variables are directly measured, and the measurements are grouped in the $q \times 1$ vector $\boldsymbol{y}(k|k)$. This value is used to initialize the recursive equation (2.12).

The last term in (2.12) is included to account for the effect of a known disturbance δ on the predicted outputs. Hence, $\boldsymbol{S}_\delta$ is the sensitivity of those variables to the known disturbance. In addition, γ is a binary variable equal to one for the instants when the known disturbance will occur, or zero otherwise.

In compact form (2.12) can be rewritten as:

$$\boldsymbol{y} = \boldsymbol{F}\boldsymbol{y}(k|k) + \Phi_y \Delta\boldsymbol{u} + \Phi_\delta \boldsymbol{\Gamma} \delta \tag{2.13}$$

with,

$$\boldsymbol{y} = \begin{bmatrix} \boldsymbol{y}(k+1|k) \\ \boldsymbol{y}(k+2|k) \\ \vdots \\ \boldsymbol{y}(k+N_p|k) \end{bmatrix}, \quad \boldsymbol{F} = \begin{bmatrix} \boldsymbol{U} \\ \boldsymbol{U} \\ \vdots \\ \boldsymbol{U} \end{bmatrix}, \quad \boldsymbol{\Gamma} = \begin{bmatrix} \gamma(k+1) \\ \gamma(k+2) \\ \vdots \\ \gamma(k+N_p) \end{bmatrix} \tag{2.14}$$

$$\Phi_y = \begin{bmatrix} \boldsymbol{S}_y & \boldsymbol{0} & \dots & \boldsymbol{0} \\ \boldsymbol{S}_y & \boldsymbol{S}_y & \dots & \boldsymbol{0} \\ \vdots & \vdots & \ddots & \vdots \\ \boldsymbol{S}_y & \boldsymbol{S}_y & \dots & \boldsymbol{S}_y \end{bmatrix}, \quad \Phi_\delta = \begin{bmatrix} \boldsymbol{S}_\delta & \boldsymbol{0} & \dots & \boldsymbol{0} \\ \boldsymbol{S}_\delta & \boldsymbol{S}_\delta & \dots & \boldsymbol{0} \\ \vdots & \vdots & \ddots & \vdots \\ \boldsymbol{S}_\delta & \boldsymbol{S}_\delta & \dots & \boldsymbol{S}_\delta \end{bmatrix} \tag{2.15}$$

where Φ_y and Φ_δ are $qN_p \times mN_c$ and $qN_p \times N_p$ matrices, respectively.

Finally, the following inequality constraints are imposed to the predicted output:

$$-\varepsilon_1 \mathbf{1} + \boldsymbol{y}^{LOW} \leq \boldsymbol{y} \leq \boldsymbol{y}^{UP} + \varepsilon_2 \mathbf{1} \tag{2.16}$$

ε_1 and ε_2 are the components of $\boldsymbol{\varepsilon}$, $\mathbf{1}$ denotes a $qN_p \times 1$ unit vector, while, $\boldsymbol{y}^{LOW}$ and $\boldsymbol{y}^{UP}$ are the lower and upper allowed output along the prediction horizon:

$$\boldsymbol{y}^{LOW} = \begin{bmatrix} \boldsymbol{y}^{low}(k+1) \\ \boldsymbol{y}^{low}(k+2) \\ \vdots \\ \boldsymbol{y}^{low}(k+N_p) \end{bmatrix}, \quad \boldsymbol{y}^{UP} = \begin{bmatrix} \boldsymbol{y}^{up}(k+1) \\ \boldsymbol{y}^{up}(k+2) \\ \vdots \\ \boldsymbol{y}^{up}(k+N_p) \end{bmatrix} \tag{2.17}$$

where $\boldsymbol{y}^{low}(k+i)$ and $\boldsymbol{y}^{up}(k+i)$ are the minimum and maximum allowed output at time $k+i$.

In order to solve the above optimization problem, it is convenient to re-arrange the equations into a standard Quadratic Programming (QP) problem:

$$\min \ \frac{1}{2} \begin{bmatrix} \Delta \boldsymbol{u} \\ \boldsymbol{\varepsilon} \end{bmatrix}^T \boldsymbol{H} \begin{bmatrix} \Delta \boldsymbol{u} \\ \boldsymbol{\varepsilon} \end{bmatrix} + \boldsymbol{f}^T \begin{bmatrix} \Delta \boldsymbol{u} \\ \boldsymbol{\varepsilon} \end{bmatrix} \tag{2.18}$$

where,

$$\boldsymbol{H} = \begin{bmatrix} \boldsymbol{R_1} + \boldsymbol{C_2^T R_2 C_2} & \boldsymbol{0} \\ \boldsymbol{0} & \boldsymbol{S} \end{bmatrix}, \quad \boldsymbol{f} = \begin{bmatrix} \boldsymbol{C_2^T R_2 (C_1 u}(k-1) - \boldsymbol{u}_{ref}) \\ \boldsymbol{0} \end{bmatrix} \tag{2.19}$$

subject to:

$$\begin{bmatrix} \Delta \boldsymbol{u}^{MIN} \\ \boldsymbol{0} \end{bmatrix} \leq \begin{bmatrix} \Delta \boldsymbol{u} \\ \boldsymbol{\varepsilon} \end{bmatrix} \leq \begin{bmatrix} \Delta \boldsymbol{u}^{MAX} \\ +\boldsymbol{\infty} \end{bmatrix} \tag{2.20}$$

$$\begin{bmatrix} \boldsymbol{u}^{MIN} - \boldsymbol{C_1 u}(k-1) \\ \boldsymbol{y}^{LOW} - \boldsymbol{F y}(k|k) - \Phi_\delta \boldsymbol{\Gamma} \delta \\ -\boldsymbol{\infty} \end{bmatrix} \leq \boldsymbol{A} \begin{bmatrix} \Delta \boldsymbol{u} \\ \boldsymbol{\varepsilon} \end{bmatrix} \leq \begin{bmatrix} \boldsymbol{u}^{MAX} - \boldsymbol{C_1 u}(k-1) \\ +\boldsymbol{\infty} \\ \boldsymbol{y}^{UP} - \boldsymbol{F y}(k|k) - \Phi_\delta \boldsymbol{\Gamma} \delta \end{bmatrix} \tag{2.21}$$

with,

$$\boldsymbol{A} = \begin{bmatrix} \boldsymbol{C_2} & \mathbf{0}_{mN_c \times 1} & \mathbf{0}_{mN_c \times 1} \\ \Phi_y & \mathbf{1}_{qN_p \times 1} & \mathbf{0}_{qN_p \times 1} \\ \Phi_y & \mathbf{0}_{qN_p \times 1} & -\mathbf{1}_{qN_p \times 1} \end{bmatrix} \tag{2.22}$$

$\mathbf{0}_{mN_c \times 1}$ is a $mN_c \times 1$ null matrix while $\mathbf{0}_{qN_p \times 1}$ and $\mathbf{1}_{qN_p \times 1}$ are $qN_p \times 1$ null and unit matrices.

In the above formulation, there are only two components in ε, the first one to relax the lower bound of all controlled variables, and the second to relax the upper bound, both over the prediction horizon. In case of different types of controlled variables, different slack variables are considered (see for instance Section 2.5). In such a case, matrix $\boldsymbol{A}$ is extended accordingly.

2.3 On the feasibility and stability of the proposed MPC formulation

2.3.1 Feasibility

The constraints imposed on the optimization problem (2.2) can be categorized into input limits (2.8, 2.9), and output limits (2.16). The input constraints arise from physical limitations on the controlled devices, and they must be always satisfied. Output constraints, on the other hand, are often not due to strict physical limitations, but rather they are included to reach/maintain a desired operating point/trajectory. More importantly, they need not be enforced strictly at all times. For instance, in the presence of disturbances or limited control means it may not be always possible for the controller to enforce the output constraints.

To reach a feasible solution, attention has to be paid while including the constraints [Mac02]. In this regard, two key techniques have been embedded into our MPC formulation which in practice guarantee feasibility:

- instead of targeting set-points for the output variables, the formulation targets a desirable range of values (acting as a "dead-band" for the controller). Hence, if all outputs lie within that range and all other constraints are satisfied, the controller does not act, while, if some outputs fall outside, the controller brings them inside the feasible set, and not to a specific reference value. Incidentally, this also provides a less intrusive control, and reduces the required efforts;

- in case the above feasible set cannot be reached (e.g. due to low system controllability), the inequality constraints on the outputs are relaxed through the ε_1 and ε_2 variables in (2.16). In other words, they are treated as *soft* constraints [QB03].

2.3.2 Stability

One of the key questions in MPC is certainly, whether it leads to stability of the controlled system. As pointed out in Section 1.3, the receding-horizon technique of applying only the first component of a sequence of optimal control actions, results in a closed-loop system behaviour, different from its open-loop counterpart. When discussing about stability, the closed-loop behaviour should be investigated. To that end, the following points should be noticed:

- It has been shown in many references that once the feasibility of the open-loop predictive control is achieved (using the two above-mentioned techniques), the stability of the closed-loop is hardly an issue. It is rather easy to obtain the stability by tuning the parameters in the problem formulation [SMR99, Mac02, FA02]. Moreover, if the MPC-based controller is applied to a stable system, the dynamic performance demanded from the controller is not very challenging.

- As explained in [Mac02], another way of ensuring stability is to have any length of horizon, but to add "terminal constraints" which forces the state to take a particular value at the end of the prediction horizon.

  It is expected that imposing the "terminal constraints" on the output variables yields the same feature in practice. Therefore, we believe that in our particular application, it would be highly unlikely to find an unstable behaviour of the closed-loop controller while bus voltages and branch currents of a DN are brought within the permissible ranges. Therefore, it is expected that using terminal constraints will avoid putting the system into such a state that will eventually be impossible to stabilize.

- Closed-loop stability becomes a more challenging issue if the controller undergoes regular redesign [Mac02]. This includes the continuous modification of the tuning parameters in the problem formulation and the re-estimation of the system model.

  As described in the rest of this chapter, in this work, the studied system does not face a severe change such as a failure, a fault or a topological change [1]. In addition, the parameters of the problem formulation are properly chosen once and remain unchanged for long periods of time. Regarding the estimation of the system model, a sensitivity-type model is considered,

[1] Nevertheless, there are some well-known techniques to handle such cases, such as the use of a "bias term" [QB03]

as detailed in Section 2.6. On some occasions, some components of this sensitivity-type model need to be updated. In this regard, the necessary considerations which, in practice, yield a smooth and stable system behaviour are provided and discussed in the same section.

Although ensuring the closed-loop stability, a drawback of targeting a particular value lies in the efforts required to meet the target at the end of the prediction horizon, which can be large, especially for short control horizons. This drawback can be mitigated by the already explained technique of targeting a desired range instead of a particular value, and also spreading the required efforts over a large enough control horizon (e.g. $N_c = 3$).

2.4 Voltage correction with minimum control effort

2.4.1 Overall objective of control

The first control goal considered consists of bringing back the DN bus voltages within some predefined limits while minimizing the control efforts, which corresponds to Objective 1 (or $w = 1$) in Eq. (2.2).

Initially, the DSO will define a target voltage for each bus in the network. This target voltage may follow a security or economical purpose, e.g. network losses minimization. However, as discussed in Section 2.3, trying to reach a given target value is impractical and likely infeasible. Alternatively, one can keep the network voltages within some limits around the target values. In the sequel, these limits are referred to as *normal operation limits*, and operating within these limits is the controller's main objective. For example, the requested band of operation for a monitored bus voltage may be set to $[0.98 \;\; 1.03]$ pu. In so far as the target range might be the result of a separate optimization, the limits might not be the same for all buses. Moreover, the range allowed for each controlled bus may depend on the load connected to it or the cost associated with regulating the voltages within a narrow band of operation.

If some bus voltages violate their limits, the controller will use the minimum control actions to bring them within the acceptable range. To do so, the controller favours the cheapest controls. However, if the problem cannot be solved by the sole cheapest controls (due to for instance low controllability of the system or severity of the violation) the controller will resort to expensive actions as well.

Note that there may be cases where the correction of some bus voltages is infeasible with the available controls. Under these circumstances, the controller should, at least, apply the control

actions that bring the problematic voltages to better values, even if they are outside the specified limits. The controller must do so until a feasible correction is found.

Let us recall that when all voltages lie within the normal operation limits, no control actions are issued any more, i.e. $\Delta \boldsymbol{u} = 0$.

2.4.2 Problem formulation

The output powers of DGUs are used to control the network voltages. The change of control variables at time instant k are:

$$\Delta \boldsymbol{u}(k) = \boldsymbol{u}(k) - \boldsymbol{u}(k-1) = \left[\begin{array}{cc} \Delta \boldsymbol{P}_g^T(k) & \Delta \boldsymbol{Q}_g^T(k) \end{array} \right]^T \tag{2.23}$$

where ^{T} denotes transposition. The MPC-based controller has to solve a Quadratic Programming (QP) problem with the objective:

$$\min_{\Delta \boldsymbol{u}, \boldsymbol{\varepsilon}, \boldsymbol{V}, \boldsymbol{I}} \quad \sum_{i=0}^{N_c-1} \|\Delta \boldsymbol{u}(k+i)\|^2_{\boldsymbol{R}_1} + \|\boldsymbol{\varepsilon}\|^2_{\boldsymbol{S}} \tag{2.24}$$

where the slack vector $\boldsymbol{\varepsilon}$ and the weighting matrices $\boldsymbol{R}_1$ and $\boldsymbol{S}$ have been introduced in Section 2.2. The weight assigned to each control variable in $\boldsymbol{R}_1$ should be related to its cost: the change of the reactive power output of a DGU is considered cheaper than that of its active power output. Therefore, if some of the voltages are outside their permissible limits, the controller will favour the adjustment of DGU reactive power outputs, and will change the active power output of DGUs in the last resort.

The objective is satisfied subject to the linearized system evolution:

for $i = 1, \ldots, N_p$:

$$\boldsymbol{V}(k+i \mid k) = \boldsymbol{V}(k+i-1 \mid k) + \boldsymbol{S}_V \Delta \boldsymbol{u}(k+i-1) \tag{2.25}$$

where $\boldsymbol{V}(k+i \mid k)$ is the predicted voltage magnitude given the measurement at time k, initialized with $\boldsymbol{V}(k \mid k)$ set to the last received measurement. $\boldsymbol{S}_V$ is sensitivity matrix of voltages with respect to control changes, and its derivation will be explained in Section 2.6. Finally, the following inequality constraints are imposed to voltages and control variables:

for $i = 1, \ldots, N_p$:

$$-\varepsilon_1 \mathbf{1} + \boldsymbol{V}^{low}(k+i) \leq \boldsymbol{V}(k+i \mid k) \leq \boldsymbol{V}^{up}(k+i) + \varepsilon_2 \mathbf{1} \tag{2.26}$$

for $i = 1, \ldots, N_c$:

$$\boldsymbol{u}^{min}(k) \leq \boldsymbol{u}(k+i) \leq \boldsymbol{u}^{max}(k) \tag{2.27}$$

$$\Delta\boldsymbol{u}^{min} \leq \Delta\boldsymbol{u}(k+i) \leq \Delta\boldsymbol{u}^{max} \tag{2.28}$$

$\boldsymbol{V}^{low}$ and $\boldsymbol{V}^{up}$ are the lower and upper limits of the predicted voltages $\boldsymbol{V}$. The proper choice of these limits over the prediction horizon to obtain a smooth system response is discussed in Section 2.5.3. $\boldsymbol{u}^{min}$, $\boldsymbol{u}^{max}$, $\Delta\boldsymbol{u}^{min}$ and $\Delta\boldsymbol{u}^{max}$ are the lower and upper limits on DGU outputs and on their rate of change. ε_1 and ε_2 are the components of $\boldsymbol{\varepsilon}$, used to relax the voltage limits, if needed.

The active power outputs of DGUs are constrained by their capacity. For example, the active power production of conventional synchronous machines is constrained by the turbine capacity. In renewable energy sources, where the production is driven by weather conditions, the corresponding variables of active power are upper bounded by the actual power extracted from the wind or the sun irradiance. That is, at any instant k, the controller cannot request more than the power that is being produced, but it can request active power reductions, i.e. partial curtailment. On the other hand, the reactive power output of renewable energy sources is considered fully controllable but subject to capacity limits. After the voltage, active and reactive power measurements have been received from the DGUs, and before the optimization is solved, the bounds $\boldsymbol{Q}_g^{min}$ and $\boldsymbol{Q}_g^{max}$ in (2.27) are updated in accordance with the DGU capability curves [VO14], assuming that the active power will not change significantly over the control horizon. Thus the bounds vary with the discrete time k, but, for legibility, the dependency on active power and voltage is omitted in the notation.

2.4.3 Illustrative example

The multi-step receding-horizon controller relying on the objective (2.24) is illustrated through simulations of the 32-bus test system introduced in Section 1.4.1.

The reactive power limits of DGUs are calculated, at any time k, given their actual operation conditions ($\boldsymbol{P}_g$ and $\boldsymbol{V}$) and their nominal capacities [VO14]. Hence, any reactive power increase requested by the controller will not compromise the DGUs active power output or violate the generator capacities.

The controller sends corrections every 10 s, and the measurements are collected with the same periodicity. The prediction and control horizons are set to $N_p = N_c = 3$. This yields a good compromise between sufficient number of MPC steps and a short enough response time to correct violations.

It is required that the monitored voltages remain all within the $[0.98 \;\; 1.03]$ pu range while minimizing the control effort.

In the objective function (2.24), identical weights have been assumed for all DGUs. The weight of active power changes has been set 50 times higher than the one of reactive power. Moreover, the weights of the slack variables ε_1 and ε_2 has been taken 1000 times higher than that of reactive power.

The line parameters used to calculate the sensitivity matrix were corrupted by a random error whose mean value is zero and standard deviation is 10% of the actual line parameter. The objective is to demonstrate that the controller is robust and can compensate for these model inaccuracies.

The measurements are collected some time after the control actions are applied. This is to wait for the system response and to avoid making decisions based on measurements taken during transients.

Let us point out that, for legibility purposes, the following plots show the exact (noiseless) voltages and DGU power outputs, as opposed to the noisy and discrete measurements received and processed by the controller.

The scenario involves a low voltage situation caused by an external voltage drop on the primary side of the main transformer. Figure 2.1 presents the voltage evolutions at a sample of monitored buses. At the initial operating point, the monitored voltages are outside the acceptable range. Therefore, it is expected that the coordinated controller uses the DGU output powers to mitigate the observed violation.

The problem is detected by the controller at $t = 10$ s. Right after, and every 10 s thereafter, the controller applies the optimum $\Delta \boldsymbol{Q}_g$ obtained as detailed in the previous section. All voltages enter the desired range of $[0.98 \; 1.03]$ pu at around $t = 80$ s. Note that further corrections after this time are trigged by the noisy measurements received by the controller, but they are very small.

Figure 2.2 presents the corresponding evolution of the DGU reactive power outputs. Initially, two of them operate at unity power factor, while the remaining two produce reactive power. As it can be seen in the figure, the reactive powers of all DGUs are increased to clear the voltage problem. The contributions differ from one DGU to another, as the result of coordinated control relying on the sensitivity matrix $\boldsymbol{S}_V$. The active power of the DGUs are not changed by the controller, since the problem can be solved by the sole reactive power adjustments.

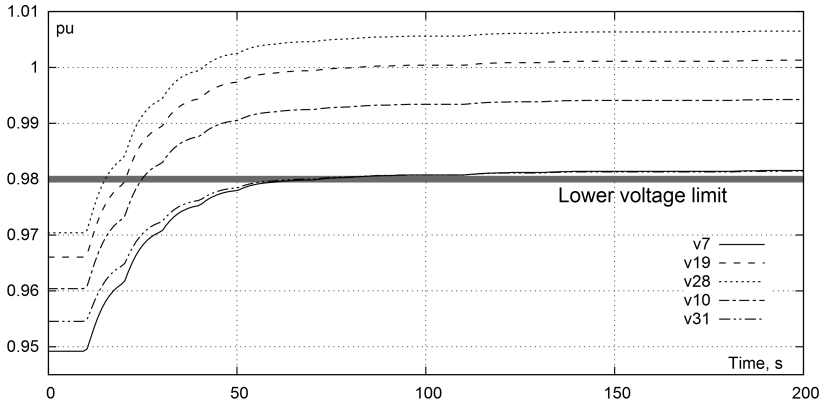

Figure 2.1: Illustrative example: Bus voltages

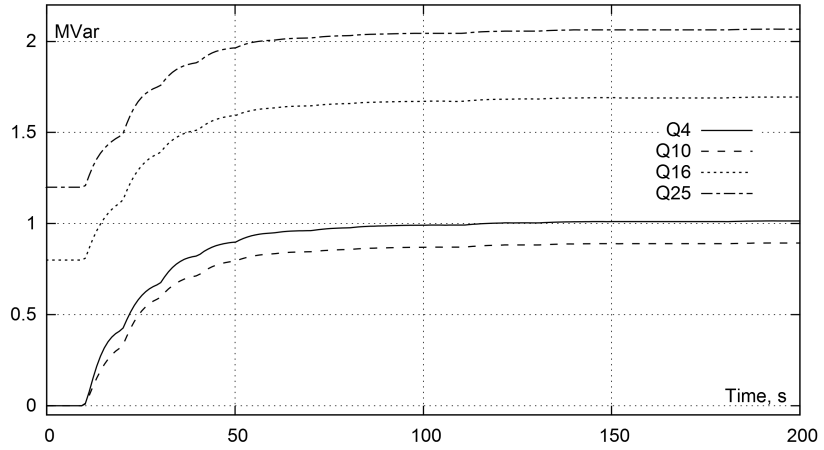

Figure 2.2: Illustrative example: Reactive power produced by DGUs

2.5 Correction of bus voltages and branch currents with minimum deviation from references

2.5.1 Overall objective of control

The second control goal corresponds to Objective 2 in Eq. (2.2) ($w = 0$). It consists in steering the DGUs to produce some reference values of active and reactive powers, while dealing with voltage and/or thermal violations experienced by the network. These reference values correspond to schedules for dispatchable units and maximum available powers for non-dispatchable ones, as will be detailed in Section 2.7.

The following features are obtained:

1. the DGU powers are set to their reference values when all operational limits are satisfied;

2. an observed (or predicted) violation is corrected (or avoided) by minimum deviations of DGU active and reactive powers from their reference values;

3. the powers are restored to the references as soon as operating conditions allow doing so.

2.5.2 Problem formulation

Here the control variables are the DGU active ($\boldsymbol{P}_g$) and reactive ($\boldsymbol{Q}_g$) powers themselves:

$$\boldsymbol{u}(k) = \begin{bmatrix} \boldsymbol{P}_g^T(k) & \boldsymbol{Q}_g^T(k) \end{bmatrix}^T \tag{2.29}$$

These variables have time-varying reference values, denoted by $\boldsymbol{P}_{ref}(k)$ and $\boldsymbol{Q}_{ref}(k)$, respectively, whose choice will be discussed in Section 2.7.

The objective is to minimize the sum of squared deviations, over the N_c future steps, between the controls and their references:

$$\min_{\boldsymbol{u},\boldsymbol{\varepsilon},\boldsymbol{V},\boldsymbol{I}} \quad \sum_{i=0}^{N_c-1} \|\boldsymbol{u}(k+i) - \boldsymbol{u}_{ref}(k+i)\|^2_{\boldsymbol{R}_2} + \|\boldsymbol{\varepsilon}\|^2_{\boldsymbol{S}} \tag{2.30}$$

where the slack variables $\boldsymbol{\varepsilon}$, and matrices $\boldsymbol{R}_2$ and $\boldsymbol{S}$ play the same role as in Section 2.2 and the weights are assigned to the control variables as explained in Section 2.4.2. The above objective is minimized subject to the linearized system evolution:

for $i = 1, \ldots, N_p$:

$$\boldsymbol{V}(k+i \mid k) = \boldsymbol{V}(k+i-1 \mid k) + \boldsymbol{S}_V \left[\boldsymbol{u}(k+i-1) - \boldsymbol{u}(k+i-2)\right] \tag{2.31}$$

$$\boldsymbol{I}(k+i \mid k) = \boldsymbol{I}(k+i-1 \mid k) + \boldsymbol{S}_I \left[\boldsymbol{u}(k+i-1) - \boldsymbol{u}(k+i-2)\right] \tag{2.32}$$

where $\boldsymbol{V}(k+i \mid k)$ and $\boldsymbol{I}(k+i \mid k)$ are the predicted bus voltages and branch currents, and $\boldsymbol{S}_V$ and $\boldsymbol{S}_I$ are sensitivity matrices of those variables with respect to control changes. The prediction is initialized with $\boldsymbol{V}(k \mid k)$ and $\boldsymbol{I}(k \mid k)$ set to the last received measurements and $\boldsymbol{u}(k-1)$ is set to the last measured value of the control variables. Finally, the following inequality constraints are imposed:

for $i = 1, \ldots, N_p$:

$$-\varepsilon_1 \mathbf{1} + \boldsymbol{V}^{low}(k+i) \leq \boldsymbol{V}(k+i \mid k) \leq \boldsymbol{V}^{up}(k+i) + \varepsilon_2 \mathbf{1} \tag{2.33}$$

$$\boldsymbol{I}(k+i \mid k) \leq \boldsymbol{I}^{up}(k+i) + \varepsilon_3 \mathbf{1} \tag{2.34}$$

and, for $i = 0, \ldots, N_c - 1$:

$$\boldsymbol{u}^{min}(k) \leq \boldsymbol{u}(k+i) \leq \boldsymbol{u}^{max}(k) \tag{2.35}$$

$$\Delta \boldsymbol{u}^{min} \leq \boldsymbol{u}(k+i) - \boldsymbol{u}(k+i-1) \leq \Delta \boldsymbol{u}^{max} \tag{2.36}$$

where $\boldsymbol{I}^{up}$ is the upper current limit on the predicted current. ε_1, ε_2 and ε_3 are the components of $\boldsymbol{\varepsilon}$. The additional slack variable ε_3 is used to relax constraint (2.34) in case of infeasibility. The entries of the 3×3 diagonal matrix $\boldsymbol{S}$ are given very high values. Inequality (2.35) includes the limits on reactive powers of DGUs, which are updated at each time step based on the measured active power and terminal voltage, as already explained in Section 2.4.2.

2.5.3 Tightening bounds and response time of the controller

In normal operation, the bus voltages lie within their limits $\boldsymbol{V}^{min}$ and $\boldsymbol{V}^{max}$, and the branch currents stay below their upper limit $\boldsymbol{I}^{max}$. In such a case, constant bounds are used in inequalities (2.26), (2.33) and (2.34) at all future times:

for $i = 1, \ldots, N_p$:

$$\boldsymbol{V}^{low}(k+i) = \boldsymbol{V}^{min} \tag{2.37a}$$

$$\boldsymbol{V}^{up}(k+i) = \boldsymbol{V}^{max} \tag{2.37b}$$

$$\boldsymbol{I}^{up}(k+i) = \boldsymbol{I}^{max} \tag{2.37c}$$

On the other hand, if after a disturbance the voltages and/or currents fall outside the above-mentioned admissible limits, the controller will correct the situation by successive actions on control means. In order to obtain a smooth system evolution, the bounds $\boldsymbol{V}^{low}(k+i)$, $\boldsymbol{V}^{up}(k+i)$ and $\boldsymbol{I}^{up}(k+i)$ on the predicted voltages and currents are tightened progressively [Mac02]. Such progressively tighter inequalities are also referred to as "funnel constraints" [QB03]. After trying several bound evolutions [VV13a, SGV14], an exponential evolution with time has been found the most appropriate. It is shown in Fig. 2.3 for respectively a lower voltage (Fig. 2.3.(a)) and a current limit (Fig. 2.3.(b)). The circles indicate voltage or current values measured at time k, which fall outside the acceptable range. The limits imposed at the successive times $k+1, \ldots, k+N_p$ are shown with solid lines. They force the voltage or current of concern to enter the acceptable range

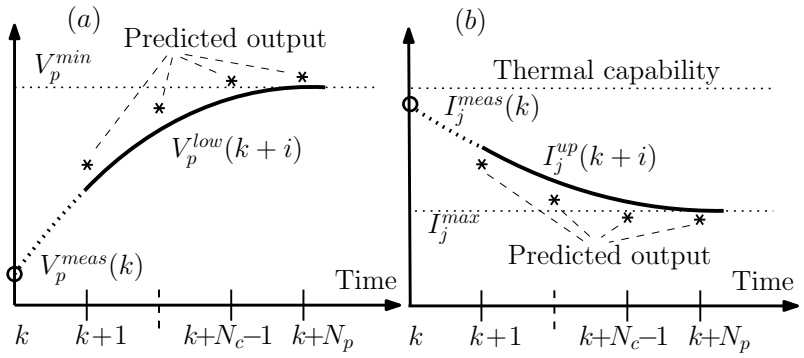

Figure 2.3: Progressive tightening of voltage and current bounds

at the end of the prediction horizon. Taking the lower voltage limit as an example, the variation is given by:

for $i = 1, \ldots, N_p$:

$$V_p^{low}(k+i) = V_p^{min} - \left(V_p^{min} - V_p^{meas}(k)\right) e^{-i/T_V} \tag{2.38}$$

where p is the bus of concern and $V_p^{meas}(k)$ is the measurement received at time k. The time constant T_V is chosen to have the predicted output at time $k + N_p$ inside the acceptable limits.

Similar variations are considered for the upper voltage and the current limits:

for $i = 1, \ldots, N_p$:

$$V_p^{up}(k+i) = V_p^{max} + \left(V_p^{meas}(k) - V_p^{max}\right) e^{-i/T_V} \tag{2.39}$$

$$I_p^{up}(k+i) = I_p^{max} + \left(I_p^{meas}(k) - I_p^{max}\right) e^{-i/T_I} \tag{2.40}$$

where T_I is the time constant considered for thermal congestion clearing.

As regards Eq. (2.40), the I^{max} value is set conservatively below the effective thermal capability monitored by the corresponding protection, as shown in Fig. 2.3.(b).

An alternative to the exponentially tightened bound is a linear one, where for instance the lower voltage limit is varying as follows:

for $i = 1, \ldots, N_p$:

$$V_p^{low}(k+i) = V_p^{min} - \left(V_p^{min} - V_p^{meas}(k)\right) \frac{N_p - i}{N_p\, \rho_V} \tag{2.41}$$

where $\rho_V \geq 1$ is tuned to modulate the limit over the prediction horizon. A larger value of ρ_V

enforces a tighter funnel constraint, leading to faster corrections. Compared to the exponential tightening, (2.41) results in a smoother voltage correction, with a proper choice of ρ_V. Indeed the needed voltage change $V_p^{min} - V_p^{meas}(k)$ is spread more evenly over the prediction horizon. In return, the violation will last longer before being fully cleared. This option can be of interest when a relatively slow correction is required.

2.6 Sensitivity derivation

In the whole thesis a static model of the system is employed in order to predict and evaluate the network response to the corrections computed by the MPC-based controller. This simplification is justified by the fast response of the power electronics based DGUs, in the order of a few seconds, compared to the MPC sampling time, in the order of ten seconds. Furthermore, the model is linear and relies on sensitivity matrices. This section is devoted to explaining how the involved sensitivities are computed and updated, if needed.

An accurate sensitivity matrix, to be used for predicting the system behaviour, should incorporate the variation of load powers with voltage, the actual network impedances, a precise Thévenin equivalent to replace the transmission system, and the actual system operation point. Unfortunately, this information is not known accurately in practice and some approximations are inevitable. The latter, however, are expected to be compensated by the MPC scheme.

2.6.1 Voltage sensitivity matrix $\boldsymbol{S}_V$

The voltage sensitivity matrix $\boldsymbol{S}_V$ can be obtained off-line from the transposed inverse of the power flow Jacobian matrix, considering constant power models for all loads. Assuming that $\boldsymbol{x}$ is the power flow state vector (bus voltage magnitudes and phase angles), $\boldsymbol{u}$ the vector of power injections and $\boldsymbol{f}$ the vector of power mismatch equations, the power flow equations can be written in compact form as $\boldsymbol{f}(\boldsymbol{x}, \boldsymbol{u}) = 0$. The voltage sensitivity matrix can be obtained from a general sensitivity formula as [CV05], [GV09]:

$$\frac{\partial \boldsymbol{V}}{\partial \boldsymbol{u}} = -\boldsymbol{f}_{\boldsymbol{u}}^T \left(\boldsymbol{f}_{\boldsymbol{x}}^T\right)^{-1} \frac{\partial \boldsymbol{V}}{\partial \boldsymbol{x}} \tag{2.42}$$

where $\boldsymbol{f}_{\boldsymbol{u}}$ (respectively, $\boldsymbol{f}_{\boldsymbol{x}}$) is the Jacobian matrix of $\boldsymbol{f}$ with respect to $\boldsymbol{u}$ (respectively $\boldsymbol{x}$), and $\frac{\partial \boldsymbol{V}}{\partial \boldsymbol{x}}$ is a trivial matrix including zero's and one's.

As an alternative, each column of $\boldsymbol{S}_V$ can be computed by running a power flow calculation with one DGU power slightly modified, and simply dividing the variations of the monitored bus

voltages by that power variation. This matrix can be updated infrequently; as already said, the errors can be compensated by the MPC scheme [VV13b], [SGV16].

2.6.2 Current sensitivity matrix $\boldsymbol{S}_I$

The current sensitivity matrix $\boldsymbol{S}_I$, on the other hand, should be updated more frequently, due to the higher variability of currents. Equation (2.32) relative to j-th branch current can be rewritten as:

$$I_j(k+1) = I_j(k) + \sum_{i=1}^{N_g} \left[\frac{\partial I_j}{\partial P_{gi}}(k)\Delta P_{gi}(k) + \frac{\partial I_j}{\partial Q_{gi}}(k)\Delta Q_{gi}(k) \right] \tag{2.43}$$

where I_j is the current magnitude, P_{gi}, Q_{gi} are the active and reactive powers generated by the i-th DGU, N_g is the number of DGUs, and $\Delta P_{gi}(k)$ and $\Delta Q_{gi}(k)$ are defined as:

$$\Delta P_{gi}(k) = P_{gi}(k) - P_{gi}(k-1) \tag{2.44a}$$

$$\Delta Q_{gi}(k) = Q_{gi}(k) - Q_{gi}(k-1) \tag{2.44b}$$

If the j-th branch is not on the path from the i-th DGU to the HV/MV transformer (source substation), the partial derivatives in (2.43) can be set to zero. Otherwise, the expression of the current is:

$$I_j = \frac{S_j}{V_k} = \frac{\sqrt{P_j^2 + Q_j^2}}{V_k} \tag{2.45}$$

where P_j, Q_j and S_j are respectively the active, reactive and apparent power flows in the branch, and V_k the voltage at the bus where the current is measured. The sensitivities can be approximated by:

$$\frac{\partial I_j}{\partial P_{gi}} \approx \frac{1}{V_k}\frac{P_j}{S_j}\frac{\partial P_j}{\partial P_{gi}} \approx \frac{P_j}{S_j} \tag{2.46a}$$

$$\frac{\partial I_j}{\partial Q_{gi}} \approx \frac{1}{V_k}\frac{Q_j}{S_j}\frac{\partial Q_j}{\partial Q_{gi}} \approx \frac{Q_j}{S_j} \tag{2.46b}$$

in which: (i) the voltage has been taken equal to 1 pu, (ii) P_j (resp. Q_j) have been assumed to not change much when Q_{gi} (resp. P_{gi}) is varied, and (iii) the change of P_j (resp. Q_j) is equal to the change in P_{gi} (resp. Q_{gi}).

Note that using Eqs. (2.46) requires to have the branch equipped with active and reactive power flow measurements.

The simplest solution consists of computing the sequence of corrective actions $u(k+i)(i = 0, \ldots, N_c - 1)$ using the sensitivities evaluated at step k. However, these sensitivities may change

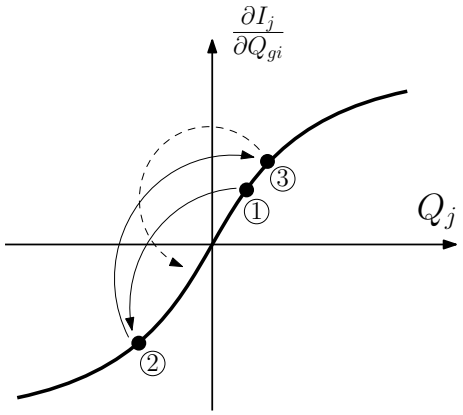

Figure 2.4: Branch current sensitivity as a function of its reactive power flow (assuming constant active power flow)

significantly with the operating point; in particular, they change sign in case of power flow reversal. This is illustrated by Fig. 2.4 which shows how a branch current sensitivity varies with its reactive power flow, assuming a constant active power flow. This significant variability may lead to over- or under-estimating the system response, especially when the active or reactive power flow crosses zero, in which case controller oscillations might occur. The black disks in the same figure, which are operating points at three successive steps, show such a case where, due to non updated sensitivities, the impact of reactive power changes is over-estimated, resulting in an oscillation around zero.

To deal with this issue, the following alternative schemes were contemplated [SGV14]:

- when the power flow approaches zero, the corresponding sensitivities are set to zero, which leads the optimization (2.30) to automatically rely on other control actions;
- using the sensitivities evaluated from measurements collected at time k, a first sequence of corrective actions is computed. At the resulting predicted states, new sensitivities are recomputed and the average between the original and the recomputed values is used to solve, for a second time, the optimization problem (2.30). The so recomputed control actions are applied to the system (the intermediate ones are ignored).

For the sake of simplicity the first proposed solution has been preferred, i.e. the sensitivities $\frac{\partial I_j}{\partial P_{gi}}$ (resp. $\frac{\partial I_j}{\partial Q_{gi}}$) are set to zero whenever the active (resp. reactive) power flow in the j-th branch becomes less than a small value. In such a case, and as long as the risk of congestion exists, any further reactive power change, due for instance to a desired reactive power output (reflected

in $\boldsymbol{Q}_{ref}$ in Objective 2), must be avoided. To do so, $\boldsymbol{Q}_{ref}$ at each discrete step is set to the last measured value of the DGU reactive power outputs.

2.7 Context of application and choice of reference values

This section is devoted to the MPC formulation of Section 2.5, minimizing deviations from references $\boldsymbol{P}_{ref}$ and $\boldsymbol{Q}_{ref}$.

This formulation can accommodate various contexts of application, depending on the interactions and information transfers between entities acting on the DGUs, in accordance with the regulatory policy. This leads to defining a number of operating modes, which are all depicted in Fig. 2.5.

The proposed controller is executed by a central entity, typically the DSO, which collects real-time measurements. The latter consists of active and reactive productions and terminal voltages of the DGUs, active and reactive power flows in critical (potentially congested) branches, and some other bus voltages. Thus, the controller relies on a dedicated measurement and communication infrastructure but, as suggested in Fig. 2.5, it could also rely on the results of a state estimator, for improved system monitoring [SPC+12, PPB+15, RTD+15].

Once the controller observes (or predicts) limit violations, it computes and sends active and/or reactive power corrections to the DGUs of concern. Those corrections are the differences between the reference and the computed controls, i.e.

$$\Delta \boldsymbol{P}_{cor}(k) = \boldsymbol{P}_{ref}(k) - \boldsymbol{P}_{g}(k) \tag{2.47a}$$

$$\Delta \boldsymbol{Q}_{cor}(k) = \boldsymbol{Q}_{ref}(k) - \boldsymbol{Q}_{g}(k) \tag{2.47b}$$

Note that these corrections stay at zero as long as no limit violation is observed (or predicted), and come back to zero (together with the objective function (2.30)) as soon as operation is no longer constrained, as explained in the sequel.

Furthermore, a distinction is made between *dispatchable* and *non-dispatchable* DGUs. The latter are typically wind turbine or photovoltaic units operated for Maximum Power Point Tracking (MPPT). In the absence of operating constraints, they are left to produce as much as it can be obtained from the renewable energy source. The dispatchable units, on the other hand, have their production schedules $\boldsymbol{P}$ and $\boldsymbol{Q}$, according to market opportunities or balancing needs, for instance.

Mode 1

This mode applies to non-dispatchable units. For MPPT purposes, at each time step k, the reference $P_{ref\,i}(k)$ of the i-th DGU should be set to the maximum power available on that unit. This information is likely to be available to the DGU MPPT controller, but is seldom transmitted outside. An alternative is to estimate that power from the measurements $\boldsymbol{P}_{meas}$. Considering the short control horizon of concern here, a simple prediction is given by the "persistence" model:

$$\boldsymbol{P}_{ref}(k+i) = \boldsymbol{P}_{meas}(k) + \Delta\boldsymbol{P}_{cor}(k-1), \quad i = 0, ..., N_c \tag{2.48}$$

As long as no power correction is applied, the last term is zero and $\boldsymbol{P}_{meas}$ is used as a short-term prediction of the available power. When a correction is applied, the right-hand side in (2.48) keeps track of what was the available power before the correction started being applied. Using this value as reference allows resetting the DGUs under the desired MPPT mode as soon as system conditions improve.

A more accurate prediction can be used, if data are available. That would result in the right-hand side of (2.48) varying with time $k + i$.

Mode 2

This mode applies to DGUs that are dispatchable but under the control of another actor than the DSO. Thus, the latter does not know the power schedule of the units of concern. In order to avoid interference with that non-DSO actor, the last measured power productions are taken as reference values over the next N_c time steps:

$$\boldsymbol{P}_{ref}(k+i) = \boldsymbol{P}_{meas}(k), \quad i = 0, ..., N_c \tag{2.49}$$

On the other hand, if a control action has been applied by the DSO, to preserve network security, this action should not be counteracted by a subsequent non-DSO action in order to avoid conflict, leading for instance to oscillation. In other word, the DSO is assumed to "have the last word" in terms of corrective actions, since it is the entity responsible for network security.

In both Modes 1 and 2, the controller lacks information to anticipate the DGU power evolution. Hence, the corrections (2.47) will be applied *ex post*, after the measurements have revealed the violation of a (voltage or current) constraint.

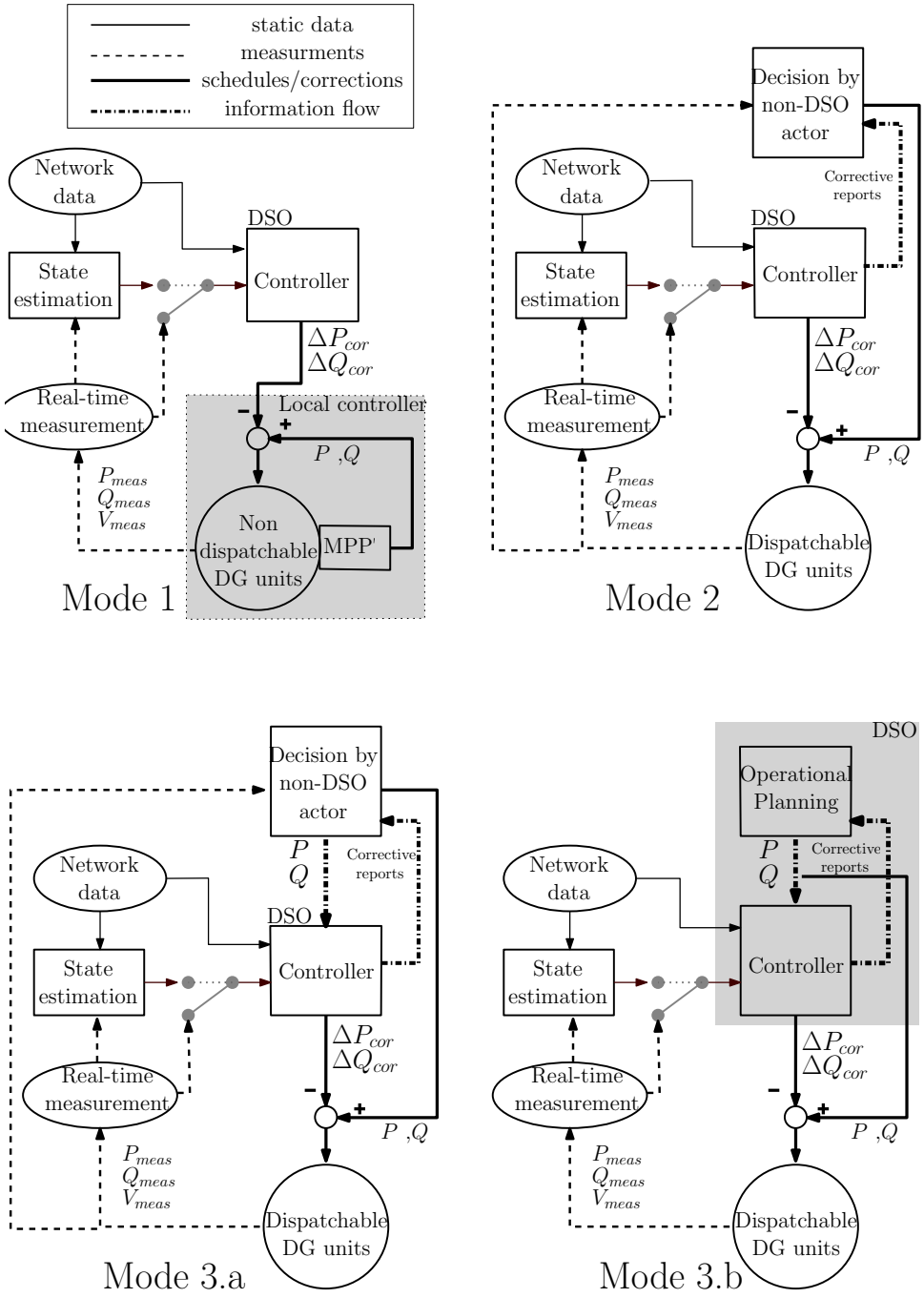

Figure 2.5: Contexts of application of the proposed control scheme

Mode 3

This mode relates to dispatchable DGUs whose power schedules are known by the controller, either because this information is transmitted by the non-DSO actors controlling the DGUs (see variant 3.a in Fig. 2.5) or because the DSO is entitled to directly control the DGUs (see variant 3.b in Fig. 2.5). The latter case may also correspond to schedules determined by the DSO operational planning. Unlike in Mode 2, the schedule imposed to the units is known by the controller, which can anticipate a possible violation under the effect of the scheduled change, and correct the productions *ex ante*. Although different from a regulatory viewpoint, Modes 3.a and 3.b are treated in the same way.

Figure 2.6 shows how the N_c future $\boldsymbol{P}_{ref}$ values are updated with the known schedule before being used as input for the controller. As long as the schedule does not change within the N_c future time steps (see Fig. 2.6.a), $\boldsymbol{P}_{ref}$ remains unchanged; otherwise, the interpolated values are used.

In principle the aforementioned choices also apply to the reference reactive powers $\boldsymbol{Q}_{ref}$. However, it is quite common to operate DGUs at unity power factor, to minimize internal losses, which amounts to setting $\boldsymbol{Q}_{ref}$ to zero, and corresponds to Mode 3.

To make system operation smoother and more secure, the identified limit violations and the corresponding corrections applied by the controller to DGUs should be communicated back to the non-DSO actors or the operational planners, as suggested by the dash-dotted arrows in Fig. 2.5.

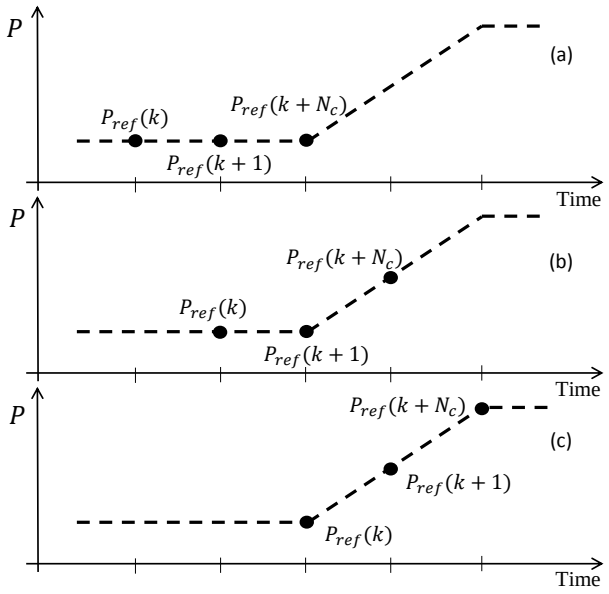

Figure 2.6: Mode 3: updating the P_{ref} values over three successive times

2.8 Simulation results: voltage and/or congestion corrections with minimum deviation from references

2.8.1 Test system and control settings

The performance of the control schemes presented in Sections 2.5 and 2.7 are going to be illustrated on the 75-bus test system introduced in Section 1.4.2.

The prediction and control horizon, the period of control actions and measurement gathering, as well as the update of the DGU reactive power limits are the same as in Section 2.4.3.

The matrices $\boldsymbol{R}_2$ and $\boldsymbol{S}$ are diagonal with entries equal to 1 for reactive powers, 25 for active powers, 500 for the slack variables ε_1 and ε_2 and 5000 for ε_3, respectively.

Note that, dealing with more sophisticated scenarios, the measurements are not affected by noise, in order to better understand the controller reactions in different time steps.

Finally, the changes in operating point applied to the system, such as wind speed variations, load increases and scheduled changes, have been made faster than in reality for a more comfortable presentation of the results.

2.8.2 Scenario A: Mode 1

All 22 DGUs are assumed to be driven by wind turbines, operated for MPPT. Thus the control of all DGUs is in Mode 1, see Fig. 2.5. Initially the dispersed generation exceeds the load, and the DN is injecting active power into the external grid. At the same time, the DGUs are operating at unity power factor, and the DN draws reactive power from the external grid.

A 10 % increase in wind speed takes place from $t = 20$ to $t = 80$ s, as shown in Fig. 2.7 [2]. This results in an increase of the active power flow in the transformer, as shown in Fig. 2.8. Around $t = 52$ s, the thermal limit of the latter, shown with heavy line in Fig. 2.9, is exceeded. This is detected by the controller through a violation of the constraint (2.34) at $t = 60$ s.

The controller corrects this congestion problem by acting first on the DGU reactive powers, which have higher priority through the weighting factors. Figure 2.10 shows that the controller makes some DGUs produce reactive power, to decrease the import through the transformer. The latter effect can be seen in the power flows (see Fig. 2.8) and the current in the transformer (see

[2] All DGUs have been assumed identical and have identical initial productions. This leads to having superimposed curves in Figs. 2.7 to 2.10

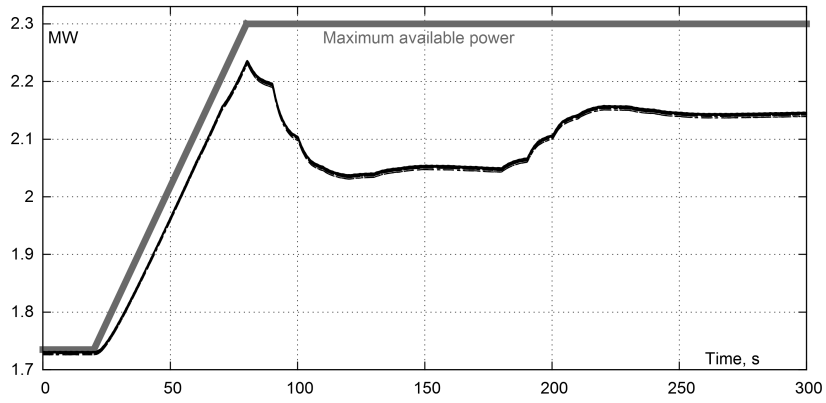

Figure 2.7: Scenario A: Active power produced by DGUs

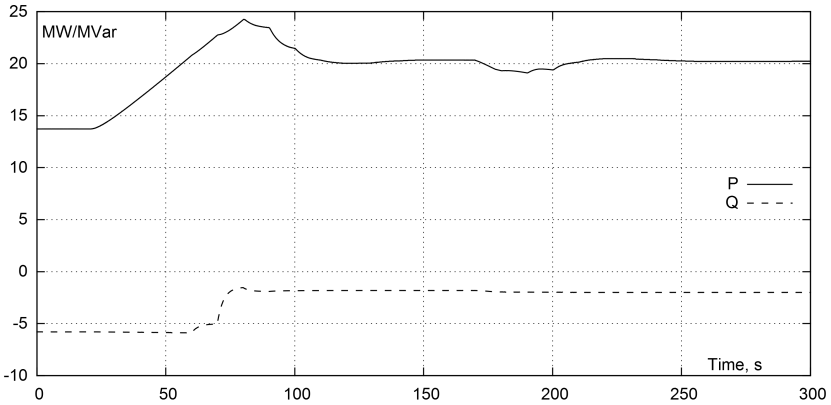

Figure 2.8: Scenario A: Power flows in the transformer

Fig. 2.9) [3]. However, the correction of DGU reactive powers alone cannot alleviate the overload, and from $t = 80$ s on, the controller curtails the active power of wind turbines as shown in Fig. 2.7. The overload is fully corrected at $t = 120$ s.

To illustrate the ability of the proposed control to steer the DGUs back to MPPT, the system operating conditions are relieved by simulating a 4.1 MW load increase starting at $t = 170$ s. The corresponding decrease of the active power flow and the current in the transformer can be observed in Figs. 2.8 and 2.9, respectively. This leaves some space to restore part of the curtailed DGU active powers. As expected, the controller increases the DGU productions until the transformer current reaches its limit again, at around $t = 210$ s. Figure 2.7 shows that, indeed, the active productions get closer to the maximum power available from wind.

[3] Assuming the active power flow is unchanged, Eq. (2.45) shows that reactive power flow should be decreased to zero to decrease the current

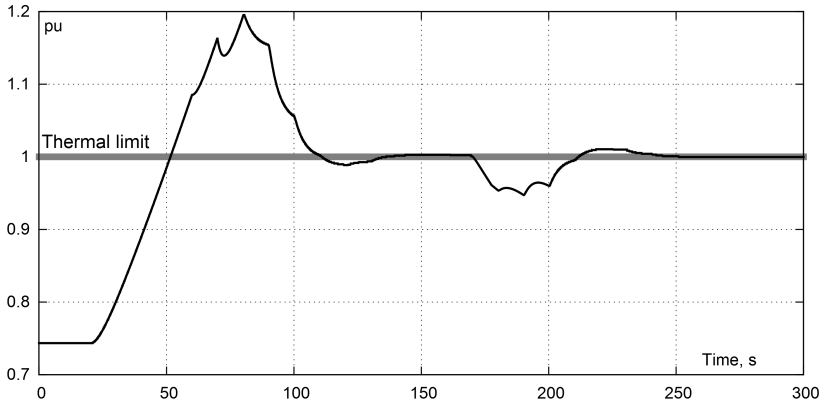

Figure 2.9: Scenario A: Current in the transformer

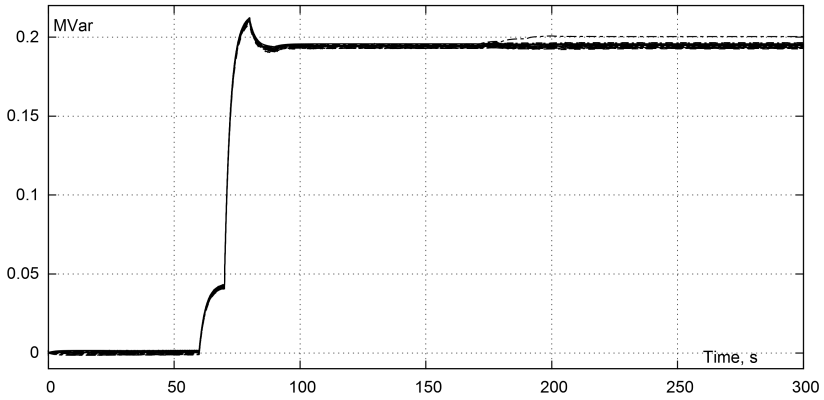

Figure 2.10: Scenario A: Reactive power produced by DGUs

In this example, the unpredicted thermal limit violation caused by the initial wind increase was corrected *ex post*. It is interesting to note that, on the contrary, when taking advantage of the load relief, the controller steers the system in such a way that it does not exceed the thermal limit.

2.8.3 Scenario B: Modes 1 and 2 combined

It is now assumed that nine units, connected respectively to buses 1118, 1119, 1129, 1132, 1138, 1141, 1155, 1159, and 1162 (see Fig. 1.4), are driven by wind turbines and are non-dispatchable. They are thus operated in Mode 1, as in Scenario A. However, since the wind speed is assumed constant in this scenario, the productions of those units remain constant.

The remaining 13 DGUs use synchronous generators and are dispatchable. They are operated in Mode 2. An increase of their active power by an actor other than the DSO, thus not known by the controller, takes place from $t = 100$ to $t = 140$ s, as shown in Fig. 2.12. The schedule leaves the

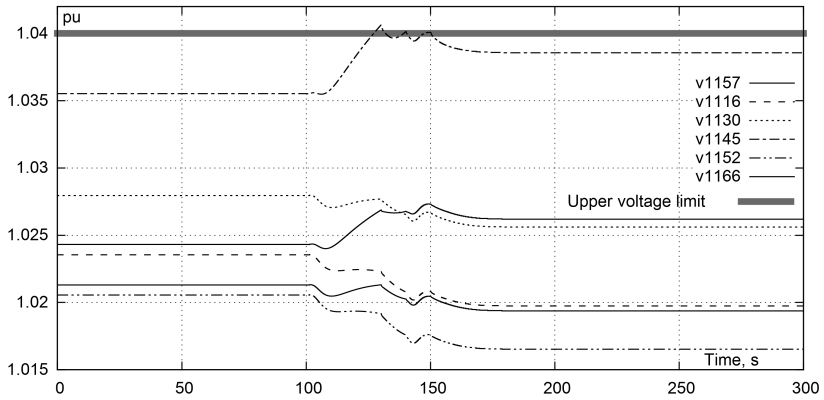

Figure 2.11: Scenario B: Bus voltages

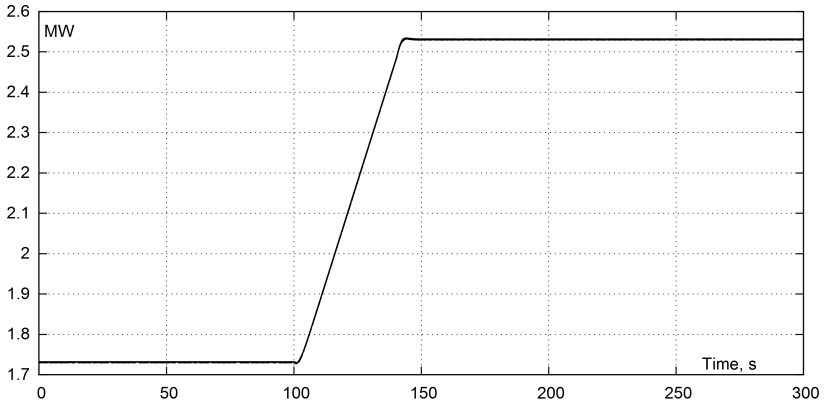

Figure 2.12: Scenario B: Active power produced by dispatchable units

reactive powers unchanged. Since the initial network voltages are close to the admissible upper limit, shown with heavy line in Fig. 2.11, the system undergoes high voltage problems.

The controller does not send corrections until $t = 130$ s, when the voltage at bus 1145 exceeds the limit. Over the 40 seconds that follow this limit violation, the controller adjusts the reactive powers of both dispatchable and non-dispatchable units, as shown by Figs. 2.13 and 2.14. It is easily seen that different corrections are applied to different DGUs, depending on their locations in the system. It is also seen from Fig. 2.11 that the voltage at bus 1145 crosses the limit several times, followed by reactive power adjustments. These *ex post* corrections were to be expected since, in this example, the DGUs are either in Mode 1 or in Mode 2.

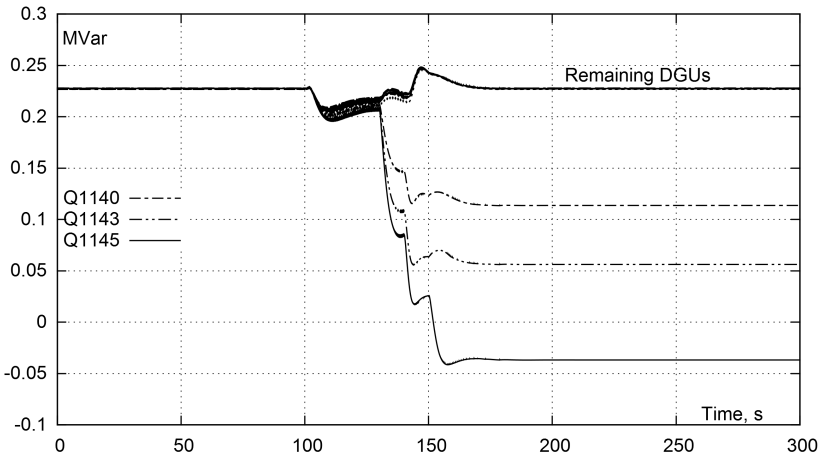

Figure 2.13: Scenario B: Reactive power produced by dispatchable units

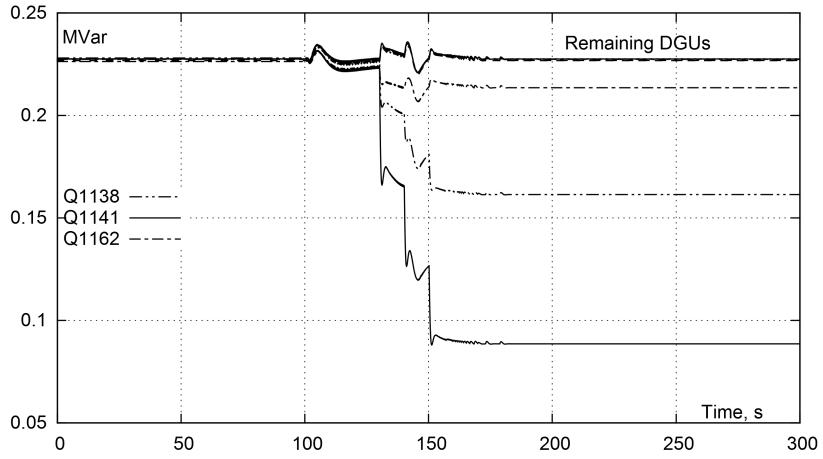

Figure 2.14: Scenario B: Reactive power produced by non-dispatchable units

2.8.4 Scenario C: Modes 1 and 3 combined

In this third scenario, some DGUs are non dispatchable and operated in Mode 1, while the dispatchable ones are operated in Mode 3, with their schedules known by the controller. The latter might come, for instance, from operational planning decisions.

Two successive changes of DGU active powers are considered: (i) an unforeseen wind speed change from $t = 20$ to $t = 70$ s increasing the production of the non-dispatchable units, and (ii) a power increase of the dispatchable units scheduled to take place from $t = 150$ to $t = 190$ s. The corresponding active power generations are shown in Fig. 2.15.

Figure 2.16 shows the resulting evolution of a few bus voltages. The increase in wind power

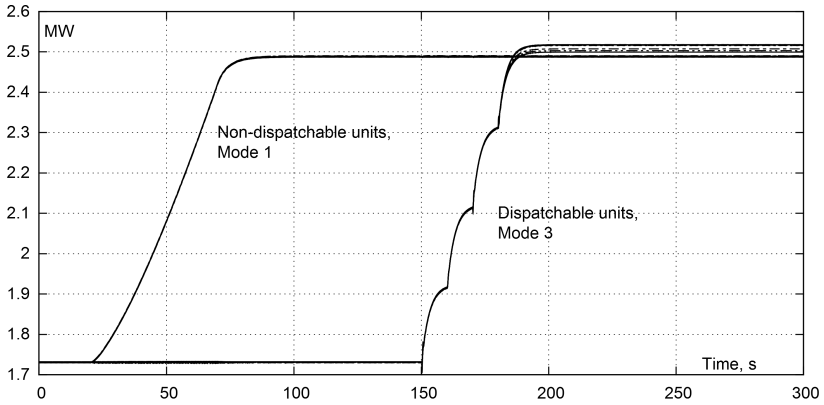

Figure 2.15: Scenario C: Active power produced by various units

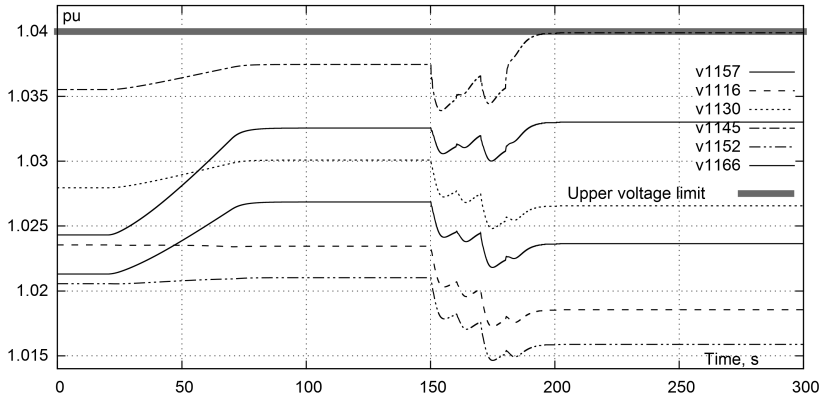

Figure 2.16: Scenario C: Bus voltages

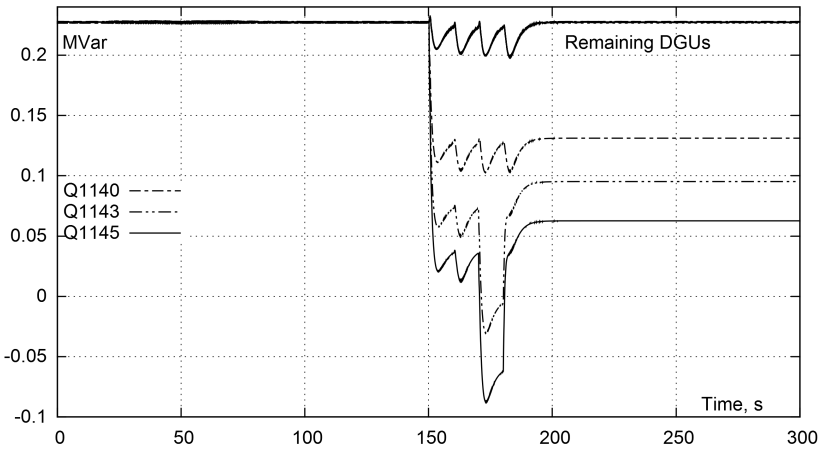

Figure 2.17: Scenario C: Reactive power produced by dispatchable units

makes them approach their limit, shown with heavy line. Without a corrective action, the subsequent scheduled change would cause a limit violation. However, the latter change is anticipated

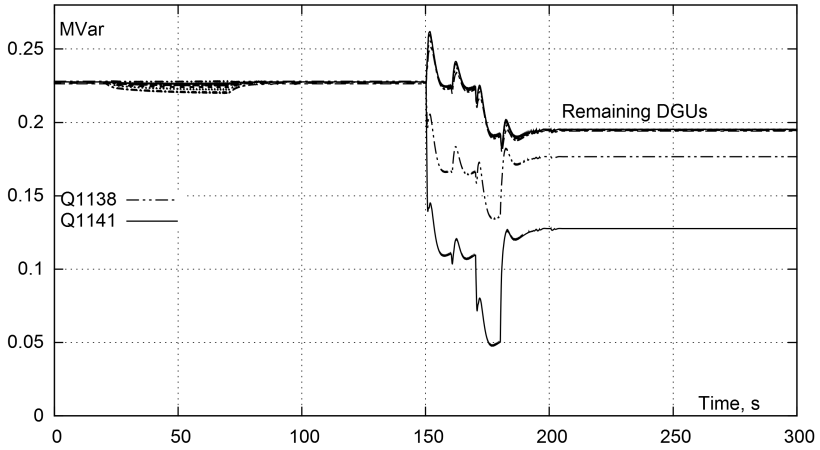

Figure 2.18: Scenario C: Reactive power produced by non-dispatchable units

by the controller, through the P_{ref} values updated as shown in Fig. 2.6. Therefore, the controller anticipatively adjusts the DGU reactive powers, as seen in Figs. 2.17 and 2.18, and no voltage exceeds the limit, while all the active power changes are accommodated. The controller anticipative behaviour is clearly seen in Fig. 2.16, where the voltage decrease resulting from the reactive power adjustment counteracts the increase due to active power increase, leading the highest voltage to land on the upper limit.

2.8.5 Data communication, processing and computing times

Each sampling period T of the centralized controller can be decomposed into the following:

1. communication delay for the centralized controller corrections to be received by all DGUs;
2. dead-time ($\simeq 2\ s$) to wait until the DGUs and their reactive power controllers have reached almost steady state in response to those corrections;
3. time window ($\simeq 2\ s$) in which the measurements $\boldsymbol{V}$ and $\boldsymbol{Q}$ are locally collected and pre-filtered [VV13b];
4. communication delay for all these measurements to be received by the centralized controller;
5. time taken by the controller to compute the corrections.

For the 75-bus test system, with $N = 22$ DGUs and $N_V = 4$ non-DGU bus voltage measurements, the amount of data exchanged is $N = 22$ for Item 1 and $3N + N_V = 70$ for Item 4. It is realistic to assume that the two data transfers together will not take more than one second.

As regards Item 5, on the same system, the elapsed time to solve one optimization problem (2.30-2.36) was found to vary between 0 and 32 ms, depending on the number of active constraints at a given time step (obtained on a standard laptop computer with a dual-core Intel-i5 processor running at 2.27 GHz with 4 GB RAM).

The sum of all the above delays amounts to $5\ s$, which leaves a very ample margin with respect to the sampling period $T = 10\ s$.

2.9 Simulation results: robustness of MPC-based control

As mentioned at several places, the closed-loop nature of MPC offers significant advantages in terms of robustness to model inaccuracies, component failures, measurement noise, etc. The objective of this section is to practically demonstrate the robustness of our controller in various situations where the model does not capture the real system behaviour. In this respect, through some examples, the behaviour of the controller is examined when:

1. The controller sampling period T does not properly correspond to the dynamics of the system components. Simply stated, the DGUs have not reached steady state by the end of the sampling period. Another situation with a similar impact is when the measurement times are badly synchronized with controller action times, i.e. they are collected early while DGU powers are still evolving.

2. There is a communication failure between the centralized controller and some DGUs under its control.

As regards item 1, the sampling period T is kept constant and equal to 10 s (as in the whole thesis), while some modifications are applied to the DGU models in order to slow down their response to the controller corrections. In practice, these limitations could be imposed by the DGU manufacturers or owners in order to avoid fast changes, and hence, increase the life-time of the generators. The instant at (or the time window in) which the measurements are collected is also playing an important role in the monitoring capability of the centralized controller.

The results are provided in six cases for the first point, and three cases for the second one. The changes from one case to the next entails additional difficulties imposed on the controller. Let us point out that, to reach some severe cases (e.g. Case 6), some assumptions have been made that might not be easily justified in practice. They have been chosen to investigate up to which point the controller can perform correctly.

The test system is the 75-bus one, introduced in Section 1.4.2, and all 22 DGUs are assumed to be driven by wind turbines, operated for MPPT. The control settings are those given in Section 2.8, unless otherwise mentioned.

2.9.1 Impact of slow DGU dynamics and early measurement sampling

As mentioned in Section 2.2, a sensitivity-type model of the system is used in this work to express the predicted system evolution. This choice has been made assuming that the sampling period of discrete-time optimization is large enough so that the DGUs have reached (almost) steady values before the measurements are collected and new controls are applied. Here the robustness of the controller is evaluated when the mentioned condition is not (fully) satisfied, due to either slower dynamics of the DGUs or early taken measurements.

In this regard, the following cases are considered:

- Case 1: the DGU parameters have the default values used throughout the rest of the thesis, and presented in Appendix B. The measurements are collected at $t = kT+8;\ \ k = 0, 1, 2, ...$
- Case 2: the reactive power control of the DGUs is made slower than in Case 1 by adjusting the integral and proportional gains of reactive power control loop (setting $K_{Qi} = 0.2$ and $K_{Qp} = 0.001$ in Fig. B.4). The measurements are collected at $t = kT + 8$.
- Case 3: the active and reactive power controls of the DGUs are made both slower than in Case 1, by doubling the mechanical time constant T_m in the speed control loop (see Fig. B.3). It means that, in this case, the generator and turbine have a higher inertia. The modification of the reactive power control is as in Case 2. The measurements are collected at $t = kT + 8$.
- Case 4: similar to Case 3, but the measurements are collected at $t = kT + 6$.
- Case 5: similar to Case 3, but the measurements are collected at $t = kT + 4$.
- Case 6: similar to Case 3, but the measurements are collected at $t = kT + 1$.

The role of the controller and the reactive and active power evolutions of the DGUs are very similar to those of Scenario A (congestion problem), presented in Section 2.8.2. The results focus on examining how the system response is impacted by the above changes.

Let us mention that all DGUs have almost identical active and reactive power productions. The powers of only one DGU is shown here, for legibility of the figures.

Cases 1, 2 and 3

All DGUs operate in Mode 1 (see Fig.2.5). Initially the total generation exceeds the load, and the DN is injecting active power into the external grid. At the same time, the DGUs are operating at unity power factor, and the DN draws reactive power from the external grid.

A 10 % increase in wind speed takes place from $t = 0$ to $t = 60$ s, yielding an active power increases of the DGUs. This results in an increase of the active power flow and, hence, the current in the transformer, as shown in Fig. 2.19. Between $t = 30$ and $t = 35$ s, the thermal limit of the latter is exceeded, as branch currents go over 1 pu in the same figure. This is detected by the controller through a violation of the constraint (2.34) at the next discrete step, i.e. $t = 40$ s.

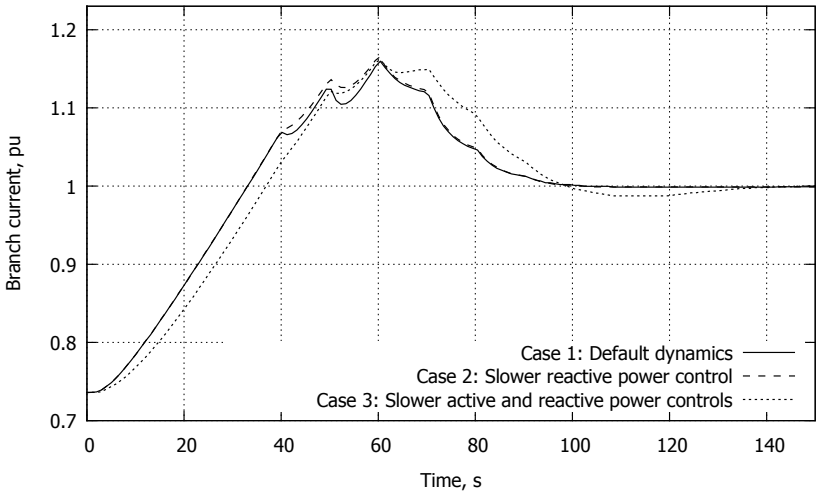

Figure 2.19: Current in main transformer

Figure 2.20 shows the active power output of DGU 1166. The curves are extremely close in Cases 1 and 2, since the time constant T_m is the same. Having a higher time constant in Case 3, the DGU reacts to the wind speed changes (from $t = 0$ to $t = 60$ s) and the corrections sent by the centralized controller (from $t = 40$ to $t = 100$ s) more slowly than in Cases 1 and 2. However, as expected, they all reach the same steady value. The slower active power evolution in Case 3 (compared to Cases 1 and 2) is reflected in the main transformer current too, as shown in Fig. 2.19.

The active power of DGU 1166 in Case 1 overlays with that of Case 2, since the mechanical inertia remains unchanged, as illustrated in Fig. 2.20.

As the result of the mentioned adjustments in reactive power control loop, it can be seen in Fig. 2.21 that the reactive power of DGU 1166 in Case 2 (dashed line) is reacting to the controller commands more slowly than in Case 1 (solid line). This results in a slightly higher current

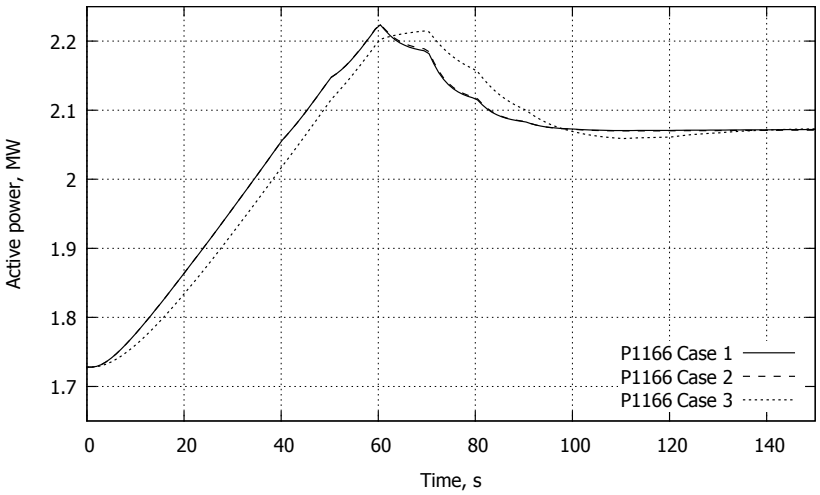

Figure 2.20: Active power produced by DGU 1166

in the transformer in the time interval from $t = 20$ until $t = 40$ s, when the reactive powers have different values (see Fig. 2.19).

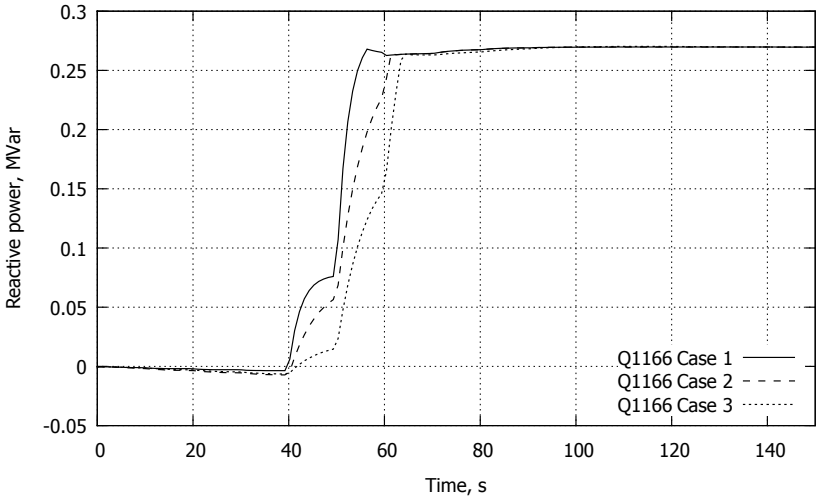

Figure 2.21: Reactive power produced by DGU 1166

Note that, although the internal DGU reactive power control is the same, the output reactive power in Case 3 has a different evolution than in Case 2. This is due to a little less severe overload, observed by the controller at $t = 40$ s, in Case 3 and, consequently, smaller reactive power (and also active power) corrections.

The current in the transformer is brought back below its thermal limit slightly later in Case 3, and the current slightly oscillates around the limit of 1 pu. This is due to the higher mechanical

time constant and hence, the slower response of the DGUs (with respect to the sampling period). This example already demonstrates the robustness of controller, which remains able to handle the congestion problem.

Cases 4, 5 and 6

The same scenario of wind increase and congestion is considered, while the impact of taking early measurements is studied. For easy comparison, the results of Case 3 are recalled in all figures.

If the measurements are collected while the DGU powers are still evolving in response to control changes, they do not capture the whole effect of the previous correction of the controller. One can also consider that the measurements used by the controller are affected by a systematic noise.

Figures 2.22 and 2.23 show the transformer current and the DGU active powers. As the measurements are collected earlier in each sampling period, three main changes can be observed: (i) the transformer experiences a higher overload, (ii) however, the latter is cleared faster, although (iii) larger oscillations take place around the limit.

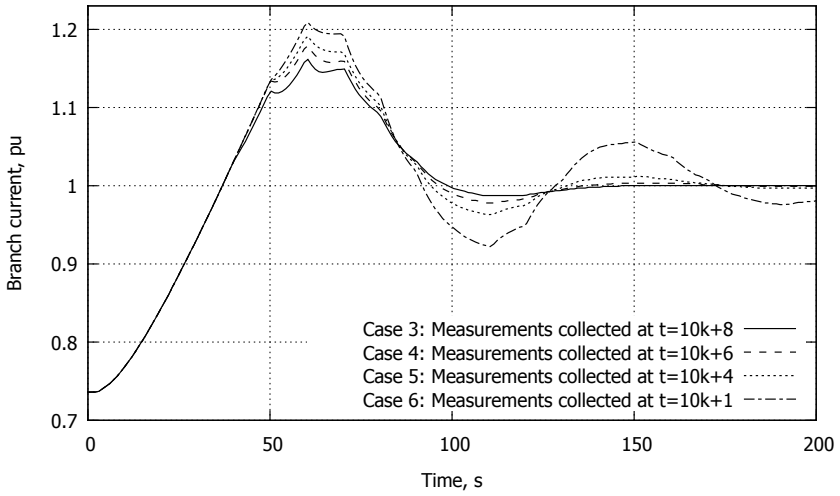

Figure 2.22: The main transformer current

When the transformer experiences an overload while the active power production of the DGUs are increasing (see the time interval from $t = 42$ until $t = 60$ s), early measurements do not allow the controller to be aware of the true severity of the congestion. Thus, the controller does not react as efficiently as it should. For similar reasons, the impact of the implemented corrections are partially observed, making the controller issue a stronger correction in the following steps (see for instance the time interval from $t = 60$ until $t = 90$ s in Fig. 2.22). The latter results in slightly earlier congestion clearing (for instance at $t = 92$ s in Case 6 versus $t = 100$ s in Case 3).

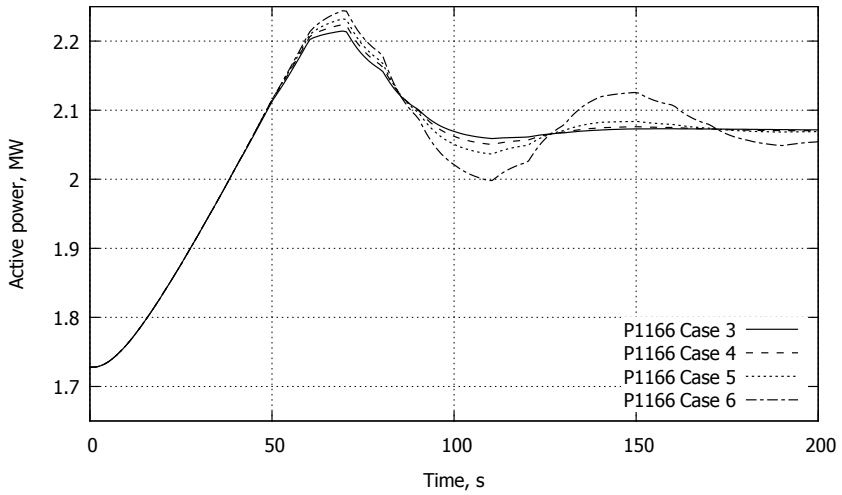

Figure 2.23: Active power produced by DGU 1166

Another impact of those excessive corrections is that even after the congestion has been removed, namely from $t = 92$ to $t = 100$ s depending on the cases, the DGU active powers are still decreased. This can be easily seen in Case 6 in Fig. 2.23, although it is less pronounced in Cases 4 and 5. This is detected by the controller after $t = 100$ s. Subsequently, the controller applies an opposite correction to the DGUs with the objective of maximizing their outputs. This cycle repeats itself, creating oscillations. The later causes a severe (resp. slight) overload in Case 6 (resp. Cases 4 and 5) culminating at $t = 150$ s.

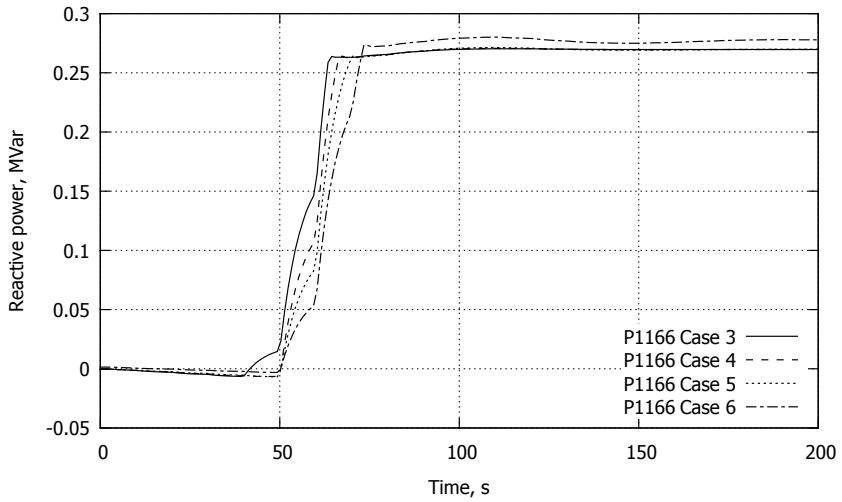

Figure 2.24: Reactive power produced by DGU 1166

As it can be seen in Figs. 2.23 and 2.24, even in Case 5 (measurements collected at $t = kT + 4$), the controller is able to handle the congestion problem very well and the oscillations are very

moderate.

The DGU reactive power follows slightly different trajectories in the various cases, as shown in Fig. 2.24. This can be explained in the same way as for Fig. 2.21.

2.9.2 Tolerance to communication failure

The ability of the controller to compensate for the errors caused by communication failures is investigated in following situations:

- Case 7: the centralized controller interacts properly with all DGUs under its control.
- Case 8: the communication links between the centralized controller and the DGUs located along the feeders that start at nodes 1137 and 1151 (see Fig. 1.4) are broken. The controller is not aware of this communication failure.
- Case 9: similar to Case 8, except that the controller is now aware of the communication failure. This information can be exploited until the problem is solved and the situation is back to Case 7.

In the above three cases, the measurements are collected at times $t = kT + 8$ and the dynamics of the DGUs are not modified (similar to Case 1).

The same test system as in Cases 1 to 6 is used, subject to a slightly different scenario, where: (i) a 12 % of wind speed increase takes place in the same time interval, and (ii) the DGUs are initially producing reactive power so that the DN is injecting active power into the transmission network at (almost) unity power factor.

Figures 2.25, 2.26 and 2.27 show the active powers of the DGUs under the effect of wind increase which results in an overload of the main transformer at around $t = 35$ s, as can be seen in Fig. 2.28. Starting from the next discrete step (i.e. $t = 40$ s), the controller sends corrections in order to curtail active power of all DGUs. Comparing the active powers and currents in the mentioned figures, the following points can be observed:

- Case 7: the active powers of all DGUs are curtailed in successive steps (see Fig. 2.25), and the congestion is fully cleared at $t = 92$ s, see Fig. 2.28.
- Case 8: some DGUs do not receive the command of the centralized controller and hence, operate at MPPT (the upper group in Fig. 2.26) Being unaware, the MPC-based controller keeps sending corrections without effect to those DGUs. As missing DGU contributions

are sensed through the measurements, the controller remarkably succeeds in solving the congestion. Expectedly, it takes more time to complete the task: the overload reaches a higher value (1.25 versus 1.21 pu in Case 7) and it lasts longer (until $t = 100$ s), as can be seen in Fig. 2.28.

- Case 9: now that the controller knows some DGUs cannot cooperate, it updates the available controls, constraints and sensitivity matrices which leads to asking a higher contribution to the remaining DGUs. It is interesting to note the very similar evolution of the transformer current compared to Case 7 (the curves relative to Cases 7 and 9 are indiscernible in Fig. 2.28), although the DGU active powers are totally different. The final value of DGU active outputs are the same in Cases 8 and 9.

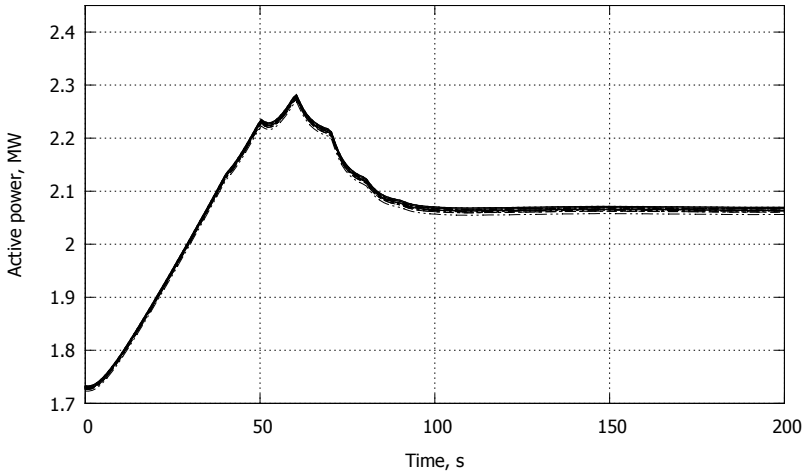

Figure 2.25: Case 7: Active power produced by the DGUs

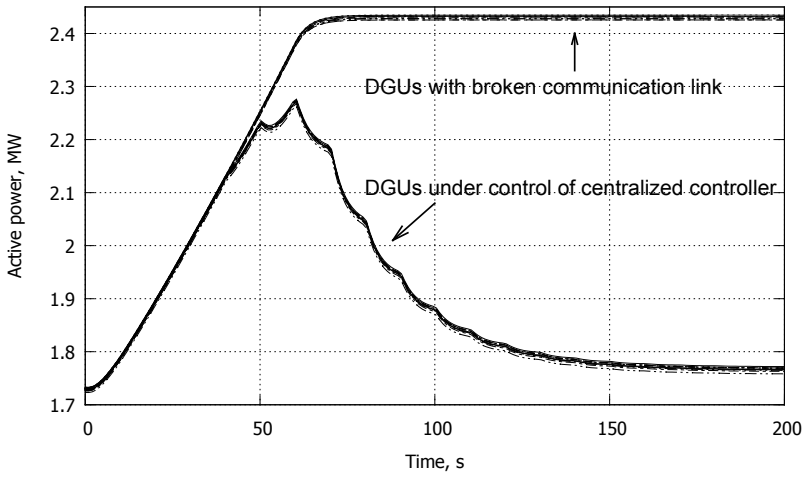

Figure 2.26: Case 8: Active power produced by the DGUs

It should added that, in Case 9, the controller was able to adjust its corrections and obtain a very similar current evolution (compared to Case 7) because the higher active power corrections requested from the participating DGUs were not limited by the rate of change of controls of Eq.(2.36).

In all three cases, the reactive power flow in the transformer is almost zero and consequently, it cannot help for congestion alleviation. Therefore, the reactive powers of the DGUs are left unchanged, as can be seen for instance for Case 7 in Figs. 2.29 and 2.30.

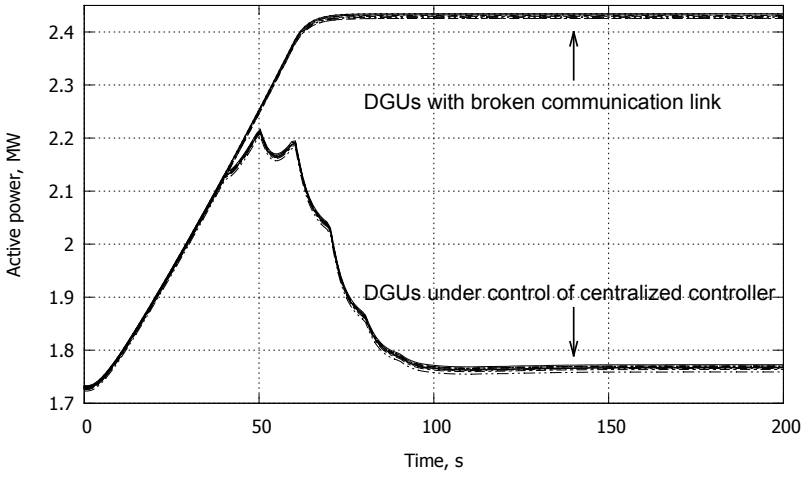

Figure 2.27: Case 9: Active power produced by the DGUs

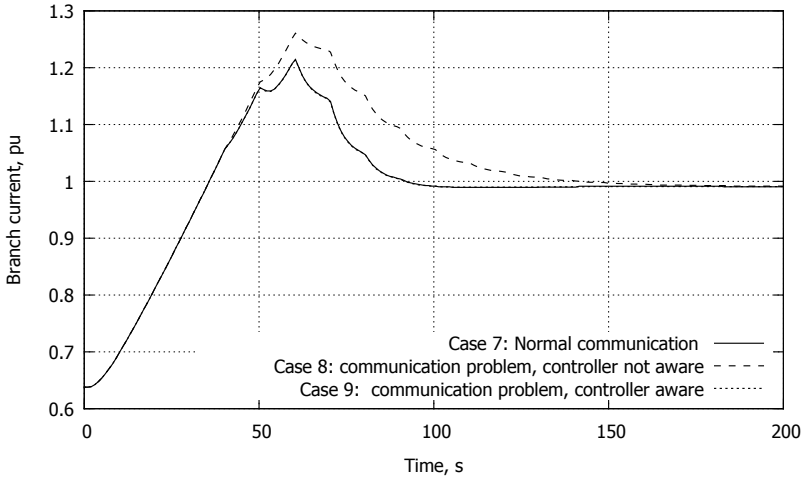

Figure 2.28: The main transformer current for Cases 7, 8 and 9

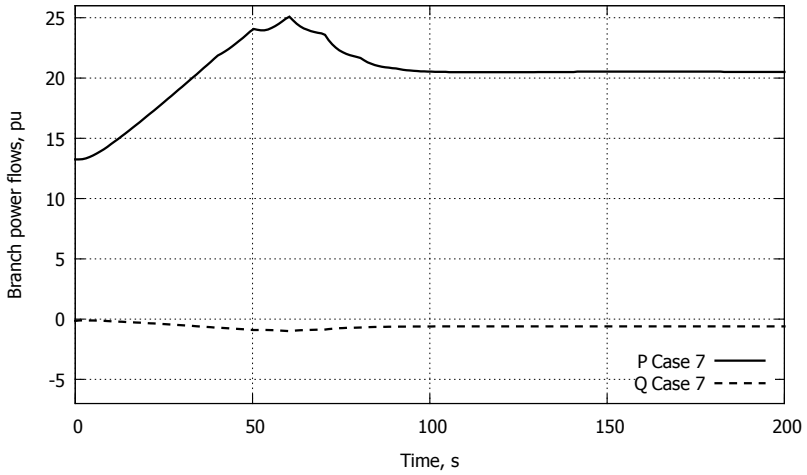

Figure 2.29: Case 7: Power flows in the main transformer

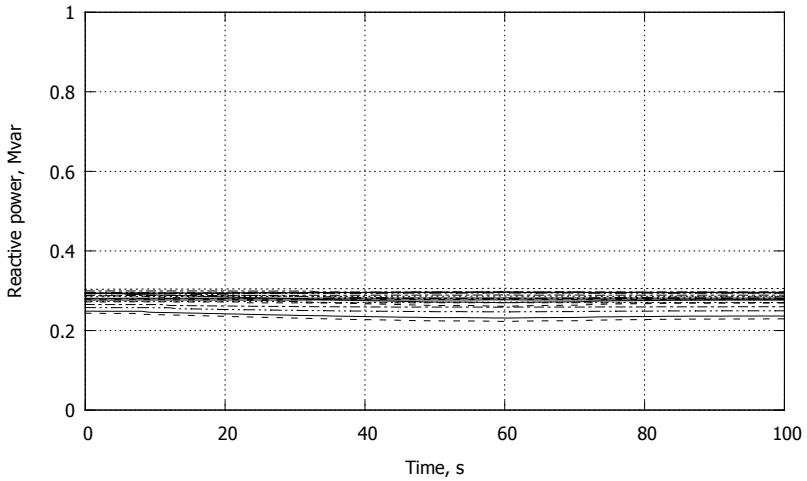

Figure 2.30: Case 7: Reactive power produced by DGUs

2.10 On the use of flexible loads in real-time

In principle, control of flexible loads (or demand side management) can be used as an additional means to alleviate the abnormal situations and, consequently, decrease generation curtailment [GG14].

Let us take a simple example where, initially the total dispersed generation exceeds the load, and the DN is injecting active power into the external grid. Assume that due to an increase of production, the main transformer starts being overloaded. By asking flexible loads located in the DN to increase their consumption at that time, the congestion could potentially be relieved without having to resort to renewable generation curtailment.

Well-known examples of flexible loads are: (i) heat pumps and electric boilers [WBK12, GLC+16a] among industrial, commercials and residential loads [MM16, HP17], and (ii) electric vehicles [TFP15]. These flexibilities are offered under certain technical and financial conditions. For instance, a range of flexibility can be offered (by these loads) in which their main purpose of operation (e.g. temperature regulation of a building by a heat pump) is not distributed. Moreover, these flexibilities are typically offered in return for some financial compensation.

As regards the financial compensations, typically there is an entity (e.g. a load aggregator) gathering the information of a group of flexible loads, and proposing its services to the DSO. This service provides all necessary information: the available potential flexibility and the cost and deviations entailed by the activation of the service. The latter are used by the DSO to take proper decisions [GLC+16b].

Modulating a flexible load at one time often impacts its consumption at later times, which is referred to as the "rebound effect" of energy constrained loads [GLC+16a]. Indeed, those flexible loads are often constrained to consume a specific amount of energy over a certain duration. In the above example, this would imply that after increasing the consumption of flexible loads over a certain time period, the DSO would later on face a decrease of their consumption, which may aggravate the congestion if the problem has not been solved in the meantime. In this context, it is important for a DSO to make decisions by planning over a relevant time horizon. In addition, due to the uncertainty on future power injections from renewable sources and to some extent on the power consumption of loads, it becomes necessary for the DSO to implement an operational planning scheme under uncertainty, which may be very challenging [Gem16].

From the viewpoint of our controller dealing with flexible loads is basically similar to using the powers of DGUs for congestion management or voltage correction. However, besides the above-mentioned energy constraints, there are some practical differences, making it more delicate to embed flexible loads into the control formulation:

1. Active and reactive power of loads cannot be controlled separately; they are linked to each other. Therefore, a change in active power consumption will modify the reactive power consumption too. The latter should be taken into account in the control formulation, namely in the sensitivity of output variables (bus voltages and branch currents) with respect to controls. It is also worth mentioning that, while monitoring the network from the MV level, several types of flexible loads (heat pumps, electric boilers, electric vehicles, industrial and residential ones) are seen as one aggregated load. Given the fact of each type has a different power factor, the average power factor of each aggregated flexible load is varying during the day and might not be easy to estimate.

2. The above-mentioned aggregated flexible loads at LV level are going to have their powers merged with other load powers, connected to the same upstream MV bus.

3. The flexible loads might not respond to requested modulation as expected. Some might follow the command with a delay (say - up to several minutes) and some others might not implement the requested change. This leads to observing a response of aggregated flexible loads as in Fig.2.31.

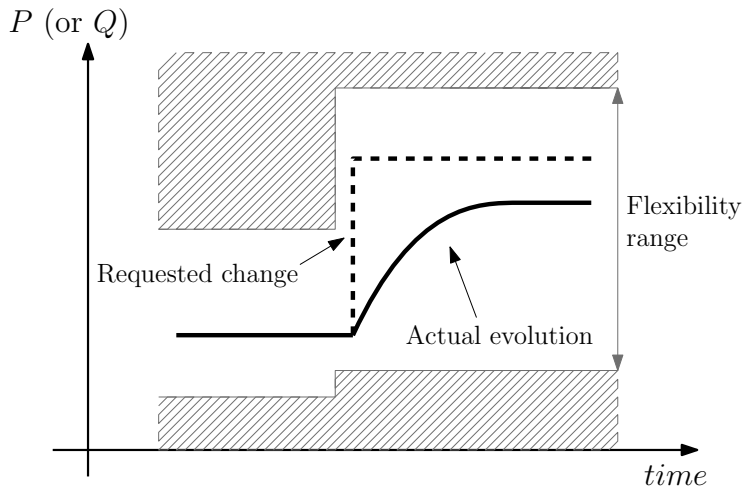

Figure 2.31: Requested change and actual evolution of consumption

A special attention has to be paid to the above point, given that the flexible loads are not all equipped with measurement devices. Thus, the controller would have to communicate the modulations "blindly" (or in "open loop"), expecting that they will be implemented. One way of addressing this issue is by using historical data of the monitored load buses and, estimating what could be the actual evolution in response to a modulation for each type of flexible load. This data could be used to adjust the modulations and hence, reach a more satisfactory result.

4. More importantly, the above-mentioned energy constraints and the time constant of the actual evolution of flexible load powers make it necessary to anticipate their effects on a much longer prediction horizon than considered so far in our controller (typically in the order of half a minute). Therefore, operational planning appears to be a better time frame for decisions dealing with demand response, keeping the real-time controller developed in this thesis as a safeguard against wrong ex ante decisions.

2.11 Extension to control of transformer Load Tap Changer

An LTC is a slowly acting device that controls the voltage on one side of the transformer by acting on its turn ratio in discrete steps [4]. The LTC performs a tap change, without interrupting the power flow, if the controlled voltage remains outside a dead-band for longer than a predefined delay [VV98]. This delay is specified to avoid frequent and unnecessary tap changes that may reduce the LTC lifetime. If more than one step is required, the LTC will move by one step at a time with delay between successive moves .

With the massive insertion of DGUs, distribution systems are prone to voltage violations and some difficulty to manage reactive power exchanges between transmission and distribution systems [VV13a, CLTB14]. Transformers equipped with LTCs connecting the distribution grid to transmission play a role in addressing such issues. In addition, having a global impact on MV voltages, the contribution of the LTC to voltage control can avoid high reactive power demand from DGUs and reactive power flows to/from the transmission system. This last point is of interest since it is in line with future requirements of the European Grid Code on Demand and Connection (DCC)[oTSOfEEE12].

However, LTCs are "fragile" devices with relatively expensive maintenance. Increasing the number of tap changes reduces the LTC lifespan [5]. This device should be used with a lower priority compared to adjustments of DGU reactive powers. This is in line with the fact that power electronics-based DGUs offer higher accuracy and speed.

Voltage support through automatic LTC can be realized in two ways: either it is directly controlled by a centralized entity, or the LTC is left to operate independently according to its local control logic. In the former case, it is convenient to have the tap changes triggered by changes of the voltage set-point itself. In the latter case, its effect should be anticipated by the controller, for good coordination of all available control means. In other words, the future actions of the locally controlled LTC will be treated as a known disturbance by the centralized controller.

The two above-mentioned control strategies, together with the possibility of support from the available DGUs can lead to several situations, in terms of DN controllability, as listed in Table 2.1.

The first case of Table 2.1 represents the situation of many conventional/present-day MV DNs; the HV/MV transformer equipped with LTC is the only control means to adjust the grid voltages. That

[4] Let us mention that alternative terms are used: on-load tap changer, under load tap changer, etc. Here we use the simpler term Load Tap Changer, as in [VV98].

[5] The lifespan (maximum number of switchings without needing maintenance) depends on technology used for the LTC, operational condition, site condition, etc. For HV/MV transformers serving varying load, this value for a typical resistor type oil-immersed LTC with traditional arc quenching is 50,000-100,000 times, and 200,000-500,000 times with a vacuum interrupter [OLT]

Table 2.1: Control means in distribution network

	LTC	DGU
1	**active (controlled locally)**	**passive**
2	**passive**	**active**
3	**active (controlled locally)**	**active**
4	**active (controlled centrally)**	**active**

is to say, either there is no DGUs in the grid (passive distribution network) or the existing DGUs are not participating in control. In such a case the LTC controls the voltage of a single bus. The latter can be the transformer MV terminal or a remote MV bus. Taking into account the historical voltage profiles at different buses of the network, the voltage set-point is properly adjusted in different seasons/months to avoid voltage violations at other buses of the grid [Kul14, FTI+07].

The second case in Table 2.1 deals with active distribution networks where DGUs are used to mitigate unsatisfactory voltages. The tap position, on the other hand, is fixed; hence, it does not contribute to voltage control. The DGUs are controlled as already detailed.

In the third case both the DGUs and the LTC contribute to keeping the voltages within the specified limits. As in the first case, the LTC acts to maintain its controlled voltage within a permitted range. The DGU outputs can be adjusted either locally or remotely [VV13a].

The last case in Table 2.1 is similar to the third one, except that the voltage set-point of the LTC is also adjusted by the centralized controller. A discrete variable can be integrated into the formulation of the centralized controller (resulting in mixed integer programming) to reflect the nature of this device [MCD+17]. Alternatively, to decrease the complexity and computational burden, a continuous approximation of the LTC effects can be embedded into the formulation [CFMS11, VV13b].

In both approaches, the non-linearities of the LTC control loop, namely the voltage dead-band and the time delays, should be taken into account for a more accurate anticipation of the voltage variations [Mor16].

The necessary extensions of the formulation, detailed in Section 2.5, to integrate the LTC as a voltage regulation device, either independently (Case 3 in Table 2.1) or in a coordinated manner (Case 4 in Table 2.1), are detailed in the rest of this section.

2.11.1 Incorporation of LTC as an independent control device

A generic model of the LTC control loop, aimed at maintaining the voltage of the controlled bus within a target range, is illustrated in Fig. 2.32. If the difference between the measured voltage V_{tr}^{meas} and its reference value V_{ref} remains outside the dead-band $[-d,\ d]$ for longer than t^{act}, a tap change will be triggered [Cal84]. V_{tr} is taken at the MV end of the transformer.

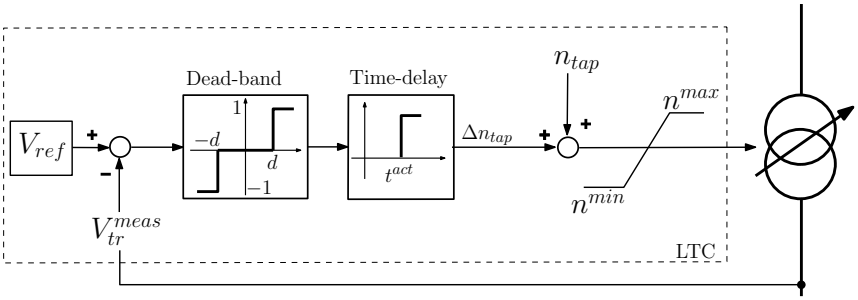

Figure 2.32: Generic model of voltage control loop of an LTC operating independently, inspired of [Cal84, Mor16]

Although the LTC is operating independently, i.e. without taking other controls into account, its operation can be predicted from basic data of the above generic model. The voltage set-point of the LTC, V_{ref}, is infrequently updated (for instance, different settings for different months/seasons). The controlled bus voltage V_{tr}^{meas} is usually known in the Distribution Management System, since this important bus is usually provided with measurement devices. Having these two values together with the dead-band and delay data, the centralized controller (hosted by the DSO) is able to anticipate the LTC operations and their impact on network voltages. To this purpose, the controller needs to estimate the number as well as the time of tap changes.

By assuming that a tap change produces a ΔV_d variation (in absolute value) of the controlled voltage, the number of tap changes can be roughly estimated by:

$$N_{op} = \begin{cases} roundup[\dfrac{V_{ref} - V_{tr}^{meas} - d}{\Delta V_d}], & \text{if } V_{ref} > V_{tr}^{meas} + d \quad \text{(tap change to increase } V_{tr}\text{)} \\ \\ roundup[\dfrac{V_{tr}^{meas} - d - V_{ref}}{\Delta V_d}], & \text{if } V_{ref} < V_{tr}^{meas} - d \quad \text{(tap change to decrease } V_{tr}\text{)} \end{cases} \tag{2.50}$$

where the function $roundup$ provides the nearest larger integer. We remind that d is half the LTC dead-band. Note that the value of ΔV_d can be obtained from the transformer technical data sheet, and is also measurable after an LTC action occurs. This value is assumed constant and known.

Furthermore, the times of LTC actions can be estimated as:

for $j = 1, \ldots, N_{op}$:

$$t_j^{act} = t_k + T_{f0} + T_f(j-1) \tag{2.51}$$

Here, t_k is the present time, T_{f0} is the time delay for the first step and T_f the time delay for each subsequent tap step. The controller can use this information to anticipate the future voltage changes due to the operation of the LTC. In order to do so, the MPC controller must extend its prediction horizon N_p until the last predicted LTC control action is included. An illustration of this is provided in Fig. 2.33. At instant k, it is predicted from (2.50) and (2.51) that three tap changes will take place at t_1^{act}, t_2^{act} and t_3^{act}, respectively, with t_2^{act} and t_3^{act} falling beyond the control horizon. In order to account for all these LTC actions, the controller extends its prediction horizon up to the smallest discrete time larger than t_3^{act}.

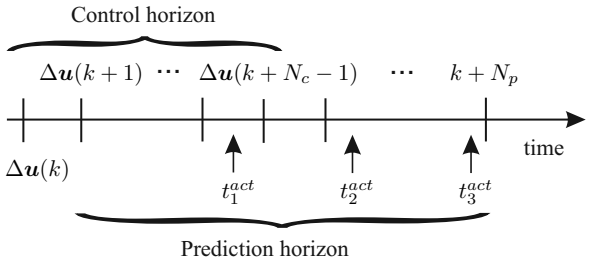

Figure 2.33: Extension of prediction horizon to include predicted LTC actions

The voltage changes are estimated using the sensitivities of bus voltages and branch currents to the LTC controlled voltage, as an extension of what was explained in Section 2.6. More precisely, the tap position changes are handled as known disturbances, accounted for by replacing (2.31, 2.32) as follows:

for $i = 1, \ldots, N_p$:

$$\begin{aligned} \boldsymbol{V}(k+i \mid k) =& \boldsymbol{V}(k+i-1 \mid k) + \boldsymbol{S}_V \left[\boldsymbol{u}(k+i-1) - \boldsymbol{u}(k+i-2)\right] \\ &+ \frac{\partial \boldsymbol{V}}{\partial V_{tr}} \Delta V_d \, \gamma(k+i) \end{aligned} \tag{2.52}$$

$$\begin{aligned} \boldsymbol{I}(k+i \mid k) =& \boldsymbol{I}(k+i-1 \mid k) + \boldsymbol{S}_I \left[\boldsymbol{u}(k+i-1) - \boldsymbol{u}(k+i-2)\right] \\ &+ \frac{\partial \boldsymbol{I}}{\partial V_{tr}} \Delta V_d \, \gamma(k+i) \end{aligned} \tag{2.53}$$

with $\gamma \in \{-1, 0, 1\}$ is equal to +1 (resp. -1) for the instants when tap changes to increase (resp. decrease) the MV voltages have been predicted, and zero otherwise. $\frac{\partial \boldsymbol{V}}{\partial V_{tr}}$ (resp. $\frac{\partial \boldsymbol{I}}{\partial V_{tr}}$) is the sensitivity matrix of the bus voltage (resp. branch current) magnitudes with respect to the voltage at the controlled bus. However, in practice, $\frac{\partial \boldsymbol{I}}{\partial V_{tr}}$ has very small elements, and can be set to zero, resulting in the same equation as (2.32).

2.11.2 Incorporation of LTC as a centrally controlled device

For simplicity (since it would be too expensive to update the many LTCs in operation) it is proposed to leave the LTC local control unchanged but act on the LTC set-point V_{tap} if appropriate. Therefore, tap changes will be triggered when changes in operating conditions make the controlled voltage V_{tr}^{meas} leave the dead-band, or when the controller requests a change of V_{tap} such that $V_{tap} - V_{tr}^{meas}$ falls outside the dead-band. Thus the model of Fig. 2.33 still applies but with the fixed reference V_{ref} replaced by the adjustable set-point V_{tap}.

Clearly, the control variables are the now active powers ($\boldsymbol{P}_g$) and reactive powers ($\boldsymbol{Q}_g$) produced by the various DGUs, together with the controlled voltage V_{tr}. The latter will be further used to determine the proper value of V_{tap} taking into account the non-linearity imposed by the LTC dead-band. The controls are thus grouped in the vector $\boldsymbol{u}(k)$, relative to time k:

$$\boldsymbol{u}(k) = [\boldsymbol{P}_g^T(k), \boldsymbol{Q}_g^T(k), V_{tr}(k)]^T \tag{2.54}$$

where ^{T} denotes transposition. Coming back to Eq. (2.30), the active and reactive powers have time-varying reference values, denoted by $\boldsymbol{P}_{ref}(k)$ and $\boldsymbol{Q}_{ref}(k)$, respectively; for the LTC the reference is the constant V_{ref} value already defined in Section 2.11.1.

Obviously, the sensitivity matrices $\boldsymbol{S}_V$ and $\boldsymbol{S}_I$ have an additional column related to the new control variable V_{tr}:

$$\boldsymbol{S}_V = \Big[\frac{\partial \boldsymbol{V}}{\partial \boldsymbol{P}_g}, \frac{\partial \boldsymbol{V}}{\partial \boldsymbol{Q}_g}, \frac{\partial \boldsymbol{V}}{\partial V_{tr}}\Big] \tag{2.55}$$

$$\boldsymbol{S}_I = \Big[\frac{\partial \boldsymbol{I}}{\partial \boldsymbol{P}_g}, \frac{\partial \boldsymbol{I}}{\partial \boldsymbol{Q}_g}, \frac{\partial \boldsymbol{I}}{\partial V_{tr}}\Big] \tag{2.56}$$

The objective is to minimize the sum of squared deviations, over the N_c future steps, between the controls and their references:

$$\begin{aligned} \min_{\boldsymbol{P}_g, \boldsymbol{Q}_g, \boldsymbol{V}_{tr}, \boldsymbol{V}, \boldsymbol{I}, \boldsymbol{\varepsilon}} \quad & \sum_{i=0}^{N_c-1} \|\boldsymbol{P}_g(k+i) - \boldsymbol{P}_{ref}(k+i)\|^2_{\boldsymbol{R}_1} + \\ & \sum_{i=0}^{N_c-1} \|\boldsymbol{Q}_g(k+i) - \boldsymbol{Q}_{ref}(k+i)\|^2_{\boldsymbol{R}_2} + \\ & \sum_{i=0}^{N_c-1} \|V_{tr}(k+i) - V_{ref}\|^2_{R_3} + \sum_{i=1}^{N_p} \|\boldsymbol{\varepsilon}(k+i)\|^2_{\boldsymbol{S}} \end{aligned} \tag{2.57}$$

where the diagonal weighting matrices $\boldsymbol{R}_1$ and $\boldsymbol{R}_2$ and the weighting factor R_3 allow prioritiz-

ing the controls, with usually lower values assigned to the DGU reactive powers than to the tap changer. The last term in (2.57) (involving the prediction horizon N_P) is aimed at relaxing the inequality constraints in case the optimization problem is infeasible; the entries of $\boldsymbol{S}$ are given very high values, forcing the constraints to be satisfied when possible.

Given the fact that any tap change computed by the controller at time k will be actuated in the LTC with a time delay, i.e. at $k+f$ where f is obtained by translating the LTC time delay in the proper number of discrete steps, the prediction horizon must be large enough to account for the impact of the LTC actions in the formulation of predicted network evolution, i.e. $N_p > f$. Moreover, to properly include this delay into the formulation, the expression of the predicted voltages and currents over the prediction horizon N_p are divided into two parts, namely until and after the future time instant $k+f$, as follows:

for $i = 1, \ldots, f$:

$$\begin{aligned}\boldsymbol{V}(k+i \mid k) =& \boldsymbol{V}(k+i-1 \mid k) + \frac{\partial \boldsymbol{V}}{\partial \boldsymbol{P}_g}\left[\boldsymbol{P}_g(k+i-1) - \boldsymbol{P}_g(k+i-2)\right] \\ &+ \frac{\partial \boldsymbol{V}}{\partial \boldsymbol{Q}_g}\left[\boldsymbol{Q}_g(k+i-1) - \boldsymbol{Q}_g(k+i-2)\right]\end{aligned} \tag{2.58}$$

$$\begin{aligned}\boldsymbol{I}(k+i \mid k) =& \boldsymbol{I}(k+i-1 \mid k) + \frac{\partial \boldsymbol{I}}{\partial \boldsymbol{P}_g}\left[\boldsymbol{P}_g(k+i-1) - \boldsymbol{P}_g(k+i-2)\right] \\ &+ \frac{\partial \boldsymbol{I}}{\partial \boldsymbol{Q}_g}\left[\boldsymbol{Q}_g(k+i-1) - \boldsymbol{Q}_g(k+i-2)\right]\end{aligned} \tag{2.59}$$

for $i = f+1, \ldots, N_p$:

$$\begin{aligned}\boldsymbol{V}(k+i \mid k) =& \boldsymbol{V}(k+i-1 \mid k) + \frac{\partial \boldsymbol{V}}{\partial \boldsymbol{P}_g}\left[\boldsymbol{P}_g(k+i-1) - \boldsymbol{P}_g(k+i-2)\right] \\ &+ \frac{\partial \boldsymbol{V}}{\partial \boldsymbol{Q}_g}\left[\boldsymbol{Q}_g(k+i-1) - \boldsymbol{Q}_g(k+i-2)\right] \\ &+ \frac{\partial \boldsymbol{V}}{\partial V_{tr}}\left[V_{tr}(k+i-1-f) - V_{tr}(k+i-2-f)\right]\end{aligned} \tag{2.60}$$

$$\begin{aligned}\boldsymbol{I}(k+i \mid k) =& \boldsymbol{I}(k+i-1 \mid k) + \frac{\partial \boldsymbol{I}}{\partial \boldsymbol{P}_g}\left[\boldsymbol{P}_g(k+i-1) - \boldsymbol{P}_g(k+i-2)\right] \\ &+ \frac{\partial \boldsymbol{I}}{\partial \boldsymbol{Q}_g}\left[\boldsymbol{Q}_g(k+i-1) - \boldsymbol{Q}_g(k+i-2)\right] \\ &+ \frac{\partial \boldsymbol{I}}{\partial V_{tr}}\left[V_{tr}(k+i-1-f) - V_{tr}(k+i-2-f)\right]\end{aligned} \tag{2.61}$$

The prediction is initialized with $\boldsymbol{V}(k \mid k)$ and $\boldsymbol{I}(k \mid k)$ set to the last received measurements. $\boldsymbol{u}(k-1)$ is also set to last collected measurements.

The inequality constraints on control and controlled variables are the same as in (2.33-2.36), and not repeated here. The limits on the new control variable V_{tr} and its rate of change are as follows:

for $i = 0, \ldots, N_c - 1$:

$$V_{tr}^{min} < V_{tr}(k+i) < V_{tr}^{max} \tag{2.62}$$

$$-\Delta V_d < V_{tr}(k+i) - V_{tr}(k+i-1) < \Delta V_d \tag{2.63}$$

where V_{tr}^{min} and V_{tr}^{max} correspond to the minimum and maximum transformer tap positions, respectively. The inequality (2.63) expresses that the tap cannot be moved by more than one position at a time.

LTC voltage set-point manipulation

To ensure that tap changes are actuated as computed, the non-linearity introduced by the LTC dead-band must be accounted for by properly manipulating the LTC voltage set-point V_{tap}.

In this regard, if the computed change in V_{tr} is large enough, the LTC voltage set-point $V_{tap}(k)$ is set outside the range $[V_{tr}^{meas}(k) - d\ ,\ V_{tr}^{meas}(k) + d]$ to make sure a tap change will be triggered. To evaluate whether the computed change in V_{tr} is large enough, the value of $V_{tr}(k) - V_{tr}(k-1)$ is compared with ΔV_d, the variation of the controlled voltage produced by one tap change. V_{tap} is adjusted as follows:

$$V_{tap}(k) = \begin{cases} V_{tr}^{meas}(k) + d, & \text{if } V_{tr}(k) - V_{tr}(k-1) > \alpha\, \Delta V_d \\ V_{tr}^{meas}(k) - d, & \text{if } V_{tr}(k) - V_{tr}(k-1) < -\alpha\, \Delta V_d \\ V_{tr}^{meas}(k) \quad , & \textit{otherwise} \end{cases} \tag{2.64}$$

where the parameter α is smaller than one. It has been set to 0.5 in our simulations.

It can be easily seen from (2.64) that small computed changes are discarded and not communicated to the LTC. This is an inevitable error when using a continuous variable (the LTC voltage set-point) to control a discrete variable (the tap position). But it is appealing to avoid introducing complexity in the formulation, and it is left to MPC to compensate for this approximation.

Note finally that, in order to have the LTC act, the adjusted voltage set-point V_{tap} must remain outside the dead-band for longer than the initial tapping delay.

2.11.3 Simulation results

The extended formulation presented above has been tested on the Belgian distribution network and the results will be presented in Chapter 3.

2.12 Conclusion

This chapter has presented a corrective control of abnormal voltages and currents relying on the concept of MPC. It has been demonstrated how temporary abnormal conditions can be corrected with coordinated actions on the DGU power outputs.

The main features of the scheme are recalled hereafter:

- Bus voltages and branch currents are corrected so that they remain within an acceptable range of operation. Hence, the controller does not act unless these limits are violated or the reference values of productions have been changed.
- The controller discriminates between “cheap” and “expensive” control actions.
- Being based on multiple time step optimization, these controller is able to smoothly drive the system from the current to the targeted operation region.
- Embedding some useful techniques, such as targeting a range for the controlled variables (outputs) as terminal constraints rather than a particular value, proper stability of the proposed control scheme can be expected, as confirmed by numerous tests.
- Due to the repeated computations and the closed-loop nature of MPC, model inaccuracies, communication failures, and unexpected dynamics of the system components can be accommodated.
- Lastly, the controller can also anticipate the effect of events that will be take place in the future. Accounting for future control actions avoids premature and maybe unnecessary control actions.

Flexible loads have been envisaged as additional control means, but discussions have been provided on challenges and practical issues to embed them into the control formulation.

The LTC has been incorporated in the formulation. It can be left to operate independently with the impact of its actions being anticipated in the prediction of the future voltages. Alternatively, its voltage set-point can be directly controlled by the centralized controller. To do so, a continuous

approximation of its effects has been considered and the necessary adjustments have been done to account for its dead-band and time delays.

Chapter 3

Application to a real-life distribution system

In the context of the GREDOR project supported by theWallonia region of Belgium (https://gredor.be), the performance of the centralized real-time controller has been evaluated on the test system stemming from a real MV network located in Wallonia, with the objective of examining the system behaviour over future years, when more DGUs would be installed. More precisely, the aim was to evaluate the capability of the real-time controller to address the over- or under-voltage and/or thermal overload issues, and, consequently, postpone network reinforcements. The main attractiveness of those tests was to assess the controller response over full days, including some periods where corrective actions were needed.

3.1 Introduction

This Chapter reports on the comprehensive testing of our centralized, coordinated control algorithm (detailed in Section 2.5 and extended in Section 2.11) aimed at correcting abnormal voltages and/or thermal overloads in a distribution network hosting numerous dispersed generation units. The tests used data of a real distribution network and plausible scenarios of future penetration of renewable energy sources. The dynamic evolution of the system has been simulated, with the controller in action, over full days where limit violations were taking place in its absence. Its capability to resolve the voltage and/or thermal issues is demonstrated. This corrective control allows postponing expensive network reinforcements and avoids to the largest possible extent curtailment of distributed generation using renewable energy sources.

The tests were performed in the context of the GREDOR project supported by the Wallonia region of Belgium (https://gredor.be), using the model of an existing distribution grid operated by a DSO partner of the project. The future year of 2030 has been considered, with typical consumption and plausible production evolutions, leading to over- or under-voltage and/or thermal overload problems in some days of that year, and for some durations during those days. The focus is on a representative sample of those situations.

The LTC control is as detailed in Section 2.11.2. The test system has been already introduced in Section 1.4.3. The overall control structure is presented in Section 3.2. To make this chapter self-supporting, some material from Chapter 2 is briefly recalled in that section. An overview of the selected scenarios and controller settings is given in Section 3.3. Section 3.4 is devoted to the results, followed by consideration on the computing times in Section 3.5. Finally, conclusions are drawn in Section 3.6.

3.2 Application of the formulation to the DGUs and transformer of a distribution grid

The environment of the proposed control scheme is sketched in Fig. 3.1. It is obtained by combining operating Modes 1 and 2 introduced in Section 2.7, with the LTC added as control means.

The available control means are the active and reactive powers of DGUs together with the voltage set point of the transformer LTC. The control scheme is aimed at being executed by a central entity, typically the DSO. This entity collects measurements in real-time and sends back control corrections, if required.

The measurements consists of active and reactive power productions and terminal voltages of the

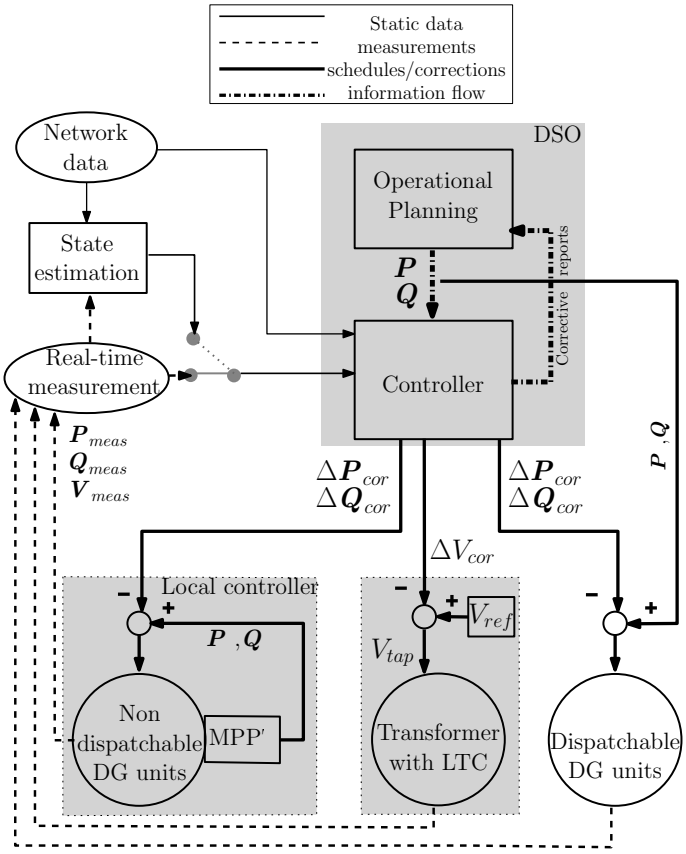

Figure 3.1: Real-time control scheme.

DGUs, active and reactive power flows in critical (potentially congested) branches, and possibly some other bus voltages. Instead of measurements, the controller could also rely on the results of a state estimator (as suggested in Fig. 3.1), for improved system monitoring.

Once the controller observes (or predicts) limit violations, it computes and sends corrections to the DGUs of concern, and possibly the transformer LTC. The corrections are the differences between the reference and the computed controls, i.e.

$$\Delta \boldsymbol{P}_{cor}(k) = \boldsymbol{P}_{ref}(k) - \boldsymbol{P}_{g}(k) \tag{3.1a}$$

$$\Delta \boldsymbol{Q}_{cor}(k) = \boldsymbol{Q}_{ref}(k) - \boldsymbol{Q}_{g}(k) \tag{3.1b}$$

$$\Delta V_{cor}(k) = V_{ref}(k) - V_{tap}(k) \tag{3.1c}$$

It must be recalled that these corrections remain at zero as long as no limit violation is observed (or predicted), and come back to zero (together with the objective function (2.57)) as soon as operation is no longer constrained.

Furthermore, a distinction is made between *dispatchable* and *non-dispatchable* DGUs. The latter are typically wind turbine or PV units operated for Maximum Power Point Tracking (MPPT). In the absence of operation constraints, they are left to produce as much as it can be obtained from their renewable energy sources. The dispatchable units, on the other hand, have their assigned (active and possibly reactive) power production schedules, according to market opportunities or balancing needs, for instance.

As regards the non-dispatchable DGUs, at each time step k, the reference $P_{ref,i}(k)$ of the i-th DGU is set to the maximum power available on that unit. This information is likely to be available to the MPPT controller of the DGU, but is seldom transmitted outside. Those powers are thus estimated from the measurements $\boldsymbol{P}_{meas}$ using the "persistence" model:

for $i = 0, \ldots, N_c - 1$:

$$\boldsymbol{P}_{ref}(k+i) = \boldsymbol{P}_{meas}(k) + \Delta\boldsymbol{P}_{cor}(k-1) \tag{3.2}$$

As long as no power correction is applied, the last term is zero and $\boldsymbol{P}_{meas}$ is used as a short-term prediction of the available power. When a correction is applied, the right-hand side in (3.2) keeps track of what was the available power before a correction started being applied. Using this value as reference allows resetting the DGUs under the desired MPPT mode as soon as system conditions improve.

Dispatchable DGUs, on the other hand, are controlled as follows. The active $\boldsymbol{P}$ and reactive power $\boldsymbol{Q}$ schedules are assumed to be known by the controller. The controller can thus anticipate a violation under the effect of the scheduled change, and correct the productions *ex ante*.

3.3 Selected scenarios and control settings

3.3.1 Selected scenarios

The simulations were run over full days, in order to assess the response of the controller to consumption/generation evolutions at different times of the day.

As already mentioned, historical data of wind speed, solar irradiance and load consumption have been exploited in this study. The data were available for the full year 2013, with a resolution of 15 min; linear interpolation has been used to obtain values at intermediate discrete times.

The following operation limits have been considered : voltages in the range $[0.95, 1.05]$ pu at all buses, and the currents in cables and transformers below their thermal ratings.

The results reported here relate to three scenarios representative of stressed operating conditions:

SD1 : a summer day with high production by the DGUs. Combined with low load, this results in a high power transfer from distribution to transmission, as shown by the evolutions of the power flows in the transformer given in Fig. 3.2. CHP units are not in operation. The voltages at a sample of MV buses are given in Fig. 3.3, showing that some voltages moderately exceed the upper limit. As expected, the voltages increase as one moves from the main substation towards the end of a feeder;

SD2 : same scenario as SD1 but with a higher production by wind generators. The corresponding same power flows are shown with heavy (black) lines in Fig. 3.4. The thermal limit of the transformer is exceeded mainly between $t \simeq 12$ and 15 h. The tap position of the transformer had been adjusted in order to avoid excessive voltages;

WD : a winter day with high power drawn from the transmission system. The wind speed is negligible and the PV units produce little power. Three CHP units come in operation during working hours. The corresponding same power flows are shown in Fig. 3.5. The two jumps in the active power are due to the rapid production changes of the CHP units. The voltage evolutions are given in Fig. 3.6. One mild and one severe under-voltage situation are experienced. In addition, the transformer is overloaded between $t \simeq 18$ and 22 h, but this situation is tolerable due to higher cooling capabilities in winter. It would be definitely safer to use the second transformer, but this option is not considered to demonstrate the effectiveness of the controller.

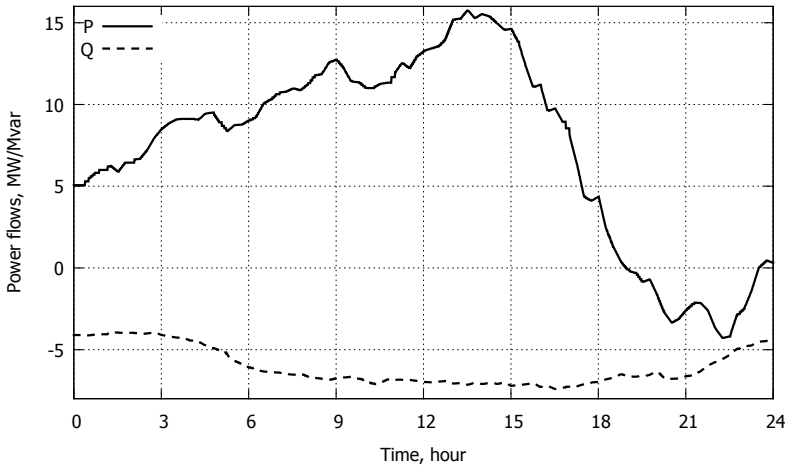

Figure 3.2: SD1, no controller: Active and reactive powers injected into the transmission system

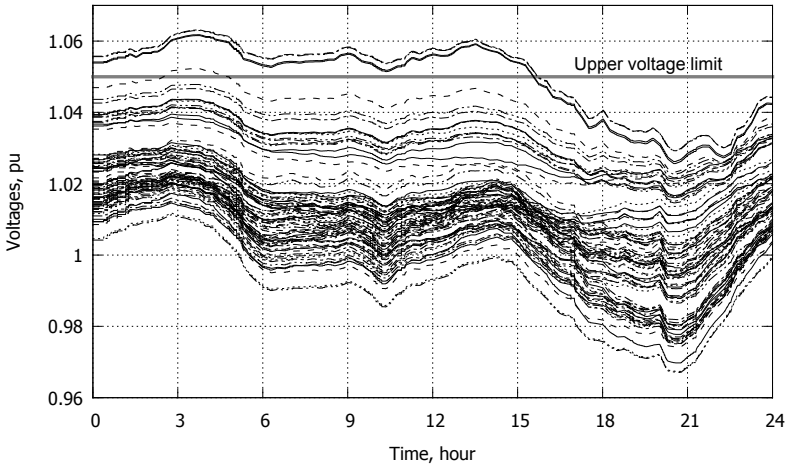

Figure 3.3: SD1, no controller: Voltages at a sample of MV buses

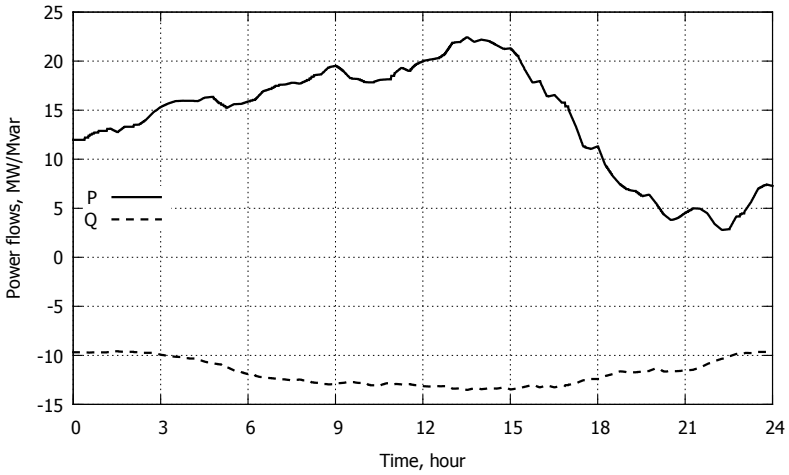

Figure 3.4: SD2, no controller: Active and reactive powers injected into the transmission system

From past recordings it is known that the voltage on the transmission side can vary from 65 kV (0.93 pu) to 77 kV (1.10 pu), depending on the system operating conditions. On the distribution side, however, voltages must be kept within the above mentioned tighter interval. In order to examine the impact of such voltage variations, two cases were considered in the simulations: variable vs. constant voltage on the transmission side of the transformer. In the former case, and in the absence of recorded data, the evolution of the voltage was assumed to be linearly related to the active power flow in the transformer, with the yearly maximum flow from transmission to distribution corresponding to 65-kV, and the yearly maximum opposite flow corresponding to 77-kV.

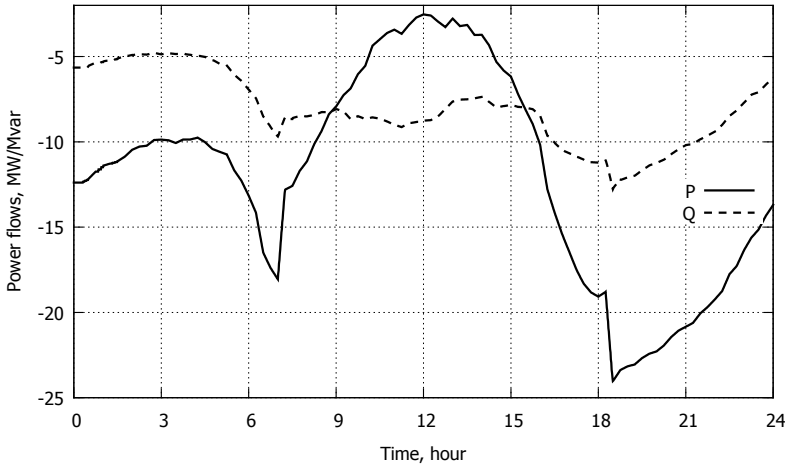

Figure 3.5: WD, no controller: Active and reactive powers injected into the transmission system

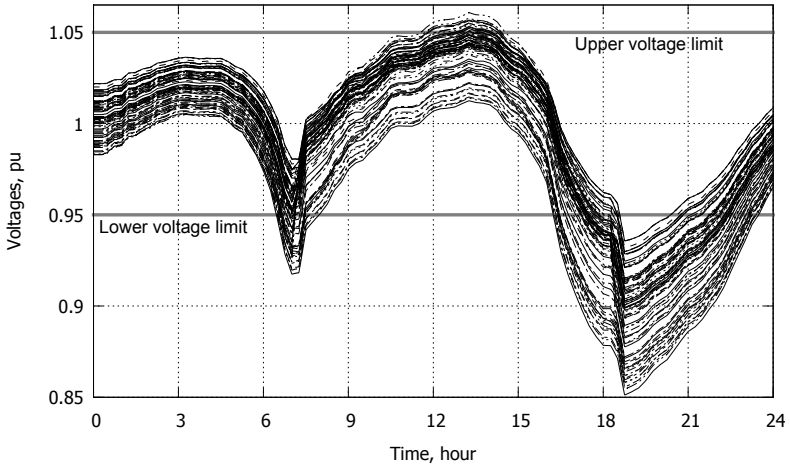

Figure 3.6: WD, no controller: Voltages at a sample of MV buses

3.3.2 Control settings

The CHP units are in operation for air-conditioning purposes mainly, their production schedule is pre-determined. Therefore, these units are categorized as dispatchable DGUs. Their active power schedules are communicated every 15 minutes to the real-time controller, which is thus aware of those productions in advance. On the other hand, the wind and solar units are left to operate in MPPT mode (unless operating conditions do not allow doing so). No prediction of wind speed and solar irradiance is available to the controller.

The measurements are assumed to be received by the controller every 10 seconds, and its corrections sent to the DGUs and the LTC with the same periodicity.

In the considered scenarios in 2030, the time evolutions of wind speed and solar irradiance are assumed to be the same as in the 2013 recordings. Wind turbines and PV units are categorized as non dispatchable units. They are assumed to be internally controlled for MPPT.

Two different capability diagrams are considered for DGUs reactive power support. The first diagram constrains the DGUs to operate between power factors of 0.9 and 1.0 in both under- and over-excited modes (triangular capability curve: see Fig. 3.7). The second capability diagram yields a wider range of reactive power reserve. Operation is allowed inside the polygonal-shaped surface shown in Fig. 3.7. The reactive power output is limited between $0.8P_{max}$ when producing, and $0.6P_{max}$ when consuming. Furthermore, in the case of low or high active power production, tighter limits are imposed. For all types of DGUs, as long as no violation is observed (or predicted), the reactive power is kept at zero with the objective of minimizing internal losses of the units.

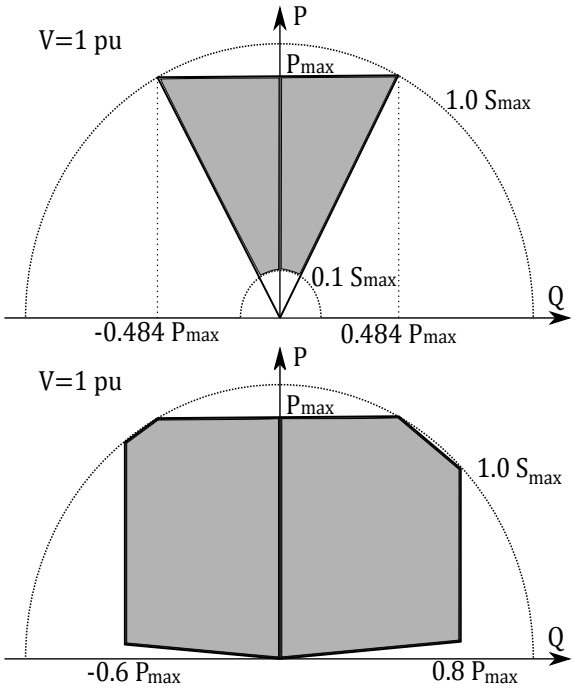

Figure 3.7: DGU capability diagram (triangular: up, polygonal: bottom); operation is allowed in the shaded area

In all simulations the sensitivity matrix $\boldsymbol{S}_I$ has been updated at each discrete step while the $\boldsymbol{S}_V$ matrix has been kept constant at all times, for simplicity and to verify the robustness of the controller.

The control and prediction horizons have been set to $N_c = N_p = 3$. Thus, the "open-loop" control horizon is $3 \times 10 = 30$ seconds. In fact, the time taken by the controller to correct violations "in closed loop", counted from its first action until a steady state is reached with all violations

corrected, is in the order of 60 seconds. This holds true as long as no rate limit (2.36) is imposed, and the references $\boldsymbol{P}_{ref}$ and $\boldsymbol{Q}_{ref}$ are not changed in the meantime. This response time is fast enough for corrective control purposes. Note finally that it can vary with the number of active inequality constraints.

Unless otherwise specified, the voltage set-point of the LTC has been included in the control variables. To avoid excessive solicitation of that device, its control has a lower priority (higher value of R_3 in Eq. 2.57) compared to DGU reactive powers, with the result that it is used only when needed.

3.4 Simulations results and discussion

3.4.1 Case 1: SD1 with constant transmission voltage, triangle-shaped capability diagram

In this case, the voltage on the transmission side of the main transformer is assumed to remain constant, while the DGUs have the triangle-shaped capability diagram shown in the upper part of Fig. 3.7.

The evolutions of the active and reactive powers produced by DGUs are shown in Figs. 3.8 and 3.9, respectively. The resulting voltage evolutions are shown in Fig. 3.10.

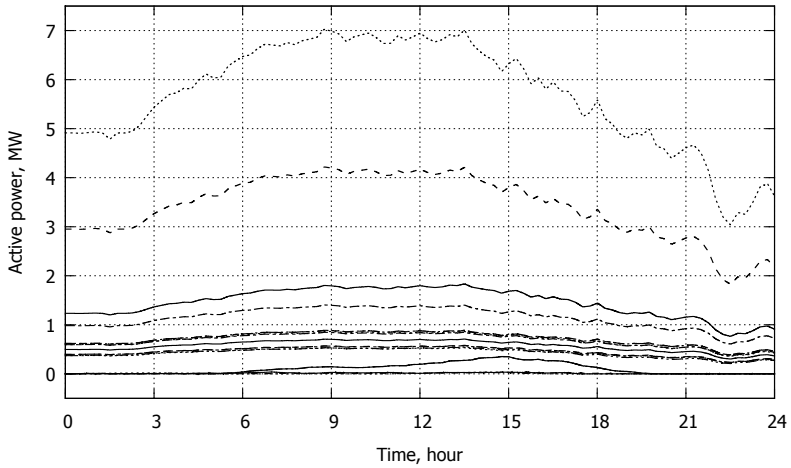

Figure 3.8: Case 1: Active powers produced by DGUs

For a little more than 15 hours, the DGUs are requested to consume reactive power in order to avoid over-voltages at the end of some feeders. It can be seen that after corrective control, the highest among all bus voltages remains equal to (or below) the maximum upper limit of 1.05 pu.

The minimum consumption level is observed between midnight and sunrise. Therefore, from midnight up to $t \simeq 4$ h, the still decreasing consumption combined with some increase of the active generation causes a voltage rise. It is smoothly counteracted by reactive power adjustments of the DGUs to keep the voltages below the limit. Figure 3.9 shows that the maximum correction takes place at $t \simeq 4$ h.

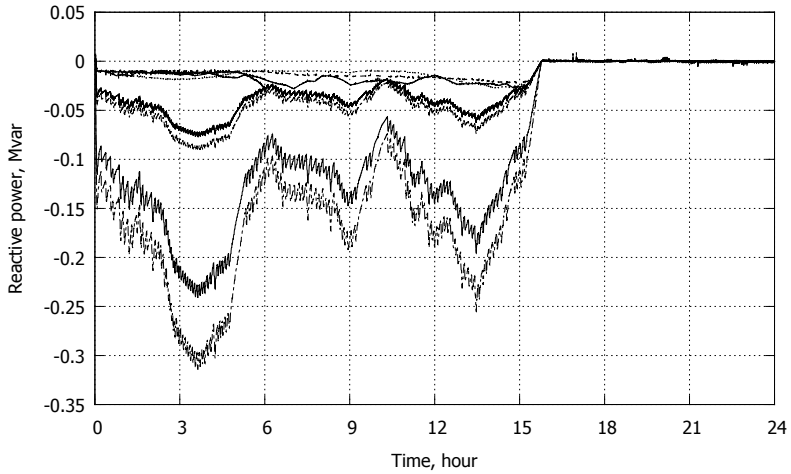

Figure 3.9: Case 1: Reactive powers produced by DGUs

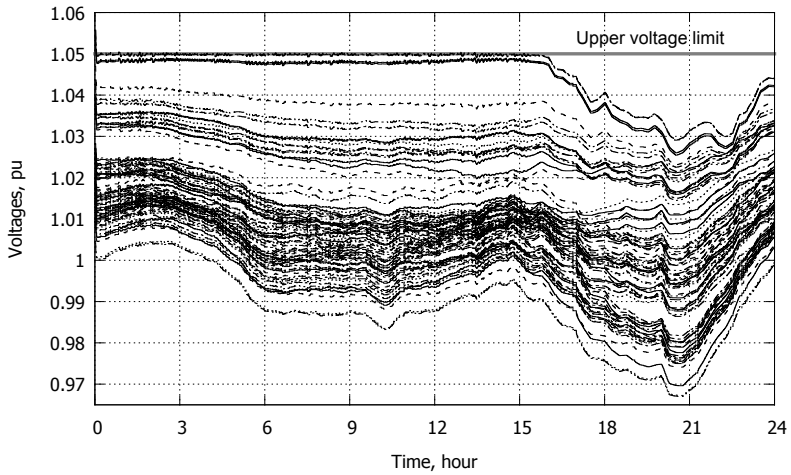

Figure 3.10: Case 1: Voltages of distribution buses

From this time till noon the production keeps on increasing, but its effects are counteracted by the consumption showing its morning ramp. Since the system is controlled in such a way that limits are obeyed with minimum deviation of DGUs from unity power factor, one can observe a "reset" effect bringing the reactive powers towards zero. Thanks to centralized control, those DGUs closer to buses with higher voltage participate more in corrective control. Furthermore, the reactive power support of DGUs is significantly limited by the triangle-shaped capability diagram. In particular, this results in low reactive power reserves on units with low active power output.

During the last third of the day, production decreases while consumption increases. This leads to a decrease of voltages in the system. All voltages move away from the upper limit. Consequently, the DGU reactive powers come back to the desired zero value.

LTC control is not used since the reactive power changes are sufficient, and they have priority through the weighting matrices.

3.4.2 Case 2: SD1 with variable transmission voltage, triangle-shaped capability diagram

This case is identical to Case 1, except for the transmission voltage which varies together with the operating point of the distribution grid. As described at the end of Section 3.3.1, this aggravates the voltage violations in the MV network.

The bus voltages after corrective control are shown in Fig. 3.11, and the DGU reactive powers are displayed in Fig. 3.12. A comparison with Case 1 clearly shows that more reactive power is consumed by the DGUs to keep voltages below the limit. The highest consumption is reached between $t \simeq 12$ to $t \simeq 15$ h. Figure 3.13 shows that this coincides with the largest active power injection in the transmission grid and, consequently, the highest transmission voltage.

On the other hand, the peak demand in the evening causes an under-voltage which is corrected by the controller imposing a small production of reactive power.

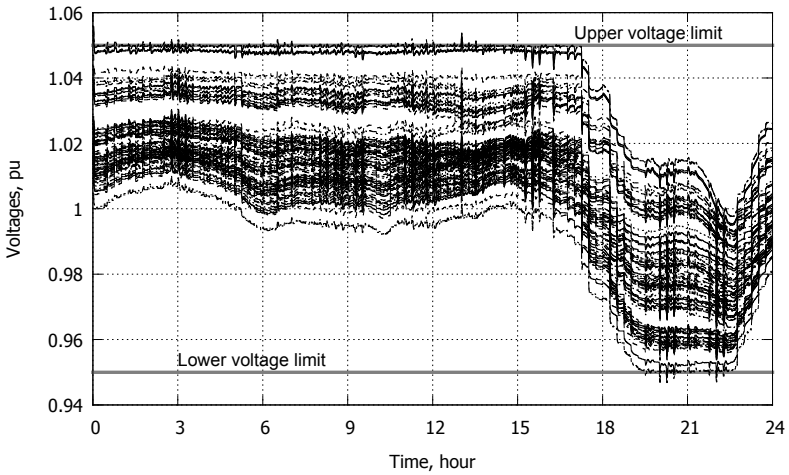

Figure 3.11: Case 2: Voltages of distribution buses

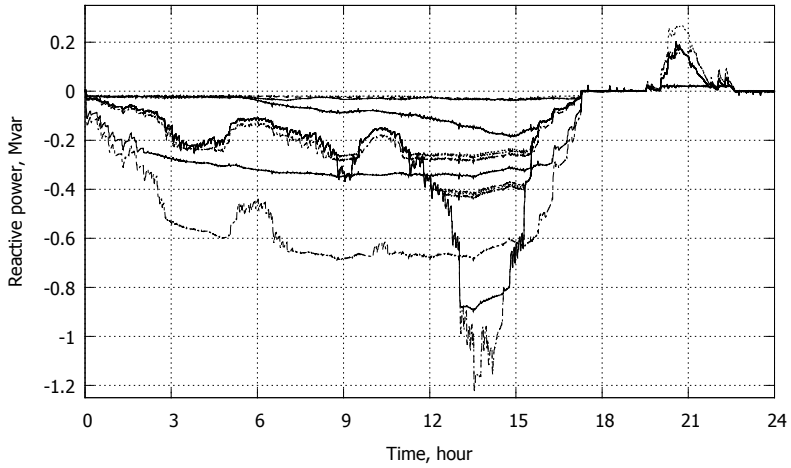

Figure 3.12: Case 2 : Reactive powers produced by DGUs

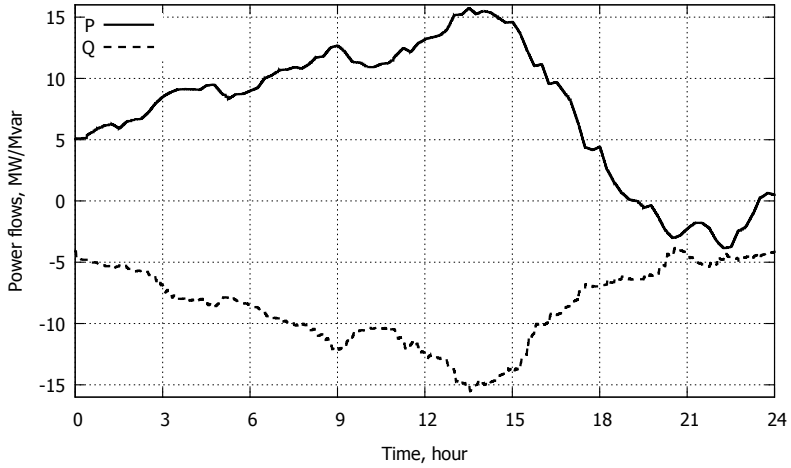

Figure 3.13: Case 2: Active and reactive powers injected into the transmission system

3.4.3 Case 3: SD2 with constant transmission voltage, polygon-bounded capability diagram, LTC non controlled

In this case, the transformer ratio is assumed constant, i.e. V_{tap} is removed from the control vector $\boldsymbol{u}$ in (2.54).

As mentioned previously, Scenario SD2 involves a violation of the transformer thermal limit, as shown by the dashed line in Fig. 3.14 relative to the current in the transformer without corrective control.

At $t \simeq 7$ h the transformer current reaches its limit. This is detected by the centralized controller from the received measurements. The controller corrects this congestion problem by acting first on the DGU reactive powers, which have higher priority. Figure 3.4 showed that the reactive power

is flowing from transmission to distribution network. To alleviate the overload, that flow must be decreased, which requires to increase the DGU reactive power productions. The latter are shown in Fig. 3.15. The solid line, which relates to a large number of DGUs with the same output, shows indeed an increase. However, an increase of all DGU reactive powers would cause over-voltages in the grid. This is why some other DGUs have their reactive power decreased, as shown by the dotted curves in Fig. 3.15.

The reactive powers are exploited until the highest voltage reaches the allowed upper limit, as shown in Fig. 3.16. At this point, the active powers of some DGUs must be decreased, until the remaining overload is cleared. Figure 3.17 shows the amount of curtailed active power of one DGU, imposed by the centralized controller.

A few hours later, a second thermal violation is detected and corrected in a similar but more pro-

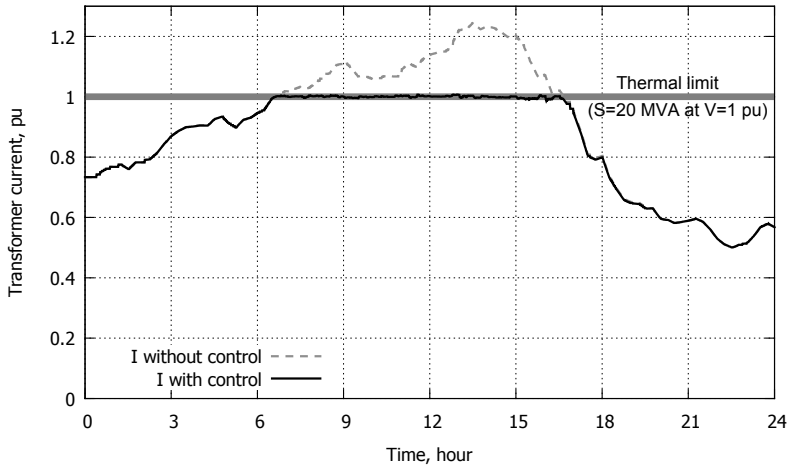

Figure 3.14: Case 3: Current in the transformer

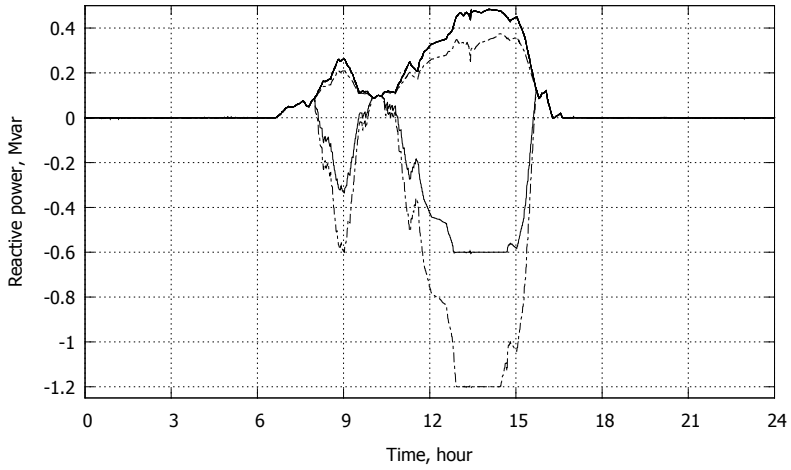

Figure 3.15: Case 3: Reactive powers produced by the DGUs

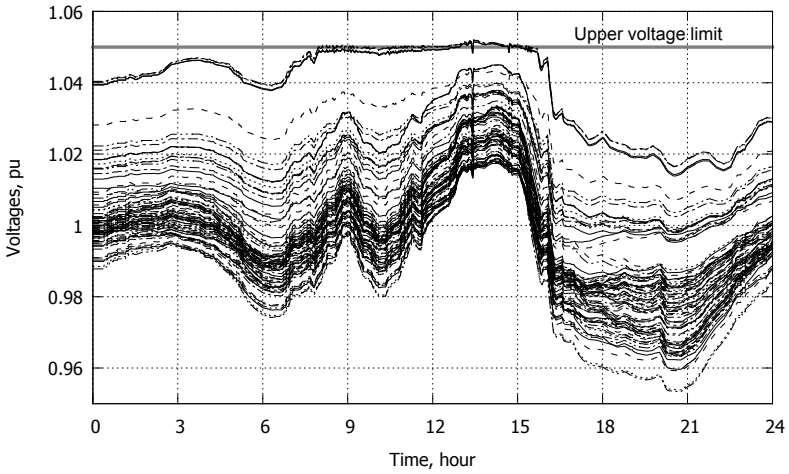

Figure 3.16: Case 3: Voltages of distribution buses

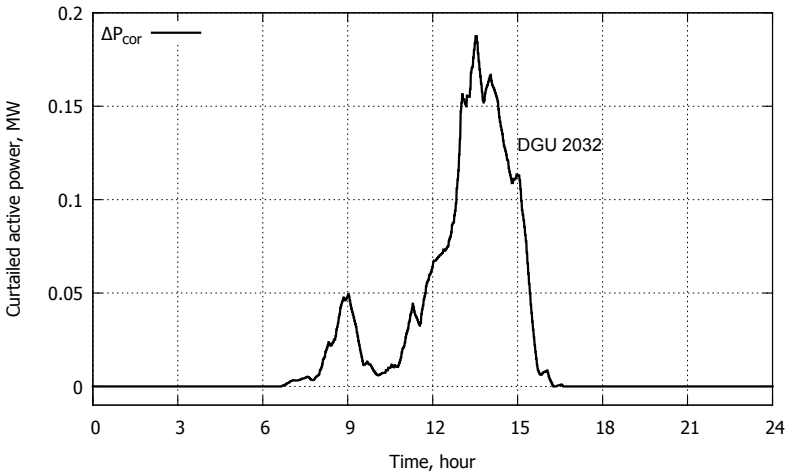

Figure 3.17: Case 3: Active power curtailment applied to DGU 2032

nounced manner. Figure 3.15 shows that two DGUs reached their maximum absorption capability.

At time $t \simeq 16$ h, the power consumption of loads increases, while the wind speed decreases. This allows the powers of the wind units to progressively reach their maximum available values, as confirmed by Fig. 3.17 showing that the correction sent by the controller decreases to zero.

3.4.4 Case 4: SD2 with constant transmission voltage, polygon-bounded capability diagram

This case is similar to the previous one, except that the centralized controller again can adjust the voltage set-point V_{tap} of the transformer LTC. The latter can be used to mitigate the over-voltages caused by DGU reactive powers, as shown hereafter.

The successful correction of the transformer overload is easily seen in Fig. 3.18.

As in Case 3, to reduce the current in the transformer, the reactive power flowing from transmission to distribution must be decreased, which requires to increase the DGU reactive powers. This is shown in Fig. 3.19.

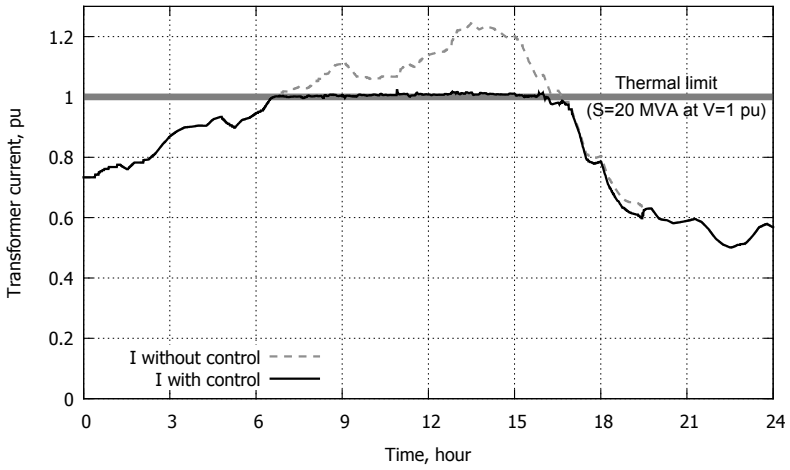

Figure 3.18: Case 4: Current in the transformer

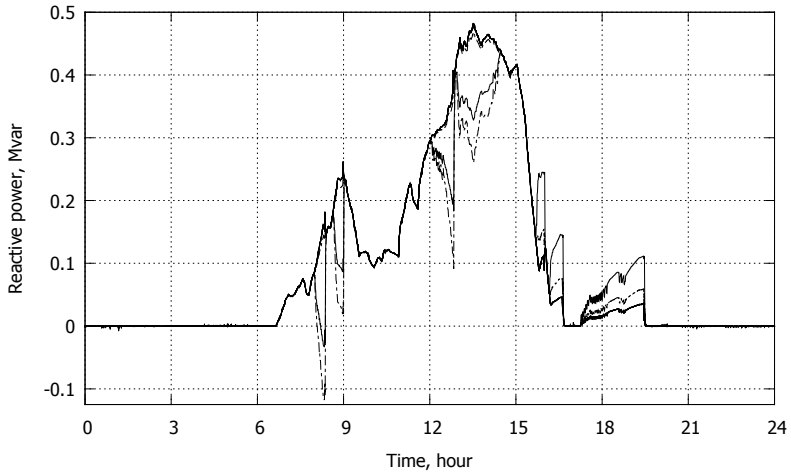

Figure 3.19: Case 4: Reactive powers produced by the DGUs

The evolution of the distribution voltages is given in Fig. 3.20. They are all kept within the allowed limits. As in Case 3, the reactive power injected by the DGUs between $t \simeq 7$ h and $t \simeq 16$ h would lead to over-voltages but the controller prevents this by decreasing the LTC voltage set-point V_{tap}. This takes place at three times, identified with down arrows in Fig. 3.20. The effects are visible in all voltage evolutions. With this contribution by the LTC, there is no need for some DGUs to consume reactive power as in Case 3 (see Fig. 3.15). On the contrary, Fig. 3.19 shows that more DGUs contribute with reactive power production.

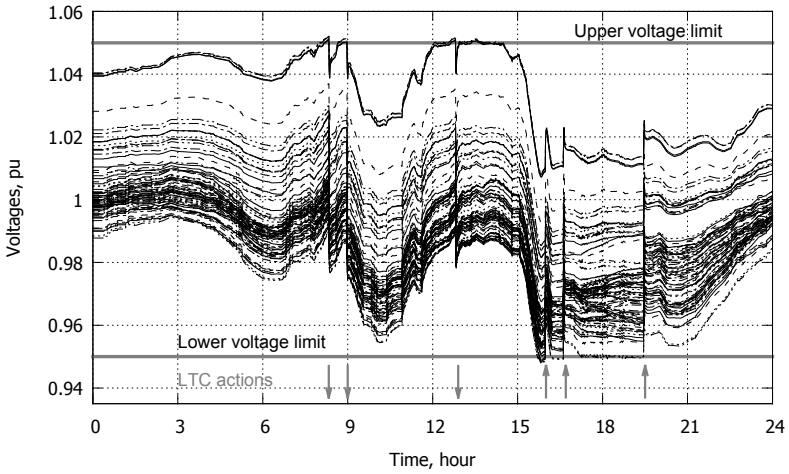

Figure 3.20: Case 4: Voltages of distribution buses

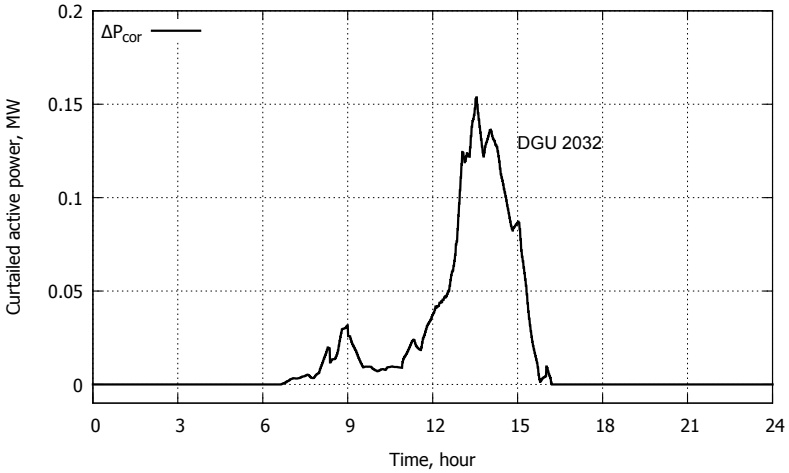

Figure 3.21: Case 4: Active power curtailment applied to DGU 2032

The main benefit of the LTC actions is the smaller amount of active power curtailment in complement to the reactive power corrections. This is illustrated in Fig. 3.21, to be compared with Fig. 3.17 of Case 3. Further evidence is given in Fig. 3.22, which compares the active power flows in the transformer in Cases 3 and 4, respectively. The additional LTC control allows exporting to the transmission system 0.4 MW more, on the average, between $t \simeq 12$ h and $t \simeq 15$ h.

From $t \simeq 16$ h to $t \simeq 19$ h, the system is exposed to under-voltages (caused by evening load increase and DGU power decrease). This voltage drop was already seen in Fig. 3.16 of Case 3, but is more severe here due to the previous LTC interventions. The controller keeps the voltages above the lower limit by changing V_{tap} in the opposite direction (as shown by the up arrows in Fig. 3.20) and by reducing the DGU reactive powers. Incidentally, this voltage adjustment explains the slightly different values of the current, with and without control (dashed vs. solid line in Fig. 3.18), while the transformer is not overloaded any more.

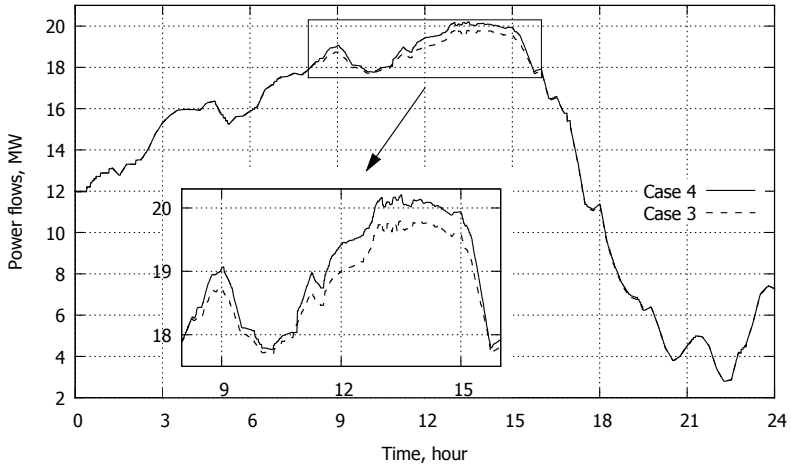

Figure 3.22: Active power injected into the transmission system: Case 3 vs. Case 4

3.4.5 Case 5: WD with variable transmission voltage, polygon-bounded capability diagram

In this case the controller acts to correct the unacceptable voltages observed in Fig. 3.6. The corrected voltage evolutions are shown in Fig. 3.23. Over-voltages are avoided at $t \simeq 13$ h and $t \simeq 23$ h, when consumption is relatively low, while under-voltages are corrected at $t \simeq 7$ h and $t \simeq 19$ h, which corresponds to morning ramp and evening peak, respectively. The corresponding adjustments of the DGU reactive powers are shown in Fig. 3.24. Although LTC control has lower priority compared to DGU reactive powers, it must be used to raise the very low evening voltages. The V_{tap} corrections result in five transformer tap changes, identified in Fig. 3.23.

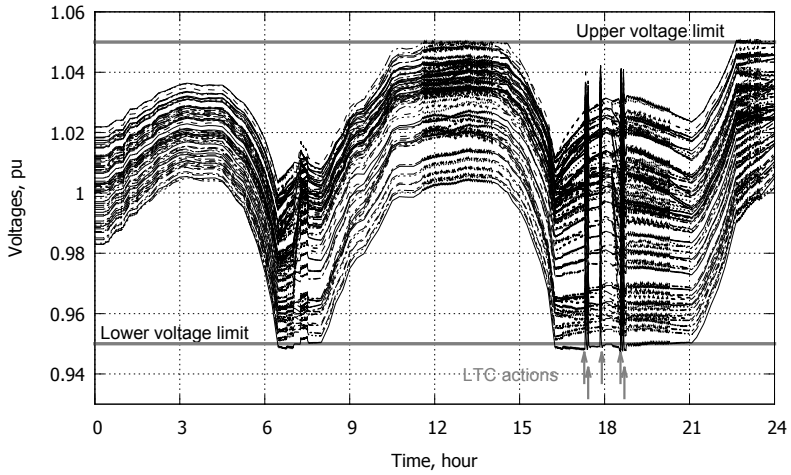

Figure 3.23: Case 5: Voltages of distribution buses

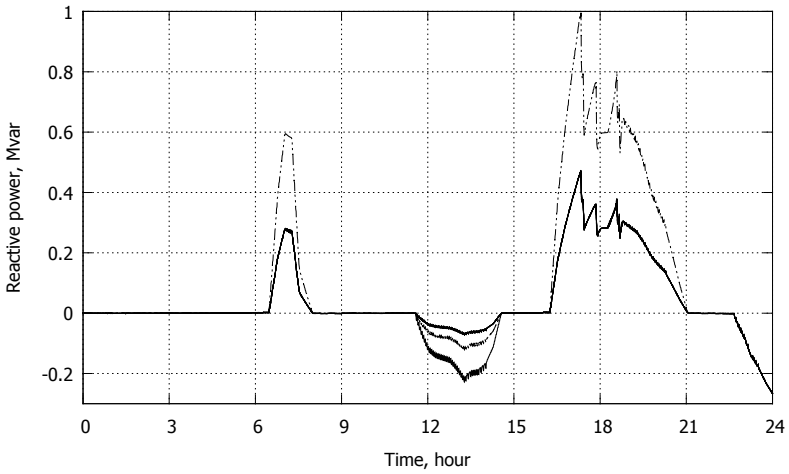

Figure 3.24: Case 5: Reactive powers produced by the DGUs

3.4.6 Case 6: WD with variable transmission voltage, triangle-shaped capability diagram

Case 5 is revisited, assuming that DGUs have tighter reactive power limits: the polygon-bounded capability diagram is replaced by the triangle-shape one (see Fig. 3.7). The controller compensates for the lack of reactive power reserves by resorting to 16 tap changes over the whole day (instead of five in Case 5). This allows keeping all voltages between limits, as shown by Fig. 3.25. A comparison with Fig. 3.23 shows that the voltage violations last longer when they are corrected by the LTC mainly. This is due to the intentional delays: 20 s on the first tap change, 10 s between subsequent tap changes.

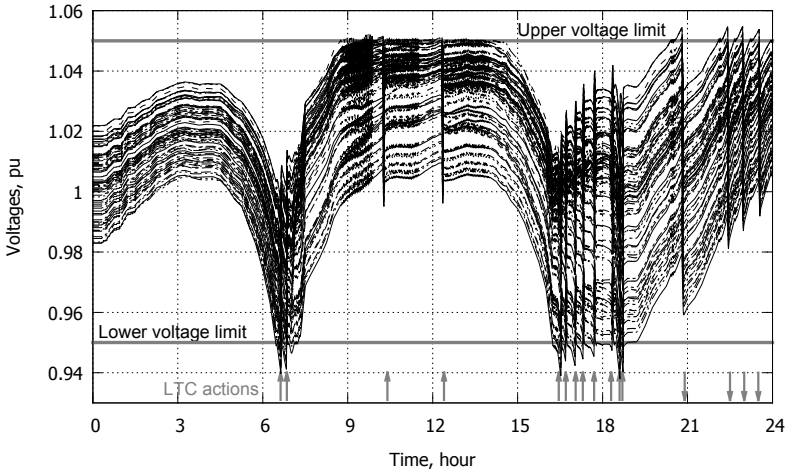

Figure 3.25: Case 6: Voltages of distribution buses

Figure 3.26 reveals very small DGU reactive power variations before $t \simeq 7$ h and after $t \simeq 19$ h. At

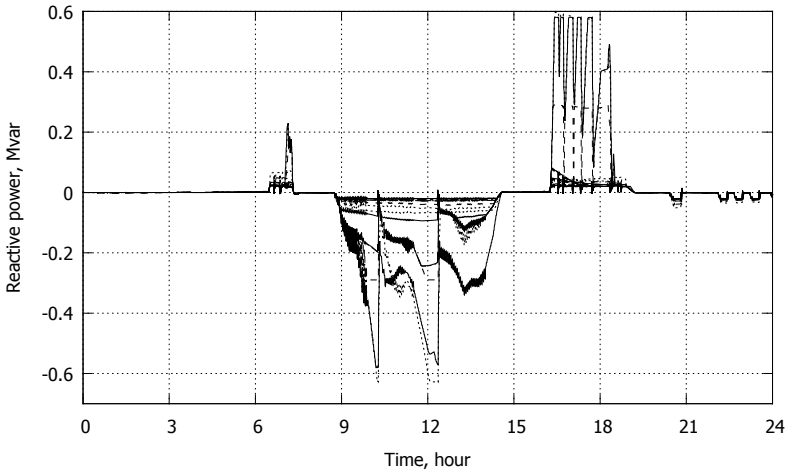

Figure 3.26: Case 6: Reactive powers produced by the DGUs

those times, the DGU active power productions are close to zero and, hence, the triangle-shaped capability diagram does not allow significant reactive power variations. In between $t \simeq 7$ and $t \simeq 19$ h, CHP and PV units are producing active power and, hence, can contribute with larger reactive power adjustments.

3.5 Computing times

As mentioned in Section 1.5, the RAMSES software has been used in all time simulations. The default time step size is 0.500 s. Since some intermediate steps are performed, the effective average time step size is 0.4945 s.

The quadratic programming problem is solved using the Harwell procedure VE17AD.

In all simulations each 15 min (900 s) of real time is represented by 1.5 min (90 s) of simulated time, for legibility of the results.

The accelerated simulation of a whole day takes on the average 17 500 time steps. Using a standard laptop computer with a dual-core Intel-i5 processor running at 2.27 GHz with 4 GB RAM, simulating the whole day takes :

- 13.2 seconds without including the MPC-based controller, and
- 28.8 seconds with the MPC-based controller acting on the system.

With the MPC controller acting every 10 seconds of accelerated time (i.e. 100 seconds of real time), the total number of control actions is $\dfrac{24 \times 3600}{100} = 864$.

Hence, the average execution time of the MPC optimization is $\frac{28\,800 - 13200}{864} = 18$ milliseconds. In fact, the computing time was found to lie between almost zero, when no constraint is active and no control change has to be computed, and 31 milliseconds when the whole constrained multi-step optimization is solved.

Needless to say, such computational efficiency is perfectly compatible with a real-time application.

3.6 Conclusion

With its "wide view of the system" (through the sensitivity matrices), the controller adjusts the DGU powers and the voltage set-point of the LTC in a coordinated manner; this performance could not be obtained with simple distributed control, and will become more important as distribution grids will host more and more DGUs.

The simulations reported in this chapter involve future scenarios of a real-life distribution system. The controller performance has been demonstrated over two full days, identified as challenging in terms of voltage and/or thermal violations. The following features were stressed: priority given to "cheap" control actions, active power curtailment minimized as much as possible, DGU powers brought back at their desired values once corrections are no longer needed.

On the premise that operation limits are exceeded for limited durations, the above demonstrated features make the proposed corrective control scheme a serious alternative to expensive network reinforcements, and contribute to removing one obstacle to the penetration of renewable energy sources in modern distribution grids.

Chapter 4

Extension to corrective control of low-voltage grids

In this chapter the formulation detailed in the Chapter 2 is extended to enable the controller to contribute to LV network voltage corrections. This is achieved by adjusting voltages on the MV side of the MV/LV transformers where a voltage problem has been detected. This extension is demonstrated on the 75-bus test system.

4.1 Introduction

The presence of distributed generation has been making significant changes in LV distribution grids. The most connected distributed sources at this voltage level are rooftop PV panels [HW16]. Their intermittent nature together with the predominantly resistive behaviour of LV cables make the system more prone to temporary over-voltages, especially at the end of the LV feeders [Eng05, KMJ13]. Furthermore, most of the MV/LV transformers have off-load tap changers, and cannot actively participate in voltage control of LV grids. For those reasons, standards and grid codes are under revision and significant attention has been paid to the possibilities offered by the DGUs connected to the LV grid to participate in network voltage control [OAEV16, oTSOfEEE16, VDE11, HW16, DMSS17].

On the other hand, as an additional possibility, adjustment of voltages on the MV side of the MV/LV transformers can help correcting abnormal LV network voltages [PMK05]. Figure 4.1 sketches an LV feeder connected to an MV bus through a transformer with an off-load tap changer. The idea is simply that, the MV voltage level can be increased when the LV feeder consumption is much larger than its production and decreased when generation exceeds the load (which is the most common situation). While keeping the MV networks within their limits (as first priority), there is a possibility for them to help improving LV network voltages.

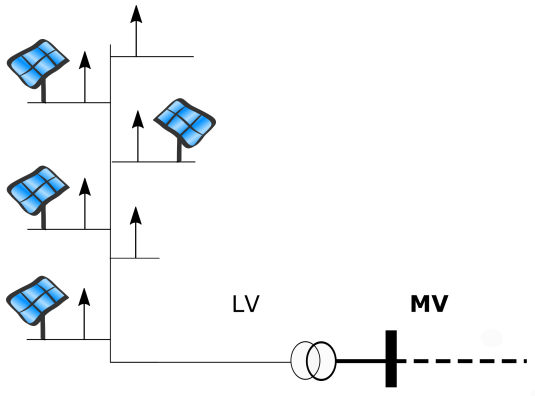

Figure 4.1: An LV feeder hosting PV units

This voltage support is the focus of this chapter, and the (simple) adjustments of the MPC-based formulation to include the latter as a second priority are going to be detailed.

While over-voltages caused by PV units are the most common issue, for generality, the dual case of under-voltage (that would be caused by a temporary high consumption) will be treated at the same time.

4.2 Method description

When an LV network experiences an over-voltage situation, the centralized controller of the upstream MV network, can adjust the voltage at the MV bus where the LV grid is connected provided that its own operational constraints allow doing so. Having a global impact on the LV grid voltage, it can help removing the violation. This is realized by modifying the allowed upper limits of voltages in the MV network.

To that purpose, it is necessary that LV networks exposed to over-voltage problems be equipped with "smart" meters, to monitor voltages at least at key buses. Here, for practical reasons, it is assumed that only one voltage signal is communicated from the LV network to the centralized controller. This signal, which is representative of the overall situation of the LV grid, should be used by the centralized controller to correct the situation.

Figure 4.2 illustrates the proposed method with an example. Initially, at $t = k$, the measured LV voltage (circle in Fig. 4.2) is above its upper limit V_{LV}^{max} (dotted line), while the corresponding MV bus (disk in the same figure) is within the prescribed limits (black dashed lines). This unsatisfactory LV voltage situation being known by the centralized controller is going to be addressed starting from the next discrete time. To do so, the upper voltage limit of the MV bus is decreased in successive discrete steps (shown by the gray dashed lines) resulting in a voltage decrease at the MV bus and, consequently, at the downstream LV buses. Finally the LV voltage is brought below its own upper limit, while the MV voltage is still within its secure limits. In this example, it is assumed that the voltages of other MV buses stay within their limits during the corrections.

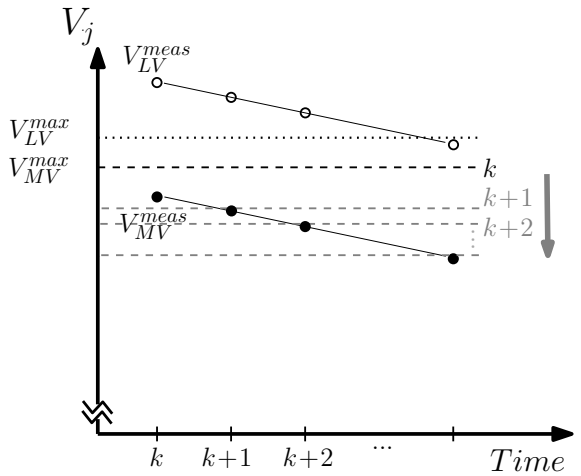

Figure 4.2: Adjustment of upper voltage limit at an MV bus to address a voltage violation in the downstream LV grid

However, more complicated cases might occur, where LV voltage reduction would interfere with the limits imposed to the MV network itself. For instance, the voltage adjustment at one MV bus, which is obtained by control of nearby DG units and possibly the LTC of the HV/MV transformer, may cause a violation at other MV buses which were close to their limits. In such a case, obviously, the priority is given to the MV network itself: the LV network is helped up to the point that it does not endanger the MV network.

Let us come back to the question of choosing an appropriate signal to communicate to the centralized controller. LV networks are hosting different types of loads such as residential, commercial and tertiary-sector over different feeders. These consumers have dissimilar daily consumption profiles, resulting in different voltage profiles from one feeder to another within the same LV network. Moreover, the presence of PV panels with their intermittent production can increase the voltage difference between feeders. The latter is more pronounced if for instance there is one feeder mainly with residential loads, and another with industrial ones. Or, one feeder producing significantly more that its consumption, and another one with a high consumption [KMJ13].

Therefore, the proper choice of a single voltage signal representing the overall situation of that LV network might be challenging in some cases. To that end, the voltage at critical buses (e.g. end of feeders) must be measured regularly, and the most critical one can be chosen and communicated to controller at the MV level. This value must be updated regularly, and it can be the voltage of different buses at different times of the day. Furthermore, the lowest voltage in the same LV grid should also be monitored, and the signal sent to the centralized controller should include this information as well. Alternatively, at each time instant, the amount of voltage change (upward or downward) to clear or mitigate all violations in the LV network could be communicated to the MV level. In this work, sending a single voltage signal is considered.

4.3 Problem formulation

The reference following formulation detailed in Section 2.5.2 is now extended to enable the centralized controller to support LV networks, as far as possible. To avoid repetitions, only the modified equations are given here. For the rest, please refer to Section 2.5.2.

The modified objective function includes a new term which becomes non-zero whenever any of the transmitted LV voltages is outside its prescribed limits:

$$\min_{\boldsymbol{u},\boldsymbol{\varepsilon},\boldsymbol{\varepsilon}_{LV},\boldsymbol{V},\boldsymbol{I}} \sum_{i=0}^{N_c-1} \|\boldsymbol{u}(k+i) - \boldsymbol{u}_{ref}(k+i)\|^2_{\boldsymbol{W}} + \|\boldsymbol{\varepsilon}\|^2_{\boldsymbol{S}} + \|\boldsymbol{\varepsilon}_{LV}\|^2_{\boldsymbol{S}_{LV}} \tag{4.1}$$

where $\boldsymbol{u}$, $\boldsymbol{u}_{ref}$, $\boldsymbol{\varepsilon}$, N_c as well as $\boldsymbol{S}$ and $\boldsymbol{W}$ are as defined in Section 2.5.2. The new slack variable

ε_{LV} relaxes the voltage constraints of the LV network. The entries of the diagonal matrix $\boldsymbol{S}_{LV}$ are given low values, compared to those of $\boldsymbol{S}$, to prioritize MV network secure operation over LV network support.

The above objective is minimized subject to the linearized system evolution (2.31, 2.32), the constraints on the control variables and their rate of changes (2.35, 2.36), the limits on predicted branch currents (2.34), and the limits on predicted bus voltages. The latter are updated to support the LV network in trouble as explained hereafter.

It should also be noted that, for simplicity, the bound tightening (please refer to Section 2.5.3) is not considered here.

4.3.1 Handling of a single LV voltage limit

Let us assume that $\boldsymbol{V}_{MV}^{min}$ and $\boldsymbol{V}_{MV}^{max}$ are the minimum and maximum MV voltage limits, respectively, which define the secure operation of the MV network while $\boldsymbol{V}_{MV}^{down}$ and $\boldsymbol{V}_{MV}^{up}$ are the effective lower and upper limits, respectively, imposed on the predicted MV voltages.

If all transmitted voltages from LV networks are within their limits, the constraints on MV voltages remain unchanged, i.e. :

$$\boldsymbol{V}_{MV}^{up}(k) = \boldsymbol{V}_{MV}^{max} \tag{4.2a}$$

$$\boldsymbol{V}_{MV}^{down}(k) = \boldsymbol{V}_{MV}^{min} \tag{4.2b}$$

otherwise, the voltage limit on the MV side of the MV/LV transformer connecting the LV network in trouble is going to be updated. This update can be performed at several MV buses at the same time if needed.

Assuming the limits $\boldsymbol{V}_{MV}^{max}$ and $\boldsymbol{V}_{MV}^{min}$ are "hard" constraints, the goal is to add a "very soft" constraint to deal with LV voltages.

Namely, when in the LV network downstream of MV bus j, the measured voltage V_{LV}^{meas} is greater than its maximum allowed value V_{LV}^{max}, the MV voltage upper limit is changed according to [1]:

$$V_{MV\ j}^{up}(k) = V_{MV\ j}^{meas}(k) - \frac{1}{\alpha}\Big(V_{LV\ j}^{meas}(k) - V_{LV\ j}^{max}\Big) \qquad \text{with} \quad \alpha > 1 \tag{4.3}$$

where $V_{MV\ j}^{meas}$ is the measured MV voltage at bus j. In the right-hand side of the above equation $\Big(V_{LV\ j}^{meas}(k) - V_{LV\ j}^{max}\Big)$ is the required voltage change on the LV side to correct the over-voltage,

[1] All voltages are per unit as usual.

and α is used to apply only a fraction of this change. At each discrete step, the second term in the right-hand side of (4.3) is subtracted from the last collected measurement, moving the upper voltage limit $V^{up}_{MV\ j}$ (see gray dashed lines in Fig. 4.2) slightly below its measured value. This shift of the upper voltage limit is done in successive steps until the violation is cleared (if possible) [2].

It is clear that, although the calculation is made in per unit, a specific voltage change at the MV side of a MV/LV transformer does not give the same exact change at the LV buses, when the transformers turn ratio is not equal to one. This can be simply taken into account by adding a new coefficient in (4.3). However, for simplicity, the latter expression is kept unchanged, since that coefficient is normally very close to one.

Coming back to "hard" and "very soft" constraints, the upper voltage limit is defined as follows:

for $j = 1, \ldots, N_{bus}$:
for $i = 1, \ldots, N_p$:

$$V_{MV\ j}(k+i) \leq V^{up}_{MV\ j}(k) + \varepsilon_2 + \varepsilon^{up}_{LV\ j} \tag{4.4}$$

$$0 \leq \varepsilon_2 \qquad \text{, highly penalized} \tag{4.5}$$

$$0 \leq \varepsilon^{up}_{LV\ j} \leq V^{max}_{MV\ j} - V^{up}_{MV\ j}(k) \qquad \text{, lightly penalized} \tag{4.6}$$

where N_{bus} is the number of monitored MV buses and $\varepsilon^{up}_{LV\ j}$ is a component of $\boldsymbol{\varepsilon}_{LV}$, upper bounded by the amount of change of MV voltage limit (the vertical distance between the black and gray dashed lines in Fig. 4.2). The light penalization of the non-zero value of $\varepsilon^{up}_{LV\ j}$ yields the following advantages:

- if it does not endanger the MV grid, the LV network voltage violations will be smoothly removed;
- if the LV voltage cannot be corrected without causing a violation of the MV voltage, the controller does what it can, and brings the problematic voltage(s) to a better value, after which it will behave as the original (non-modified) formulation of Section 2.5.2, i.e. only the operation of the MV network is taken into account. More precisely, in such a case, the problem becomes infeasible and the constraints on voltage have to be relaxed through slack variables $\boldsymbol{\varepsilon}$ and/or $\varepsilon^{up}_{LV\ j}$. Since the latter is penalized much lighter than $\boldsymbol{\varepsilon}$, it will increase and eventually hit its maximum value $V^{max}_{MV\ j} - V^{up}_{MV\ j}(k)$. Then, the upper limit in (4.4) becomes:

$$V^{up}_{MV\ j}(k) + \varepsilon_2 + \overbrace{\left[V^{max}_{MV\ j} - V^{up}_{MV\ j}(k)\right]}^{\varepsilon^{up}_{LV\ j}} = V^{max}_{MV\ j} + \varepsilon_2 \tag{4.7}$$

[2] Of course, attention must be paid to not decrease the upper voltage limit so much that $V^{up}_{MV\ j} < V^{down}_{MV\ j}$, in which case the optimization becomes infeasible.

and, consequently, (4.4-4.6) become:

for $i = 1, \ldots, N_{bus}$:
for $i = 1, \ldots, N_p$:

$$V_{MV\,j}(k+i) \leq V_{MV\,j}^{max} + \varepsilon_2 \tag{4.8}$$

$$0 \leq \varepsilon_2 \tag{4.9}$$

which involves the MV voltage only.

4.3.2 Combined MV and LV voltage constraints

Considering similar formulation in the case of low LV voltage, the whole set of inequality constraints can be written as follows:

for $j = 1, \ldots, N_{bus}$:
for $i = 1, \ldots, N_p$:

$$-\varepsilon_{LV\,j}^{down} - \varepsilon_1 + V_{MV\,j}^{down}(k) \leq V_{MV\,j}(k) \leq V_{MV\,j}^{up}(k) + \varepsilon_2 + \varepsilon_{LV\,j}^{up} \tag{4.10a}$$

$$0 \leq \varepsilon_1, \varepsilon_2 \tag{4.10b}$$

$$0 \leq \varepsilon_{LV\,j}^{down} \leq V_{MV\,j}^{down}(k) - V_{MV\,j}^{min} \tag{4.10c}$$

$$0 \leq \varepsilon_{LV\,j}^{up} \leq V_{MV\,j}^{max} - V_{MV\,j}^{up}(k) \tag{4.10d}$$

where:

$$V_{MV\,j}^{down}(k) = \begin{cases} V_{MV\,j}^{meas}(k) + \frac{1}{\alpha}(V_{LV\,j}^{min} - V_{LV\,j}^{meas}(k)), & \text{under-voltage in } j\text{th LV network} \\ V_{MV\,j}^{min}\,, & \text{otherwise} \end{cases} \tag{4.11}$$

and,

$$V_{MV\,j}^{up}(k) = \begin{cases} V_{MV\,j}^{meas}(k) - \frac{1}{\alpha}(V_{LV\,j}^{meas}(k) - V_{LV\,j}^{max}), & \text{over-voltage in } j\text{th LV network} \\ V_{MV\,j}^{max}\,, & \text{otherwise} \end{cases} \tag{4.12}$$

where $\varepsilon_{LV\,j}^{down}$ is another component of $\boldsymbol{\varepsilon}_{LV}$.

The extended formulation including LV network support consists of minimizing the objective (4.1) subject to the constraints (4.10) together with (2.31, 2.32) and (2.34-2.36).

It should be noted that the above formulation assumes that the MV counterparts of all LV networks have their voltage measured, while, for instance, in the 75-bus test system only 26 buses are

equipped with a voltage measurement device. To deal with this issue, the voltage of non-measured MV buses could be estimated by a state estimator and the limit (4.10a) applied on the estimated value. Alternatively, the limit adjustments can be performed at the closest monitored MV bus. Indeed, a voltage correction at one MV bus affects the neighbouring buses similarly, and it is expected to obtain acceptable results, if the monitored MV bus is relatively close to the LV network experiencing problem. It also requires that the voltage measurement devices are rather uniformly distributed over the MV grid. An example dealing with this choice is presented in Section 4.4.2.

4.4 Simulation results

The performance of the proposed method will be illustrated on the 75-bus, 11-kV network already used in Chapter 2 (see also Section 1.4.2). In this section, all 22 MV DGUs are assumed to be wind turbine units.

The LV grids, including their consumers and their PV panels are not represented as such but replaced by aggregated loads connected to the upstream MV buses. Therefore, LV voltage measurements have been artificially produced to simulate over-voltage problems at LV level. This is done by linearly relating the LV voltage signals to their upstream MV voltage measurements [3].

In all scenarios, one of the LV networks is assumed to face an over-voltage due to the high production of PV panels. The MV network is assumed to be the only control means to solve the problem.

The MV upper and lower voltage limits are set to 1.05 and 0.95 pu, and those of the LV network to 1.1 and 0.9 pu, respectively. The parameter α in (4.12) is set to 1.5. The weight assigned to the slack variables $\varepsilon_1, \varepsilon_2$ is 500 times larger than that assigned to reactive power corrections, while the weight assigned to the $\varepsilon_{LV\ j}$ variables ($j = 1, \ldots N_{bus}$) is only five times larger.

4.4.1 Case 1

A new operating point has been considered, in which all wind generations, connected to the MV level, and PV panels, connected to the LV level, are producing a high amount of active power. Thus, the LV networks are injecting active power into the MV grid, and the latter also exports active power to the external grid. Reactive power, on the other hand, is imported from the external grid to cover the loads and the losses.

[3] i.e. x% of voltage change in the MV bus is assumed to create the same change of the voltage at the critical LV bus.

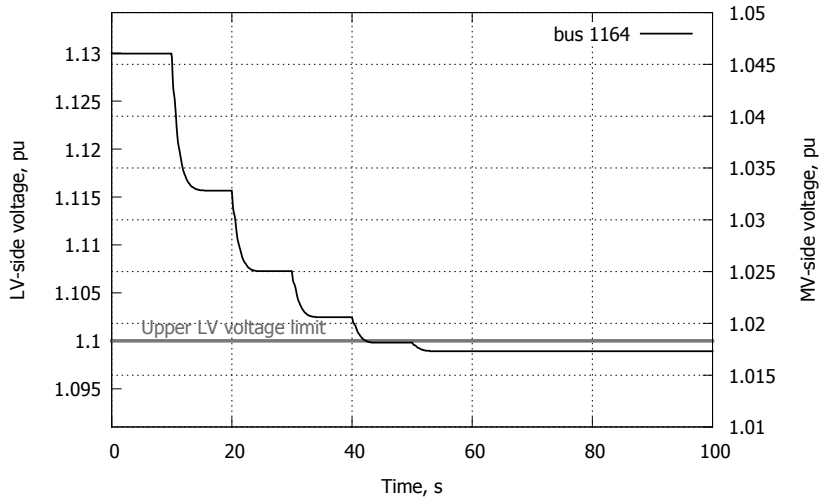

Figure 4.3: Case 1: Voltage at MV Bus 1164 and in the corresponding connected LV grid [4]

It is assumed that at the initial operating point, the communicated LV voltage reveals an overvoltage situation in the LV grid connected to the MV Bus 1164 (see Fig. 4.3), which is located almost at the end of the longest MV feeder. This bus has its voltage magnitude measured. The centralized controller reacts to this violation by adjusting the DGU reactive powers. It decreases the voltage of the feeder including Bus 1164, and hence the voltage of the connected LV grid. Figure 4.3 shows that the latter goes below its limit in five successive steps. The smooth voltage evolution is achieved thanks to the choice of parameter α in (4.12), and the weight assigned to the $\varepsilon_{LV\ j}$ variables. Using the sensitivity matrix $\boldsymbol{S}_V$, the centralized controller shares the corrective efforts among all DGUs. Expectedly, those DGUs located closer to Bus 1164 have a larger contribution than the others, resulting in the maximum voltage change in their neighbourhood, as illustrated in Fig. 4.4.

These adjustments impact the voltages at other MV buses as well. However, as shown in Fig. 4.5, in this example, the voltages throughout the MV grid are initially far from the lower limit $V_{MV}^{min} = 0.95$ pu and the decrease to support the LV network do not make them approach the lower voltage limit. Thus, it is expected that this voltage support is achieved without having to relax the constraint (4.4); the slack variable $\varepsilon_{LV\ 1164}$ should remain equal to zero. On the contrary, Fig. 4.6 reveals that, initially, this slack variable has a non-zero value, although it goes to zero after four steps. In fact, this happens due to the very small weight assigned to $\varepsilon_{LV\ j}$ (only five times larger than reactive power corrections). More precisely, this choice leads the optimization, for instance at $t = 10$ s, to resort to: (i) reactive power corrections, as well as (ii) relaxation of the upper limit on voltage (by assigning a non-zero value to $\varepsilon_{LV\ 1164}^{up}$) in order to satisfy the voltage con-

[4] Both LV and MV voltages can be shown in one curve, since they are assumed to be linearly related. It is expected to have (slightly) different MV and LV voltage evolutions if the LV networks are modelled in detail.

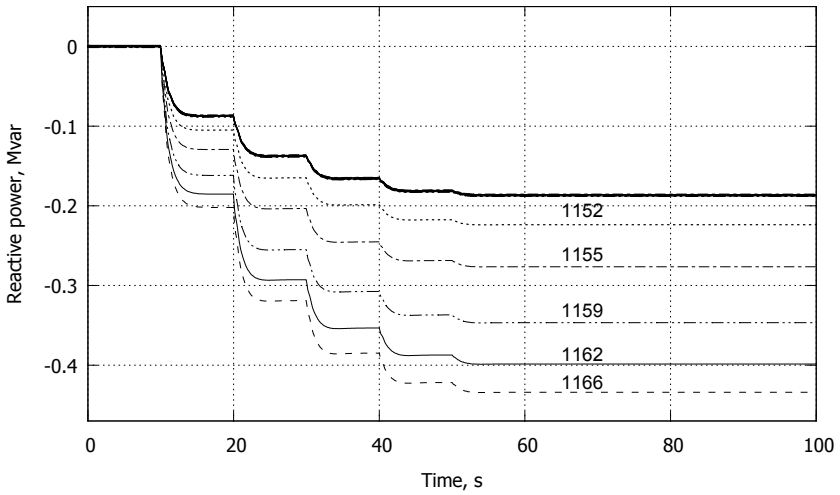

Figure 4.4: Case 1: Reactive powers produced by DGUs in the MV grid

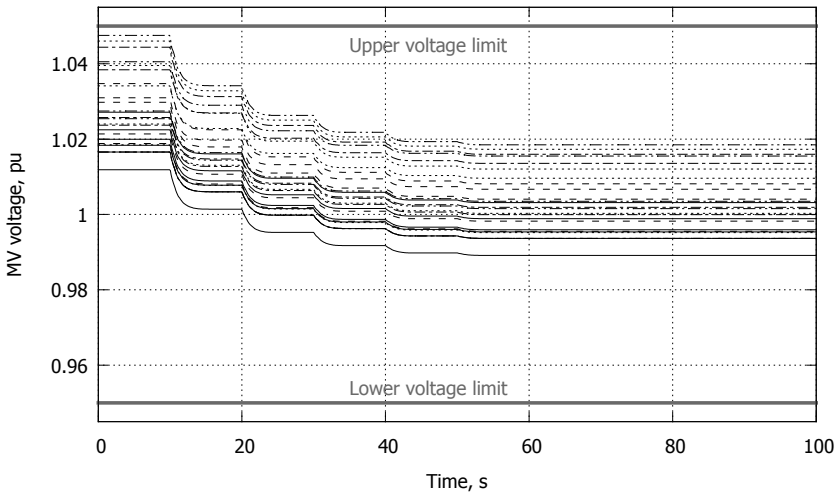

Figure 4.5: Case 1: Bus voltages in the MV grid

straint (4.10a). However, Item (ii) is used only very slightly, as shown by the very small value of $\varepsilon^{up}_{LV\ 1164}$ in Fig. 4.6, shown with "+" sign. Indeed, $\varepsilon^{up}_{LV\ 1164}$ is far below its upper limit $V^{max}_{MV\ 1164} - V^{up}_{MV\ 1164}(k)$ in Inequality (4.10d) (shown with circles in the same figure). In the following steps, as the DGU reactive power adjustments alleviate the problem, the whole effort is progressively shifted to Item (i) and $\varepsilon^{up}_{LV\ 1164}$ reaches zero in four successive steps.

In fact, the initial non-zero value of $\varepsilon^{up}_{LV\ 1164}$ comes from the low value of the associated weight $\boldsymbol{S}_{LV}$ in the objective (4.1), which in turn comes from the hierarchy of control priorities in the optimization problem. The use of penalty factors starts reaching its limits, although in this particular case, the optimization problem is solved and the violations corrected very properly.

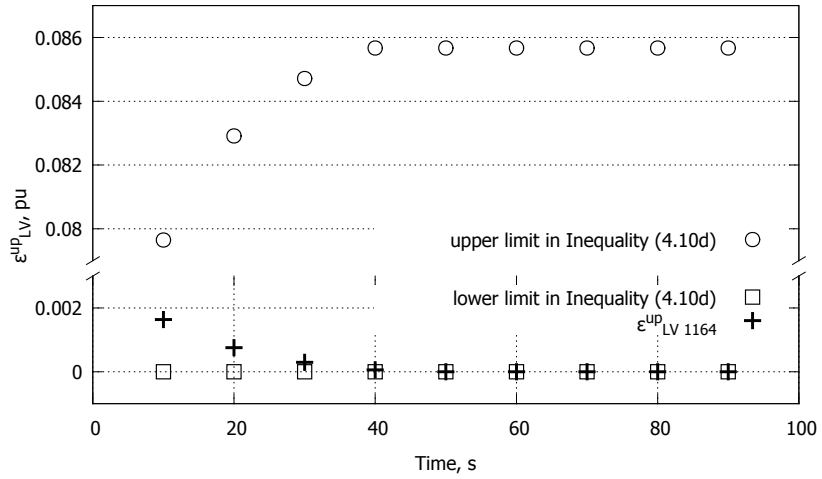

Figure 4.6: Case 1: Slack variable of voltage constraint corresponds to the LV network connected to Bus 1164

It is interesting to add that the initial non-zero value of the $\varepsilon^{up}_{LV\ 1164}$ slack variable makes the whole correction process slower than expected. However, the correction speed can be easily increased by adjusting the value of α in (4.12).

4.4.2 Case 2

It is now assumed that an over-voltage takes place in an LV network connected to Bus 1151, which is not voltage measured and is located next to the main substation of the MV grid (see Fig. 1.4). Bus 1100 is taken by the centralized controller as neighbouring monitored bus, and the limit adjustment (4.10a) is applied to that bus. The LV network voltage, shown in Fig. 4.7, is decreased under the effect of DGUs reactive power changes.

Since the centralized controller adjusts the voltage of the main substation (MV side of the main transformer), one can expect all the DGUs reactive power corrections to be the same, since regardless of their location within the MV grid, they have almost the same impact on the main substation voltage. This is indeed confirmed by Fig. 4.8, showing almost identical reactive power changes for the multiple DGUs.

Figure 4.9 shows how the MV voltages evolve at different buses. Similar to the first case, they all remain within their specified limits during LV network voltage support.

It should be noted that, although the over-voltage was observed in the LV network connected to Bus 1151, the updated voltage limits have been applied to the closest monitored Bus 1100,

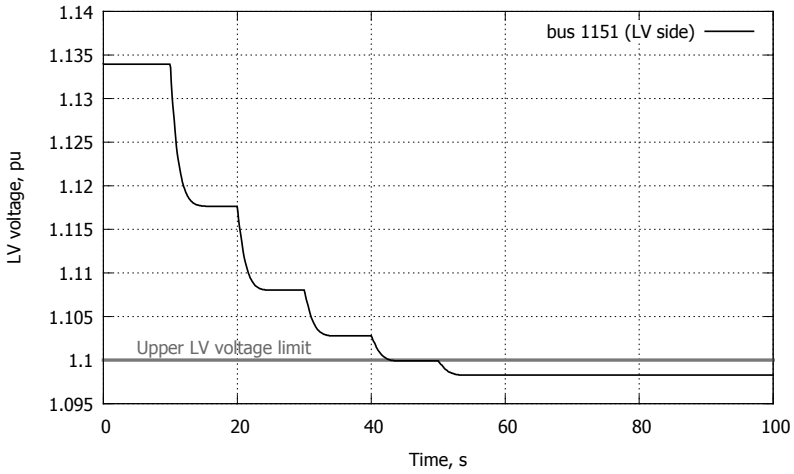

Figure 4.7: Case 2: Voltage in the LV grid connected to bus 1151

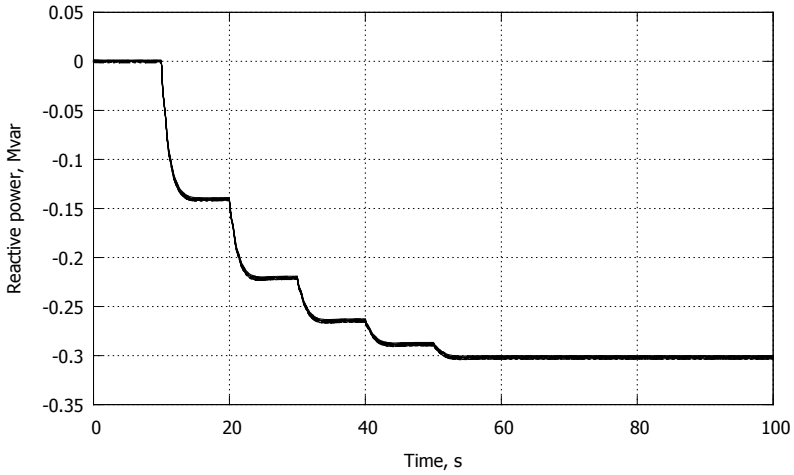

Figure 4.8: Case 2: Reactive powers produced by DGUs in the MV grid

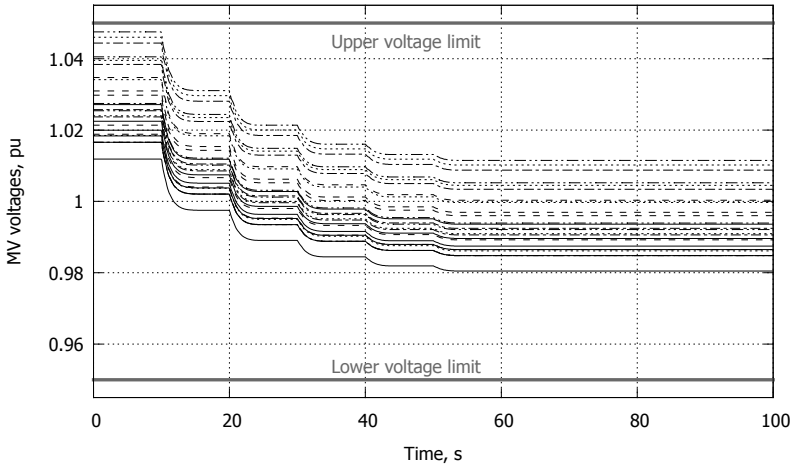

Figure 4.9: Case 2: Bus voltages in the MV grid

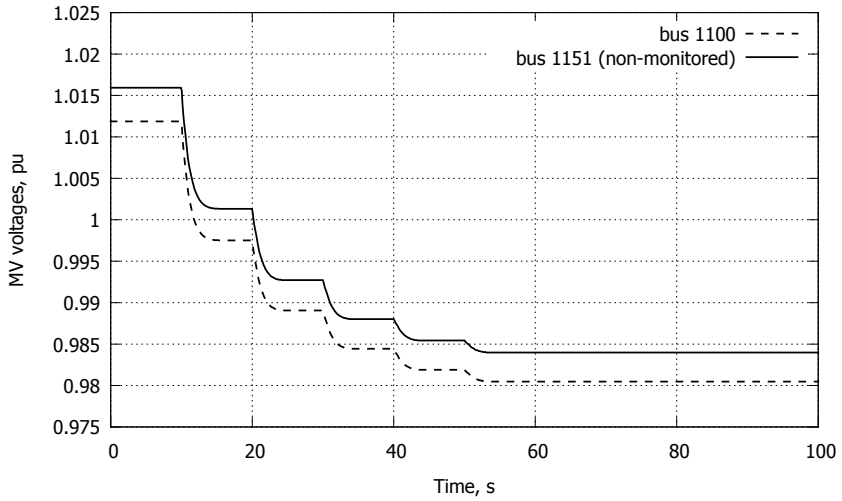

Figure 4.10: Case 2: Voltages at Buses 1100 and 1151

assuming that both voltage will change by the same value. For comparison reasons, Fig. 4.10 shows these two bus voltages. The difference is approximately 0.004 pu and remains constant. It means that the choice of the closest monitored bus in this example is quite acceptable.

4.4.3 Case 3

A different initial operating point is considered now, with the MV voltages initially closer to their lower limit of $V_{MV}^{min} = 0.95$ pu. Consequently, there is less margin (compared to the first two cases) to help mitigating over-voltages in the LV networks.

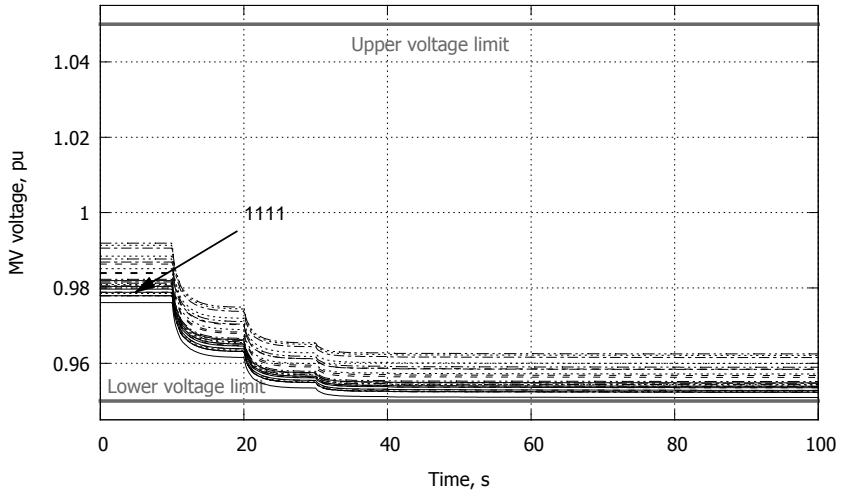

Figure 4.11: Case 3: Bus voltages in the MV grid

It is assumed that an over-voltage is detected in the LV network connected to the monitored Bus 1111. Figure 4.12 shows the mentioned LV network voltage together with its MV-side counterpart. Therefore, starting from $t = 10$ s, the centralized controller decreases the voltages of the MV network taking into account the available margin. It continues decreasing until one of the MV voltages reaches the minimum allowed value. At this point (i.e. at $t = 40$ s), the LV network voltage is much lower than its initial value but still above the upper limit. However, the centralized controller stops helping the LV grid, since the constraints on MV buses have higher priority. This is obtained by assigning a non-zero value to $\varepsilon^{up}_{LV\ 1111}$ which relaxes Inequality (4.10d), as shown in Fig. 4.13. The initial non-zero values of $\varepsilon^{up}_{LV\ 1111}$ can be explained as in Case 1.

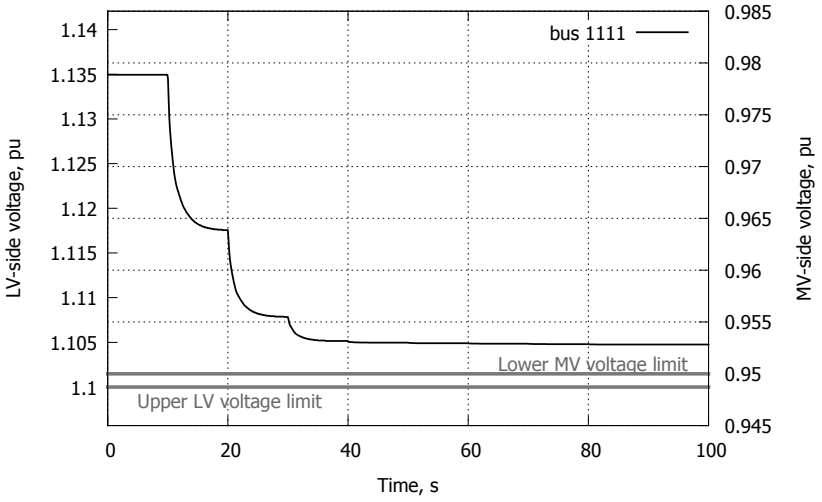

Figure 4.12: Case 3: Voltage at Bus 1111 and its downstream LV grid

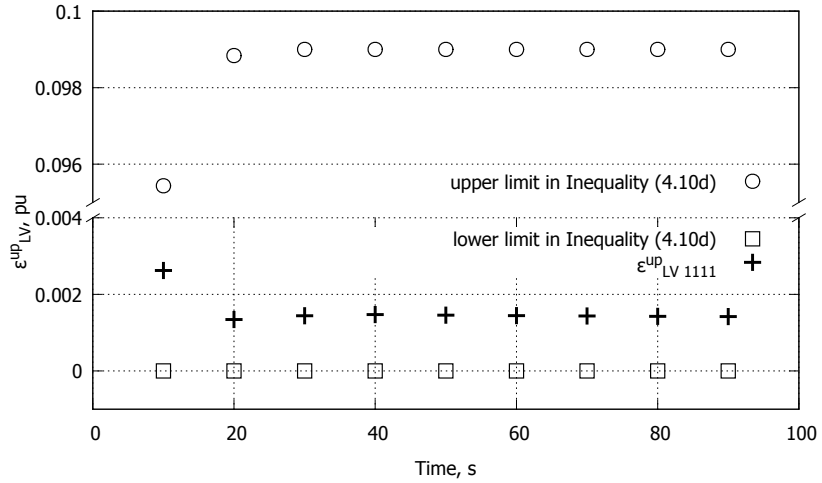

Figure 4.13: Case 3: Slack variable $\varepsilon_{LV\ 1111}$ of voltage constraint corresponding to the LV network connected to Bus 1111

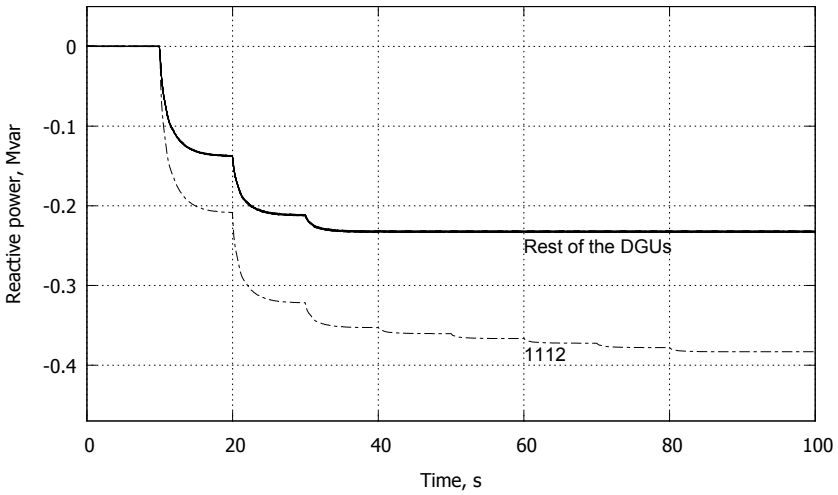

Figure 4.14: Case 3: Reactive powers produced by DGUs

Figure 4.14 illustrates that all DGUs are asked to contribute by reducing their reactive power outputs. It is, however, interesting to note that a bigger reactive power change is assigned to DGU 1112, which is in the same feeder as Bus 1111, than to the others. The rest of the DGUs have almost the same impact on the voltage at Bus 1111, and hence they are requested to change their reactive powers by almost the same value.

It should be also noted that, the voltage at Bus 1111 is among the lowest (see Fig. 4.11) and eventually lands very close to the lower limit $V_{MV}^{min} = 0.95$ pu.

4.4.4 Case 4

A similar scenario to Case 3 is considered here, except that the LV network over-voltage is detected at the monitored Bus 1164. The latter is located almost at the end of the longest feeder, and its voltage is initially among the largest, as can be seen from Fig. 4.15.

As shown in Fig. 4.16, from $t = 10$ s to $t = 40$ s, the DGU reactive powers are all decreased, to reduce the voltage at Bus 1164. The contributions differ from one DGU to another, as already noted. At the end of the mentioned time interval, an MV bus voltage reaches its lower limit (see Fig. 4.15) while the voltage at Bus 1164 is still at some distance of the lower limit. From there on, the centralized controller keeps decreasing the reactive power of DGUs close to the mentioned bus, and starts increasing that of some other DGUs. In this way, both the mentioned MV bus voltage and the downstream LV voltage decrease, while the voltage of some other MV buses (mainly those close to the main substation) are increased to avoid an under-voltage situation. Figure 4.17 shows that the LV network over-voltage is fully cleared at $t = 60$ s.

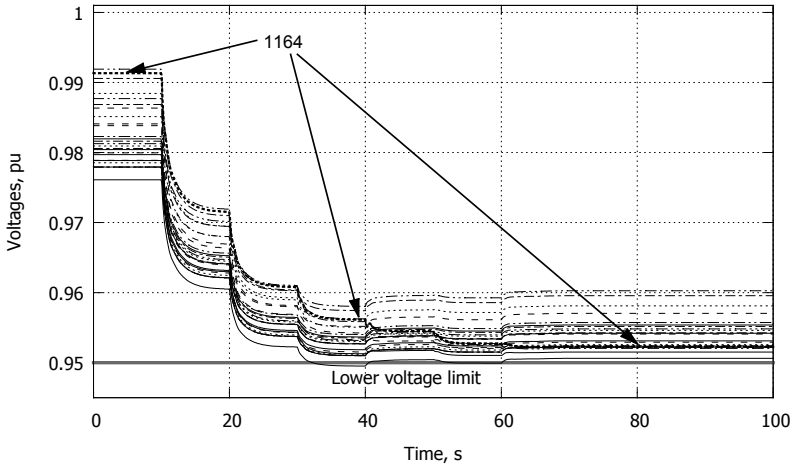

Figure 4.15: Case 4: Bus voltages in the Mv grid

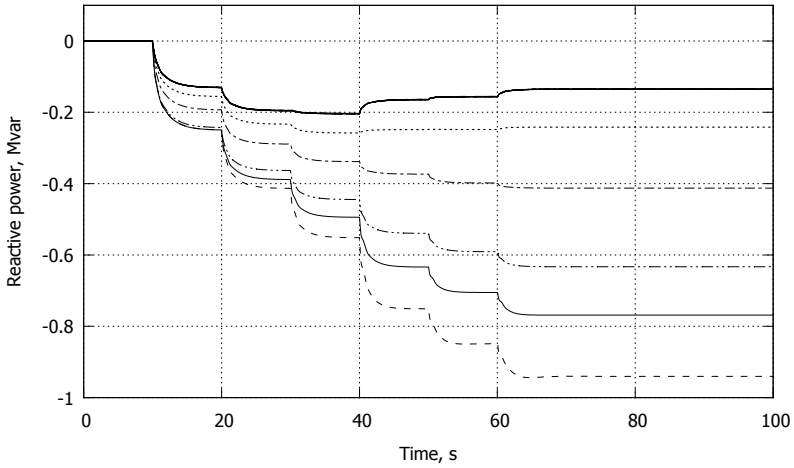

Figure 4.16: Case 4: Reactive powers produced by DGUs

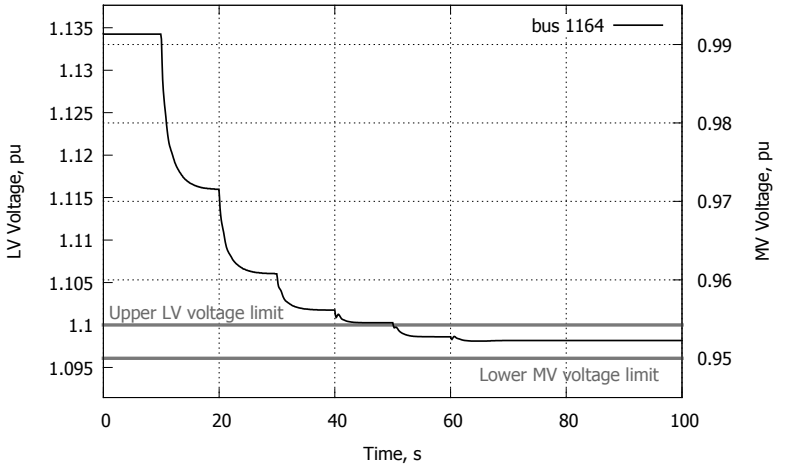

Figure 4.17: Case 4: Voltage at Bus 1164 and its downstream LV grid

This example shows that, having a wide-area view of the system, the coordinated controller is able to ask the proper corrections from different DGUs in order to clear the problem in the LV network in the best possible way.

4.5 Conclusion

The centralized controller has been extended to contribute to voltage correction in downstream LV networks. To that end, it would be necessary to equip LV grids with voltage measurements and communication infrastructure, broadening the area monitored by the controller. The extended controller is able to adjust the MV bus voltages to clear/mitigate unsatisfactory voltages in LV grids. It has been shown in particular that, if the LV voltage cannot be fully corrected without creating abnormal MV bus voltages, at least the controller brings the problematic LV voltage to a better value, but keeps the control of MV voltages as its first priority.

Chapter 5

Two-level voltage control schemes

The real-time corrective control of DNs is extended to accommodate a two-level control architecture combining the previously presented centralized controller with multiple local controllers. The local control provides fast response after a disturbance, reducing its impact and enhancing voltage quality. The centralized control uses measurements collected throughout the network to bring the voltages inside tighter limits and balance the various DGU contributions. To this purpose, it adjusts in a coordinated way their reactive power set-points, taking into account the local controls. As a variant, a hybrid control structure is also considered where, the centralized controller is acting on some of the DGUs only. This hybrid control is of practical interest where the deployment of the upper level control is not feasible or affordable over all DGUs. The proposed method effectiveness is demonstrated on the 75-bus test system.

5.1 Introduction

The thermal overload of branches needs to be addressed in a centralized manner, since some/all of the down-stream DGUs of the network should be employed to mitigate the violation. On the other hand, voltage control can be implemented through different architectures taking into account practical needs, technical limitations of the DGUs, and regulatory policies. Two broad categories are the local and the centralized architectures, depicted in Figs. 5.1.a and 5.1.b, respectively. Local control is implemented inside the equipment and adjusts the reactive power of each DGU based on local measurements only, typical terminal voltage and active power. The measurements are collected without communication delay. Thus, a fast reaction is obtained while no communication infrastructure is required. A centralized controller, on the other hand, periodically gathers measurements and sends set-point corrections to the controlled devices. Having a wider view of the system, it is able to share the corrective efforts over multiple DGUs. This scheme has been already detailed and demonstrated in Chapter 2.

Combining the local and centralized schemes, as depicted in Fig. 5.1.c, offers enhanced control possibilities. At the local level, the DGUs are equipped with controllers adjusting reactive powers in response to terminal voltage variations. At the upper level, a discrete-time controller receives measurements and adjusts set-points of the local controllers in order to improve the overall system behaviour. In this manner, with the objective of combining the respective advantages of both schemes:

- in a couple of seconds, the local level provides the fast response to a disturbance, reducing its impact and enhancing voltage quality;
- in some tens of seconds, the central level coordinates the various DGUs in order to refine the local corrections and balance the various DGU contributions;
- the local level acts as back-up in case of communication failures between the DGUs and the centralized controller, which adds to the overall reliability.

In some DNs, due to practical constraints, the deployment of the upper level over all DGUs might not be feasible or affordable. For instance, it may not be justified to centrally control DGUs of small nominal powers, or those based on an older technology. This leads to considering the hybrid control architecture of Fig. 5.1.d. In the latter, a subset of DGUs are under Combined Local and Centralized (CLC) control while the remaining are under local control only. The architectures of Figs. 5.1.a and 5.1.c are thus combined. This requires the centralized controller to take into account the (faster) reaction of all local controllers, including those of the DGUs that are not

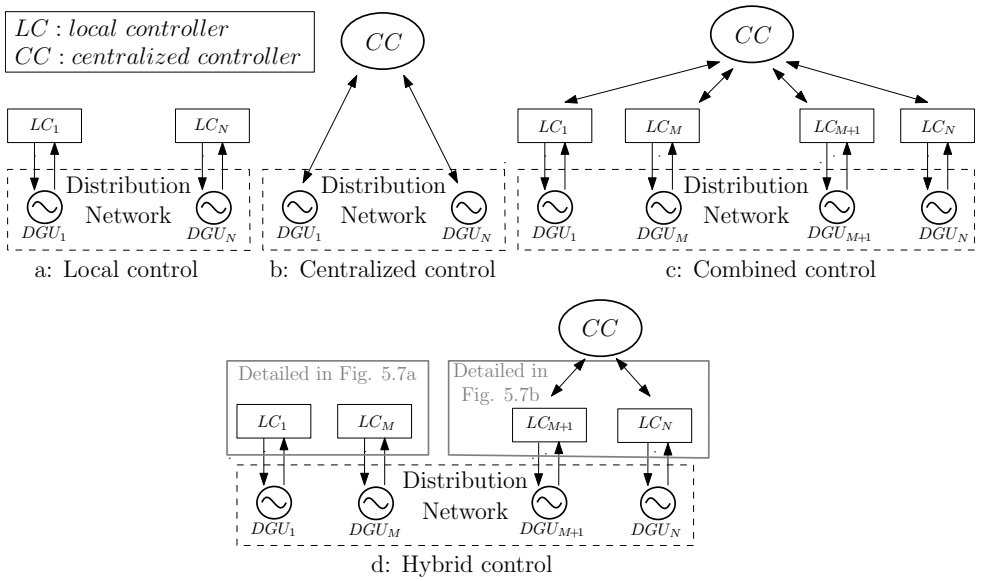

Figure 5.1: Voltage control architectures

under its control. One of the purposes of this scheme is to demonstrate the performance of the upper level having limited controllability of the DGUs.

Recently attention has been paid to multi-layer controllers exploiting the capability of different control means. For instance, a combined scheme was proposed in [CKN+12] in which local controllers provide fast responses and a centralized controller uses power injection predictions for the next hours to update the droop parameters of the local controllers, ensuring that the voltages are kept within their limits in the forecast time interval. The authors in [FLEBP13] present a dynamic control strategy in which the fast and expensive sources, such as gas turbine generators, are used to modify the voltage and power balance of distribution system during transients and let slower and cheaper generators gradually take over after transients have died out. Reference [JWS14] proposes a two-stage strategy for distributed energy storage management. In day-ahead, the optimized battery charge/discharge schedules are calculated centrally. Then, they are communicated to local controllers for further short-term adjustments, when approaching real-time. Using a dynamic model of the system, Ref. [FGM+15] suggested a multi-layer control structure. At the upper level, a static OPF computes reference values of reactive powers. The latter are communicated to the next layer, an MPC-based centralized controller, which handles the operation constraints.

As briefly mentioned, combined scheme includes fast controllers at the lower level and a centralized slower one at the higher level. Such a scheme has been developed, embedding the centralized controller presented in previous chapters of this thesis.

The formulation detailed in Chapter 2 has been extended to account for the lower level, as detailed in the next section.

5.2 Combined Control Scheme

5.2.1 Lower-level: local control

Reactive power control of a DGU

In steady state the reactive power output of a DGU under local control varies according to the piecewise linear VQ characteristic shown in Fig. 5.2. Such characteristic was proposed for instance in [BSB10, TSBC11, KKW+14, RHSS16]. As long as the measured terminal voltage lies within the dead-band $[V_{loc}^{min1}, V_{loc}^{max1}]$, the produced reactive power Q_g is kept at zero, which is usually preferred to minimize DGU internal losses. Outside the above mentioned dead-band, the DGU reacts to over or under-voltage by consuming or producing reactive power, respectively. The DGU is locked at its maximum reactive power production Q^{max} (resp. consumption Q^{min}), if the voltage stays below V_{loc}^{min2} (resp. above V_{loc}^{max2}).

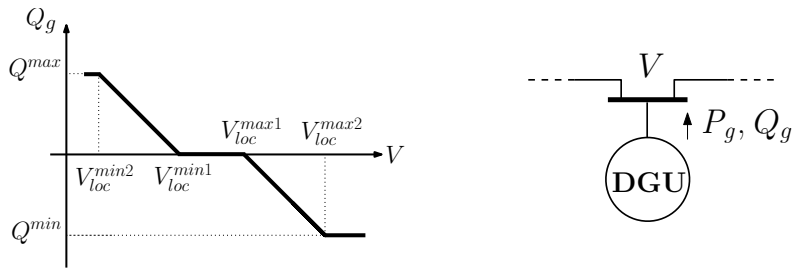

Figure 5.2: Local level: steady-state VQ characteristic

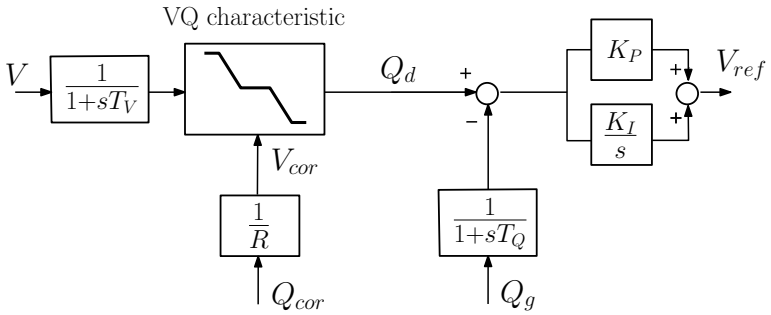

Figure 5.3: Local level: generic model of DGU reactive power control

A generic model of DGU reactive power control is shown in Fig. 5.3. The terminal voltage V and the generated reactive power Q_g are measured, with the corresponding time constants T_V and T_Q. The desired reactive power output Q_d is given by the VQ characteristic using the measured voltage. The difference between Q_d and the measured reactive power is processed by a Proportional-Integral controller. The output V_{ref} is used as field voltage reference in a synchronous generator,

or terminal voltage reference in a power-electronics based DGU. Let us stress that the above model does not encompass all practical voltage control schemes (see e.g. [CMSG10]), but it serves the main purpose of this work.

For coordination purposes the local controller receives a reactive power correction Q_{cor} updated and sent at discrete times by the centralized controller. This correction results in a shift of the VQ characteristic, as detailed in the next section.

The change of reactive power output of one DGU affects the voltages at other buses, including DGU buses. Assuming that these DGUs are not operating in the dead-band of their VQ characteristics, they will react to the voltage change by also adjusting their reactive powers. The interactions between locally controlled DGUs are such that the reactive power increase of a DGU causes reactive power decreases of other DGUs. The response time is at most a couple of seconds.

5.2.2 Correction from the centralized controller

As suggested in Fig. 5.3, the correction Q_{cor} received from the centralized controller modifies the VQ characteristic. Namely, the piecewise linear characteristic is shifted parallel to the V axis. The purpose of this is better explained with an example.

Figure 5.4 shows an over-voltage situation and the subsequent actions at both levels to remove the violation. The initial operating point of the DGU, shown with a black dot, is at the intersection of the DGU and network VQ characteristics. In the example of Fig. 5.4.a, the voltage lies in the dead-band; therefore, initially, the DGU operates at unity power factor. Under the effect of a disturbance, the network characteristic changes and the DGU terminal voltage exceeds the upper limit V_{loc}^{max1}. The circle in Fig. 5.4.b shows the situation with no control. Although the violation is partly corrected by a first and fast reaction of the local controller (black dot in Fig. 5.4.b), the voltage is still above the upper voltage limit V_{cnt}^{max} monitored by the centralized controller. The latter computes a sequence of corrections ΔQ_{cor} and sends them to the local controller.

At the lower level, the successively received corrections are cumulated as shown in Fig. 5.5, where k is the discrete time, T the sampling period and Q_{cor} the cumulated (or discrete integral) correction. The latter is used to shift the VQ characteristic as shown in Fig. 5.4.c. Assuming operation on the sloping part of the VQ characteristic, the voltage shift V_{cor} corresponding to a given value of Q_{cor} is:

$$V_{cor} = \frac{Q_{cor}}{R} \tag{5.1}$$

where R is the local droop of the VQ characteristic.

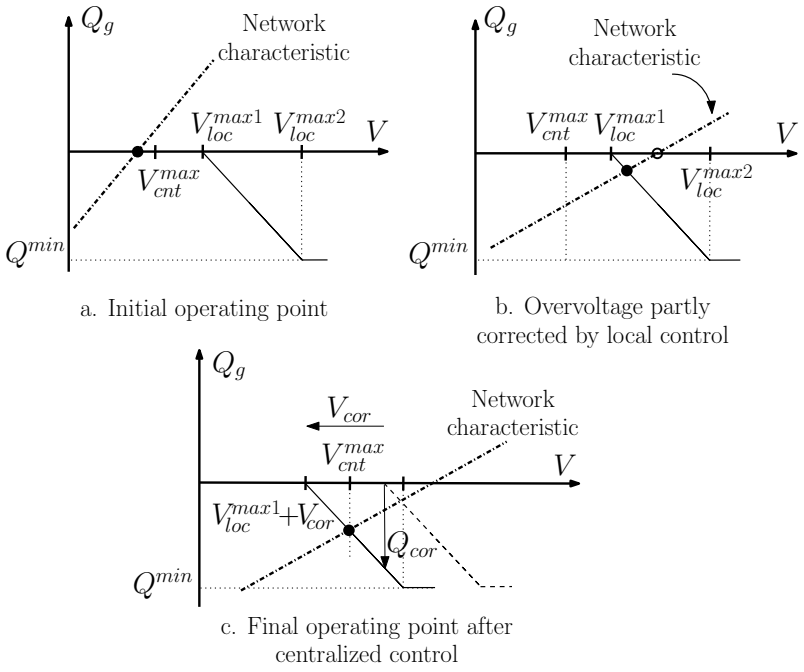

Figure 5.4: Example of over-voltage correction by local and centralized controls (only high voltage part of the characteristic is shown). The smaller slope of the VQ curve in sub-figures 5.4.b and 5.4.c compared to 5.4.a corresponds to a larger Thévenin impedance seen by the DGU

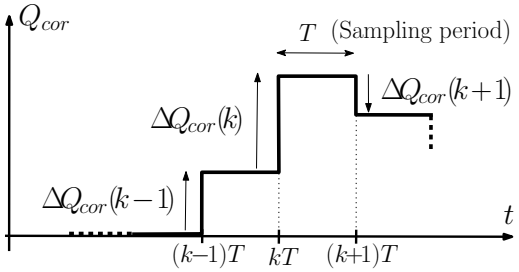

Figure 5.5: Local level: cumulation of reactive power corrections received from the centralized controller

The upper level keeps on sending ΔQ_{cor} corrections until the voltage is brought at the V_{cnt}^{max} limit, as illustrated by the black dot in Fig. 5.4.c.

Note that the cumulated correction Q_{cor} received from the centralized controller is different from the DGU effective reactive power change, as seen from Fig. 5.4.c. A linear relation between both can be used, as detailed in Section 5.2.3.

Note also that different voltage limits are specified in the local and centralized controls. Local control aims at mitigating the voltage excursion in the very first seconds after a disturbance. The centralized control acts only if the resulting voltage exceeds the limit V_{cnt}^{max}.

A similar behaviour is obtained in case of under-voltage.

With the above correction, the expression of the "VQ characteristic" block in Fig. 5.3 can be detailed as follows:

$$Q_d = \begin{cases} Q^{max} & \text{if } V - V_{cor} \leq V_{loc}^{min2} \\ R(V_{loc}^{min1} + V_{cor} - V) & \text{if } V_{loc}^{min2} < V - V_{cor} < V_{loc}^{min1} \\ 0 & \text{if } V_{loc}^{min1} \leq V - V_{cor} \leq V_{loc}^{max1} \\ -R(V - V_{loc}^{max1} - V_{cor}) & \text{if } V_{loc}^{max1} < V - V_{cor} < V_{loc}^{max2} \\ Q^{min} & \text{if } V - V_{cor} \geq V_{loc}^{max2} \end{cases} \tag{5.2}$$

where the various voltage thresholds are defined in Fig. 5.2, and the same droop R has been considered for under- and over-voltage, for simplicity.

5.2.3 Upper level: centralized control

The aim of the upper-level controller is to bring voltages inside tighter limits and balance the various DGU contributions. It relies on measurements collected throughout the network.

For clarity, the formulation in the following section involves only the corrections $\Delta \boldsymbol{Q}_{cor}$ sent to lower level, while extensions to DGU active powers and LTC voltage set-point are discussed afterwards in the same section.

MPC formulation

At a discrete time k, the objective is to minimize over the next N_c steps the deviations of the reactive powers of these DGUs, $\boldsymbol{Q}_g(k+i)$, from their last measured values, $\boldsymbol{Q}_g^m(k)$:

$$\min_{\boldsymbol{Q}_g, \boldsymbol{V}, \Delta \boldsymbol{Q}_g, \Delta \boldsymbol{Q}_{cor}, \boldsymbol{\varepsilon}} \quad \sum_{i=0}^{N_c-1} \|\Delta \boldsymbol{Q}_g(k+i)\|_{\boldsymbol{W}}^2 + \|\boldsymbol{\varepsilon}\|_{\boldsymbol{S}}^2 \tag{5.3}$$

where for $i = 0, \ldots, N_c - 1$:

$$\Delta \boldsymbol{Q}_g(k+i) = \boldsymbol{Q}_g(k+i) - \boldsymbol{Q}_g^m(k) \tag{5.4}$$

and $\boldsymbol{W}$ is a diagonal matrix allowing to give different weights to different DGUs. The second term in (5.3) involves the slack variables $\boldsymbol{\varepsilon}$ aimed at relaxing the inequality constraints (detailed hereafter) in case of infeasibility. Matrix $\boldsymbol{S}$ is also diagonal with large diagonal elements to force the constraints.

The minimization is subject to the linearized relation between $\Delta \boldsymbol{Q}_g$ and the control variables:

for $i = 0, \ldots, N_c - 1$:

$$\Delta \boldsymbol{Q}_g(k+i) = \boldsymbol{S}_{QQ}\, \Delta \boldsymbol{Q}_{cor}(k+i) \tag{5.5}$$

as well as the linearized predicted evolution of voltages over the future N_p steps:

for $i = 1, \ldots, N_p$:

$$\boldsymbol{V}(k+i) = \boldsymbol{V}^m(k) + \boldsymbol{S}_{VQ}\, \Delta \boldsymbol{Q}_g(k+i-1) \tag{5.6}$$

$$\boldsymbol{I}(k+i) = \boldsymbol{I}^m(k) + \boldsymbol{S}_{IQ}\, \Delta \boldsymbol{Q}_g(k+i-1) \tag{5.7}$$

where $\boldsymbol{V}(k+i)$ and $\boldsymbol{I}(k+i)$ are the vectors of predicted bus voltages and branch currents at time $k+i$. The prediction is initialized with the last gathered measurements $\boldsymbol{V}^m(k)$ and $\boldsymbol{I}^m(k)$. $\boldsymbol{S}_{QQ}$ and $\boldsymbol{S}_{VQ}$ are sensitivity matrices whose derivation is detailed in the next section, and $\boldsymbol{S}_{IQ}$ relates the branch current variation to DGU reactive power changes.

Finally, the following inequality constraints are imposed:

$$\boldsymbol{\varepsilon} = \begin{bmatrix} \varepsilon_1 & \varepsilon_2 \end{bmatrix} \geq \boldsymbol{0} \tag{5.8}$$

for $i = 1, \ldots, N_p$:

$$(-\varepsilon_1 + V_{cnt}^{min})\, \boldsymbol{1} \leq \boldsymbol{V}(k+i) \leq (V_{cnt}^{max} + \varepsilon_2)\, \boldsymbol{1} \tag{5.9}$$

$$\boldsymbol{I}(k+i) \leq \boldsymbol{I}^{max} \tag{5.10}$$

for $i = 0, \ldots, N_c - 1$:

$$\boldsymbol{Q}_g^{min}(k) \leq \boldsymbol{Q}_g(k+i) \leq \boldsymbol{Q}_g^{max}(k) \tag{5.11}$$

$$\Delta \boldsymbol{Q}_g^{min} \leq \boldsymbol{Q}_g(k+i) - \boldsymbol{Q}_g(k+i-1) \leq \Delta \boldsymbol{Q}_g^{max} \tag{5.12}$$

where $\boldsymbol{1}$ denotes a unit vector, $\boldsymbol{Q}_g^{min}$, $\boldsymbol{Q}_g^{max}$, $\Delta \boldsymbol{Q}_g^{min}$ and $\Delta \boldsymbol{Q}_g^{max}$ are the lower and upper limits on DGU reactive powers and on their rates of change. In (5.12), $\boldsymbol{Q}_g(k-1)$ is set to $\boldsymbol{Q}_g^m(k)$.

After the voltage, active and reactive power measurements have been received from the DGUs, and before the optimization is solved, the bounds $\boldsymbol{Q}_g^{min}$ and $\boldsymbol{Q}_g^{max}$ in (5.11) are updated in accordance with the DGU capability curves, as explained in Section 2.4.2.

The above formulation is very similar to the one used in Section 2.4. However, a significant difference lies in the fact that the objective (5.3) does not involve the deviations of control variables but $\Delta \boldsymbol{Q}_g$, which is a linear function of the control variables $\Delta \boldsymbol{Q}_{cor}$. This modification was required to properly account for the lower level control.

The formulation is such that, if all voltages and currents lie inside the feasible set defined by (5.9, 5.10), the obvious solution is $\Delta \boldsymbol{Q}_{cor} = \boldsymbol{0}$, i.e. no control is sent to the DGUs.

Derivation of sensitivity matrices

The sensitivity matrix $\boldsymbol{S}_{VQ}$ (resp. $\boldsymbol{S}_{QQ}$) expresses how much the bus voltages (resp. the DGU reactive powers) change after a small change $\Delta\boldsymbol{Q}_{cor}$ of the control variables.

A graphic view is given in Fig.5.6, showing the voltage and reactive power changes induced a variation of ΔQ_{cor} in one DGU. Assuming operation on the inclined part of the VQ characteristic, the figure shows the resulting change of voltage ΔV and reactive power ΔQ_g.

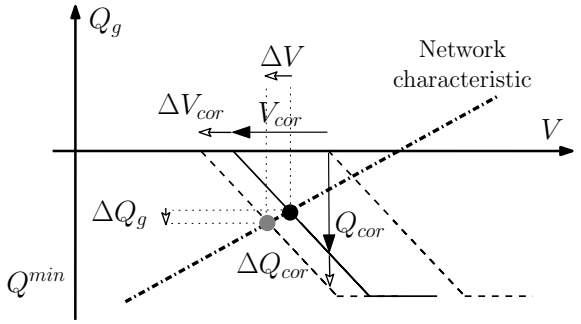

Figure 5.6: Graphic representation of the effects of a small control change ΔQ_{cor}

The equation of the solid black line is:

$$Q_g - Q_{cor} = -R\,(V - V_{loc}^{max1}) \tag{5.13}$$

involving the already defined droop R. Considering small deviations denoted with Δ, (5.13) gives:

$$\Delta Q_g - \Delta Q_{cor} = -R\,\Delta V \tag{5.14}$$

This equation can be written in matrix form for all DGUs as:

$$\Delta\boldsymbol{Q}_g = \Delta\boldsymbol{Q}_{cor} - \boldsymbol{R}\Delta\boldsymbol{V} \tag{5.15}$$

where $\boldsymbol{R}$ is a diagonal matrix whose diagonal elements are the various droop coefficients.

The variation of the bus voltages with the DGU reactive powers is given by:

$$\Delta\boldsymbol{V} = \boldsymbol{S}_{VQ}\Delta\boldsymbol{Q}_g \tag{5.16}$$

where $\boldsymbol{S}_{VQ}$ can be obtained from the transposed inverse of the power flow Jacobian matrix. Alternatively, each column of the matrix can be computed by running a power flow calculation with one DGU reactive power slightly modified, and dividing the bus voltage variations by the reactive power variation considered.

By substituting (5.16) in (5.15), one easily obtains:

$$\Delta \boldsymbol{Q}_g = (\boldsymbol{U} + \boldsymbol{R}\,\boldsymbol{S}_{VQ})^{-1} \Delta \boldsymbol{Q}_{cor} \tag{5.17}$$

where $\boldsymbol{U}$ is a unit matrix. The sought matrix is thus given by:

$$\boldsymbol{S}_{QQ} = (\boldsymbol{U} + \boldsymbol{R}\,\boldsymbol{S}_{VQ})^{-1} \tag{5.18}$$

The above calculation is made under the assumption that all DGUs operate on the sloping portion of their VQ characteristics. This could be justified by the fact that, after a significant voltage disturbance, the DGUs contributing the most to local voltage control will have their operating points moved to those sloping portions. The fact remains, however, that for DGUs operating in their dead-band, (5.18) is inexact.

One option would be for the centralized controller to know the status of operation of each DGU and update $\boldsymbol{S}_{QQ}$ to reflect the changes. This would entail too much complexity. It is more appealing to work with a non-updated $\boldsymbol{S}_{QQ}$ matrix and leave it to MPC to compensate for the error, taking advantage of its ability to operate with a somewhat inaccurate model.

More precisely, when the centralized controller assigns a correction ΔQ_{cor} to a DGU assuming implicitly that it operates on the sloping portion of its VQ characteristic, while it lies (and remains) in its dead-band, the DGU does not respond with the expected additional reactive power. This will cause the MPC to repeat its requests at subsequent times. In the best case, the VQ curve is enough shifted so that the DGU eventually operates on the sloping portion (and hence adjusts its reactive power). If those repeated attempts remain unsuccessful, other DGUs will be solicited and the voltage correction is likely to take some more time.

An example of this situation is presented in Section 5.3, scenario 3.

Extension to DGU active power control

The DGU reactive powers are the preferred control means to correct abnormal voltages. In severe conditions where there are not enough DGUs, or they are not properly located in the network, the optimization problem (5.3-5.12) may become infeasible. This is easily detected by a non-zero value of ε, which gives a warning that other control means are needed, namely the voltage set-point of the LTC and, in the last resort, the DGU active powers. LTC control is discussed in the next section, while an extension that encompasses both active and reactive power controls is given hereafter.

Note that this extension is also needed when the initial problem is a thermal overload that cannot be solved by changing reactive powers only.

The objective function (5.3) becomes:

$$\min \sum_{i=0}^{N_c-1} \|\Delta \boldsymbol{Q}_g(k+i)\|^2_{\boldsymbol{W}_Q} + \|\Delta \boldsymbol{P}_g(k+i)\|^2_{\boldsymbol{W}_P} + \|\boldsymbol{\varepsilon}\|^2_{\boldsymbol{S}} \tag{5.19}$$

where $\Delta \boldsymbol{P}_g$ is the vector of active power corrections:

$$\Delta \boldsymbol{P}_g(k+i) = \boldsymbol{P}_g(k+i) - \boldsymbol{P}_g^m(k) \tag{5.20}$$

and the entries of $\boldsymbol{W}_P$ are set much higher than those of $\boldsymbol{W}_Q$ in order to give priority to reactive power changes. Similar to (5.11, 5.12), the following constraints are imposed on active powers and their rates of change ($i = 0, \ldots, N_c - 1$):

$$\boldsymbol{P}_g^{min}(k) \leq \boldsymbol{P}_g(k+i) \leq \boldsymbol{P}_g^{max}(k) \tag{5.21}$$

$$\Delta \boldsymbol{P}_g^{min} \leq \boldsymbol{P}_g(k+i) - \boldsymbol{P}_g(k+i-1) \leq \Delta \boldsymbol{P}_g^{max} \tag{5.22}$$

The choice of $\boldsymbol{P}_g^{max}(k)$ is discussed in Section 2.7.

The equality constraints (5.5)-(5.7) are extended as follows to account for active power changes:

$$\Delta \boldsymbol{Q}_g(k+i) = \boldsymbol{S}_{QQ}\, \Delta \boldsymbol{Q}_{cor}(k+i) + \boldsymbol{S}_{QP}\, \Delta \boldsymbol{P}_g(k+i) \tag{5.23}$$

$$\boldsymbol{V}(k+i) = \boldsymbol{V}^m(k) + \boldsymbol{S}_{VQ}\, \Delta \boldsymbol{Q}_g(k+i-1) + \boldsymbol{S}_{VP}\, \Delta \boldsymbol{P}_g(k+i-1) \tag{5.24}$$

$$\boldsymbol{I}(k+i) = \boldsymbol{I}^m(k) + \boldsymbol{S}_{IQ}\, \Delta \boldsymbol{Q}_g(k+i-1) + \boldsymbol{S}_{IP}\, \Delta \boldsymbol{P}_g(k+i-1) \tag{5.25}$$

The extended formulation including active power changes consists in minimizing the objective (5.19) subject to the constraints (5.8)-(5.12) together with (5.20)-(5.25).

The sensitivity matrix $\boldsymbol{S}_{VP}$ (resp. $\boldsymbol{S}_{IP}$) is determined similarly to $\boldsymbol{S}_{VQ}$ (resp. $\boldsymbol{S}_{IQ}$). The $\boldsymbol{S}_{QP}$ matrix is derived as follows. The variations of bus voltages with the DGU active and reactive powers is now given by:

$$\Delta \boldsymbol{V} = \boldsymbol{S}_{VQ}\, \Delta \boldsymbol{Q}_g + \boldsymbol{S}_{VP}\, \Delta \boldsymbol{P}_g \tag{5.26}$$

Substituting this expression for $\Delta \boldsymbol{V}$ in (5.15) yields:

$$\Delta \boldsymbol{Q}_g = \Delta \boldsymbol{Q}_{cor} - \boldsymbol{R}\, \boldsymbol{S}_{VQ}\, \Delta \boldsymbol{Q}_g - \boldsymbol{R}\, \boldsymbol{S}_{VP}\, \Delta \boldsymbol{P}_g \tag{5.27}$$

which can be rewritten as:

$$(\boldsymbol{U} + \boldsymbol{R}\boldsymbol{S}_{VQ})\,\Delta\boldsymbol{Q}_g = \Delta\boldsymbol{Q}_{cor} - \boldsymbol{R}\,\boldsymbol{S}_{VP}\,\Delta\boldsymbol{P}_g \tag{5.28}$$

from which the sought sensitivity matrices are obtained as:

$$\boldsymbol{S}_{QQ} = (\boldsymbol{U} + \boldsymbol{R}\boldsymbol{S}_{VQ})^{-1} \tag{5.29}$$

$$\boldsymbol{S}_{QP} = -(\boldsymbol{U} + \boldsymbol{R}\boldsymbol{S}_{VQ})^{-1}\,\boldsymbol{R}\,\boldsymbol{S}_{VP} \tag{5.30}$$

Extension to transformer ratio control

As already discussed in Section 2.11, another option for voltage control consists of adjusting the ratio of the transformer connecting the distribution grid to transmission.

However, increasing the number of tap changes reduces the LTC lifetime, and considering the higher accuracy and speed offered by power electronics-based DGUs, the latter are progressively preferred to actions on LTCs.

For this reason, and also for the sake of clarity, in this chapter, voltage correction is performed without the contribution of the LTC. But it could be included as described in Section 2.11.

Interactions between local and centralized controls

As already explained a disturbance triggers a fast reaction of local controllers, followed by a slower corrections by the centralized controller. There are basically two cases:

- the measurements used by the centralized controller are collected after the DGU powers have reached (almost) steady state. In this case there is clear separation between local and centralized controls. Furthermore, the centralized controller will benefit from measurements that already reflect the contribution of local controls;

- the measurements used by the centralized controller are collected while the DGU powers are still evolving in response to the disturbance. The measurements are thus affected by these transients, which can be seen as noise, compensated by the closed-loop feature of the centralized controller.

5.3 Simulation results: Combined control scheme

5.3.1 Test system and control settings

The performance of the combined control is illustrated on the 75-bus distribution network introduced in Section 1.4.2. The same network topology, measurement locations and controller settings are assumed as in Section 2.8.

The network hosts 22 DGUs, of which 13 are synchronous generators driven by turbines, and the remaining are doubly fed induction generators driven by wind-turbines.

Moreover, it is assumed that each DGUs can operate in the shaded area of the capability diagram shown in Fig. 5.7 [CEN15], where S^{max} is the rated apparent power. The area is defined by: power factor between 0.9 and 1.0 in both under- and over-excited modes, active power smaller than the maximum P^{max} defined in the figure, apparent power $S \geq 0.1 S^{max}$.

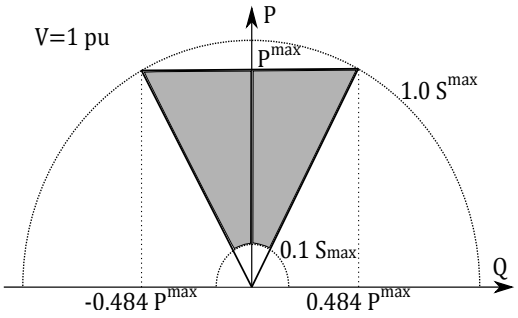

Figure 5.7: DGU capability diagram; operation is allowed in the shaded area

The measurements are received by the centralized controller every 10 seconds. The corrections $\Delta \boldsymbol{Q}_{cor}$, obtained from (5.32)-(5.12), are sent to the DGUs with the same periodicity. The DGUs respond to these corrections within a few seconds, due to their internal dynamics.

Table 5.1: Voltage thresholds and limits

local control (see Fig. 5.2)	centralized control (bounds in (5.11))
$V_{loc}^{min2} = 0.92$ pu	
$V_{loc}^{min1} = 0.97$ pu	$V_{cnt}^{min} = 0.97$ pu
$V_{loc}^{max1} = 1.03$ pu	$V_{cnt}^{max} = 1.03$ pu
$V_{loc}^{max2} = 1.08$ pu	

The voltage thresholds and limits used in all simulations are given in Table 5.1. At local level, the VQ characteristics were chosen to obtain progressive reactive power changes.

In the objective function (5.3), $\boldsymbol{W}$ has been set to a unit matrix and the diagonal entries of $\boldsymbol{S}$ to 10^4, where all voltages and slack variables are in per unit on the network voltage base.

5.3.2 Scenario 1: Local control only

In this first scenario, the voltages are initially within the 0.97-1.03 pu dead-band of both control levels, and all DGUs operate at unity power factor. All DGUs produce active power, which results in higher voltages as one moves away from the transformer towards the end of a feeder. The grid exports 13.7 MW and imports 6.5 MVar.

The assumed disturbance is a 0.05 pu drop of the Thévenin voltage at $t = 30\ s$. For reasons explained in Section 5.2.3, the transformer LTC is inoperative.

The voltage evolutions at various MV buses are shown in Fig. 5.8. The voltage drop is large enough to move the operating point outside the dead-band of some VQ characteristics (see Fig. 5.2). Therefore, those DGUs with a terminal voltage lower than $V_{loc}^{min1} = 0.97$ pu start producing reactive power right after the disturbance. The other DGUs keep operating at unity power factor. For comparison purposes, the light gray rectangle in Fig. 5.8 shows the range of bus voltages if there was no local control. The voltages are partly but rapidly corrected, leading to fewer buses in low voltage situation.

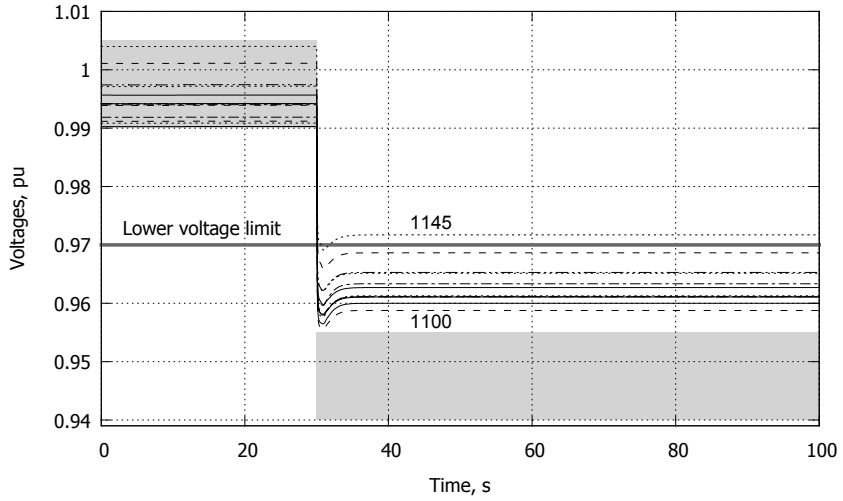

Figure 5.8: Scenario 1: Voltages at a sample of MV buses

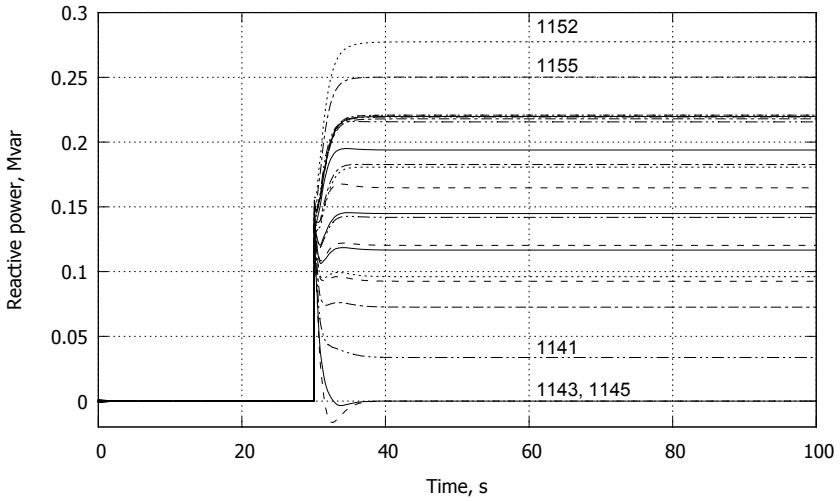

Figure 5.9: Scenario 1: Reactive power produced by a sample of DGUs

The reactive powers produced by various DGUs are shown in Fig. 5.9. No DGU reaches its maximum reactive power limit. It can be seen that generators 1143 and 1145 transiently produce reactive power but return to unity power factor in steady state, as they keep on operating in the dead-band of their static VQ characteristics. For those DGUs which eventually produce reactive power, the contribution varies with the terminal voltage and, hence, with the location.

5.3.3 Scenario 2: Local and centralized control

In this scenario, the operating point and the disturbance are unchanged but the centralized controller now sends the $\Delta \boldsymbol{Q}_{cor}$ corrections to the local controllers, shifting their VQ characteristics until the desired reactive powers are obtained.

The bus voltages are shown in Fig. 5.10. Again, the corrective action of the local controllers can be assessed by comparing the light gray rectangle with the voltages reached a little before $t = 40\ s$, when the first $\Delta \boldsymbol{Q}_{cor}$ correction is applied. Although improved, the voltages of many buses are still below the specified lower limit.

As long as all voltages are inside the $[V_{cnt}^{min}\ \ V_{cnt}^{max}]$ range, the upper level does not issue any correction. It acts for the first time at $t = 40$ s, after some measured voltages have been found lower than $V_{cnt}^{min} = 0.97$ pu. Two control steps are enough to bring them all in the desired range, bus 1100 being just at the limit.

Figure 5.11 shows the variations of reactive power generations of various DGUs. From $t = 30$ to $t = 40\ s$, the DGU reactive powers either increase or remain at zero, as in Scenario 1, while

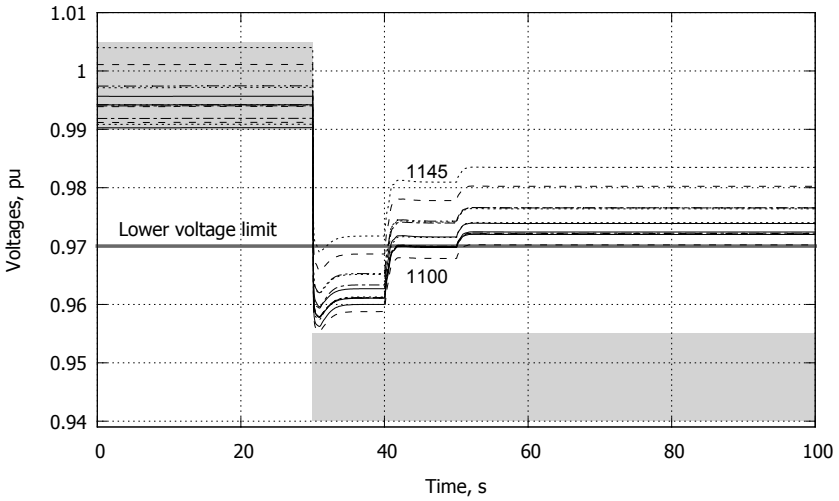

Figure 5.10: Scenario 2: Voltages at a sample of MV buses

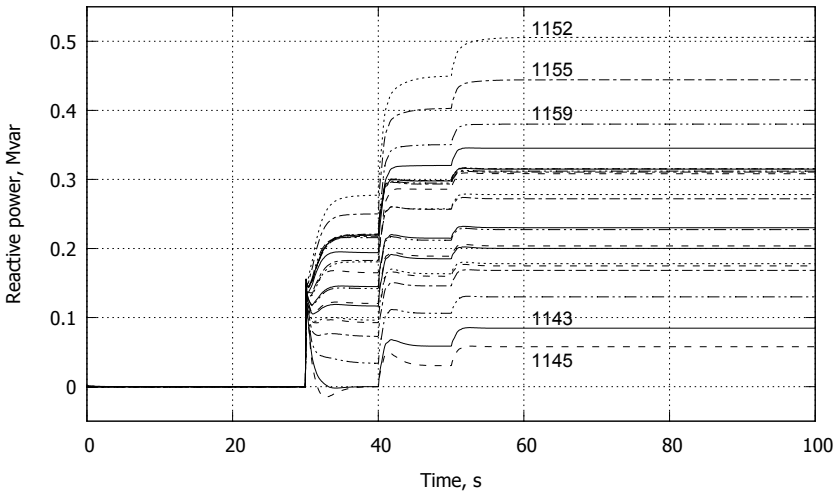

Figure 5.11: Scenario 2: Reactive power produced by a sample of DGUs

at $t = 40$ and 50 s, the centralized controller increases all of them in a coordinated way. The contributions differ from one DGU to another, as the result of coordinated control relying on the sensitivity matrices $\boldsymbol{S}_{VQ}$ and $\boldsymbol{S}_{QQ}$. They would also be influenced by unequal weights in $\boldsymbol{W}$.

These corrections issued by both control levels decrease the reactive power imported by the distribution network. Given that the exported active power remains (almost) unchanged, the current in the transformer decreases, as shown in Fig. 5.12.

However, a branch overload problem could appear in other scenarios, for instance when the DGUs decrease their reactive power to correct an over-voltage problem. In such a case the controller

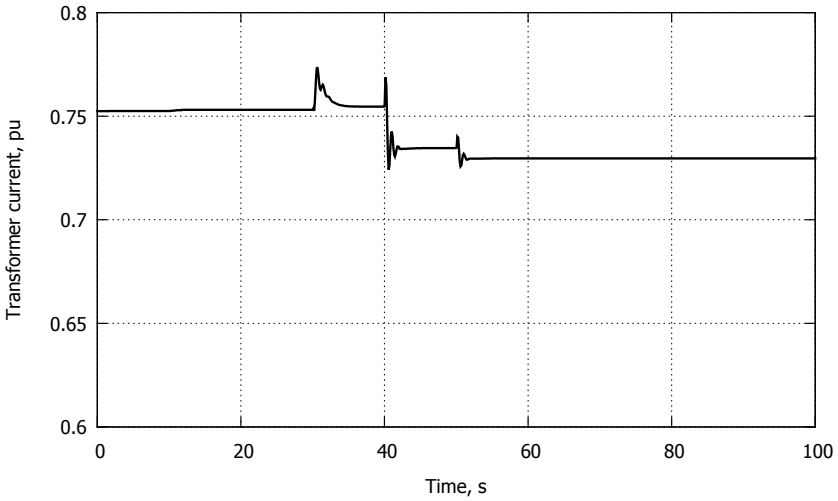

Figure 5.12: Scenario 2: Current flowing in the 33/11 kV transformer

would keep correcting voltages until the transformer current reaches its hard upper limit constraint (5.10). At this point, the optimization problem (5.3)-(5.12) being infeasible, the voltage constraints (5.9) would be relaxed through a nonzero ε_2. This issue would be properly handled using the extended optimization problem (5.19)-(5.25) allowing active power corrections.

5.3.4 Scenario 3: Local and centralized control with limited reactive reserves

In this third scenario, a different initial operating point is considered, with a lower active power generation by the DGUs along the feeders that start at nodes 1151, 1115, 1101, 1104, 1110 and 1107. At this operating point, the MV grid receives active power from the external grid. The power flow results in lower voltages as one moves away from the transformer towards the end of the above listed feeders. As a wider range of active powers is considered, there is also a greater variety of reactive power limits.

The assumed disturbance is a 0.04 pu drop of the Thévenin voltage at $t = 30$ s.

As shown in Fig. 5.13, some of the voltages are initially close to the lower limit and, hence, most of the buses experience under-voltage after the occurrence of the disturbance. As in the previous scenarios, the voltage fall is mitigated by the local voltage control.

The corresponding reactive power generations are shown in Fig. 5.14. From $t = 30$ to $t = 40$ s, under the effect of local control, the DGUs which undergo low voltages inject reactive power, while the others remain with a zero injection. Following the first correction, sent by the centralized controller at $t = 40$ s, the grid voltages are already significantly improved. In fact, the buses with

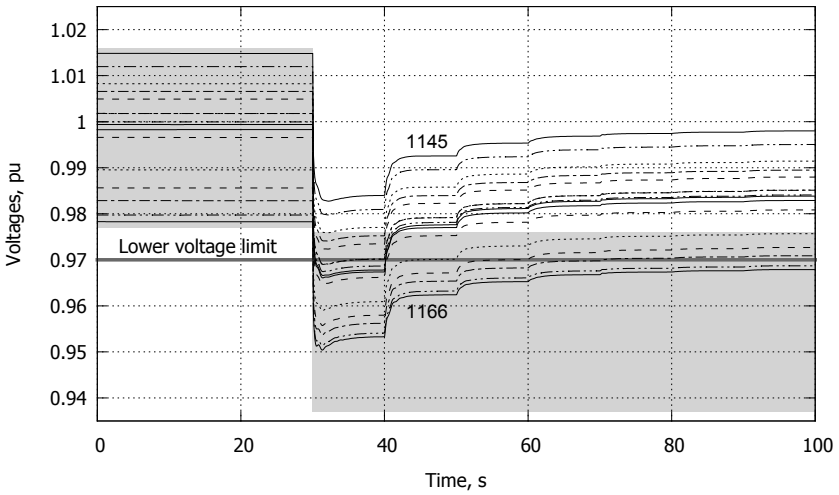

Figure 5.13: Scenario 3: Voltages at a sample of MV buses

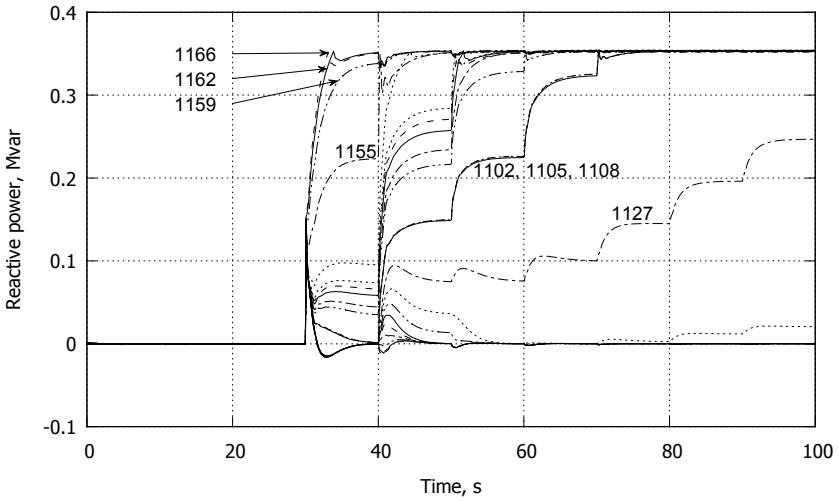

Figure 5.14: Scenario 3: Reactive power produced by a sample of DGUs

a measured voltage still below the limit at $t \simeq 49$ s are 1166, 1162, 1159 and 1157, all located along the same, long feeder. Figure 5.14 shows that the DGUs at buses 1166, 1162 and 1159 have reached their maximum reactive power and, hence, cannot further help correcting the voltages. Therefore, the controller adjusts the reactive power of other DGUs, including some located in other branches, in order to raise the network voltages and correct the remaining unsatisfactory voltages. This is done smoothly in several time steps.

It is clearly seen that, in this scenario, voltages recover more slowly than in Scenario 2. Moreover, after six control steps, the voltages in the neighbourhood of bus 1166 are very close but still below the desired value. This is due to the fact that some of DGUs operate in the dead-band of their

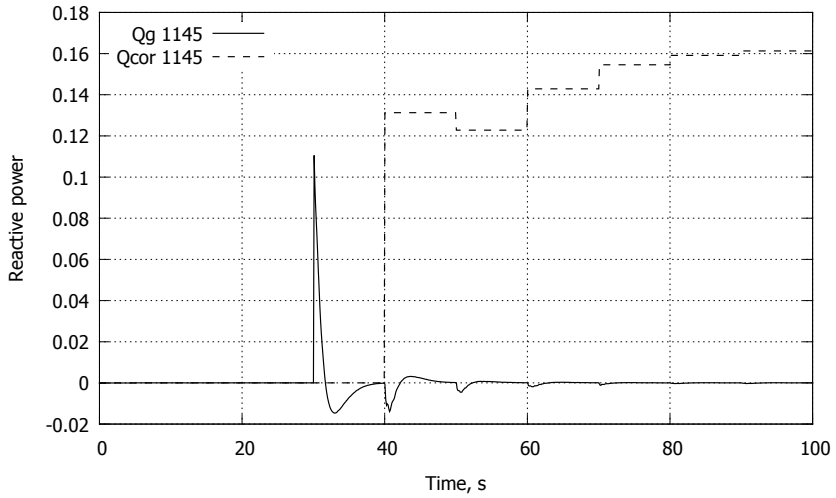

Figure 5.15: Scenario 3: Reactive power corrections and DGU response

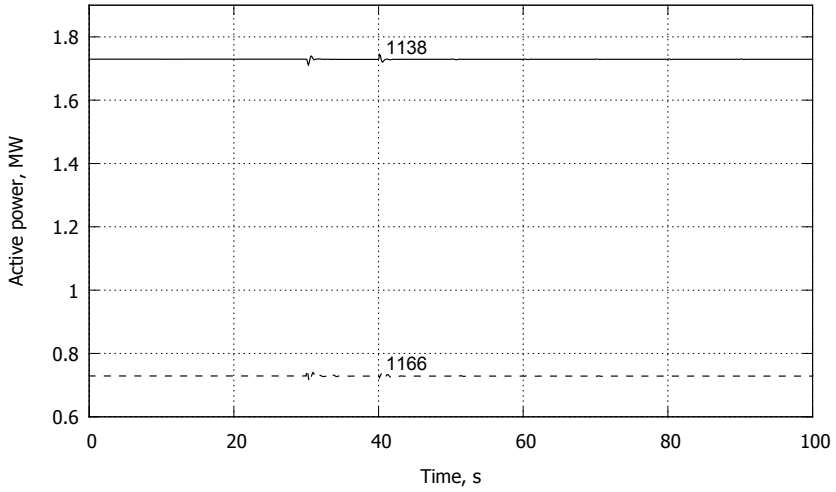

Figure 5.16: Scenario 3: Active powers produced by two DGUs

VQ characteristic, while the centralized controller assumes they operate on the sloping portion, as explained in Section 5.2.3. Thus the DGUs of concern do not respond as expected, which leads to more control steps.

An illustration is provided in Fig. 5.15, comparing respectively the cumulated reactive power correction Q_{cor} and the effective reactive power production Q_g of the DGU at bus 1145. Before $t = 40$ s, since its terminal voltage is above V_{loc}^{min1}, its output reactive power remains at zero, in accordance with the VQ characteristic. The same holds true during the successive corrections applied by the centralized controller, which are insufficient to move the operating point on the sloping part. The situation is not known by the controller but is compensated by the closed-loop nature of MPC, which leads to a final operating point with only little violations of the voltage constraint.

In some cases, voltage violations can be corrected by acting on active power, with a higher "cost". This option was not contemplated in this part of the work. Figure 5.16 shows for instance the active powers of two DGUs, which remain constant apart from tiny transients due to reactive power adjustments.

5.4 Hybrid Control Scheme

As mentioned in Section 5.1, the hybrid scheme is a practical alternative when the deployment of the upper-level coordinated control can not be feasible or affordable over all DGUs. The corresponding formulation is presented in this section. It should be noted that due to the strong similarities between the hybrid and the combined schemes, the common explanations and formulations are not repeated here and only the differences are pointed out.

5.4.1 Lower-level: local control

Reactive power control of a DGU

Figure 5.1.d shows all DGUs are equipped with local control. However, they can be categorised in two subsets: those which are additionally adjusted by a higher level (under CLC control, as defined in the Introduction), and the rest under local control only. The employed local control of the former group, as shown in Fig. 5.17.b, is exactly as explained in Section 5.2.1. Obviously, the latter group does not have any interaction with the upper level. Thus, as shown in Fig. 5.17.a, the desired reactive power output Q_d is given by the VQ characteristic using the measured voltage only. The difference between Q_d and the measured reactive power is processed by a Proportional-Integral controller. The output V_{ref} is the terminal voltage reference in a power-electronics based DGU, or the field voltage in a synchronous generator.

The "adjustableVQ characteristic" block in Fig. 5.17.b can be expressed as of the combined scheme (please see (5.2)), and the "VQ characteristic" one in Fig. 5.17.a can be detailed as follows:

$$Q_d = \begin{cases} Q^{max} & \text{if } V \leq V_{loc}^{min2} \\ R(V_{loc}^{min1} - V) & \text{if } V_{loc}^{min2} < V < V_{loc}^{min1} \\ 0 & \text{if } V_{loc}^{min1} \leq V \leq V_{loc}^{max1} \\ -R(V - V_{loc}^{max1}) & \text{if } V_{loc}^{max1} < V < V_{loc}^{max2} \\ Q^{min} & \text{if } V \geq V_{loc}^{max2} \end{cases} \tag{5.31}$$

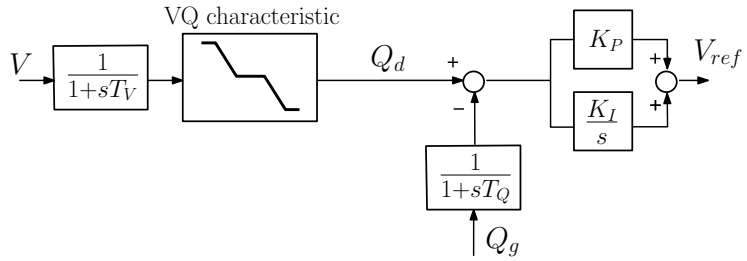

a: no interaction with the centralized controller

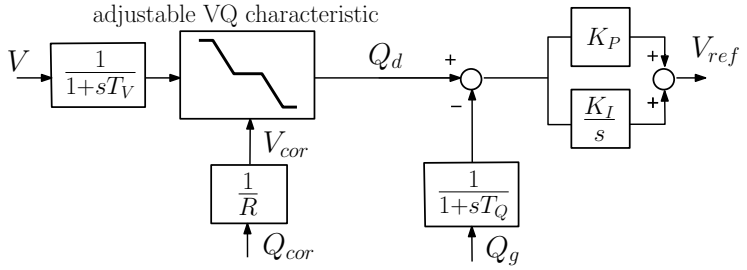

b: interaction with the centralized controller

Figure 5.17: Local level: generic model of DGU reactive power control

Correction from the centralized controller

The correction Q_{cor} received from the centralized controller modifies the VQ characteristic of the subset of DGUs under CLC control. The considerations in Section 5.2.2 apply to those DGUs also and are not repeated here.

5.4.2 Upper level: centralized control

MPC formulation

The multi-step MPC formulation is similar to the one already given in Section 5.2.3. However, it should be noted that a subset of the DGUs are not controlled by the centralized control while, due to their VQ characteristic, they react to any reactive power change of DGUs in CLC subset. Thus, the centralized controller needs to take into account the reaction of all local controllers, including those of the DGUs that are not under its control. Therefore, the formulation is adapted to act on the subset of DGUs under CLC control.

The control variables are the corrections $\Delta \boldsymbol{Q}_{cor}$ sent to the DGUs under CLC control.

At a discrete time k, the objective is to minimize over the next N_c steps the deviations of the

reactive powers of *all* DGUs, $\boldsymbol{Q}_g(k+i)$, from their last measured values, $\boldsymbol{Q}_g^m(k)$:

$$\min_{\boldsymbol{Q}_g, \boldsymbol{V}, \Delta\boldsymbol{Q}_g, \Delta\boldsymbol{Q}_{cor}, \boldsymbol{\varepsilon}} \quad \sum_{i=0}^{N_c-1} \|\Delta\boldsymbol{Q}_g(k+i)\|_{\boldsymbol{W}}^2 + \|\boldsymbol{\varepsilon}\|_{\boldsymbol{S}}^2 \tag{5.32}$$

where ($i = 0, \ldots, N_c - 1$):

$$\Delta\boldsymbol{Q}_g(k+i) = \boldsymbol{Q}_g(k+i) - \boldsymbol{Q}_g^m(k) \tag{5.33}$$

The minimization is subject to the linearized relation between $\Delta\boldsymbol{Q}_g$ and the control variables

for $i = 0, \ldots, N_c - 1$:

$$\Delta\boldsymbol{Q}_g(k+i) = \boldsymbol{S}_{QQ}^{'}\, \Delta\boldsymbol{Q}_{cor}(k+i) \tag{5.34}$$

$\boldsymbol{S}_{QQ}^{'}$ is sensitivity matrix whose derivation is detailed in the next section. It relates the reactive powers of all DGUs to the corrections imposed to DGUs under CLC control. Thus, it is not a square matrix as in Section 5.2.

The linearized voltages evolution, operating voltage and current constraints, and limits on control variables and their rate of changes are same as those detailed for combined scheme in Section 5.2.3 (see (5.6-5.12)).

Derivation of sensitivity matrix

The sensitivity matrix $\boldsymbol{S}_{QQ}^{'}$ expresses by how much the DGU reactive powers (also including those under local control only) vary following a small change $\Delta\boldsymbol{Q}_{cor}$ of the control variables. This matrix can be derived similar to $\boldsymbol{S}_{QQ}$ detailed in Section 5.2.3. However, it should be noted that for instance Eqs. (5.13) and (5.14) in that section correspond to a DGU under CLC control. The corresponding equation for a DGU under local control only can be easily derived by setting ΔQ_{cor} to zero. Therefore, the whole set of equations can be written in compact matrix form as:

$$\Delta\boldsymbol{Q}_g = \begin{bmatrix} \boldsymbol{0} \\ \Delta\boldsymbol{Q}_{cor} \end{bmatrix} - \boldsymbol{R}\Delta\boldsymbol{V} \tag{5.35}$$

where the size of the zero vector $\boldsymbol{0}$ is the number of DGUs under local control only, and $\boldsymbol{R}$ is a diagonal matrix whose diagonal elements are the various droop coefficients.

The variation of the bus voltages with the DGU reactive powers is given by:

$$\Delta\boldsymbol{V} = \boldsymbol{S}_{VQ}\Delta\boldsymbol{Q}_g \tag{5.36}$$

By substituting (5.36) in (5.35), one easily obtains:

$$\Delta \boldsymbol{Q}_g = (\boldsymbol{U} + \boldsymbol{R}\,\boldsymbol{S}_V)^{-1} \begin{bmatrix} \boldsymbol{0} \\ \Delta \boldsymbol{Q}_{cor} \end{bmatrix} \tag{5.37}$$

$$\Delta \boldsymbol{Q}_g = \boldsymbol{S}'_{QQ} \Delta \boldsymbol{Q}_{cor} \tag{5.38}$$

where $\boldsymbol{S}'_{QQ}$ is obtained from $(\boldsymbol{U} + \boldsymbol{R}\,\boldsymbol{S}_V)^{-1}$ by removing the columns relative to DGUs under local control only.

Similar to the combined scheme, the above calculation is made under the assumption that all DGUs operate on the sloping portion of their VQ characteristics.

5.5 Simulation result: Hybrid control scheme

The performance of the proposed controls is illustrated on the (much-used) 75-bus, 11-kV network. Given the fact that the DGUs under CLC control needs to be distinguished from those under LC only, the network one-line diagram is repeated in Fig. 5.18, but showing the former subset with gray filled disks.

The type of the DGUs remains unchanged. But, ten DGUs are assumed to be under local control only. The remaining twelve, under CLC control, are spread over different feeders.

The measurements are received every 10 s by the centralized controller, which sends the corrections $\Delta \boldsymbol{Q}_{cor}$ at the same rate. The units respond to these corrections within a few seconds, due to their internal dynamics.

The voltage thresholds shown in Table 5.1 were used in all simulations.

In the objective function (5.32), $\boldsymbol{W}$ has been set to a unit matrix and the diagonal entries of $\boldsymbol{S}$ to 10^4, where all voltages and slack variables are in per unit on the network voltage base.

In the fourth scenario of this chapter, all voltages are initially within the $[0.97\ 1.03]$ pu dead-band common to both control levels, and all DGUs operate with a unity power factor.

The simulation results deal with the response to a 0.05 pu drop of the external grid voltage at $t = 10$ s.

Figure 5.19 shows the voltage evolutions at a sample of buses throughout the grid. The voltage drop at $t = 10$ s is large enough to move the operating point outside the dead-band of many VQ

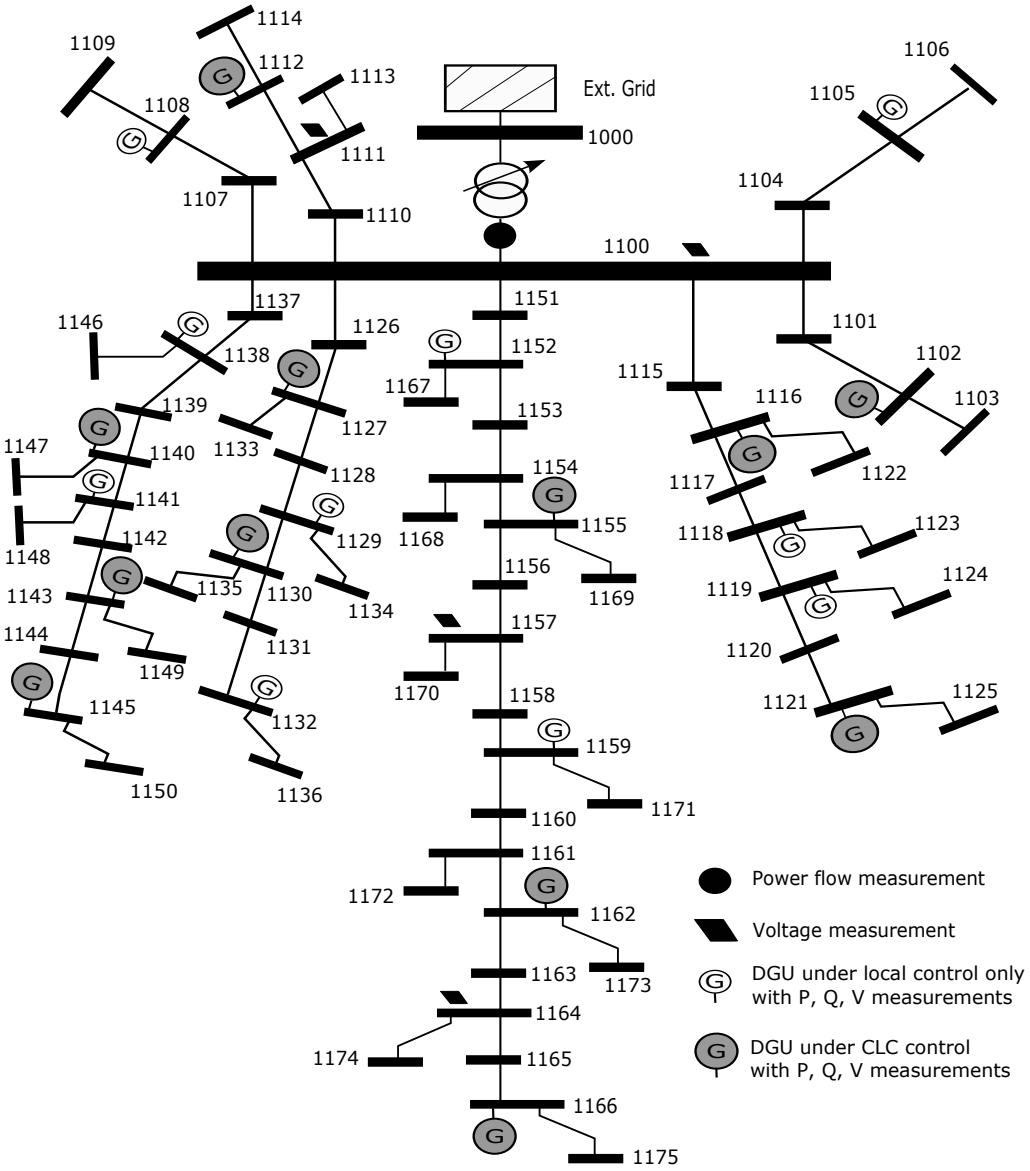

Figure 5.18: 75-bus test system: Network topology and measurement allocation with only some DGUs under the centralized control (Hybrid scheme)

characteristics (see Fig. 5.2). Therefore, the DGUs whose terminal voltage drops below $V_{loc}^{min1} = 0.97$ pu start producing reactive power right after the disturbance. The other DGUs keep operating at unity power factor. The voltages are partly but rapidly corrected, leading to fewer buses in low voltage situation.

At the next discrete time step, $t = 20$ s, the centralized controller, which has sensed the unsatisfactory voltages, starts sending corrections. The latter shift the VQ characteristics of the 12 DGUs under CLC control, leading them to increase their reactive power productions. It succeeds bringing

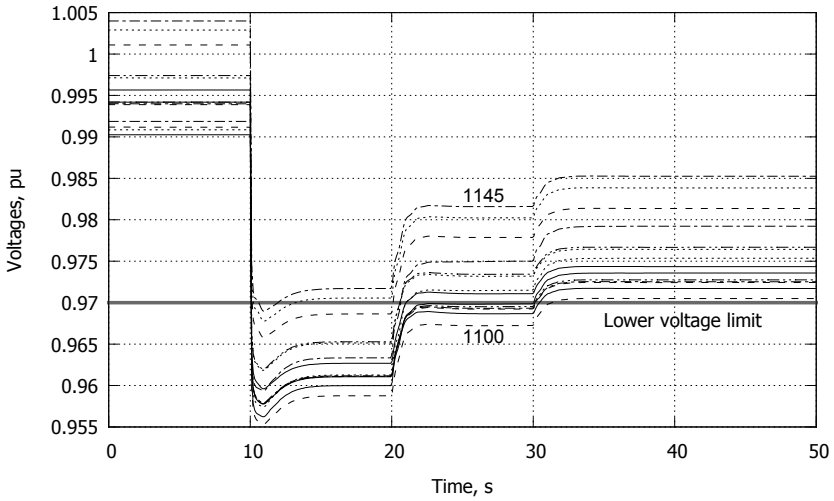

Figure 5.19: Scenario 4: Voltages at a sample of MV buses

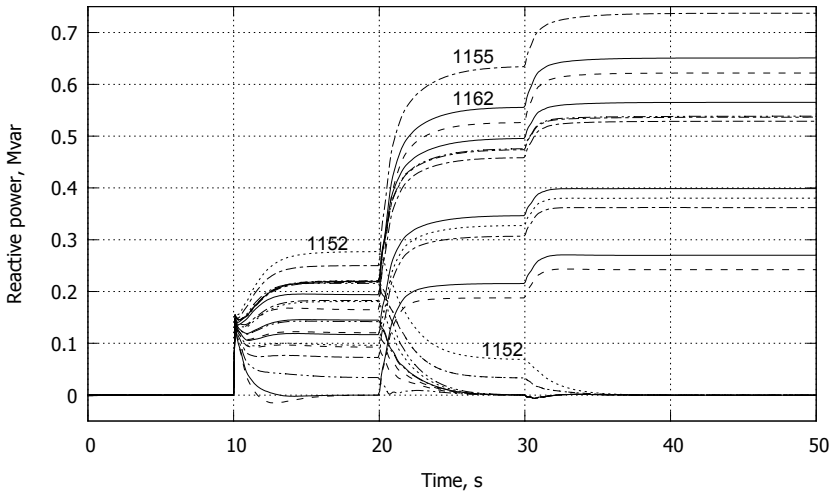

Figure 5.20: Scenario 4: Reactive power produced by a sample of DGUs

all voltages within the desired limits in two discrete steps (at $t = 20$ and 30 s, respectively).

Figure 5.20 shows how DGUs interact. As the centralized controller increases the reactive power of the DGUs under its control (e.g. see DGU at bus 1155 or 1162), the network voltages increase and the DGUs under local control only have their reactive power decreased (e.g. see DGU at bus 1152) and return to unity power factor at $t \simeq 35$ s.

In other words, DGUs under local control only participate in the initial correction of the voltage violation, and inject reactive power for a few tens of seconds only. The centralized controller anticipates this behaviour (through its sensitivity matrices) and properly adjust the DGUs under its control.

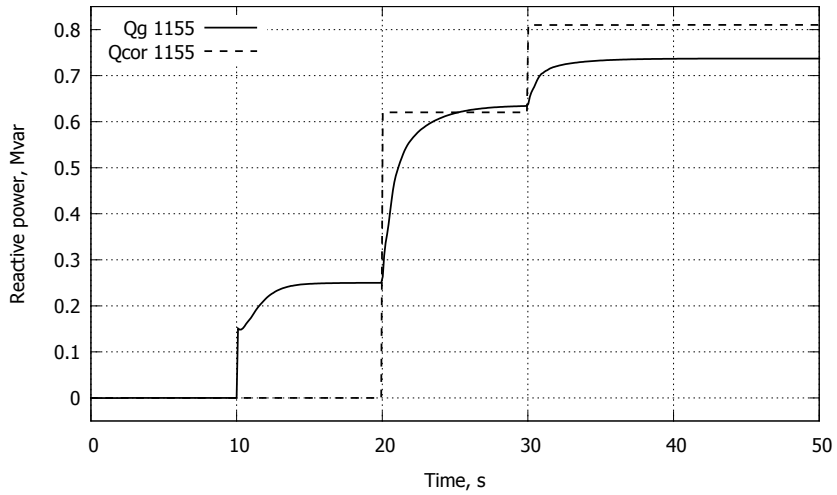

Figure 5.21: Scenario 4: DGU at bus 1155: cumulated correction vs. reactive power production

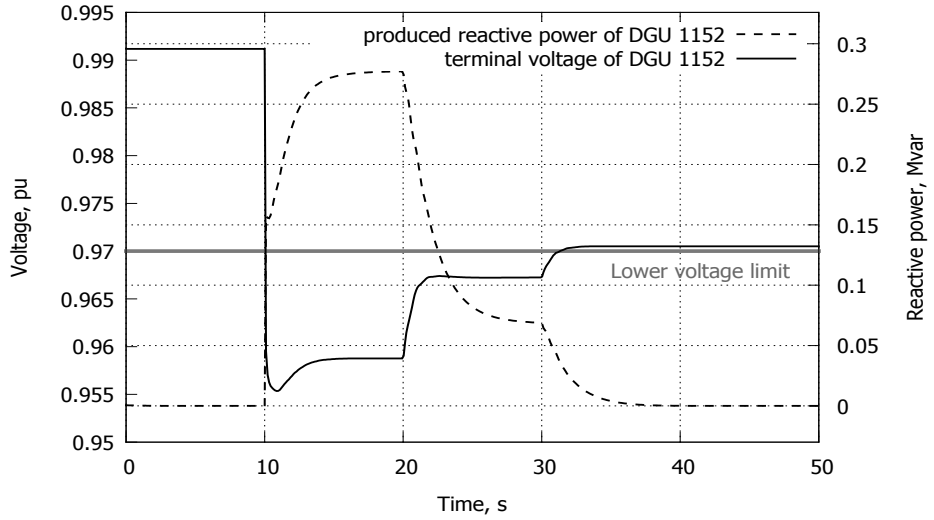

Figure 5.22: Scenario 4: DGU at bus 1152: terminal voltage and reactive power

Figure 5.21, focusing on the DGU at bus 1155, shows the cumulated correction Q_{cor} (dashed line), received from the centralized controller, and the resulting reactive power production Q_g (solid line). The former is increased in two steps, and the latter follows according to the DGU dynamics. In the final steady state, the two curves differ since: (i) a correction ΔQ_{cor} applied to a DGU does not yield an equal variation ΔQ_g of the that DGU, as shown graphically in Fig. 5.4; (ii) the reactive power of a DGU is impacted by the corrections applied to the other DGUs. This last effect is captured by the off-diagonal elements of matrix $\boldsymbol{S}'_{QQ}$, which show that the DGUs with the largest impact are those connected to buses 1162 and 1166.

Figure 5.22 shows the reactive power and the voltage of the DGU at bus 1152. Since this unit is under local control only, it does not produce reactive power as long as the voltage lies in between $V_{loc}^{min1} = 0.97$ and $V_{loc}^{max1} = 1.03$ pu. In response to the initial disturbance, the voltage drops below 0.97 pu and the unit increases its reactive power. The time taken to reach the maximum, around 5 s, is due to the measurement time constant, the PI controller (see Fig. 5.17), and other delays in the DGU excitation system. This response time is still short with respect to the 10 s sampling time of the centralized controller, which allows using a static, sensitivity-based model in the MPC formulation.

5.6 Conclusion

In this chapter combined and hybrid control architectures have been presented for corrective control of voltages in active distribution networks. Both methods, consist of two levels.

At the lower one, DGU reactive powers are controlled locally according to a piecewise linear static VQ characteristic. This local control provides a fast response to disturbances. It includes a dead-band to keep DGUs operating at unity power factor as far as possible.

The upper (centralized) level coordinates the various DGU reactive power corrections. In the combined scheme, the upper level communicates with all DGUs, while only a subset of DGUs are under the control of the upper level in the hybrid scheme. The latter is of interest when all DGUs cannot be controlled centrally.

To keep the centralized control simple and, consequently, the computational burden low, constant sensitivity matrices are used regardless of the operating point on the VQ characteristics. This is made possible by the robustness of MPC.

The reported simulation results clearly show the combination of a fast but partial correction by the local controllers, followed by the smooth, coordinated control of the DGU reactive powers by the upper-level control. The latter is able to complement the actions taken locally, taking into account the various DGU reactive power reserves as well as the cost and impact of DGU reactive power adjustments.

The results obtained with the hybrid scheme confirm that, if the voltage limits specified in the centralized control correspond to the dead-band of the lower level VQ characteristics, the whole reactive power effort is eventually transferred to the centrally controlled DGUs.

Chapter 6

Multi-step optimization for preventive security restoration

In this chapter the time frame of the centralized controller is extended with preventive security restoration. The latter uses near-future production/consumption predictions to determine if the active distribution network is going to operate within prescribed limits and, if not, to determine appropriate preventive decisions that can be used, for instance, as reference for the real-time corrective controller. The most distinctive feature of that preventive analysis is that it re-uses the multi-step constrained optimization formulation of our MPC-based real-time controller.

6.1 Introduction

preventive security restoration refers to studying the near-future network state, identifying limit violations, and taking preventive actions. This preventive analysis issues decisions (or only recommendations) to the other actors of the power system including the real-time control in order to, first, prevent the anticipated violations, and second, provide useful information for power balancing purposes and market objectives. It is stated as an Optimal Power Flow (OPF) problem, more precisely a feasibility restoration problem. In this chapter it is shown that the multi-step optimization at the heart of the MPC-based real-time controller can be re-used to solve that problem.

The correlation between the effective wind speed (or solar irradiation) and its prediction is expected to be relatively high in the horizon of few hours ahead [WGH11]. This information can be used to achieve a more secure and cost-effective operation of DNs. More precisely, some voltage and/or thermal violations can be avoided in advance, relieving the real-time controller from *ex post* corrective actions and, consequently, enhancing power quality. Moreover, these ahead-of-time preventive decisions, which are reflected on production schedules, can be of interest to other actors such as those responsible for maintaining a balance between consumption and production [KA14, MLEC16]. These decisions are taken in a horizon from a few hours to 15 minutes ahead of real-time.

The real-time corrective controller is then responsible for both implementing these schedules as well as handling unforeseen incidents and performing complementary adjustments to cope with imprecise predictions. It steers the DGUs to follow the desired power schedule (reflecting the decisions taken ahead of time) while monitoring the network through the collected measurements. If the latter reveals an unexpected violation, the real-time controller calculates and imposes *ex post* corrections to the units to bring the network back within admissible limits [SGV16].

Since it is in charge of fast control, the real-time controller has to clear the unexpected violations relatively fast. Thus, apart from minimizing communication delays and measurement time intervals, a short computing time is a key feature. To that purpose, a simple sensitivity-based model of the system is used, as explained in Chapter 2. On the other hand, for preventive security restoration, dealing with a longer time horizon, a higher computing time is acceptable.

In this chapter a sequential OPF formulation is presented in Section 6.2 for the preventive security restoration. Then the combination of the preventive and the corrective controls is discussed in Section 6.3. Simulation results are reported in Section 6.4.

6.2 Preventive security restoration: Open-loop sequential OPF

6.2.1 Problem statement

Using the most recently updated forecasts, the preventive analysis checks the near-future system state, identifies the limit violations, and runs an OPF to determine preventive actions, if necessary. To this end, the following objective is considered:

$$\min_{\boldsymbol{u},\boldsymbol{V},\boldsymbol{\theta}} \ \|\boldsymbol{u}-\hat{\boldsymbol{u}}\|^2_{\boldsymbol{W}} \tag{6.1}$$

where the control variables $\boldsymbol{u}$, consisting mainly of DGU power outputs, are requested to deviate as few as possible from their predicted values $\hat{\boldsymbol{u}}$. $\boldsymbol{W}$ is a diagonal matrix allowing to give different weights to different component of $\boldsymbol{u}$. The following constraints are imposed, while minimizing the objective:

$$\boldsymbol{f}(\boldsymbol{u},\hat{\boldsymbol{c}},\boldsymbol{V},\boldsymbol{\theta})=\boldsymbol{0} \tag{6.2a}$$

$$\boldsymbol{V}^{min}\leq\boldsymbol{V}\leq\boldsymbol{V}^{max} \tag{6.2b}$$

$$\boldsymbol{I}(\boldsymbol{V},\boldsymbol{\theta})\leq\boldsymbol{I}^{max} \tag{6.2c}$$

$$\boldsymbol{u}^{min}\leq\boldsymbol{u}\leq\boldsymbol{u}^{max} \tag{6.2d}$$

Solving the power flow equations (6.2a) with the anticipated consumptions $\hat{\boldsymbol{c}}$ yields the corresponding bus voltage magnitudes $\boldsymbol{V}$ and phase angles $\boldsymbol{\theta}$. Using the latter, the vector of branch currents $\boldsymbol{I}$ is obtained, which must be below its upper limit $\boldsymbol{I}^{max}$. The bus voltages also must be within the admissible limits $\boldsymbol{V}^{max}$ and $\boldsymbol{V}^{min}$. $\boldsymbol{u}^{max}$ and $\boldsymbol{u}^{min}$ define the control variable acceptable range.

It is clearly seen that, if the predicted production and consumption do not cause any violation, the above formulation returns the control variables $\boldsymbol{u}$ equal to their predicted values $\hat{\boldsymbol{u}}$. It means that the DGUs can be left to operate for Maximum Power Point tracking (MPPT) or any other desired strategy. Otherwise, it becomes a feasibility restoration problem, and the solution of the optimization problem serves as preventive decisions.

It should be also noted that satisfying the constraints (6.2b, 6.2c) might not be feasible in some difficult cases. Then, the constraints should be relaxed to a wider range to reach a solution.

6.2.2 Sequential quadratic programming

One way of solving the optimization problem (6.1, 6.2) is sequential quadratic programming. This well-known method [NCD00, Nej99] consists of linearizing the constraints around the current operating point, and solving repeatedly the resulting quadratic programming problems until convergence takes place. In more detail, the problem is as follows:

1. Initialize:

$$\begin{aligned} \boldsymbol{u}(0) &= \hat{\boldsymbol{u}} \\ k &= 1 \end{aligned}$$

   where k is the iteration counter number.

2. Solve the power flow equations:

$$\boldsymbol{f}(\boldsymbol{u}(k-1), \hat{\boldsymbol{c}}, \boldsymbol{V}(k), \boldsymbol{\theta}(k)) = \boldsymbol{0} \tag{6.3}$$

   to obtain $\boldsymbol{V}(k), \boldsymbol{\theta}(k)$ and hence $\boldsymbol{I}(\boldsymbol{V}(k), \boldsymbol{\theta}(k))$.

3. Compute the bus voltage and branch current sensitivity matrices $\boldsymbol{S}_V$ and $\boldsymbol{S}_I$, respectively, at the operating point $\boldsymbol{V}(k), \boldsymbol{\theta}(k)$.

   The sensitivity derivation has been detailed in Section 2.6.

4. Solve the quadratic problem:

$$\min_{\boldsymbol{u}(k), \boldsymbol{V}(k), \boldsymbol{\theta}(k), \boldsymbol{\varepsilon}} \ \|\boldsymbol{u}(k) - \hat{\boldsymbol{u}}\|^2_{\boldsymbol{W}} + \|\boldsymbol{\varepsilon}\|^2_{\boldsymbol{S}} \tag{6.4}$$

   subject to the linearized constraints:

$$\boldsymbol{V}(k+1) = \boldsymbol{V}(k) + \boldsymbol{S}_V \Big(\boldsymbol{u}(k) - \boldsymbol{u}(k-1)\Big) \tag{6.5a}$$

$$\boldsymbol{I}(k+1) = \boldsymbol{I}(\boldsymbol{V}(k), \boldsymbol{\theta}(k)) + \boldsymbol{S}_I \Big(\boldsymbol{u}(k) - \boldsymbol{u}(k-1)\Big) \tag{6.5b}$$

$$-\varepsilon_1 \boldsymbol{1} + \boldsymbol{V}^{min} \leq \boldsymbol{V}(k+1) \leq \boldsymbol{V}^{max} + \varepsilon_2 \boldsymbol{1} \tag{6.5c}$$

$$\boldsymbol{I}(k+1) \leq \boldsymbol{I}^{max} + \varepsilon_3 \boldsymbol{1} \tag{6.5d}$$

$$\boldsymbol{u}^{min} \leq \boldsymbol{u}(k) \leq \boldsymbol{u}^{max} \tag{6.5e}$$

$$\varepsilon_1, \varepsilon_2, \varepsilon_3 \geq 0 \tag{6.5f}$$

   where the second term in (6.4) involves the slack variables $\varepsilon_1, \varepsilon_2$ and ε_3 aimed at relaxing the inequality constraints in case of infeasibility. Matrix $\boldsymbol{S}$ is diagonal with large diagonal

elements to enforce the constraints. Note that $\boldsymbol{u}(k-1)$ is either the initial value of the control variables (for $k=1$) or the control variables obtained from the previous iteration of the sequence (for $k \geq 2$).

5. If $\|\boldsymbol{u}(k) - \boldsymbol{u}(k-1)\| < \delta$ stop; else $k = k+1$, go to Step 2.

It is easily shown that, if the above algorithm converges, the sequence of controls $\boldsymbol{u}(1), \boldsymbol{u}(2), \ldots, \boldsymbol{u}(k)$ converges to a solution of the original problem (6.1, 6.2). Indeed let $(\boldsymbol{u}^*, \boldsymbol{V}^*, \boldsymbol{\theta}^*)$ be the solution reached when convergence has taken place.

$$\boldsymbol{u}(k) \simeq \boldsymbol{u}(k-1) \simeq \boldsymbol{u}^* \tag{6.6a}$$
$$\boldsymbol{V}(k) \simeq \boldsymbol{V}(k-1) \simeq \boldsymbol{V}^* \tag{6.6b}$$
$$\boldsymbol{\theta}(k) \simeq \boldsymbol{\theta}(k-1) \simeq \boldsymbol{\theta}^* \tag{6.6c}$$

Let us also assume that the optimization problem (6.4, 6.5) solved in the last iteration was feasible, i.e.

$$\boldsymbol{\varepsilon} \simeq \mathbf{0} \tag{6.7}$$

Introducing (6.6) and (6.7) into (6.3, 6.4, 6.5) gives:

$$\boldsymbol{u}^* = \arg\min \|\boldsymbol{u}^* - \hat{\boldsymbol{u}}\|^2_{\boldsymbol{W}} \tag{6.8}$$

with:

$$\boldsymbol{f}(\boldsymbol{u}^*, \hat{\boldsymbol{c}}, \boldsymbol{V}^*, \boldsymbol{\theta}^*) = \mathbf{0} \tag{6.9a}$$
$$\boldsymbol{V}^{min} \leq \boldsymbol{V}^* \leq \boldsymbol{V}^{max} \tag{6.9b}$$
$$\boldsymbol{I}(\boldsymbol{V}^*, \boldsymbol{\theta}^*) \leq \boldsymbol{I}^{max} \tag{6.9c}$$
$$\boldsymbol{u}^{min} \leq \boldsymbol{u}^* \leq \boldsymbol{u}^{max} \tag{6.9d}$$

which shows obviously that $(\boldsymbol{u}^*, \boldsymbol{V}^*, \boldsymbol{\theta}^*)$ is a solution of the original problem (6.1, 6.2).

6.2.3 Multi-step sequential quadratic problem

Although, compared to the original problem (6.1, 6.2), the quadratic problem (6.4, 6.5) offers less computational burden, the sensitivities may change significantly with the operating point, making the linear approximation inaccurate. It is particularly the case for branch currents, since their sensitivities have a relatively high variability; in particular, they change sign in case of power flow

reversal, as discussed in Section 2.6. To cope with the inaccuracy, the control change ($\boldsymbol{u}(k) - \boldsymbol{u}(k-1)$) should be small enough so that the linear approximation is valid. in this respect, the following two solutions can be thought of:

- apply only a fraction of the control change obtained from the quadratic problem (6.4, 6.5).

  More precisely, at each iteration of the sequential quadratic problem detailed in Section 6.2.2, if the computed control is not "close enough" to the control obtained at the previous iteration, only a fraction of the difference is applied to obtain the next-iteration operating point.

- reuse the multi-step formulation at the heart of the MPC-based real-time control, since the latter is known to progressively enforce the violated constraints. This will lead to using the MPC algorithm but with the real-time measurements now replaced by values obtained from the power flow solution of (6.3).

In the first approach, it remains to find a strategy to properly select the mentioned fraction. On the other hand, in the second (MPC-like) approach, the change of control variables can be made small, since the total effort is spread over several successive steps. Based on the experience accumulated in the context of real-time control, the MPC-based solution has been preferred.

The detailed procedure is as follows:

1. Initialize:

$$\begin{aligned} \boldsymbol{u}(0) &= \hat{\boldsymbol{u}} \\ k &= 1 \end{aligned}$$

2. Solve the power flow equations:

$$\boldsymbol{f}(\boldsymbol{u}(k-1), \hat{\boldsymbol{c}}, \boldsymbol{V}(k), \boldsymbol{\theta}(k)) = \boldsymbol{0} \tag{6.10}$$

   to obtain $\boldsymbol{V}(k), \boldsymbol{\theta}(k)$ and hence $\boldsymbol{I}(\boldsymbol{V}(k), \boldsymbol{\theta}(k))$.

3. Compute the bus voltage and branch current sensitivity matrices $\boldsymbol{S}_V$ and $\boldsymbol{S}_I$, respectively, at the operating point $\boldsymbol{V}(k), \boldsymbol{\theta}(k)$.

4. Solve the quadratic problem involving N_c steps:

$$\min_{\boldsymbol{u}(k), \boldsymbol{V}(k), \boldsymbol{\theta}(k), \boldsymbol{I}(k), \boldsymbol{\varepsilon}} \sum_{i=0}^{N_c-1} \|\boldsymbol{u}(k+i) - \hat{\boldsymbol{u}}\|^2_{\boldsymbol{W}} + \|\boldsymbol{\varepsilon}\|^2_{\boldsymbol{S}} \tag{6.11}$$

subject to the linearized constraints:

for $i = 1, \ldots, N_c$:

$$\boldsymbol{V}(k+i) = \boldsymbol{V}(k) + \boldsymbol{S}_V \left(\boldsymbol{u}(k+i-1) - \boldsymbol{u}(k-1)\right) \tag{6.12a}$$

$$\boldsymbol{I}(k+i) = \boldsymbol{I}(\boldsymbol{V}(k), \boldsymbol{\theta}(k)) + \boldsymbol{S}_I \left(\boldsymbol{u}(k+i-1) - \boldsymbol{u}(k-1)\right) \tag{6.12b}$$

$$-\varepsilon_1 \mathbf{1} + \boldsymbol{V}^{low}(k+i) \leq \boldsymbol{V}(k+i) \leq \boldsymbol{V}^{up}(k+i) + \varepsilon_2 \mathbf{1} \tag{6.12c}$$

$$\boldsymbol{I}(k+i) \leq \boldsymbol{I}^{up}(k+i) + \varepsilon_3 \mathbf{1} \tag{6.12d}$$

$$\boldsymbol{u}^{min} \leq \boldsymbol{u}(k+i-1) \leq \boldsymbol{u}^{max} \tag{6.12e}$$

and,

$$\varepsilon_1, \varepsilon_2, \varepsilon_3 \geq 0 \tag{6.13}$$

The bounds on the predicted voltages and currents $\boldsymbol{V}^{low}(k+i)$, $\boldsymbol{V}^{up}(k+i)$ and $\boldsymbol{I}^{up}(k+i)$ are tightened progressively over the control horizon. To obtain very smooth changes, the linear tightening is chosen, as explained in Section 2.5.3.

5. Consider the first element $\boldsymbol{u}(k)$ of the sequence of control actions $\boldsymbol{u}(k), \boldsymbol{u}(k+1), \ldots$:

   If $\|\boldsymbol{u}(k) - \boldsymbol{u}(k-1)\| < \delta$ stop; else $k = k+1$, go to Step 2.

It must be stressed that for $N_c = 1$, the optimization problem (6.11, 6.12, 6.13) is identical to the sequential quadratic formulation (6.4, 6.5). By using $N_c > 1$ the control effort is spread over several steps, and $\boldsymbol{u}$ is adjusted more smoothly.

Another point to be mentioned is that the objective (6.11) is a variant of Objective 2 defined in Section 2.5, i.e. minimizing the sum of squared deviations between the controls and their references, where the reference values have been set to the prediction $\hat{\boldsymbol{u}}$.

Again, let us show that, if convergence takes place, the successive controls tend to a solution of original problem (6.1, 6.2). Let $(\boldsymbol{u}^*, \boldsymbol{V}^*, \boldsymbol{\theta}^*)$ be the solution reached when convergence has taken place, i.e.

$$\boldsymbol{u}(k+i) \simeq \boldsymbol{u}(k-1) \simeq \boldsymbol{u}^* \qquad i = 0, \ldots, N_c - 1 \tag{6.14a}$$

$$\boldsymbol{V}(k+i) \simeq \boldsymbol{V}(k) \simeq \boldsymbol{V}^* \qquad i = 1, \ldots, N_c \tag{6.14b}$$

$$\boldsymbol{\theta}(k+i) \simeq \boldsymbol{\theta}(k) \simeq \boldsymbol{\theta}^* \qquad i = 1, \ldots, N_c \tag{6.14c}$$

Let us also assume that the optimization problem (6.11, 6.12) solved at the last iteration was feasible, i.e.

$$\boldsymbol{\varepsilon} \simeq \mathbf{0} \tag{6.15}$$

Introducing (6.14) and (6.15) into (6.11) gives:

$$\begin{aligned} \boldsymbol{u}^* &= \arg\min \sum_{i=0}^{N_c-1} \|\boldsymbol{u}^* - \hat{\boldsymbol{u}}\|^2_{\boldsymbol{W}} \\ &= \arg\min N_c \|\boldsymbol{u}^* - \hat{\boldsymbol{u}}\|^2_{\boldsymbol{W}} \\ &= \arg\min \|\boldsymbol{u}^* - \hat{\boldsymbol{u}}\|^2_{\boldsymbol{W}} \end{aligned} \tag{6.16}$$

while (6.10) and (6.12) becomes:

$$\boldsymbol{f}(\boldsymbol{u}^*, \hat{\boldsymbol{c}}, \boldsymbol{V}^*, \boldsymbol{\theta}^*) = \boldsymbol{0} \tag{6.17a}$$

$$\boldsymbol{V}^{min} \leq \boldsymbol{V}^* \leq \boldsymbol{V}^{max} \tag{6.17b}$$

$$\boldsymbol{I}(\boldsymbol{V}^*, \boldsymbol{\theta}^*) \leq \boldsymbol{I}^{max} \tag{6.17c}$$

$$\boldsymbol{u}^{min} \leq \boldsymbol{u}^* \leq \boldsymbol{u}^{max} \tag{6.17d}$$

Equations (6.16, 6.17) express that $(\boldsymbol{u}^*, \boldsymbol{V}^*, \boldsymbol{\theta}^*)$ is a solution of the original problem (6.1, 6.2).

It is thus concluded that the same multi-step optimization can be used for both preventive analysis and real-time corrective control. The latter uses the measurements collected in the network, while the preventive analysis uses the solution of the power flow equations (6.10) for a similar purpose. The similarity between both approaches is depicted in Fig. 6.1.

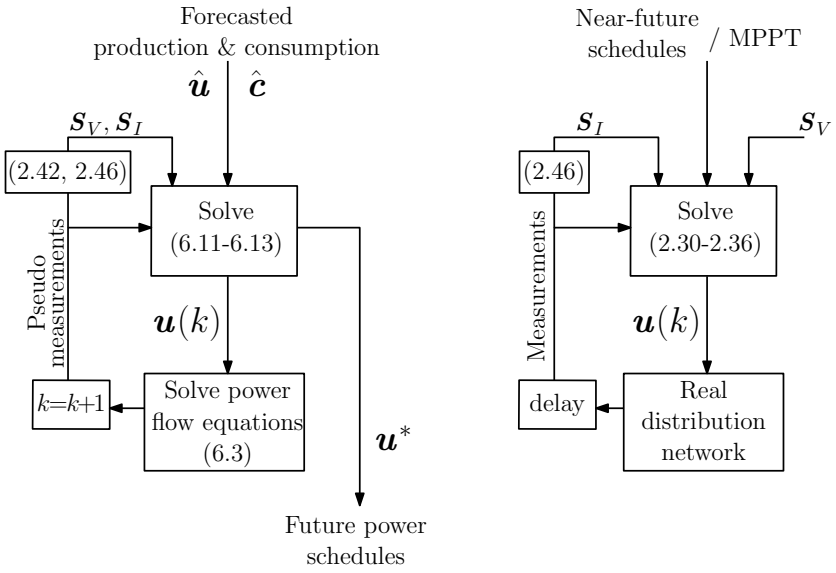

a) preventive security restoration b) real-time corrective control

Figure 6.1: Comparison of preventive analysis and corrective control

It should be noted that the corrective actions of the real-time controller are reflected on the measurements after a delay. The latter accounts for communication delay, dead-time until the DGUs have reached steady state, and time window in which the measurements are collected and pre-filtered. In the preventive analysis, there is no notion of time; k is only an iteration counter.

6.3 Combining preventive analysis and real-time control

As the name indicates, in the preventive approach, the necessary adjustments of DGUs to avoid anticipated violations are determined ahead of time. However, the fact remains that due to uncertainties (e.g. imprecise consumption or generation prediction, and incidents) the network might be driven to limit violations in real-time. Thus, using the last updated measurements, the MPC-based real-time controller supplements the decisions made by the preventive security restoration, if necessary. Therefore, these two control entities need to be properly combined for a secure and cost-effective operation of the distribution network; in this regard, three types of interaction can be envisaged, as explained in the following three sub-sections.

6.3.1 First option : Communicating both active and reactive power schedules

In this first scheme, the preventive analysis sends active and reactive power schedules $\boldsymbol{P}^*, \boldsymbol{Q}^*$ to the real-time corrective controller. The latter makes sure that the DGUs follow the desired productions. If the system evolves exactly as predicted, no supplementary adjustment is needed from the real-time controller. Otherwise, in case of an unforeseen violation, the latter adds some corrective actions on the units to bring the network back within limits.

Let us recall that the real-time controller is dealing with a shorter time horizon than the preventive one (e.g. 10 s vs. 15 min). Hence, the values $\boldsymbol{P}^*, \boldsymbol{Q}^*$ which relate to some time in the future have to be reflected in the reference values of the real-time controller, namely:

$$\boldsymbol{u}_{rt,\,ref}(k) = \left[\begin{array}{cc} \boldsymbol{P}^T_{rt,\,ref}(k) & \boldsymbol{Q}^T_{rt,\,ref}(k) \end{array} \right]^T \tag{6.18}$$

In this chapter, all notations related to the real-time controller are the same as in the previous chapters but with subscript rt. For example, $P_{rt,\,ref}$ is P_{ref} of the real-time controller.

Figure 6.2 illustrates how the active power references could be updated in real-time through a simple linear interpolation of two successive schedules, determined by the preventive security restoration. Those references are updated as the real-time controller moves to the next discrete time-step. The reactive power references $\boldsymbol{Q}_{rt,\,ref}$ are obtained similarly.

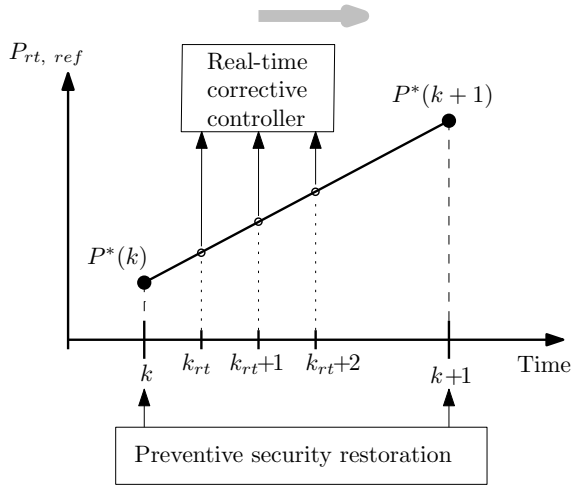

Figure 6.2: Extraction of active power references by linear interpolation of preventive schedules (similarly for reactive power)

The $\boldsymbol{P}^*, \boldsymbol{Q}^*$ values are of interest to other actors of the power system such as balance responsible parties, transmission system operator, etc. [KA14, MLEC16]. These near-future information should be communicated to those actors early enough, leaving them time to take proper decisions.

6.3.2 Second option : Communicating only active power schedules

Although a prediction of active power consumptions and generations with a relatively good accuracy can be obtained at a horizon of at most a few hours (the same does not hold true for reactive power in general), it is very likely that, in real-time, the network does not exactly evolve towards the predicted values. Therefore, an alternative to the previous option is that the preventive analysis communicates only active power schedules $\boldsymbol{P}^*$ to the real-time corrective controller, leaving the reactive power adjustments for real-time, when the actual network operating point, possibly different from the predicted, is observed through measurements. In such a case, the active power schedule, which plays a much more important role in market objectives than its reactive counterpart, is also available in advance to other actors of the power system.

6.3.3 Third option : Having DGUs controlled in real-time only

The choice of adjusting DGUs in real-time only is of practical interest when the renewable generation units operate for MPPT. The following two situations can lead to this choice:

- no limit violation is anticipated by the preventive analysis;

- although prediction shows a limit violation, the DGUs are left to operate for MPPT in order to maximize the captured active power. The expected violation will be cleared by the real-time controller, right after it is observed. Moreover, the curtailed DGUs are reset back to MPPT as soon as the operating conditions allow doing so (see Section 2.7).

Obviously in this case the sole real-time corrective controller takes care of violations, and the preventive analysis decisions are not enforced. However, as already mentioned, the near-future schedules determined by the latter may still be of interest to other actors of the power system, as they allow anticipating power imbalances.

6.4 Simulation results

6.4.1 Test system

The performance of the preventive security restoration and its coupling with the real-time corrective control are now illustrated on the already used 75-bus, 11-kV network. The information on loads, DGUs, measurements, etc. can be found in Section 1.4.2. In this section, all 22 DGUs are assumed to be wind turbine driven units.

It is assumed that initially all units operate for MPPT, and at unity power factor. This leads to exporting active power from the distribution network to the external grid, but importing reactive power to feed the loads and cover the losses.

Based on the predicted data, wind speed is expected to increase by 10% in the following 15 minutes (unless stated otherwise). This variation is large enough to cause a thermal overload of the transformer. The consumption, on the other hand, is assumed to be unchanged in this period (unless stated otherwise).

6.4.2 Comparison of multi- and single-step optimizations

The objective of this section is threefold:

- illustrate the better performance of the multi-step formulation of Section 6.2.3, with $N_c > 1$, compared to the successive quadratic programming method of Section 6.2.2;
- confirm through simulations that the multi-step formulation of Eqs. (6.10-6.13) gives the same result (assuming the algorithm converges, of course) independently of the value of $N_c > 1$. This has been shown mathematically in Eqs. (6.16, 6.17);

- identify an appropriate value for N_c.

It is assumed that the above-mentioned congestion problem is anticipated in the following 15 minutes.

The sequential quadratic programming method has been implemented by merely setting $N_c = 1$ in the multi-step formulation of Eqs. (6.10-6.13), as already mentioned. The sequence of transformer current values is shown in Fig. 6.3 while the successive values of the active and reactive powers of one DGU are shown in Fig. 6.4. It is clearly seen that the sequence does not converge. This is due to the wrong sensitivity matrix S_I when the current passes through a minimum under the effect of reverse reactive power flow, as explained in Section 2.6.

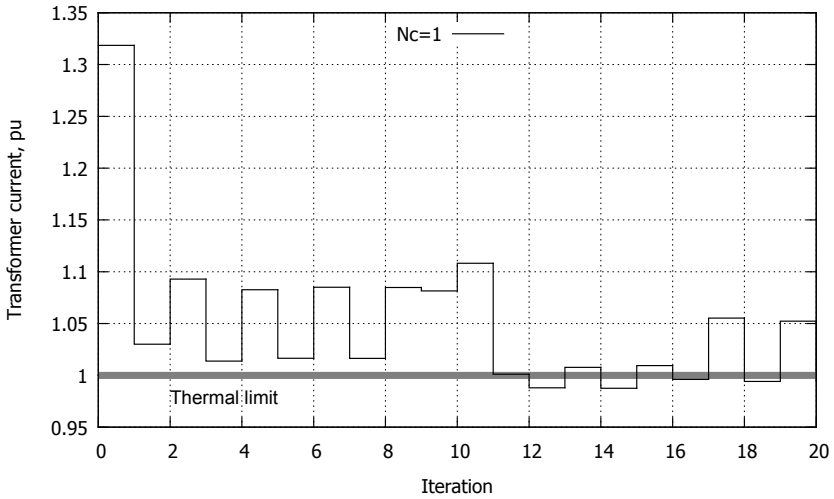

Figure 6.3: Sequence of current in the transformer using sequential quadratic programming

The result of the multi-step formulation of Section 6.2.3, for various values of $N_c > 1$ are given in Figs. 6.5 to 6.8 showing the successive values of respectively: the current in the transformer (to be compared to Fig. 6.3), the active power of the same DGU (to be compared to Fig. 6.4), the reactive power of the same DGU (to be compared to Fig. 6.4) and the objective function (6.1). It is clear that all variants result in the same, feasible operating point. It is noteworthy that already with $N_c = 2$ the sequence converges smoothly.

Since both $N_c = 2$ and $N_c = 4$ result in the solution being reached after eight iterations, for the sake of security (i.e. to have a smooth sequence), it seems appropriate to choose $N_c = 4$.

This choice as been adopted in all simulations reported in the rest of this chapter.

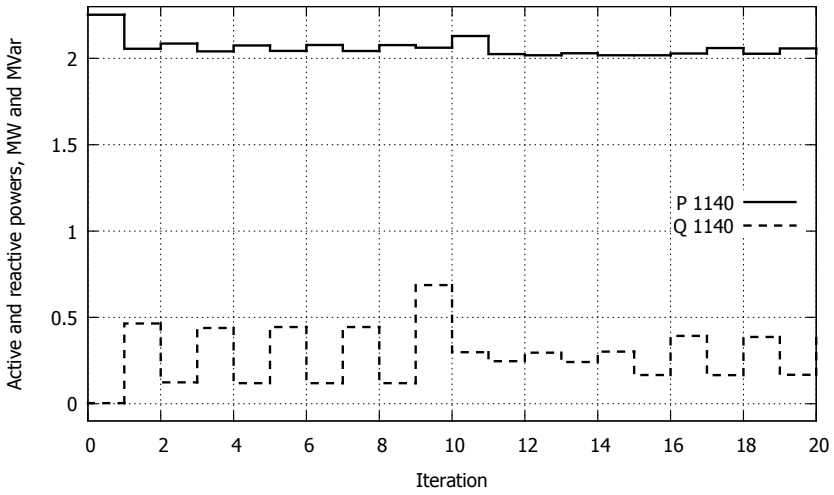

Figure 6.4: Sequence of active and reactive power outputs of DGU 1140 using sequential quadratic programming

6.4.3 Combinations of preventive analysis and corrective control in various scenarios

The performance of the preventive and/or corrective controls, in the time interval of 15 minutes, is investigated in eight scenarios. Table 6.1 introduces these scenarios by indicating the accuracy of the wind speed/load evolution prediction, the active controls (preventive and/or real-time), and their coupling. In Scenarios 2 to 4 and 7 a perfect wind speed prediction is assumed, while in the scenarios 5, 6 and 8 an imprecise wind speed prediction is considered.

In all cases no voltage violation is predicted/observed and the results mainly relate to solving the thermal violation. It should be mentioned that all DGUs are treated in the same manner (i.e. the same schedule or correction is sent to all of them), since the congested branch is the transformer connecting the whole DN to the external grid.

Moreover, for the ease of comparisons, Tables 6.2, 6.3 and 6.4 provide the total DGU active (resp. reactive) power curtailment (resp. adjustment) decided in real-time and preventively, as well as the final operating point when the congestion is avoided/cleared. For instance, the expression of the total amount of active power curtailment in real-time is:

if the units operate for MPPT:

$$\sum_{i=1}^{N_{DG}} (P_{rt,\,i}(k) - P_{MPPT,\,i}(k)) \tag{6.19}$$

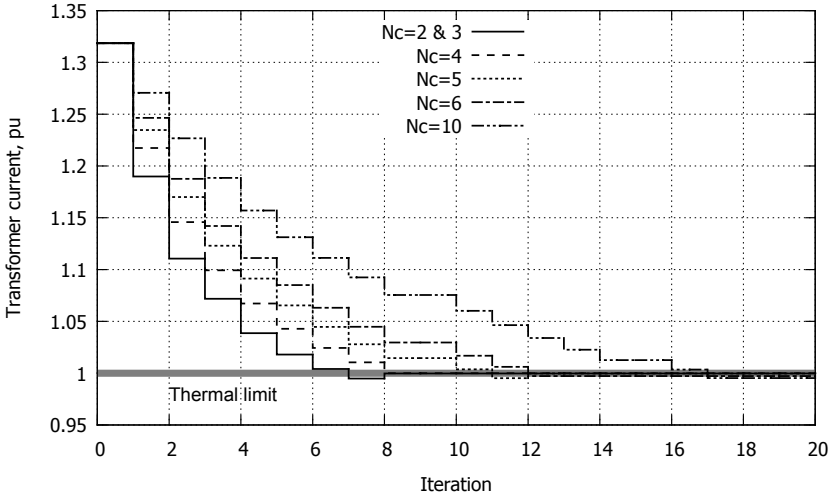

Figure 6.5: Sequence of current values in the transformer using multi-step optimizations

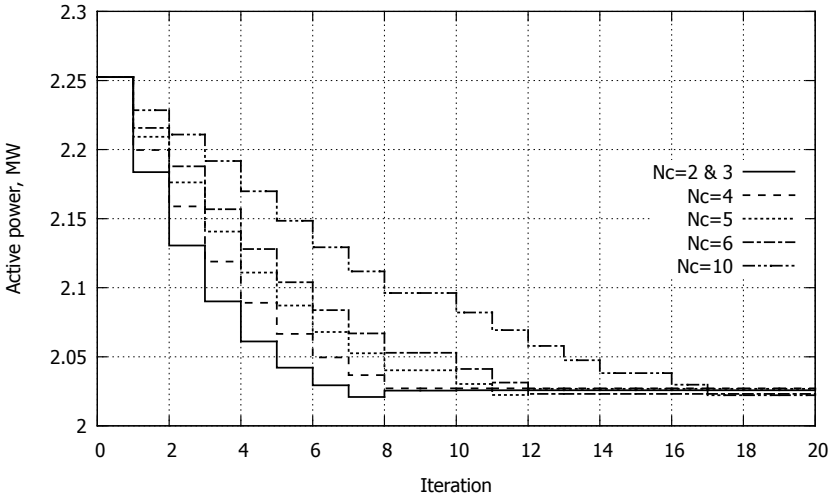

Figure 6.6: Sequence of active power values of DGU 1140 using multi-step optimizations

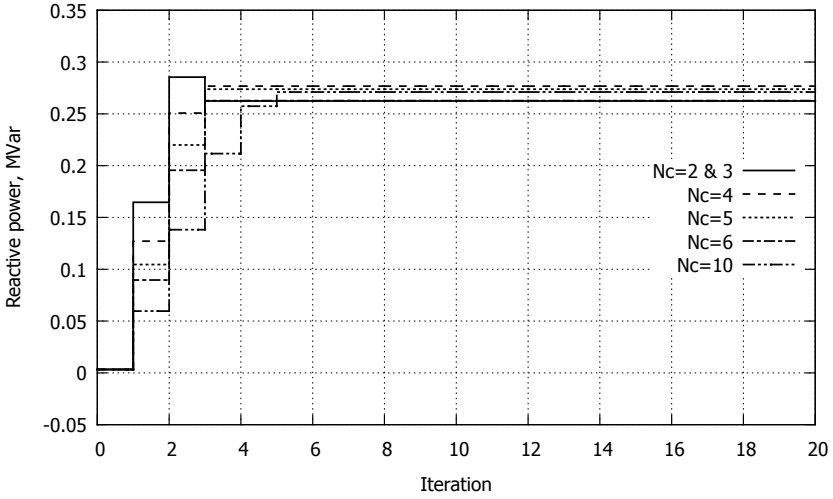

Figure 6.7: Sequence of reactive power values of DGU 1140 using multi-step optimizations

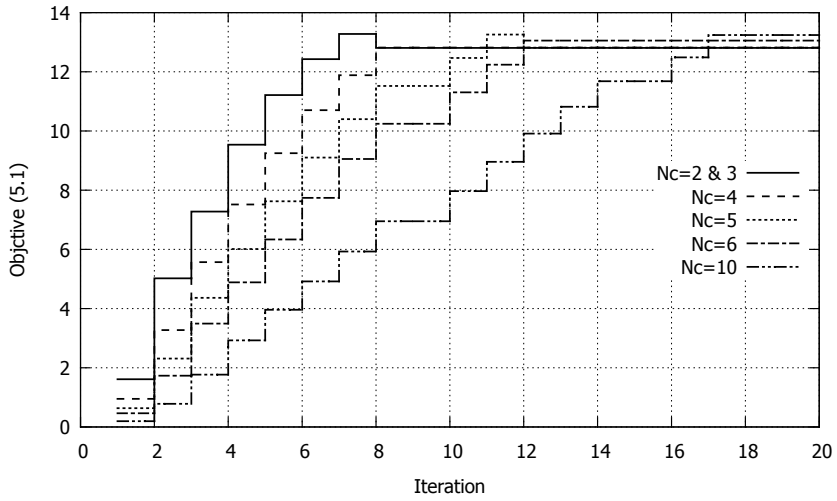

Figure 6.8: Successive values of the objective function (6.1) over successive iterations

Table 6.1: Scenarios specifications

	Prediction quality		Real-time		
	Wind speed	**Consumption**	**corrective control**	**preventive analysis**	**Coupling**
1	not applicable	assumed constant	active	inactive	not applicable
2	accurate	assumed constant	inactive	active	not applicable
3	accurate	assumed constant	active	active	P^* and Q^*
4	accurate	assumed constant	active	active	P^*
5	underestimating the severity	assumed constant	active	active	P^* and Q^*
6	overestimating the severity	assumed constant	active	active	P^* and Q^*
7	accurate	unforeseen load decrease	active	active	P^* and Q^*
8	underestimating the severity	assumed constant	active	active	MPPT

if the units follow a power reference:

$$\sum_{i=1}^{N_{DG}} (P_{rt,\,i}(k) - P_i^*(k)) \tag{6.20}$$

where N_{DG} is number of DGUs in the distribution network and k indicates the last time step of the 15-min period. P_{MPPT} and P_{rt} are the maximum available power, and the effective active power output, respectively.

Reactive power expressions are defined similarly.

In Table 6.2 the values in Columns 4 and 5 are the expected active power curtailments, and the effective active power curtailment, respectively, which are equal only if the wind speed prediction is infinitely accurate. These two values are defined similarly to (6.19, 6.20).

Scenario 1

Only the real-time controller is assumed to be acting in this first scenario. Therefore, the congestion is corrected when it is detected from the collected measurements. To correct the violation, first, the unit reactive power productions are increased, in order to decrease the reactive power flow in the transformer (final value of -0.974 MVar)[1], and hence its current. Then, since the sole reactive power change cannot solve the problem, a total amount of 5.086 MW of DGU active power is curtailed until the transformer current reaches 0.9999 pu, just below the thermal limit of 1 pu. The total reactive power adjustments and active power curtailments together with the final active/reactive power flows in the transformer are given in the tables.

Scenario 2

In this opposite scenario, it is assumed that the real-time controller is inoperative. Taking into account the wind speed prediction, the preventive analysis computes $\boldsymbol{u}^*$ to avoid the congestion problem. It must be mentioned that the real-time controller should be kept in operation for secure operation of the grid. In fact, this scenario is provided only to compare the accuracy of decisions made at the preventive stage and in real-time (Scenario 1), both treating the same problem.

Comparing the transformer active and reactive power flows at the end of 15-min horizon with that of the previous scenario (see Table 6.4), it can be seen that the preventive analysis better exploits the reactive power (reactive power flow of 0.069 MVar instead of -0.974 MVar), leading to a lower active power curtailment (total of 4.969 MW instead of 5.086 MW). This more satisfactory performance of the preventive analysis is achieved thanks to smaller control actions. The latter are the result of imposing linear tightening bounds [2] on the violated current (please see Section 2.5.3). Furthermore, the following factors contribute to the observed difference:

- both the preventive analysis and the corrective control stop taking actions as soon as the network enters the secure limits. Thus, even if a violation is cleared in real-time with a non-optimal exploitation of cheap and expensive control means, the controller does not issue the corrections any more (i.e. the previous corrections are not further refined);
- unlike the preventive analysis, the corrective controller modifies the operating points by taking relatively big steps (which is in accordance with the real-time control needs) at the price of less precise linear approximations. Thus, a change slightly bigger than what is needed (or the non-optimal exploitation of reactive power) might take place.

[1] The non-zero value comes from the treatment of the sensitivity of branch current with respect to DGU reactive powers, as explained in Section 2.6

[2] and not the exponential one

Table 6.2: Adjustments by the preventive analysis to prevent a congestion

Scenario	**preventive analysis**				
	P^* Individual DGU production (MW)	Q^* Individual DGU production $(MVar)$	Expected total active power curtailment (MW)	Effective total active power curtailment (MW)	Total reactive power adjustment $(MVar)$
1	–	–	–	–	–
2	2.031	0.277	4.969	4.969	5.823
3	2.031	0.277	4.969	4.969	5.823
4	2.031	–	4.969	4.969	0.000
5	2.031	0.277	4.969	7.624	5.823
6	2.031	0.277	4.969	2.303	5.823
7	2.031	0.277	4.969	4.969	5.823
8	(MPPT)	(MPPT)	0.000	0.000	0.000

Table 6.3: Adjustments by the real-time controller to correct a congestion

Scenario	**Real-time control**	
	Total active power curtailment (MW)	Total reactive power adjustment $(MVar)$
1	5.086	4.863
2	–	–
3	0.000	0.000
4	0.269	4.489
5	0.000	0.000
6	0.000	0.000
7	1.073	0.000
8	5.086	4.863

Table 6.4: Transformer power flows and current at the end of 15-min horizon

Scenario	P_{tr} (MW)	Q_{tr} $(MVar)$	I_{tr} (pu)
1	19.991	- 0.974	0.99990
2	20.206	0.069	1.00396
3	20.206	0.069	1.00396
4	19.956	- 1.341	1.00090
5	20.117	0.070	1.00030
6	20.117	0.070	1.00030
7	20.121	0.068	1.00053
8	19.991	- 0.974	0.99990

Scenario 3

In this scenario the schedules P^* and Q^* are communicated to the real-time controller, and the DGUs are steered by the latter to follow those references (with the linear evolution explained in Fig. 6.2). Assuming an infinitely accurate prediction, the thermal violation is avoided while no contribution is needed from the real-time controller. The final power flows of the transformer are the ones of Scenario 2.

This is an example showing how a precise prediction can be exploited to extract maximum possible power from renewable generation units while avoiding any limit violation.

Scenario 4

A similar case to Scenario 3 is considered here, where only the active power schedule P^* is communicated by the preventive analysis to the real-time one, leaving the reactive power adjustment for the latter, when the actual network operating point, possibly different from the predicted, is observed through the measurements.

In such a case, it is expected to observe a thermal violation in real-time, since the preventive decisions on active power are not sufficient. However, thanks to the active power corrections received preventively, it is also expected that a significantly less severe congestion takes place, which can be cleared by acting on the DGU reactive powers only. Contrary to this, the results reveal that in addition to reactive power adjustments, a very small amount of active power (total of 0.269 MW) is also curtailed by the real-time controller to reach the target; the reactive power

is not fully exploited (the final transformer reactive power flow is 1.341 MVar instead of the -0.069 MVar value reached in Scenarios 2 and 3). This can be explained by the imprecise current sensitivity matrix $\boldsymbol{S}_I$ (see Section 2.6) employed by the real-time controller, which is not updated through the iterations. The impact, however, is very small.

Scenario 5

In this case, Scenario 3 is revisited assuming that wind speed change is predicted to be 10%, while the real value is 12%. The situation is sketched in Fig. 6.9. The predicted active power and its effective value (observed in real-time) are shown with a circle and a black disk, respectively, for one DGU. As in the other scenarios, the preventive analysis computes the power schedules as the maximum DGU active power productions ($P^* = 2.031$ MW for all DGUs) which do not create a congestion. This value is shown with a cross in the same figure, and is smaller than the predicted production with no control. Although the real wind speed is different from the predicted value, the active power schedule P^* guarantees no limit violation, relieving the real-time controller from any further effort. In fact, the imprecise wind speed prediction, which yields a non-accurate maximum available power, results in the expected total active power curtailment of 4.969 MW (the sum over all DGUs of the distance between the cross and the circle in Fig. 6.9) while the effective value is 7.624 MW (the sum over all DGUs of the distance between the disk and the circle in Fig. 6.9).

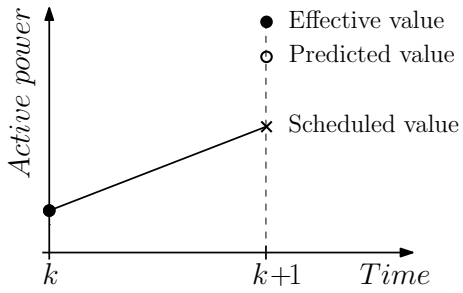

Figure 6.9: Scenario 5: Predicted, scheduled and effective active powers of a DGU in case of imprecise prediction

This example shows that, when a renewable generation unit is meant to follow a scheduled value of production (and not operate for MPPT), the active power in excess is curtailed to satisfy the security limits.

Scenario 6

Another example of imprecise wind speed change is considered but here the change is predicted to be 10%, while the real value is 8%. Accordingly, as shown in Fig. 6.10, the effective active

power (shown with the disk) is smaller than its predicted value (shown with the circle), but still larger than the scheduled value (the cross). Similarly to Scenario 5, this results in a different value of total active power curtailment (2.303 MW) than the expected value (4.969 MW), while the network does not experience any violation and no contribution is needed from the real-time controller.

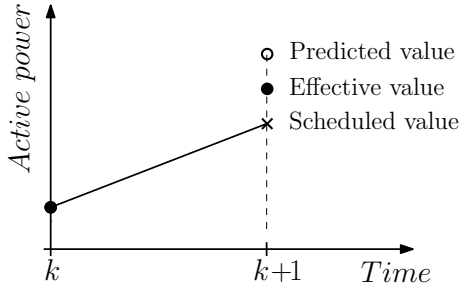

Figure 6.10: Scenario 6: Predicted, scheduled and effective active powers a DGU in case of imprecise prediction

Clearly, there can be also cases where the real wind speed is significantly lower than the predicted one and, consequently, the maximum available power is lower than the scheduled active power. Obviously, in such a case the units cannot produce the scheduled value (computed from an imprecise prediction), and they operate for MPPT.

Scenario 7

Scenario 3 is revisited, assuming that an unforeseen 1-MW load decrease takes place at the very end of the 15-minute interval. Since the distribution network exports active power to the external grid, this load change leads to an increase of the active power export and, hence, a larger transformer overload. The latter, is not anticipated by the preventive analysis but is detected by the real-time controller and corrected by curtailing a total amount of 1.073 MW of DGU active power. The DGU reactive powers are not further adjusted, since the transformer reactive power flow is already close to zero.

Scenario 8

In this last scenario, it is assumed that the DGUs initially operate for MPPT, and the predicted wind speed change, which is 5%, does not reveal any violation. This is sketched in Fig. 6.11 where the predicted value of the active power (shown with the circle) is smaller than its maximum allowed value (shown with the cross). Therefore, after performing a preventive security checking

it is decided that the DGUs can be left to operate for MPPT. However, in real-time the units are subject to a higher wind speed increase of 10% by the end of the 15-min time interval, which results in DGU effective active powers (shown with the black disk in Fig. 6.11) exceeding the maximum allowed value.

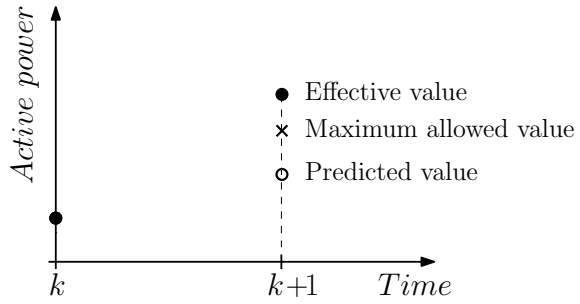

Figure 6.11: Scenario 8: Predicted, maximum allowed and effective active powers a DGU in case of imprecise prediction

Unlike in Scenarios 5 and 6, the real-time controller takes care of handling the unexpected situation. The production increases are large enough to create a thermal violation. The latter is corrected by the real-time controller when it is detected through the collected measurements.

6.5 Conclusion

In this chapter a preventive security restoration was introduced. The latter uses near-future production/consumption predictions to determine if the active distribution network is going to operate within prescribed limits and, if not, determine appropriate preventive actions with minimal deviations from the expected operating point. The results of this analysis can be communicated as production schedules to the real-time corrective controller. The latter is then responsible for both implementing these schedules as well as handling unforeseen incidents and performing complementary adjustments to cope with imprecise predictions. The main distinctive feature of that preventive analysis is that it re-uses the multi-step constrained optimization algorithm present in our real-time controller.

Chapter 7

General conclusion

7.1 Summary of work and main contributions

This thesis has focused on voltage control and congestion management in active distribution networks. In this context, a number of methods and algorithms have been devised, developed and tested which can allow DSOs to enhance the real-time monitoring and control of their grids. The central contribution of this work lies in the development of a real-time corrective controller which is able to tackle various practical challenges existing in real-life MV DNs. To do so, appropriate control schemes and proven optimization methods have been used in progressively extended formulations covering various applications.

More precisely, the original contributions can be listed as follows:

- A centralized control scheme has been designed to correct abnormal voltages and branch overloads in real-time. The formulation relies on the concept of MPC which involves a multi-step optimization over a receding horizon. It was chosen mainly for its closed-loop nature, a key feature missing in most published works, while being needed for on-line applications. Relying on the appropriate measurement and communication infrastructures, the centralized controller acts on active and reactive powers of DGUs as well as voltage set-point of the transformer LTC in order to smoothly drive the system from an unsatisfactory operating point to a targeted secure operation region. The proposed method has been successfully tested to confirm its robustness.

- The performance of the real-time controller, has been evaluated on a test system stemming from a real MV network, with the objective of examining the system behaviour over future

years, when more DGUs would be installed. One of the main attractiveness of those tests was to assess the controller response over full days, focusing on challenging ones in terms of voltage and/or thermal violations. On the premise that operation limits are exceeded for limited durations, the demonstrated features of the corrective real-time controller make it a serious alternative to expensive network reinforcements.

- The above control scheme has been extended to contribute to correcting abnormal (mainly too high) voltages in the LV network, if the operating conditions of the MV grid allow doing so. This is achieved by adjustment of voltages on the MV side of the MV/LV transformers through which the LV grid of concern is connected.
- The approach has been also extended to accommodate a two-level control architecture combining the previously presented centralized controller with multiple local, simple and faster acting controllers. The resulting scheme has the following features:
  - local control provides fast response after a disturbance, reducing its impact and enhancing voltage quality;
  - a hybrid control structure is possible where, at the upper level, only a subset of the DGUs are centrally controlled.
- The time frame has been extended with a preventive security restoration. Using near-future production/ consumption predictions, appropriate preventive decisions are computed in open loop, that can be used as references for the real-time corrective controller, when network limit violations are anticipated. The same multi-step constrained optimization is used in those complementary preventive and real-time decisions.

7.2 Directions for future work

The algorithms developed in the framework of this thesis could be further improved or extended along the following directions:

- The DGUs were assumed to react faster than the MPC sampling period (of typically 10 seconds). This justifies using a static representation, through sensitivity matrices, to predict the future system evolution. Although the control scheme has been shown to be quite robust, a true dynamic modelling could better deal with slower responding devices or with smaller MPC sampling periods.
- To add to the robustness of the centralized controller, the scheme could be further extended with a fault-tolerance feature. For instance, using the output feedback, a “bias term” could

be added to the measured values processed by the controller to compensate for the observed discrepancies between the predicted and the observed values. This technique is expected to be an appropriate choice for voltage control in the DN, and needs further investigations for congestion management.

- The preventive analysis presented in Chapter 6 could be extended to incorporate the control of the available flexible loads in the DN. The preventive analysis relates to a longer, future time interval than the real-time controller, and that time frame can encompass the response time of energy-constrained flexible loads. Such incorporation, however, should take into account the practical aspects discussed in Section 2.10.

- State estimation is not as common at distribution level as it is at transmission level. The main reason is the lack of real-time measurements. This is why the real-time controller has been developed without assuming that state estimation was available (see for instance Fig. 2.5). That being said, the availability of such an estimator and the resulting improved situational awareness could benefit the real-time controller. As a first step, the most appropriate locations for additional real-time measurements should be identified. Then, the state estimator would provide an estimate of the complex voltages at all buses of the network, from which any quantity of interest can be computed. In particular, it would provide the active and reactive power flows in the various network branches, which are required to properly deal with overloads, as detailed in Section 2.6.2. More generally, the estimates could be used to improve the quality of the model used by the real-time controller.

- The real-time control of the MV network could be also extended to support the transmission system when the latter operates in stressed conditions. To do so, additional constraints can be included in the multi-step optimization solved by the real-time controller. For instance, those constraints could deal with the reactive power exchanged (or the power factor) at the interface with the transmission grid. Of course, proper priorities should be assigned to the new constraints compared to those relative to the security of the MV grid itself. The grid codes should be extended to cover this (still not very common) mutual assistance.

- There is room for improvement of the signal(s) transmitted to the real-time controller to deal with abnormal voltages in the LV grids. Although there is a tendency to install more "smart meters" at LV level, in the absence of such real-time measurements, the voltages should be estimated from the available information, most likely in the MV/LV transformers.

- Capacitor banks can be also used in DNs as additional control means for voltage support and/or power factor correction. The capacitor bank can be switched on/off using local measurements (e.g. the power factor), or it can be controlled by a central entity such as the real-time controller presented in this thesis. In order to handle the status of the capacitor

bank together with the other control variables, an integer variable should be integrated into the formulation, resulting in mixed integer programming. This requires a higher computational effort. Most likely the latter remains reasonable if only two states (namely, connected or disconnected) have to be considered, but it could become significant if a higher combinatorial has to be taken into account (compensation in several steps, or at different locations in the MV network).

- Energy storages are a promising solution to the issues raised by the intermittency of renewable energy sources. They are mainly used to accumulate or restitute active power to the system. However, being connected to the grid through converters, they have the ability to consume or produce reactive power as well. Energy storages can be used for voltage control, congestion management, maximizing the captured power of renewable DGUs, and minimizing network losses. In order to include them together with the other control variables, they can be treated similarly to DGUs but with some differences. Besides allowing power consumption, their active power output does not depend on weather conditions (wind speed or solar radiation), but an energy constraint involving the stored energy must be satisfied (as for energy-constrained flexible loads).

- In this whole work, the MV grid has been assumed to operate in balanced three-phase conditions, which is usually considered acceptable in most European countries. If needed, and if measurements are available, the models could be extended to three phases. As far as the LV grid is concerned (see Chapter 4), phase imbalances should be considered.

Appendix A

Test system parameters

Table A.1: 32-bus test system: Branch data
(one-line diagram is shown in Fig. 1.3)

From Bus	To Bus	R Ω	X Ω	B Ω^{-1}
N31	N30	0.0723	0.2058	0
N30	N1	0.0723	0.2058	0
N1	N2	0.1220	0.3430	0
N2	N3	0.1342	0.3773	0
N2	N4	0.1708	0.4802	0
N4	N5	0.1220	0.3430	0
N4	N6	0.1220	0.3430	0
N6	N7	0.1342	0.3773	0
N7	N8	0.1464	0.4116	0
N1	N9	0.1464	0.4116	0
N9	N10	0.1464	0.4116	0
N15	N16	0.1342	0.3773	0
N16	N17	0.1220	0.3430	0
N16	N18	0.1586	0.4459	0
N18	N19	0.1342	0.3773	0
N18	N20	0.1220	0.3430	0
N15	N21	0.1464	0.4116	0
N21	N22	0.1464	0.4116	0
N22	N23	0.1342	0.3773	0
N22	N24	0.1220	0.3430	0
N21	N25	0.1586	0.4459	0
N10	N11	0.1220	0.3430	0
N10	N12	0.1220	0.3430	0
N12	N13	0.1220	0.3430	0
N13	N14	0.1220	0.3430	0
N9	N15	0.1342	0.3773	0
N25	N26	0.1464	0.4116	0
N25	N27	0.1464	0.4116	0
N27	N28	0.1586	0.4459	0
N27	N29	0.1342	0.3773	0
Transformer		0	0.075 pu	0

Table A.2: 75-bus test system: Branch data (one-line diagram is shown in Fig. 1.4)

From Bus	To Bus	R Ω	X Ω	B Ω^{-1}	From Bus	To Bus	R Ω	X Ω	B Ω^{-1}
1100	1101	0.2038	0.1056	0	1138	1139	0.0917	0.0706	0
1101	1102	0.2038	0.1056	0	1139	1140	0.0917	0.0706	0
1102	1103	0.0624	0.0170	0	1140	1141	0.0917	0.0706	0
1100	1104	0.2038	0.1056	0	1141	1142	0.0917	0.0706	0
1104	1105	0.2038	0.1056	0	1142	1143	0.0917	0.0706	0
1105	1106	0.0624	0.0170	0	1143	1144	0.0917	0.0706	0
1100	1107	0.2038	0.1056	0	1144	1145	0.0917	0.0706	0
1107	1108	0.2038	0.1056	0	1138	1146	0.0571	0.0155	0
1108	1109	0.0624	0.0170	0	1140	1147	0.0571	0.0155	0
1100	1110	0.2660	0.1378	0	1141	1148	0.0571	0.0155	0
1110	1111	0.2660	0.1378	0	1143	1149	0.0571	0.0155	0
1111	1112	0.2660	0.1378	0	1145	1150	0.0571	0.0155	0
1111	1113	0.0663	0.0180	0	1100	1151	0.0665	0.0512	0
1112	1114	0.0663	0.0180	0	1151	1152	0.0665	0.0512	0
1100	1115	0.0745	0.0574	0	1152	1153	0.0665	0.0512	0
1115	1116	0.0745	0.0574	0	1153	1154	0.0665	0.0512	0
1116	1117	0.0745	0.0574	0	1154	1155	0.0665	0.0512	0
1117	1118	0.0745	0.0574	0	1155	1156	0.0665	0.0512	0
1118	1119	0.0745	0.0574	0	1156	1157	0.0665	0.0512	0
1119	1120	0.0745	0.0574	0	1157	1158	0.0665	0.0512	0
1120	1121	0.0745	0.0574	0	1158	1159	0.0665	0.0512	0
1116	1122	0.0542	0.0147	0	1159	1160	0.0665	0.0512	0
1118	1123	0.0542	0.0147	0	1160	1161	0.0665	0.0512	0
1119	1124	0.0542	0.0147	0	1161	1162	0.0665	0.0512	0
1121	1125	0.0542	0.0147	0	1162	1163	0.0665	0.0512	0
1100	1126	0.0745	0.0574	0	1163	1164	0.0665	0.0512	0
1126	1127	0.0745	0.0574	0	1164	1165	0.0665	0.0512	0
1127	1128	0.0745	0.0574	0	1165	1166	0.0665	0.0512	0
1128	1129	0.0745	0.0574	0	1152	1167	0.0729	0.0198	0
1129	1130	0.0745	0.0574	0	1154	1168	0.0729	0.0198	0
1130	1131	0.0745	0.0574	0	1155	1169	0.0729	0.0198	0
1131	1132	0.0745	0.0574	0	1157	1170	0.0729	0.0198	0
1127	1133	0.0542	0.0147	0	1159	1171	0.0729	0.0198	0
1129	1134	0.0542	0.0147	0	1161	1172	0.0729	0.0198	0
1130	1135	0.0542	0.0147	0	1162	1173	0.0729	0.0198	0
1132	1136	0.0542	0.0147	0	1164	1174	0.0729	0.0198	0
1100	1137	0.0917	0.0706	0	1166	1175	0.0729	0.0198	0
1137	1138	0.0917	0.0706	0					
Transformer		0	0.072 pu	0					

Appendix B

DGU models

Simplified models of the Doubly Fed Induction Generation (DFIG) and synchronous generator have been used, in accordance with the type of dynamics considered in this work. The models and parameters with full dynamics and details were taken from [TNV09, CMSG10, HBM99].

B.1 Model of the Doubly-Fed Induction Generator

Wind units using the DFIG technology (type III) have been assumed in this work, and detailed hereafter.

The symbols not defined in the text are briefly described in Table B.2.

B.1.1 Overview of the DFIG

A typical scheme of wind turbine equipped with DFIG is shown in Fig. B.1.

The stator of a DFIG is directly connected to the grid, while the wound-rotor is connected to a partially rated power electronic frequency converter consisting of two PWM inverters/rectifiers connected back-to-back via an intermediate DC-link.

The rotor current is fed by the rotor-side converter. According to the typical vector control strategy, the *dq* synchronous reference frame for the vector control of the rotor side converter is oriented along the stator flux vector position. Neglecting the stator resistance is equivalent to setting the q-axis on the terminal voltage phasor. This results in the electromagnetic torque being proportional to $i_q^{'}$ which is the q-axis component of the rotor current. Consequently, the rotor speed can be

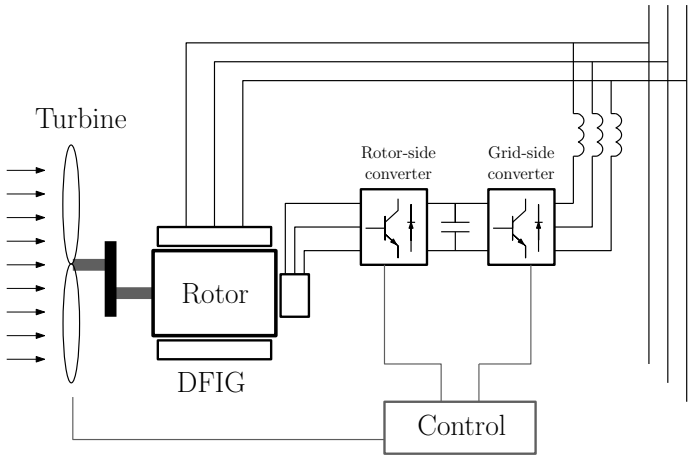

Figure B.1: The wind turbine and the DFIG system

controlled through $i_q^{'}$. On the other hand, the d-axis component of the rotor current $i_d^{'}$ is used to control the reactive power Q injected into the grid by the induction machine stator.

As regards the grid-side converter, the active power flow is controlled in order to keep the DC voltage constant, while the reactive power is usually kept at zero.

B.1.2 Generator and converter

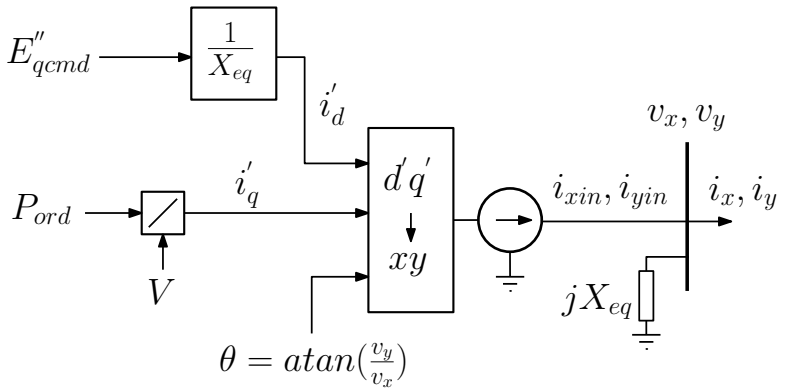

Figure B.2: Simplified generator and converter model

Figure B.2 gives the block-diagram of the model used to represent the generator and the converter. The following relations hold for the current injected into the network:

$$i_{xin} = i_q^{'} \cos(\theta) + \frac{E_{qcmd}^{''}}{X_{eq}} \sin(\theta) \tag{B.1}$$

$$i_{yin} = i_q^{'} \sin(\theta) - \frac{E_{qcmd}^{''}}{X_{eq}} \cos(\theta) \tag{B.2}$$

$$0 = -i_{yin} + i_y \frac{S_{base}}{S_{nom}} - \frac{v_x}{X_{eq}} \tag{B.3}$$

$$0 = -i_{xin} + i_x \frac{S_{base}}{S_{nom}} + \frac{v_y}{X_{eq}} \tag{B.4}$$

where θ is the angle reference of the rotor-side converter. v_x, v_y are the rectangular components of the terminal voltage V, and i_x, i_y the rectangular components of the current injected into the network. S_{base} and S_{nom} are the base apparent power of the network and the generator nominal apparent power, respectively.

B.1.3 Speed control

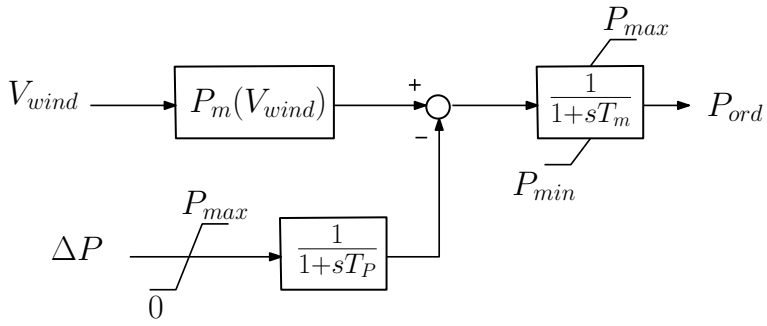

Figure B.3: Speed controller

The speed controller uses the wind speed V_{wind} as an input signal. The corresponding maximum mechanical power P_m which can be captured at this speed, is calculated assuming the pitch angle of the blades equal to zero.

$$P_m = \frac{1}{2} \rho \, \pi \, R^2 \, V_{wind}^3 \, C_p \, \frac{n_{turb}}{S_{nom}} \tag{B.5}$$

where C_p is the aerodynamic power coefficient, set to its maximum value.

ΔP in Fig. B.3 is the amount of active power curtailment requested by the centralized controller. This value is processed with time constant T_p which corresponds to the mechanical delay introduced by pitch angle adjustment. It is, then, subtracted from the maximum available mechanical

power P_m to obtain the desired value of active power production P_{ord}. T_m represents a mechanical time constant related to the generator and the wind turbine.

B.1.4 Reactive power control

As shown in Fig. B.4, depending upon the control strategy (indicated by "mode" in the same figure), Q_{cmd} can be one of the following:

- Q_d is the desired reactive power when the unit is in local control mode and varies its reactive power with voltage according to the piecewise linear VQ characteristic (see Section 5.2.1). In such a case, Q_d is obtained as shown in Fig. 5.17a.
- $P\ \tan(\Phi_{ref})$, which leads the generator to operating at a specified power factor $\cos(\Phi_{ref})$.

  This has not been used in the reported simulations.
- Q_{ref} is the reactive power requested when operating in reactive power mode.

  This mode of operation has been used in the whole work, except in the context of the two-level voltage control (see Chapter 5).

The output Q_{cmd} is compared with the generated reactive power Q_g, and then processed with a proportional-integral controller, whose output is the reference emf E''_{qcmd} shown in Fig. B.4.

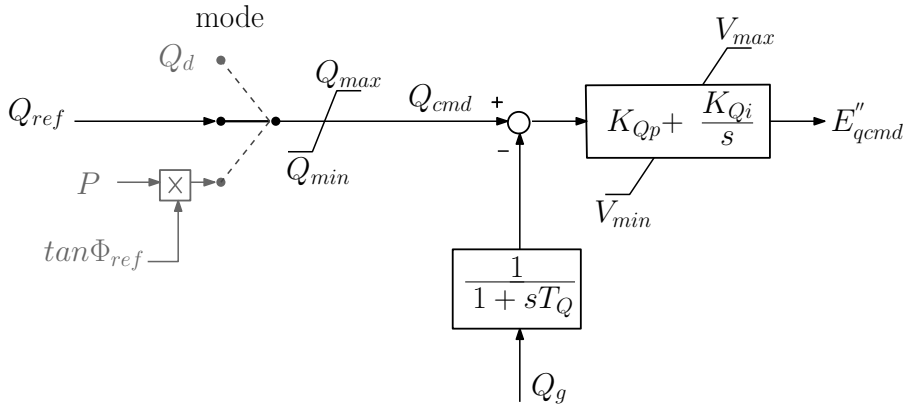

Figure B.4: Reactive power control

In per unit on the generator base, the reactive power appearing in Fig. B.4 is easily obtained as:

$$Q = v_y i_x \frac{S_{base}}{S_{nom}} - v_x i_y \frac{S_{base}}{S_{nom}} \tag{B.6}$$

B.1.5 Data and parameters

Table B.1: Data of the DFIG model

S_{nom}	n_{turb}	P_{nom}	X_{eq}	R	$ratio$	$P\ (poles)$	ρ	T_p
3.334	2	1.5	0.8	35.25	90	4	1.225	0.3

K_{Qi}	K_{Qp}	V_{min}	V_{max}	Q_{min}	Q_{max}	P_{min}	P_{max}	T_m	$mode$
0.5	0.05	0.9	1.1	-0.725	0.495	0.05	1.5	4	2

Table B.2: Parameters used in the DFIG model

S_{nom}, P_{nom}	generator nominal apparent and active powers
n_{turb}	number of turbines
X_{eq}	equivalent reactance
R	blade radius
$ratio$	gearbox ratio
$P\ (poles)$	number of poles
ρ	air density (kg/m3)
K_{Qi}, K_{Qp}	reactive power controller parameters
T_m	generator and wind turbine time constant
V_{min}, V_{max}	limits on reference voltage
Q_{min}, Q_{max}	generated reactive power limits
P_{min}, P_{max}	limits on ordered active power
T_p	pitch actuator time constant

B.2 Model of synchronous generator

This section deals with the modelling of small distributed synchronous machines. The generator is provided with a reactive power control.

B.2.1 Torque control

The model of the constant torque control used in this work is shown in Fig. B.5. This model receives the active power set-point P requested by the centralized controller. The time constant

T_m is used to represent the delay introduced by the turbine. Finally, the rotor speed ω is used to obtain the mechanical torque T_{mech}.

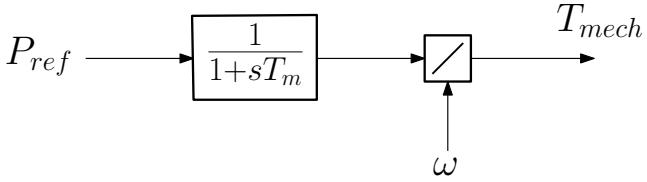

Figure B.5: Torque control

B.2.2 Reactive power control

The generic model of reactive power control of a generator under local control has been given in Fig. 5.17a.

The generic model of a generator under reactive power control is shown in Fig. B.6. The generated reactive power of the synchronous generator Q_g is measured, with the corresponding time constant T_Q. The reactive power requested by the centralized controller Q_{ref} is compared with the generated one, and processed by a Proportional-Integral controller. The gains K_{Qp} and K_{Qi} have been tune to minimize rotor oscillations. The output V_{ref} is the field voltage of the synchronous generator. This model has been used in the whole work, except in Chapter 5.

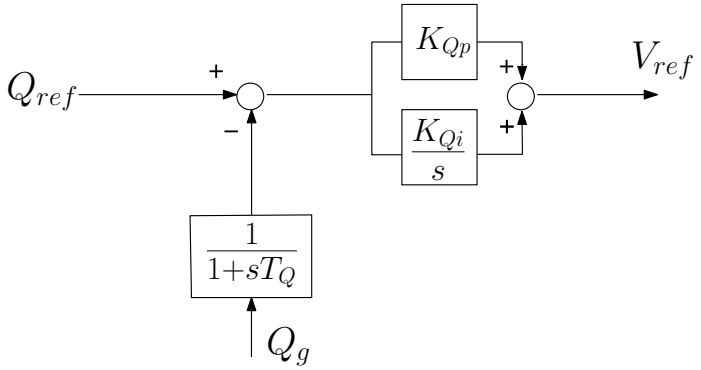

Figure B.6: Reactive power control

The data of the synchronous generator used are as follows:

Table B.3: Data of the torque and reactive power controls

T	T_Q	K_{Qp}	K_{Qi}
3	0.02	1	1

Bibliography

[ACA17] I. Abdelmotteleb and J.P. Chaves-Avila. Benefits of PV Inverter Volt-Var Control on Distribution Network Operation. In *Proc. IEEE PowerTech Conference*, Manchester (UK), 2017.

[AFV14] P. Aristidou, D. Fabozzi, and T. Van Cutsem. Dynamic Simulation of Large-Scale Power Systems Using a Parallel Schur-Complement-Based Decomposition Method. *IEEE Transactions on Parallel and Distributed Systems*, 25(10):2561–2570, oct 2014.

[ALV16] P. Aristidou, S. Lebeau, and T. Van Cutsem. Power System Dynamic Simulations Using a Parallel Two-Level Schur-Complement Decomposition. *IEEE Transactions on Power Systems*, 31(5):3984–3995, sep 2016.

[Ari15] P. Aristidou. *Time-domain simulation of large electric power systems using domain-decomposition and parallel processing methods*. PhD thesis, Université de Liège, Liège (Belgium), jun 2015.

[AZLV17] S. Asadollah, R. Zhu, M. Liserre, and C. Vournas. Decentralized Reactive Power and Voltage Control of Wind Farms with Type-4 Generators. In *Proc. IEEE PowerTech Conference*, Manchester (UK), 2017.

[BBG+10] A. Borghetti, M. Bosetti, S. Grillo, S. Massucco, C. A. Nucci, M. Paolone, and F. Silvestro. Short-Term Scheduling and Control of Active Distribution Systems with High Penetration of Renewable Resources. *IEEE Systems Journal*, 4(3):313–322, sep 2010.

[BCP16] M. Bahramipanah, R. Cherkaoui, and M. Paolone. Decentralized Voltage Control of Clustered Active Distribution Network by Means of Energy Storage Systems. *Electric Power Systems Research*, 136:370–382, jul 2016.

[BEM07] M. E. Baran and I. M. E. Markabi. A Multiagent-Based Dispatching Scheme

for Distributed Generators for Voltage Support on Distribution Feeders. *IEEE Transactions on Power Systems*, 22(1):52–59, feb 2007.

[BM99] A. Bemporad and M. Morari. Robust model predictive control: A survey. In *Robustness in identification and control*, pages 207–226. Springer, London (UK), 1999.

[BNCP15] M. Bahramipanah, M. Nick, R. Cherkaoui, and M. Paolone. Network Clustering for Voltage Control in Active Distribution Network Including Energy Storage Systems. In *proc. 6th IEEE PES Innovative Smart Grid Technologies (ISGT)*, Washington (USA), feb 2015.

[BSB10] J. Backes, C. Schorn, and H. Basse. Cost-Efficient Integration of Dispersed Generation Using Voltage Dependent Reactive Power Control. In *Proc. CIRED Workshop*, number 107, Lyon (France), jun 2010.

[BTCP16] M. Bahramipanah, D. Torregrossa, R. Cherkaoui, and M. Paolone. A Decentralized Adaptive Model-Based Real-time Control for Active Distribution Networks Using Battery Energy Storage Systems. *IEEE Transactions on Smart Grid*, PP(99), nov 2016.

[Cal84] M. Calovic. Modeling and Analysis of Under-Load Tap-Changing Transformer Control Systems. *IEEE Transactions on Power Apparatus and Systems*, 103(7):1909–1915, jul 1984.

[CCC09] S. Chowdhury, S. P. Chowdhury, and P. Crossley. *Microgrids and Active Distribution Networks*. The Institution of Engineering and Technology (IET), London (UK), 2009.

[CEN15] CENELEC. Requirements for Generating Plants to be Connected in Parallel With Distribution Networks - Part 2: Connection to a MV Distribution Network. Technical specification, CLC/TS 50549-2, 2015.

[CFMS11] A. Casavola, G. Franzè, D. Menniti, and N. Sorrentino. Voltage Regulation in Distribution Networks in the Presence of Distributed Generation: A Voltage Set-Point Reconfiguration Approach. *Electric Power Systems Research*, 81:25–34, jan 2011.

[CIG14] CIGRE Working Group C6.19. Planning and Optimization Methods for Active Distribution Systems. Technical report, aug 2014.

[CKN+12] Y. Chistyakov, E. Kholodova, K. Netreba, A. Szabo, and M. Metzger. Combined Central and Local Control of Reactive Power in Electrical Grids with Distributed

Generation. In *2012 IEEE International Energy Conference and Exhibition (ENERGYCON)*, pages 325–330, Florence (Italy), sep 2012. IEEE.

[CLTB14] L. Chen, H. Li, V. Turnham, and S. Brooke. Distribution Network Supports for Reactive Power Management in Transmission Systems. In *proc. 5th IEEE PES Innovative Smart Grid Technologies (ISGT)*, Istanbul (Turkey), oct 2014.

[CMSG10] K. Clark, N.W. Miller, and J.J. Sanchez-Gasca. Modeling of GE wind turbine-generators for grid studies. Technical report, apr 2010.

[CV05] F. Capitanescu and T. Van Cutsem. Unified Sensitivity Analysis of Unstable or Low Voltages Caused by Load Increases or Contingencies. *IEEE Transactions on Power Systems*, 20(1):321–329, feb 2005.

[CVGE15] B. Cornélusse, D. Vangulick, M. Glavic, and D. Ernst. Global Capacity Announcement of Electrical Distribution Systems: A Pragmatic Approach. *Sustainable Energy, Grids and Networks*, 4:43–53, dec 2015.

[DDK+12] M.J. Dolan, E.M. Davidson, I. Kockar, G.W. Ault, and S.D.J. McArthur. Distribution Power Flow Management Utilizing an Online Optimal Power Flow Technique. *IEEE Transactions on Power Systems*, 27(2):790–799, may 2012.

[DMSS17] F. D'Agostino, S. Massucco, M. Saviozzi, and F. Silvestro. Real time control of a low voltage microgrid through a Distribution Management System. In *Proc. 6th International Conference on Clean Electrical Power (ICCEP)*, pages 133–138, Santa Margherita Ligure (Italy), jun 2017.

[DNA+17] K. Das, E. Nuno Martinez, M. Altin, A. Daniela Hansen, and G. Wad Thybo. Facing the Challenges of Distribution Systems Operation with High Wind Power Penetration. In *Proc. IEEE PowerTech Conference*, Manchester (UK), 2017.

[EGH16] V.A. Evangelopoulos, P.S. Georgilakis, and N.D. Hatziargyriou. Optimal Operation of Smart Distribution Networks: A Review of Models, Methods and Future Research. *Electric Power Systems Research*, 140:95–106, nov 2016.

[Eng05] A. Engler. Applicability of Droops in Low Voltage Grids. *International Journal of Distributed Energy Resources and Smart Grids*, 1(1):3–15, jan 2005.

[FA02] Rolf Findeisen and Frank Allgöwer. An Introduction to Nonlinear Model Predictive Control. In *21st Benelux Meeting on Systems and Control*, pages 119–141, Veldhoven (The Netherlands), mar 2002.

[FCHV13] D. Fabozzi, A. S. Chieh, B. Haut, and T. Van Cutsem. Accelerated and Localized Newton Schemes for Faster Dynamic Simulation of Large Power Systems. *IEEE Transactions on Power Systems*, 28(4):4936–4947, nov 2013.

[Fer] Ferdowsi, https://en.wikipedia.org/wiki/Ferdowsi.

[FGM+15] M. Farina, A. Guagliardi, F. Mariani, C. Sandroni, and R. Scattolini. Model Predictive Control of Voltage Profiles in MV Networks with Distributed Generation. *Control Engineering Practice*, 34:18–29, jan 2015.

[FLDV14] F. Faghihi, J.C. Labeau, P.E. Maun, V. De Wilde, and A. Vergnol. A risk-based Approach to Long-term Grid Planning in Presence of Active Network Management. In *proc. of 2014 CIGRE conference*, Brussels (Belgium), mar 2014.

[FLEBP13] M. Falahi, S. Lotfifard, M. Ehsani, and K. Butler-Purry. Dynamic Model Predictive-Based Energy Management of DG Integrated Distribution Systems. *IEEE Transactions on Power Delivery*, 28(4):2217–2227, oct 2013.

[FTI+07] M. Fila, G.A. Taylor, M.R. Irving, J. Hiscock, P. Lang, and P. Aston. Systematic Modelling and Analysis of TAPP Voltage Control Schemes. In *proc. 42nd International Universities Power Engineering Conference (UPEC)*, number 2, pages 349–356, Brighton (USA), sep 2007.

[Gem16] Q. Gemine. *Active Network Management for Electrical Distribution Systems*. PhD thesis, Université de Liège, Liège (Belgium), nov 2016.

[GG14] L. Gelazanskas and K.A.A. Gamage. Demand Side Management in Smart Grid: A Review and Proposals for Future Direction. *Sustainable Cities and Society*, 11(Supplement C):22 – 30, 2014.

[GH15] P.S. Georgilakis and N.D. Hatziargyriou. A review of power distribution planning in the modern power systems era: Models, methods and future research. *Electric Power Systems Research*, 121:89–100, apr 2015.

[GKEC13] Q. Gemine, E. Karangelos, D. Ernst, and B. Cornélusse. Active Network Management: Planning Under Uncertainty for Exploiting Load Modulation. In *Proc. IREP Symposium on Bulk Power System Dynamics and Control*, Rethymnon (Greece), aug 2013.

[GLC+16a] E. Georges, V. Lemort, B. Cornélusse, D. Ernst, Q. Louveaux, and S. Mathieu. Direct Control Service from Residential Heat Pump Aggregation with Specified Payback. In *Proc. 19th Power System Computation Conference (PSCC)*, Genova (Italy), jun 2016.

[GLC+16b] E. Georges, V. Lemort, B. Cornélusse, D. Ernst, Q. Louveaux, and S. Mathieu. Direct control service from residential heat pump aggregation with specified payback. In *Proc. 19th Power System Computation Conference (PSCC)*, Genova (Italy), jun 2016.

[GRMC16] R. Godina, E.M.G. Rodrigues, J.C.O. Matias, and J.P.S. Catalão. Smart Electric Vehicle Charging Scheduler for Overloading Prevention of an Industry Client Power Distribution Transformer. *Applied Energy*, 178:29–42, sep 2016.

[GV09] M. Glavic and T. Van Cutsem. Wide-Area Detection of Voltage Instability From Synchronized Phasor Measurements. Part I: Principle. *IEEE Transactions on Power Systems*, 24(3):1408–1416, aug 2009.

[HB11] J. Hambrick and R.P. Broadwater. Configurable, Hierarchical, Model-Based Control of Electrical Distribution Circuits. *IEEE Transactions on Power Systems*, 26(3):1072–1079, aug 2011.

[HBM99] J.D. Hurley, L.N. Bize, and C.R. Mummert. The Adverse Effects of Excitation System Var and Power Factor Controllers. *IEEE Transactions on Energy Conversion*, 14(4):1636–1645, dec 1999.

[HP17] M.S. Hoosain and B.S. Paul. Smart Homes: A Domestic Demand Response and Demand Side Energy Management System for Future Smart Grids. In *Proc. International Conference on the Domestic Use of Energy (DUE)*, pages 285–291, Cape Town (South Africa), apr 2017.

[hsl11] HSL. A Collection of Fortran Codes for Large Scale Scientific Computation. *Available: http://www.hsl.rl.ac.uk*, 2011.

[HW16] M.M. Haque and P. Wolfs. A Review of High PV Penetrations in LV Distribution Networks: Present Status, Impacts and Mitigation Measures. *Renewable and Sustainable Energy Reviews*, 62:1195–1208, sep 2016.

[JWS14] N. Jayasekara, P. Wolfs, and M. Sherkat Masoum. An Optimal Management Strategy for Distributed Storages in Distribution Networks with High Penetrations of PV. *Electric Power Systems Research*, 116:147–157, nov 2014.

[KA14] L. Kane and G. Ault. A Review and Analysis of Renewable Energy Curtailment Schemes and Principles of Access: Transitioning Towards Business as Usual. *Energy Policy*, 72:67 – 77, 2014.

[KHBL13] P. Kotsampopoulos, N. Hatziargyriou, B. Bletterie, and G. Lauss. Review, Analysis and Recommendations on Recent Guidelines for the Provision of Ancillary

Services by Distributed Generation. In *Proc. IEEE International Workshop on Inteligent Energy Systems (IWIES)*, pages 185–190, Vienna (Austria), nov 2013.

[KK09] E. Kgi-Kolisnychenko. *Distribution management system including dispersed generation and storage in a liberalized market environment*. PhD thesis, Ecole Polytechnique Federale de Lausanne, Lausanne (Switzerland), 2009.

[KKW+14] T. Kerber, G. Kerber, M. Werner, M. Finkel, and M. Wiest. Decentralized Voltage Control in 20 kV Distribution Grids by Controlling Reactive Power of Inverters. In *Proc. CIRED Workshop*, number 0112, Rome (Italy), jun 2014.

[KMJ13] M. Kaspirek, D. Mezera, and J. Jiricka. Problems of Voltage Stabilization in MV and LV Distribution Grids Due to the Operation of Renewable Energy Sources. In *Proc. 22nd International Conference and Exhibition on Electricity Distribution (CIRED)*, number 0062, Stockholm (Sweden), jun 2013.

[Kul14] A. Kulmala. *Active Voltage Control in Distribution Networks Including Distributed Energy Resources*. PhD thesis, Tampere University of Technology, Tampere (Finland), may 2014.

[LHM+07] J.A. Peças Lopes, N. Hatziargyriou, J. Mutale, P. Djapic, and N. Jenkins. Integrating Distributed Generation into Electric Power Systems: A Review of Drivers, Challenges and Opportunities. *Electric Power Systems Research*, 77(9):1189–1203, jul 2007.

[LHO02] M. Larsson, D.J. Hill, and G. Olsson. Emergency Voltage Control Using Search and Predictive Control. *International Journal of Electrical Power & Energy Systems*, 24(2):121 – 130, 2002.

[Mac02] J. M. Maciejowski. *Predictive Control with Constraints*. Prentice-Hall, Essex (UK), 2002.

[MCD+17] J. Morin, F. Colas, J. Y. Dieulot, S. Grenard, and X. Guillaud. Embedding OLTC Nonlinearities in Predictive Volt Var Control for Active Distribution Networks. *Electric Power Systems Research*, 143:225–234, feb 2017.

[MH17] J.A. Martin and I.A. Hiskens. A Model-Predictive Control Strategy for Alleviating Voltage Collapse. In *proc. IREP Symposium : X Bulk Power Systems Dynamics and Control Symposium*, number 100, Espinho (Portugal), aug 2017.

[MLEC16] S. Mathieu, Q. Louveaux, D. Ernst, and B. Cornlusse. DSIMA: A Testbed for the Quantitative Analysis of Interaction Models within Distribution Networks . *Sustainable Energy, Grids and Networks*, 5:78 – 93, mar 2016.

[MM16] B. Mattlet and J.C. Maun. Assessing the Benefits for the Distribution System of a Scheduling of Flexible Residential Loads. In *Proc. IEEE International Energy Conference (ENERGYCON)*, Leuven (Belgium), apr 2016.

[Mor16] J. Morin. *Joint TSO-DSO Voltage and Reactive Power Control at the HV/MV Systems Interface and Development of Real-Time Volt Var Control of Distribution Networks*. Ph.D. thesis, Ecole nationale supérieure d'arts et métiers - ENSAM, Paris (France), November 2016.

[MZ16] N. Mahmud and A. Zahedi. Review of Control Strategies for Voltage Regulation of the Smart Distribution Network with High Penetration of Renewable Distributed Generation. *Renewable and Sustainable Energy Reviews*, 64:582–595, oct 2016.

[NCD00] I. M. Nejdawi, K. A. Clements, and P. W. Davis. An Efficient Interior Point Method for Sequential Quadratic Programming Based Optimal Power Flow. *IEEE Transactions on Power Systems*, 15(4):1179–1183, Nov 2000.

[Nej99] I.M. Nejdawi. *Optimal Power Flow Using Sequential Quadratic Programming*. PhD thesis, Worcester Polytechnic Institute, Massachusetts (US), Nov 1999.

[OAEV16] F. Olivier, P. Aristidou, D. Ernst, and T. Van Cutsem. Active Management of Low-Voltage Networks for Mitigating Overvoltages Due to Photovoltaic Units. *IEEE Transactions on Smart Grid*, 7(2):926–936, mar 2016.

[OLT] Technical Data of Oil-Immersed Load Tap Changer (OILTAP). Technical report, Available online: http://www.reinhausen.com.

[oTSOfEEE12] European Network of Transmission System Operators for Electricity (ENTSO-E). Network Code on Demand Connection. Technical report, Available online: https://www.entsoe.eu, dec 2012.

[oTSOfEEE16] European Network of Transmission System Operators for Electricity (ENTSO-E). Draft Establishing a Network Code on Requirements for Grid Connection of Generators. Technical report, Available online: https://www.entsoe.eu, apr 2016.

[PMK05] F. Provoost, J. Myrzik, and W. Kling. Optimized Voltage Control in Autonomously Controlled Networks. In *Proc. IEEE International Conference on Future Power Systems*, Amsterdam (Netherlands), Nov 2005.

[PPB+15] M. Pignati, M. Popovic, S. Barreto, R. Cherkaoui, G. Dario Flores, J.Y. Le Boudec, M. Mohiuddin, M. Paolone, P. Romano, S. Sarri, T. Tesfay, D.C. Tomozei, and L. Zanni. Real-time State Estimation of the EPFL-campus Medium-

Voltage Grid by Using PMUs. In *proc. 6th IEEE PES Innovative Smart Grid Technologies (ISGT)*, Washington (USA), feb 2015.

[QB03] S.J. Qin and T.A. Badgwell. A Survey of Industrial Model Predictive Control Technology. *Control Engineering Practice*, 11(7):733–764, jul 2003.

[RHDG13] B.A. Robbins, C.N. Hadjicostis, and A.D. Dominguez-Garcia. A Two-Stage Distributed Architecture for Voltage Control in Power Distribution Systems. *IEEE Transactions on Power Systems*, 28:1470–1482, May 2013.

[RHSS16] M. Rylander, Huijuan Li, J. Smith, and W. Sunderman. Default Volt-Var Inverter Settings to Improve Distribution System Performance. In *Proc. IEEE PES General Meeting*, Boston (USA), jul 2016.

[RTD+15] P. Rousseaux, J.F. Toubeau, Z. De Greve, F. Vallee, M. Glavic, and T. Van Cutsem. A New Formulation of State Estimation in Distribution Systems Including Demand and Generation States. In *Proc. IEEE PowerTech Conference*, Eindhoven (The Netherlands), Jun 2015.

[SFC+17] S.F. Santos, D.Z. Fitiwi, M.R.M. Cruz, C.M.P. Cabrita, and J.P.S. Catalao. Impacts of Optimal Energy Storage Deployment and Network Reconfiguration on Renewable Integration Level in Distribution Systems. *Applied Energy*, 185:44–55, jan 2017.

[SGV14] H. Soleimani Bidgoli, M. Glavic, and T. Van Cutsem. Model Predictive Control of Congestion and Voltage Problems in Active Distribution Networks. In *Proc. CIRED Workshop*, number 0108, Rome (Italy), Jun 2014.

[SGV16] H. Soleimani Bidgoli, M. Glavic, and T. Van Cutsem. Receding-horizon Control of Distributed Generation to Correct Voltage or Thermal Violations and Track Desired Schedules. In *Proc. 19th Power System Computation Conference (PSCC)*, Genova (Italy), jun 2016.

[SKR14] A. Seack, J. Kays, and C. Rehtanz. Time Series Based Distribution Grid Planning Approach with Decentralised Voltage Regulation. In *Proc. 18th Power System Computation Conference (PSCC)*, Wroclaw (Poland), aug 2014.

[SMR99] P.O.M. Scokaert, D.Q. Mayne, and J.B. Rawlings. Suboptimal Model Predictive Control (Feasibility Implies Stability). *IEEE Transactions on Automatic Control*, 44(3):648–654, mar 1999.

[SOH12] T. Sansawatt, L.F. Ochoa, and G.P. Harrison. Smart Decentralized Control of DG for Voltage and Thermal Constraint Management. *IEEE Transactions on Power Systems*, 27(3):1637–1645, aug 2012.

[SPC+12] S. Sarri, M. Paolone, R. Cherkaoui, A. Borghetti, F. Napolitano, and C.A. Nucci. State Estimation of Active Distribution Networks: Comparison between WLS and Iterated Kalman-Filter Algorithm Integrating PMUs. In *Proc. 3rd IEEE PES Innovative Smart Grid Technologies (ISGT)*, Washington (USA), oct 2012.

[SV] H. Soleimani Bidgoli and T. Van Cutsem. Combined Local and Centralized Voltage Control in Active Distribution Networks. *IEEE Transactions on Power Systems (in Press)*.

[SVA+] H. Soleimani Bidgoli, G. Valverde, P. Aristidou, M. Glavic, and T. Van Cutsem. Operation of Distribution Systems within Secure Limits Using Real-Time Model Predictive Control. In *Dynamic Vulnerability Assessment and Intelligent Control for Sustainable Power Systems (in Press)*.

[tes05] United Kingdom generic distribution network (UKGDS). *Available: http://sedg.ac.uk.*, 2005.

[TFP15] S. Tong, T. Fung, and J.W. Park. Reusing Electric Vehicle Battery for Demand Side Management Integrating Dynamic Pricing. In *Proc. IEEE International Conference on Smart Grid Communications (SmartGridComm)*, pages 325–330, Miami (USA), nov 2015.

[TNV09] G. Tsourakis, B.M. Nomikos, and C.D. Vournas. Effect of Wind Parks with Doubly Fed Asynchronous Generators on Small-Signal Stability. *Electric Power Systems Research*, 79(1):190–200, jan 2009.

[TSBC11] K. Turitsyn, P. Sulc, S. Backhaus, and M. Chertkov. Options for Control of Reactive Power by Distributed Photovoltaic Generators. *Proceedings of the IEEE*, 99(6):1063–1073, jun 2011.

[VDE11] VDE-AR-N 4105. Power Generation Systems Connected to the Low-voltage Distribution Network: Technical Minimum Requirements for the Connection to and Parallel Operation with Low-voltage Distribution Networks. Technical report, Available online: https://www.vde-verlag.de/, Aug 2011.

[VHRW06] A.N. Venkat, I.A. Hiskens, J.B. Rawlings, and S.J. Wright. Distributed MPC strategies for automatic generation control. In *proc. 5th IFAC Symposium on Power Plants and Power Systems Control*, volume 5, pages 383–388, Kananaskis (Canada), jun 2006.

[VKWH07] P. N. Vovos, A. E. Kiprakis, A. R. Wallace, and G. P. Harrison. Centralized and Distributed Voltage Control: Impact on Distributed Generation Penetratio. *IEEE Transactions on Power Systems*, 22(1):476–483, feb 2007.

[VO14] G. Valverde and J.J. Orozco. Reactive Power Limits in Distributed Generators from Generic Capability Curves. In *Proc. IEEE PES General Meeting*, Washington DC (USA), jul 2014.

[VV98] T. Van Cutsem and C. Vournas. *Voltage Stability of Electric Power Systems*. Springer, Boston (USA), 1998.

[VV13a] G. Valverde and T. Van Cutsem. Control of Dispersed Generation to Regulate Distribution and Support Transmission Voltages. In *Proc. IEEE Grenoble Conference*, Grenoble (France), jun 2013.

[VV13b] G. Valverde and T. Van Cutsem. Model Predictive Control of Voltages in Active Distribution Networks. *IEEE Transactions on Smart Grid*, 4(4):2152–2161, dec 2013.

[VZ13] A. Vaccaro and A.F. Zobaa. Voltage Regulation in Active Networks by Distributed and Cooperative Meta-Heuristic Optimizers. *Electric Power Systems Research*, 99:9–17, jun 2013.

[WBK12] C.J.C. Williams, J.O. Binder, and T. Kelm. Demand Side Management Through Heat Pumps, Thermal Storage and Battery Storage to Increase Local Self-Consumption and Grid Compatibility of PV Systems. In *Proc. 3rd IEEE PES Innovative Smart Grid Technologies Europe (ISGT Europe)*, Berlin (Germany), oct 2012.

[WGH11] X. Wang, P. Guo, and X. Huang. A Review of Wind Power Forecasting Models. *Energy Procedia*, 12:770–778, dec 2011.